KINETIC INVESTIGATION AND MECHANISMS OF REDUCTION OF N, N'-PHENYLENEBIS(SALICYLIDENEIMINATO)COBALT(III) ION BY SOME REDUCING AGENTS IN DMSO-H_2O MEDIUM

BY

SAFIYA ABDULSALAM

DEPARTMENT OF CHEMISTRY,
FACULTY OF PHYSICAL SCIENCES,
AHMADU BELLO UNIVERSITY,
ZARIA, NIGERIA

DECEMBER, 2021

KINETIC INVESTIGATION AND MECHANISMS OF REDUCTION OF N, N'-PHENYLENEBIS(SALICYLIDENEIMINATO)COBALT(III) ION BY SOME REDUCING AGENTS IN DMSO-H_2O MEDIUM

BY

SAFIYA ABDULSALAM

B.Tech. (ATBU 2011), M.Sc. (ABU 2015)

P15SCCH9071

A THESIS SUBMITTED TO THE SCHOOL OF POSTGRDUATE STUDIES, AHMADU BELLO UNIVERSITY, IN PARTIAL FULFILLMENT OF THE REQUIREMENTS FOR THE AWARD OF A DOCTOR OF PHILOSOPHY DEGREE IN INORGANIC CHEMISTRY

DEPARTMENT OF CHEMISTRY,
FACULTY OF PHYSICAL SCIENCES,
AHMADU BELLO UNIVERSITY,
ZARIA, NIGERIA

DECEMEBER, 2021

DECLARATION

I declare that the work in this thesis entitled "Kinetic Investigation and Mechanisms of Reduction of N, N'-phenylenebis(salicylideneiminato)cobalt(III) Ion by Some Reducing Agents in DMSO-H_2O Medium" have been carried out by me in the Department of Chemistry, Ahmadu Bello University, Zaria. The information derived from literature have been duly acknowledged in the text and a list of references provided. No part of this thesis was previously presented for another degree or diploma in this or any other institution.

Safiya ABDULSALAM	_____	_____
Name of Student	Signature	Date

CERTIFICATION

This thesis entitled "**Kinetic investigation and mechanisms of reduction of N,N'-phenylenebis(salicylideneiminato)cobalt(III) ion by some reducing agents in DMSO-H_2O medium**" by Safiya ABDULSALAM, meets the regulations governing the award of the degree of Doctor of Philosophy in Inorganic Chemistry of Ahmadu Bello University, and is approved for its contribution to knowledge and literary presentation.

Prof. S. O. Idris Chairman, Supervisory Committee	_____ Signature	_____ Date
Dr. G.A. Shallangwa Member, Supervisory Committee	_____ Signature	_____ Date
Dr. A. D. Onu Member, Supervisory Committee	_____ Signature	_____ Date
Prof. G. I. Ndukwe Head of Department	_____ Signature	_____ Date
Prof. S. A. Abdullahi Dean, School of Postgraduate Studies	_____ Signature	_____ Date

DEDICATION

This work is dedicated to my beloved parents, Alhaji Mustapha Abdulsalam and Hajiya Maimunat Badamasi. May Allah have mercy on them, just as they had on me when I was young! Amen.

ACKNOWLEDGEMENTS

All praises and gratitude are due to Almighty Allah, the All and All; I thank you for seeing me through this academic journey. Your unquantifiable love to me is overwhelming. May the Peace and Blessings of Allah continue to cascade upon the Noble Prophet Muhammad (*SAW*), his household, his companions and all who follow them till the day of reckoning! Amin.

To the Chairman, Supervisory Committee, Prof. S. O. Idris who is not only a supervisor but a father, mentor and a role model, thank you for your support and dedication especially during the COVID-19 pandemic. May God Almighty grant you good health, long life and prosperity and bless your generation, amin. My profound and sincere appreciation go to the rest of the Supervisory Committee Members, Dr. G. A. Shallangwa and Dr. A. D. Onu for their patience, encouragement and contributions toward the success of this work. May God Almighty answer your prayers! Amin. I would like to thank the Head of Department, Prof. G. I. Ndukwe and the entire Staff of the Department for their contributions from the time I started my postgraduate studies in the Department till date.

I am very grateful to the following lecturers; Dr. Z. N. Garba, Dr. I. Abdulkadir, Dr. (Mrs) O. R. A. Iyun, Dr. H. Ibrahim, Mrs. S. A. Hamza, Mrs. M. Imam, Dr. I. Bello, Dr. M. J. Zubairu, Dr. Abdulfatai Usman, Mr. I. Ibrahim, Dr. A. B. Aliyu, Mr. A. Haruna, Dr. N. Tajuddeen, Dr. N. Lawal, Dr. A. B. Umar, Dr. M. T. Ibrahim, Mr. M. A. Lawal, Mr. M. Abdulrahman and Mr. Z. Y. Ibrahim for their support, encouragement and advice, May Allah reward you in abundance. Also, the Chief Technologist of the Department, Malam Saidu Musa and all the members of non-academic staff especially Malam Ja'afar Adam, Malam Maikudi Jinjiri and Malama Safiya Aliyu, thank you for the help and encouragements toward the success of this research. The assistance of Mr. Silas Ekwuribe of Multi-User Science Research Laboratory and his team in providing the facilities for this work is gratefully acknowledged. The efforts of Mr. I. U. Nkole towards the success of this work is highly appreciated.

My appreciation also goes to my entire family (The Mustaphas), my husband, Engineer Yusuf Badamasi, my children, Fatima, Abdulrahman, Aisha and Ummulkhair, and my house help Zakhriyya for their support, encouragement, love and care. To my faithful friends (known and unknown), I owe you people a lot. To all who have contributed in one way or the other towards my success, I said thank you.

Nevertheless, I would like to specially appreciate my beloved parents, my uncles, my brothers and sisters for their support, spiritually and morally. May Allah reserve the highest palace for you in Jannah! Amin.

ABSTRACT

The kinetic investigation and mechanisms of reduction of N,N'-phenylenebis(salicyalideneiminato)cobalt(III) ion (hereafter denoted as $[Co(salophen)]^{+}$) by L-cysteine (LSH), thioglycol (RSH), thioglycolic acid (TSH), 1,5-diphenylcarbazide (DPCI) thiosemicarbazide (TSCZ), acetaldehyde (CH_3CHO), formaldehyde (HCHO), iodide ion (I^-), ascorbic acid (H_2A) and thiodiglycol ($S(R)_2$) were studied in aqueous hydrochloric acid (HCl) medium, except for TSH which was monitored in the absence of acid. The stoichiometry was found to be 1:2 (reductant/complex) in the CH_3CHO, HCHO and $S(R)_2$, 3:2 for H_2A and 1:1 for LSH, RSH, TSH, DPCI, TSCZ and I^- systems. The rate of reaction was first order in both the [oxidant] and [reductants] for all the systems and second order overall. Addition of acid had inverse effect on the rates of reaction for the $[Co(salophen)]^{+}$ - TSH and $[Co(salophen)]^{+}$ - H_2A systems, and direct dependence for the $[Co(salophen)]^{+}$ - LSH and $[Co(salophen)]^{+}$ - RSH systems but was found to be independent on the rate of the rest reactions. The overall rate equation for the reactions can be given as;

$$-\frac{d}{dt}[Co(salophen)^{+}] = (a + b[H^{+}]^{-1})[Co(salophen)^{+}][reductants]$$

where reductant = H_2A and TSH

$$-\frac{d}{dt}[Co(salophen)^{+}] = (a + b[H^{+}])[Co(salophen)^{+}][reductants]$$

where reductants = LSH and RSH

Varying the ionic strength (μ) and dielectric constant (D) of the reaction medium had no effect on rates of the reactions of DPCI, TSCZ, CH_3CHO, HCHO, I^- and $S(R)_2$, while in the case of LSH and RSH reactions, increase in μ led to an increase in rate while decrease in D led to decrease in rate of the reactions. For the TSH and H_2A reactions, increase in μ led to the decrease in the reaction rates and decrease in D led to an increase in the rate of reactions. Added

ions (Ca^{2+}, Mg^{2+}, SO_4^{2-}, CH_3COO^- and $HCOO^-$) catalysed and/or inhibited the rate of the reactions for all the systems except for I^- reaction where added ions had no effect on the reaction rate. Free radicals were identified in all the systems except for DPCI and TSCZ systems. The temperature dependence study showed a negative entropy of activation ($\Delta S^{\ddagger}$) for all the systems except in the case of TSH reaction where positive entropy was observed. Spectroscopic information and the results of the Michaelis – Menten's plots suggest lack of formation of stable and detectable intermediate complex prior to electron transfer for all the systems. For LSH, RSH, TSH and TSCZ systems, disulphide was found to be the oxidation product, sulphoxide for $S(R)_2$, 1,5-diphenylcarbazone (DPCO) for DPCI, dehydroascorbic acid for H_2A, iodine for I^- and acetic acid and formic acid for CH_3CHO and HCHO reactions respectively. Based on the results obtained in the investigations, the reactions are proposed to have proceeded through the outer-sphere electron transfer mechanism.

TABLE OF CONTENTS

Cover Page	i
Fly Leaf	ii
Title Page	iii
Declaration	iv
Certification	v
Dedication	vi
Acknowledgement	vii
Abstract	viii
Table of Contents	x
List of Tables	xv
List of Figures	xix
List of Schemes	xxvii
Appendices	xxviii
Abbreviations	xxix

CHAPTER ONE

1.0 INTRODUCTION	**1**
1.1 Statement of Research Problem	**3**
1.2 Justification	**4**
1.3 Aim and Objectives	**5**

CHAPTER TWO

2.0 LITERATURE REVIEW	**6**
2.1 Chemistry of Cobalt(III) Complexes	**6**

2.2 Reactions of L-cysteine **8**

2.3 Reactions of Thioglycol **11**

2.4 Reactions of Thioglycolic Acid **13**

2.5 Reactions of Thiosemicarbazide **15**

2.6 Reactions of 1,5-diphenylcarbazide **18**

2.7 Reactions of Acetalaldehyde **19**

2.8 Reactions of Formaldehyde **20**

2.9 Reactions of Iodide Ion **21**

2.10 Reactions of L-ascorbic Acid **22**

2.11 Reactions of Thiodiglycol **25**

CHAPTER THREE

3.0 MATERIALS AND METHODS **27**

3.1 Materials **27**

3.1.1 Reagents and chemicals 27

3.1.2 Equipment 27

3.2 Methods **28**

3.2.1 Preparation of 0.5 mol dm^{-3} l-cysteine solution 28

3.2.2 Preparation of 0.5 mol dm^{-3} l-ascorbic acid solution 28

3.2.3 Preparation of thioglycolic acid solution 28

3.2.4 Preparation of thioglycol solution 28

3.2.5 Preparation of 0.08 mol dm^{-3} 1,5-diphenylcarbazide solution 29

3.2.6 Preparation of 0.5 mol dm^{-3} potassium iodide solution 29

3.2.7 Preparation of 0.5 mol dm^{-3} acetaldehyde solution 29

3.2.8 Preparation of 0.5 mol dm^{-3} formaldehyde solution 29

3.2.9 Preparation of 0.5 mol dm^{-3} thiodiglycol solution 29

3.2.10 Preparation of 0.5 mol dm^{-3} thiosemicarbazide solution 30

3.2.11 Preparation of 1.5 mol dm^{-3} sodium chloride solution 30

3.2.12 Preparation of 0.1 mol dm^{-3} sodium carbonate solution 30

3.2.13 Preparation of standard solution of hydrochloric acid 30

3.2.14 Preparation of 2.0 mol dm^{-3} solution of perchloric acid 30

3.2.15 Preparation of 1.0 mol dm^{-3} solution of sulphuric acid 31

3.2.16 Preparation of salt solutions 31

3.2.17 Preparation of 0.1 mol dm^{-3} acrylamide solution 31

3.2.18 Preparation of 0.2 mol dm^{-3} potassium thiocyanate solution 31

3.2.19 Preparation of 0.5 mol dm^{-3} hydrogen peroxide solution 31

3.2.20 Synthesis and characterization of the ligand and the complex 32

3.2.21 Stoichiometric studies 33

3.2.22 Product analysis 35

3.2.23 Kinetic measurements 36

3.2.24 Determination of the effect of $[H^+]$ on the reaction rates 37

3.2.25 Determination of the effect of change in ionic strength of reaction medium on rate of reaction 38

3.2.26 Determination of the effect of change in dielectric constant of reaction medium on rate of reactions 38

3.2.27 Determination of the effect of added of ions on the rate of reactions 39

3.2.28 Determination of the effect of change in temperature on the reaction rates 39

3.2.29 Test for the participation of free radicals in the reaction 40

3.2.30 Test for the formation of intermediate complex prior to electron transfer 40

CHAPTER FOUR

4.0 RESULTS 41

4.1 Characterisation and Stability of the Complex 41

4.2 Stoichiometry Studies 41

4.3 Products Analyses 53

4.4 Pseudo-first Order and Second Order Rate Constants and Order of Reaction 54

4.5 Effect of Hydrogen Ion Concentration on the Rate of Reaction 86

4.6 Effect of Change in Ionic Strength of Reaction Medium on the Reaction Rate 97

4.7 Effect of Change in Dielectric Constant of Reaction Medium on the Reaction Rate 97

4.8 Effect of Added Ions on the Reaction Rates 97

4.9 Dependence of Reactions Rate on Temperature 165

4.10 Free Radical Test 165

4.11 Test for the Formation of Intermediate Complex 165

4.11.1 Kinetic test (Michaelis-Menten plots) 165

4.11.2 Spectroscopic test 165

CHAPTER FIVE

5.0 DISCUSSION 206

5.1 Reaction of [Co(salophen)]$^+$ with L-cysteine and Thioglycol **206**

5.2 Reaction of [Co(salophen)]$^+$ with Thioglycolic Acid **211**

5.3 Reaction of [Co(salophen)]$^+$ with Thiosemicarbazide **214**

5.4 Reaction of [Co(salophen)]$^+$ with 1,5-diphenylcarbazide **217**

5.5 Reaction of [Co(salophen)]$^+$ with Acetaldehyde and Formaldehyde **220**

5.6 Reaction of [Co(salophen)]$^+$ with Iodide Ion **223**

5.7 Reaction of [Co(salophen)]$^+$ with Ascorbic Acid **225**

5.8 Reaction of [Co(salophen)]$^+$ with Thiodiglycol **229**

5.9 Comparative Study **231**

5.9.1 Comparison of [Co(salophen)]$^+$ with thiols (LSH, RSH, TSH, and $S(R)_2$) systems 231

5.9.2. Comparison of [Co(salophen)]$^+$ with carbazides 232

5.9.3 Comparison of [Co(salophen)]$^+$ with aldehydes 232

5.9.4 Comparison of [Co(salophen)]$^+$ with thiols, carbazides and aldehydes 232

CHAPTER SIX

6.0 SUMMARY, CONCLUSION AND RECOMMENDATIONS **233**

6.1 Summary **233**

6.2 Conclusion **234**

6.3 Recommendations **234**

REFERENCES **236**

LIST OF APPENDICES **249**

LIST OF TABLES

4.1 Pseudo-first Order and Second Order Rate Constants for the Redox Reaction of $[Co(salophen)]^+$ and LSH 76

4.2 Pseudo-first Order and Second Order Rate Constants for the Redox Reaction of $[Co(salophen)]^+$ and RSH 77

4.3 Pseudo-first Order and Second Order Rate Constants for the Redox Reaction of $[Co(salophen)]^+$ and TSH 78

4.4 Pseudo-first Order and Second Order Rate Constants for the Redox Reaction of $[Co(salophen)]^+$ and TSCZ 79

4.5 Pseudo-first Order and Second Order Rate Constants for the Reaction of $[Co(salophen)]^+$ and DPCI 80

4.6 Pseudo-first Order and Second Order Rate Constants for the Redox Reaction of $[Co(salophen)]^+$ and CH_3CHO 81

4.7 Pseudo-first Order and Second Order Rate Constants for the Reaction of $[Co(salophen)]^+$ and HCHO 82

4.8 Pseudo-first Order and Second Order Rate Constants for the Reaction of $[Co(salophen)]^+$ and I^- 83

4.9 Pseudo-first Order and Second Order Rate Constants for the Redox Reaction of $[Co(salophen)]^+$ and H_2A 84

4.10 Pseudo-first Order and Second Order Rate Constants for the Redox Reaction of $[Co(salophen)]^+$ and $S(R)_2$ 85

4.11 Acid Dependence Effect on the Rate of Reaction of $[Co(salophen)]^+$ and TSH 87

4.12 Effect of Dielectric Constant on the Redox Reaction of $[Co(salophen)]^+$ and LSH 102

4.13 Effect of Dielectric Constant on the Redox Reaction of $[Co(salophen)]^+$ and RSH 103

4.14 Effect of Dielectric Constant on the Redox Reaction of $[Co(salophen)]^+$ and TSH 104

4.15 Effect of Dielectric Constant on the Redox Reaction of $[Co(salophen)]^+$ and TSCZ 105

4.16 Effect of Dielectric Constant on the Rate of Reaction of $[Co(salophen)]^+$ and DPCI 106

4.17 Effect of Dielectric Constant on the Redox Reaction of $[Co(salophen)]^+$ and CH_3CHO 107

4.18 Effect of Dielectric Constant on the Rate of Reaction of $[Co(salophen)]^+$ and HCHO 108

4.19 Effect of Dielectric Constant on the Rate of Reaction of $[Co(salophen)]^+$ and I^- 109

4.20 Effect of Dielectric Constant on the Redox Reaction of $[Co(salophen)]^+$ and H_2A 110

4.21 Effect of Dielectric Constant on the Redox Reaction of $[Co(salophen)]^+$ and $S(R)_2$ 111

4.22 Effect of Added Cation on the Redox Reaction of $[Co(salophen)]^+$ and LSH 112

4.23 Effect of Added Anion on the Redox Reaction of $[Co(salophen)]^+$ and LSH 113

4.24 Effect of Added Cation on the Redox Reaction of $[Co(salophen)]^+$ and RSH 114

4.25 Effect of Added Anion on the Redox Reaction of $[Co(salophen)]^+$ and RSH 115

4.26 Effect of Added Cation on the Redox Reaction of $[Co(salophen)]^+$ and TSH 116

4.27 Effect of Added Anion on the Redox Reaction of $[Co(salophen)]^+$ and TSH 117

4.28 Effect of Added Cations on the Redox Reaction of $[Co(salophen)]^+$ and TSCZ 118

4.29 Effect of Added Anion on the Redox Reaction of $[Co(salophen)]^+$ and TSCZ 119

4.30 Effect of Added Cation on the Rate of Reaction of $[Co(salophen)]^+$ and DPCI 120

4.31 Effect of Added Anion on the Rate of Reaction of $[Co(salophen)]^+$ and DPCI 121

4.32 Effect of Added Cation on the Redox Reaction of $[Co(salophen)]^+$ and CH_3CHO 122

4.33 Effect of Added Anion on the Redox Reaction of $[Co(salophen)]^+$ and CH_3CHO 123

4.34 Effect of Added Cation on the Rate of Reaction of $[Co(salophen)]^+$ and HCHO 124

4.35 Effect of Added Anion on the Rate of Reaction of $[Co(salophen)]^+$ and HCHO 125

4.36 Effect of Added Cation on the Rate of Reaction of $[Co(salophen)]^+$ and I^- 126

4.37 Effect of Added Anion on the Rate of Reaction of $[Co(salophen)]^+$ and I^- 127

4.38 Effect of Added Cation on the Redox Reaction of $[Co(salophen)]^+$ and H_2A 128

4.39 Effect of Added Anion on the Redox Reaction of $[Co(salophen)]^+$ and H_2A 129

4.40 Effect of Added Cation on the Redox Reaction of $[Co(salophen)]^+$ and $S(R)_2$ 130

4.41 Effect of Added Anion on the Redox Reaction of $[Co(salophen)]^+$ and $S(R)_2$ 131

4.42 Temperature Dependent Rate constants and Activation Parameters for the Redox Reaction of $[Co(salophen)]^+$ and LSH 166

4.43 Temperature Dependent Rate Constants and Activation Parameters for the Redox Reaction of $[Co(salophen)]^+$ and RSH 167

4.44 Temperature Dependent Rate Constants and Activation Parameters on the Redox Reaction of $[Co(salophen)]^+$ and TSH 168

4.45 Temperature Dependent Rate Constants and Activation Parameters for the redox reaction of $[Co(salophen)]^+$ and TSCZ 169

4.46 Temperature Dependent Rate Constants and Activation Parameters for the Reaction of $[Co(salophen)]^+$ and DPCI 170

4.47 Temperature Dependent Rate Constants and Activation Parameters for the Redox Reaction of $[Co(salophen)]^+$ and CH_3CHO 171

4.48 Temperature Dependent Rate Constants and Activation Parameters for the Reaction of $[Co(salophen)]^+$ and HCHO 172

4.49 Temperature Dependent Rate Constants and Activation Parameters for the Reaction of $[Co(salophen)]^+$ and I^- 173

4.50 Temperature Dependent Rate Constants and Activation Parameters for the Redox Reaction of $[Co(salophen)]^+$ and H_2A 174

4.51 Temperature Dependent Rate Constants and Activation Parameters for the Redox Reaction of $[Co(salophen)]^+$ and $S(R)_2$ 175

LIST OF FIGURES

2.1	Structure of L-cysteine	8
2.2	Structure of Thioglycol	11
2.3	Structure of Thioglycolic Acid	13
2.4	Structure of Thiosemicarbazide	15
2.5	Structure of 1,5-diphenylcarbazide	18
2.6	Structure of L-ascorbic Acid	22
2.7	Structure of Thiodiglycol	25
4.1	Plot of Absorbance Versus Mole Ratio for the Redox Reaction of $[Co(salophen)]^+$ and LSH	42
4.2	Plot of Absorbance Versus Mole Ratio for the Redox Reaction of $[Co(salophen)]^+$ and RSH	43
4.3	Plot of Absorbance Versus Mole Ratio for the Redox Reaction of $[Co(salophen)]^+$ and TSH	44
4.4	Plot of Absorbance Versus Mole Ratio for the Redox Reaction of $[Co(salophen)]^+$ and TSCZ	45
4.5	Plot of Absorbance Versus Mole Ratio for the Redox Reaction of $[Co(salophen)]^+$ and DPCI	46
4.6	Plot of Absorbance Versus Mole Ratio for the Redox Reaction of $[Co(salophen)]^+$ and CH_3CHO	47
4.7	Plot of Absorbance Versus Mole Ratio for the Redox Reaction of $[Co(salophen)]^+$ and HCHO	48
4.8	Plot of Absorbance Versus Mole Ratio for the Redox Reaction of $[Co(salophen)]^+$ and I^-	49
4.9	Plot of Absorbance Versus Mole Ratio for the Redox Reaction of $[Co(salophen)]^+$ and H_2A	50
4.10	Plot of Absorbance Versus Mole Ratio for the Redox Reaction of $[Co(salophen)]^+$ and $S(R)_2$	51

4.11 Typical Pseudo-first Order Plot for the Redox Reaction of $[Co(salophen)]^+$ and LSH 55

4.12 Typical Pseudo-first Order Plot for the Redox Reaction of $[Co(salophen)]^+$ and RSH 56

4.13 Typical Pseudo-first Order Plot for the Redox Reaction of $[Co(salophen)]^+$ and TSH 57

4.14 Typical Pseudo-first Order Plot for the Redox Reaction of $[Co(salophen)]^+$ and TSCZ 58

4.15 Typical Pseudo-first Order Plot for the Redox Reaction of $[Co(salophen)]^+$ and DPCI 59

4.16 Typical Pseudo-first Order Plot for the Redox Reaction of $[Co(salophen)]^+$ and CH_3CHO 60

4.17 Typical Pseudo-first Order Plot for the Redox Reaction of $[Co(salophen)]^+$ and HCHO 61

4.18 Typical Pseudo-first Order Plot for the Redox Reaction of $[Co(salophen)]^+$ and I^- 62

4.19 Typical pseudo-first order plot for the redox reaction of $[Co(salophen)]^+$ and H_2A 63

4.20 Typical Pseudo-first Order Plot for the Redox Reaction of $[Co(salophen)]^+$ and $S(R)_2$ 64

4.21 Plot of log k_1 Versus log [LSH] for the Redox Reaction of $[Co(salophen)]^+$ and LSH 65

4.22 Plot of logk_1 Versus log [RSH] for the Redox Reaction of $[Co(salophen)]^+$ and RSH 66

4.23 Plot of log k_1 Versus log [TSH] for the Redox Reaction of $[Co(salophen)]^+$ and TSH 67

4.24 Plot of log k_1 versus log [DPCI] for the redox reaction of $[Co(salophen)]^+$ and DPCI 68

4.25 Plot of log k_1 Versus log [TSCZ] for the Redox Reaction of $[Co(salophen)]^+$ and TSCZ 69

4.26 Plot of log k_1 Versus log [CH_3CHO] for the Redox Reaction of [Co(salophen)]$^+$ and CH_3CHO 70

4.27 Plot of log k_1 Versus log [HCHO] for the Redox Reaction of [Co(salophen)]$^+$ and HCHO 71

4.28 Plot of log k_1 Versus log [I^-] for the Redox Reaction of [Co(salophen)]$^+$ and I^- 72

4.29 Plot of log k_1 Versus log [H_2A] for the Redox Reaction of [Co(salophen)]$^+$ and H_2A 73

4.30 Plot of log k_1 Versus log [$S(R)_2$] for the Redox Reaction of [Co(salophen)]$^+$ and $S(R)_2$ 74

4.31 Plot of log k_1 Versus log [H^+] for the Redox Reaction of [Co(salophen)]$^+$ and LSH 88

4.32 Plot of log k_1 Versus log [H^+] for the Redox Reaction of [Co(salophen)]$^+$ and RSH 89

4.33 Plot of log k_1 Versus log [H^+]$^{-1}$ for the Redox Reaction of [Co(salophen)]$^+$ and TSH 90

4.34 Plot of log k_1 Versus log [H^+]$^{-1}$ for the Redox Reaction of [Co(salophen)]$^+$ and H_2A 91

4.35 Plot of k_2 Versus [H^+] for the Redox Reaction of [Co(salophen)]$^+$ and LSH 92

4.36 Plot of k_2 Versus [H^+] for the Redox Reaction of [Co(salophen)]$^+$ and RSH 93

4.37 Plot of k_2 Versus 1/[H^+] for the Redox Reaction of [Co(salophen)]$^+$ and TSH 94

4.38 Plot of k_2 Versus 1/[H^+] for the Redox Reaction of [Co(salophen)]$^+$ and H_2A 95

4.39 Plot of log k_2 Versus $\sqrt{\mu}$ for the Redox Reaction of [Co(salophen)]$^+$ and LSH 98

4.40 Plot of log k_2 Versus $\sqrt{\mu}$ for the Redox Reaction of [Co(salophen)]$^+$ and RSH 99

4.41 Plot of log k_2 Versus $\sqrt{\mu}$ for the Redox Reaction of $[Co(salophen)]^+$ and TSH 100

4.42 Plot of log k_2 Versus $\sqrt{\mu}$ for the Redox Reaction of $[Co(salophen)]^+$ and H_2A 101

4.43 Plot of k_2 Versus $[Mg^{2+}]$ for the Redox Reaction of $[Co(salophen)]^+$ and LSH 132

4.44 Plot of k_2 Versus $[Ca^{2+}]$ for the Redox Reaction of $[Co(salophen)]^+$ and LSH 133

4.45 Plot of k_2 Versus $[SO_4^{2-}]$ for the Redox Reaction of $[Co(salophen)]^+$ and LSH 134

4.46 Plot of k_2 Versus $[CH_3COO^-]$ for the Redox Reaction of $[Co(salophen)]^+$ and LSH 135

4.47 Plot of k_2 Versus $[Mg^{2+}]$ for the Redox Reaction of $[Co(salophen)]^+$ and RSH 136

4.48 Plot of k_2 Versus $[Ca^{2+}]$ for the Redox Reaction of $[Co(salophen)]^+$ and RSH 137

4.49 Plot of k_2 Versus $[SO_4^{2-}]$ for the Redox Reaction of $[Co(salophen)]^+$ and RSH 138

4.50 Plot of k_2 Versus $[Mg^{2+}]$ for the Redox Reaction of $[Co(salophen)]^+$ and TSH 139

4.51 Plot of k_2 Versus $[Ca^{2+}]$ for the Redox Reaction of $[Co(salophen)]^+$ and TSH 140

4.52 Plot of k_2 Versus $[SO_4^{2-}]$ for the Redox Reaction of $[Co(salophen)]^+$ and TSH 141

4.53 Plot of k_2 Versus $[Mg^{2+}]$ for the Redox Reaction of $[Co(salophen)]^+$ and TSCZ 142

4.54 Plot of k_2 Versus $[Ca^{2+}]$ for the Redox Reaction of $[Co(salophen)]^+$ and TSCZ 143

4.55 Plot of k_2 Versus $[HCOO^-]$ for the Redox Reaction of $[Co(salophen)]^+$ and TSCZ 144

4.56 Plot of k_2 Versus $[Mg^{2+}]$ for the Reaction of $[Co(salophen)]^+$ and DPCI 145

4.57 Plot of k_2 Versus $[Ca^{2+}]$ for the Reaction of $[Co(salophen)]^+$ and DPCI 146

4.58 Plot of k_2 Versus $[SO_4^{2-}]$ for the Reaction of $[Co(salophen)]^+$ and DPCI 147

4.59 Plot of k_2 Versus $[CH_3COO^-]$ for the Reaction of $[Co(salophen)]^+$ and DPCI 148

4.60 Plot of k_2 Versus $[Mg^{2+}]$ for the Redox Reaction of $[Co(salophen)]^+$ and CH_3CHO 149

4.61 Plot of k_2 Versus $[Ca^{2+}]$ for the Redox Reaction of $[Co(salophen)]^+$ and CH_3CHO 150

4.62 Plot of k_2 Versus $[SO_4^{2-}]$ for the Redox Reaction of $[Co(salophen)]^+$ and CH_3CHO 151

4.63 Plot of k_2 Versus $[CH_3COO^-]$ for the Redox Reaction of $[Co(salophen)]^+$ and CH_3CHO 152

4.64 Plot of k_2 Versus $[Mg^{2+}]$ for the Redox Reaction of $[Co(salophen)]^+$ and HCHO 153

4.65 Plot of k_2 Versus $[Ca^{2+}]$ for the Redox Reaction of $[Co(salophen)]^+$ and HCHO 154

4.66 Plot of k_2 Versus $[SO_4^{2-}]$ for the Reaction of $[Co(salophen)]^+$ and HCHO 155

4.67 Plot of k_2 Versus $[CH_3COO^-]$ for the Redox Reaction of $[Co(salophen)]^+$ and HCHO 156

4.68 Plot of k_2 Versus $[Mg^{2+}]$ for the Redox Reaction of $[Co(salophen)]^+$ and H_2A 157

4.69 Plot of k_2 Versus $[Ca^{2+}]$ for the Redox Reaction of $[Co(salophen)]^+$ and H_2A 158

4.70 Plot of k_2 Versus $[SO_4^{2-}]$ for the Redox Reaction of $[Co(salophen)]^+$ and H_2A 159

4.71 Plot of k_2 Versus $[CH_3COO^-]$ for the Redox Reaction of $[Co(salophen)]^+$ and H_2A 160

4.72 Plot of k_2 Versus $[Mg^{2+}]$ for the Redox Reaction of $[Co(salophen)]^+$ and $S(R)_2$ 161

4.73 Plot of k_2 Versus $[Ca^{2+}]$ for the Redox Reaction of $[Co(salophen)]^+$ and $S(R)_2$ 162

4.74 Plot of k_2 Versus $[SO_4^{2-}]$ for the Redox Reaction of $[Co(salophen)]^+$ and $S(R)_2$ 163

4.75 Plot of k_2 Versus $[CH_3COO^-]$ for the Redox Reaction of $[Co(salophen)]^+$ and $S(R)_2$ 164

4.76 Plot of $\ln\left(\frac{k_2}{T}\right)$ Versus $\left(\frac{1}{T}\right)$ for the Redox Reaction of $[Co(salophen)]^+$ and LSH 176

4.77 Plot of $\ln\left(\frac{k_2}{T}\right)$ Versus $\left(\frac{1}{T}\right)$ for the Redox Reaction of $[Co(salophen)]^+$ and RSH 177

4.78 Plot of $\ln\left(\frac{k_2}{T}\right)$ Versus $\left(\frac{1}{T}\right)$ for the Redox Reaction of $[Co(salophen)]^+$ and TSH 178

4.79 Plot of $\ln\left(\frac{k_2}{T}\right)$ Versus $\left(\frac{1}{T}\right)$ for the Redox Reaction of $[Co(salophen)]^+$ and TSCZ 179

4.80 Plot of $\ln\left(\frac{k_2}{T}\right)$ Versus $\left(\frac{1}{T}\right)$ for the Reaction of $[Co(salophen)]^+$ and DPCI 180

4.81 Plot of $\ln\left(\frac{k_2}{T}\right)$ Versus $\left(\frac{1}{T}\right)$ for the Redox Reaction of $[Co(salophen)]^+$ and CH_3CHO 181

4.82 Plot of $\ln\left(\frac{k_2}{T}\right)$ Versus $\left(\frac{1}{T}\right)$ for the Reaction of $[Co(salophen)]^+$ and HCHO 182

4.83 Plot of $\ln\left(\frac{k_2}{T}\right)$ Versus $\left(\frac{1}{T}\right)$ for the Reaction of $[Co(salophen)]^+$ and I^- 183

4.84 Plot of $\ln\left(\frac{k_2}{T}\right)$ Versus $\left(\frac{1}{T}\right)$ for the Redox Reaction of $[Co(salophen)]^+$ and H_2A 184

4.85 Plot of $\ln\left(\frac{k_2}{T}\right)$ Versus $\left(\frac{1}{T}\right)$ for the Redox Reaction of $[Co(salophen)]^+$ and $S(R)_2$ 185

4.86 Michaelis-Menten Plot for the Redox Reaction of $[Co(salophen)]^+$ and LSH 186

4.87 Michaelis-Menten Plot for the Redox Reaction of $[Co(salophen)]^+$ and RSH 187

4.88 Michaelis-Menten Plot for the Redox Reaction of $[Co(salophen)]^+$ and TSH 188

4.89 Michaelis-Menten Plot for the Redox Reaction of $[Co(salophen)]^+$ and TSCZ 189

4.90 Michaelis-Menten Plot for the Redox Reaction of $[Co(salophen)]^+$ and DPCI 190

4.91 Michaelis-Menten Plot for the Redox Reaction of $[Co(salophen)]^+$ and CH_3CHO 191

4.92 Michaelis-Menten Plot for the Redox Reaction of $[Co(salophen)]^+$ and HCHO 192

4.93 Michaelis-Menten Plot for the Redox Reaction of $[Co(salophen)]^+$ and I^- 193

4.94 Michaelis-Menten Plot for the Redox Reaction of $[Co(salophen)]^+$ and H_2A 194

4.95 Michaelis-Menten Plot for the Redox Reaction of $[Co(salophen)]^+$ and $S(R)_2$ 195

4.96 Plot for Spectrophotometric Test for the Redox Reaction of $[Co(salophen)]^+$ and LSH 196

4.97 Plot for Spectrophotometric Test for the Redox Reaction of $[Co(salophen)]^+$ and RSH 197

4.98 Plot for Spectrophotometric Test for the Redox Reaction of $[Co(salophen)]^+$ and TSH 198

4.99 Plot for Spectrophotometric Test for the Redox Reaction of $[Co(salophen)]^+$ and TSCZ 199

4.100 Plot for Spectrophotometric Test for the Redox Reaction of $[Co(salophen)]^+$ and DPCI 200

4.101 Plot for Spectrophotometric Test for the Redox Reaction of $[Co(salophen)]^+$ and CH_3CHO 201

4.102 Plot for Spectrophotometric Test for the Redox Reaction of $[Co(salophen)]^+$ and HCHO 202

4.103 Plot for Spectrophotometric Test for the Redox Reaction of $[Co(salophen)]^+$ and I^- 203

4.104 Plot for Spectrophotometric Test for the Redox Reaction of $[Co(salophen)]^+$ and H_2A 204

4.105 Plot for Spectrophotometric Test for the Redox Reaction of $[Co(salophen)]^+$ and $S(R)_2$ 205

LIST OF SCHEMES

3.1	Reaction of 2-hydroxybenzaldehyde(salicyldehyde) and O-phenylene-diamine to give Bis(salicylidene)phenylenediamine	32
3.2	Reaction of Bis(salicylidene)phenylenediamine and Cobalt(II)chloride to give Phenylenebis(salicylideneiminato)cobalt(III) Complex	33

LIST OF APPENDICES

I. FT-IR Spectrum of the Salophen Ligand 247

II. FT-IR Spectrum of the Co(III)salophen Complex 248

III. UV-Visible Spectrum for DMSO-H_2O Solution of $[Co(salophen)]^+$ Complex at 4.0×10^{-4} mol dm^{-3} 249

IV. UV-Visible Spectrum of Product of LSH Oxidation by $[Co(salophen)]^+$ and Hydrogen Peroxide 250

V. UV-Visible Spectrum of Product of RSH Oxidation by $[Co(salophen)]^+$ and Hydrogen Peroxide 251

VI. UV-Visible Spectrum of Product of TSH Oxidation by $[Co(salophen)]^+$ and Hydrogen Peroxide 252

VII. UV-Visible Spectrum of Product of TSCZ Oxidation by $[Co(salophen)]^+$ and Hydrogen Peroxide 253

VIII. UV-Visible Spectrum of Diphenylcarbazide (DPCI) in DMSO - H_2O Solvent 254

IX. UV-Visible Spectrum of Product of DPCI Oxidation by $[Co(salophen)]^+$ in DMSO – H_2O Solvent 255

X. FT-IR Spectral of Diphenylcarbazide 256

XI. FT-IR Spectral of the Product of Reaction of $[Co(salophen)]^+$/DPCI 257

ABBREVIATIONS

Abbreviation	Definition
Abs	Absorbance
A_t	Absorbance at time ‘t”
A_∞	Absorbance at infinity
AR	Analar reagent
Aq	Aqueous
BM	Bohr magneton
BDH	British drug house
C	Coulomb
Conc.	Concentrated
$[Co(salophen)]^+$	N,N¹-phenylenebis(salicylideneiminato)cobalt(III) complex ion
D	Dielectric constant
DPCI	1,5-diphenylcarbazide
DPCO	1,5-diphenylcarbazone
DMSO	Dimethylsulphoxide
E_a	Activation energy
FT-IR	Fourier transformed infrared
^1H NMR	Proton nuclear magnetic resonance
h	Planck’s constant
K	Equilibrium constant
k_B	Boltzmann’s constant
k_1	First order rate constant

k_2	Second order rate constant
LSH	L-cysteine
R	Molar gas constant
RS^-	Thiolate
RSH	Thioglycol
$RS^{\cdot}$	Thyl radical
Redox	Reduction – oxidation
salophen	bis(salicylidene)-1,2-phenylenediamine
$S(R)_2$	Thiodiglycol
T	Absolute Temperature
TSH	Thioglycolic acid
TSCZ	Thiosemicarbazide
UV	Ultraviolet visible
Δ_{oct}	Crystal field splitting energy
$\Delta S^{\ddagger}$	Entropy of activation
$\Delta H^{\ddagger}$	Enthalpy of activation
$\Delta G^{\ddagger}$	Gibb's free energy of activation
μ	Ionic strength
λ_{max}	Wavelength of maximum absorption

CHAPTER ONE

1.0 INTRODUCTION

Redox reactions in which oxidation and reduction process occur simultaneously between chemical entities, are numerous, and have been attracting extra-ordinary attention throughout the globe. They have been widely acclaimed to be very important as they play pivotal role in a number of natural processes. Oxidation is a chemical change in which any of the processes like loss of electron, addition of oxygen, loss of hydrogen or increase in the oxidation number take place where as reduction is a process that follows the reverse conditions of oxidation. In redox reactions, the transfer of one or more electrons between the interacting species usually brings change in oxidation number of both oxidant and the reductant (Asperger, 2003; Santosh, 2006).

Cobalt is an essential trace element required for human development and can occur in organic and inorganic forms. The organic form is a necessary component of vitamin B_{12} and plays a very important role in forming amino acids and some proteins in nerve cells, and in creating neurotransmitters that are indispensable for normal functioning of the organism. It is present in small quantities in compounds with sulphur and arsenic. This element is used in numerous industrial applications like welding, diamond tooling, grinding, chemical catalyses, and nuclear power plants (Roesems *et al.,* 2000; Ortega *et al.,* 2009). In nuclear plants, it can occur in two radioactive forms of cobalt, ^{58}Co and ^{60}Co, which are formed from corrosion-erosion of alloys containing cobalt and other metals. These two forms produce high-energy γ photons, which can be used in radiotherapy to fight tumours (Bresson *et al*., 2008; Gault *et al*., 2010).

There has been increased interest in the chemistry of transition metal complexes containing N_2O_2 coordination sites, such as salicylidenes, due to their broad range of applications

in areas such as catalysis, functional materials, non-linear optics, molecular magnetism, and organic electronics (Gaur *et al*., 2012, Kianfar and Khavasi, 2016). Salicylidenes are a type of schiff base derived from the condensation of a primary amine with a salicylaldehyde derivative. Numerous substituents can be placed on the phenol ring, and the imine bridge allows for tuning the size and the shape of the complexes to control their self-assembly on surfaces. Their easiness along with the synthesis and modulation of the physicochemical properties of salicylidenes make them a versatile and interesting class of molecules. Their molecular structure and coordination sites make salicylidenes a flexible coordination compounds with several metal ions (Rodrigo *et al.,* 2018). A variety of metal ions (diamagnetic and paramagnetic) can be introduced in the coordination site, in most cases forming square planar or octahedral array frameworks (Di-Bella *et al.*, 2012; Staykov *et al*., 2014).

Among the salophen-type complexes are cobalt(III) salophens with applications in catalysis and biological processes (Yu-Ling *et al*., 2003; Mohammad *et al*., 2019). Interestingly, in spite of the numerous kinetic data on various metal complexes, such as superoxobinuclear cobalt(III) (Osunlaja *et al.,* 2013), tetrakis(2,2¹-bipyridine)-µ-oxodiiron(III) (Anweting, 2016), aminocarboxylatocobalt(III) (Abiti *et al.,* 2018), aminocarboxylatoiron(III) (Nkole *et al.,* 2018a), iron(III) dimer ([(Fe(saloph))2-µ-dicarpy]) (Ukoha *et al*., 2018), tris(1,10-phenanthroline)-cobalt(III) (Osunkwo *et al.,* 2018) and 2-(hydroxyethyl)ethylenediaminetriacetatoiron(III) (Nkole *et al.,* 2021), the kinetic studies of their reactions have proven inexhaustible. This can only be attributed to the great potency of synthesising numerous metal complexes from different starting materials at different experimental conditions, and also the wide range of other available reducing and oxidising agents (Davies, 1992; Hamzeh, 2001).

1.2 Statement of Research Problem

Schiff base complexes of cobalt(III) are utilised as impetuses for the oxygenation reactions of organic molecules (Niederhoffer *et al.,* 1984), eminently in the preparative oxygenation of phenols (Matsuura, 1977), indols (Nishinaga *et al.,* 1993) and amines (Nishinaga *et al.,* 1988); a reversible process similar to Co(III)/Co(II) redox potential (Hirotsu *et al.,* 1996). Cobalt(III) complexes have been discovered to have applications in oxidative coupling catalytic reactions of phenols and oxidation of olefins (Zhang *et al.,* 2017). The catalytic activity of Co(III) salen (b*is*(salicylidene)ethylenediamine) complexes demonstrates the catalytically active species to be cobalt in +3 oxidation state (Eichhorn and Speiser, 1994; Speiser and Stahl, 1995; Eichhorn *et al.,* 1997).

On the other hand, these complexes have been utilised extensively to imitate cobalamin (B_{12}) coenzymes (Polson *et al.,* 1997; Aly, 1998; Cini *et al.,* 1998; Amirnasr *et al.,* 2001), classified as an oxygen carrier (Niederhoffer *et al.,* 1984) and oxygen activators (Bianchini and Zoellner, 1996; Henson *et al.,* 1999; Yamada, 1999). Metal complexes of salophen (*bis*(salicylidene)phenylenediamine) and salen-type ligands also find applications in the intercalation of DNA base pairs (Kocak *et al.,* 2016; Yilmaz *et al.,* 2017) and for potentiometric discoveries of basic anions existing in biological and environmental systems (Kleij *et al.,* 2006). Co(III) salophen complexes have been additionally utilised as nitrite sensors (Ganjali *et al.,* 2004) and antimicrobial agents (Böttcher *et al.,* 1997).

Furthermore, Co(III)salen complexes have shown an outstanding selectivity to poly(propylenecarbonate) development with 99% of carbonate linkages (Lu and Wang, 2004;

Luinstra *et al.*, 2005; Cohen and Coates, 2006; Hošt'álek *et al.*, 2015). Recently, Solomon *et al.* (2018) studied the effective electrochemical behaviour and reduction properties of Co(III)salen complexes in the presence of CO_2 and reported the complexes existing as multi-electron reducing agents.

Despite the wide applicability of this complex, there is need to dwell more on the field of its kinetics and mechanistic pathway. This has led to significant efforts being made to probe mechanistic pathway of its reactions with a view to have a better understanding of its redox reactions.

1.3 Justification

Salophen complexes have received less attention since their application potential in catalysis (homogeneous) has been considered limited. They have been neglected for a long time despite the fact that they have greater advantages over their salen analogues. They represent π-conjugated ligand systems with tunable photophysical properties than the corresponding salen ligands. For these reasons, such salophen systems have excellent potential as building blocks in material science amongst other applications (Wezenberg and Kleij, 2008).

Also, the rigid geometry around the metal center that is dictated by the salophen ligand can be used to manipulate properties such as the Lewis acid character of the metal and therefore can be effectively used to increase the reactivity of the resulting complex (Kianfar and Khavasi, 2016).

The kinetic data on electron transfer reaction of cobalt(III) complex, *N,N′*-phenylenebis(salicylideneiminato)cobalt(III), ($[Co(salophen)]^+$), is very scarce, thus the need to carry out investigations on the redox reaction between the complex and the reductants of interest.

Moreover, the interaction of metal ions with bioactive molecules in physiological systems is very complex and interesting. The mechanisms of their reactions are complex and are relatively unknown. Hence, the need to embark on the kinetic investigations of its reactions with some biologically important molecules like ascorbic acid, thioglycol, thioglycolic acid, formaldehyde, acetaldehyde, L-cysteine, iodide, thiosemicarbazide, thiodiglycol, and 1,5-diphenylcarbazide.

1.4 Aim and Objectives

The aim of the research is to investigate the kinetics of the reactions of *N,N′*-phenylenebis(salicylideneiminato)cobalt(III) ion, ($[Co(salophen)]^+$) with thiols, aldehydes, carbazides, ascorbic acid and iodide ion in DMSO-H_2O medium.

The specific objectives are to:

i. synthesise and characterise the $[Co(salophen)]^+$ complex through schiff base platform;

ii. determine the stoichiometry, the order of the reaction and analyse the product of the reactions;

iii. study the effect of change in hydrogen ion concentration, ionic strength, dielectric constant and added ions on the rate of the reactions;

iv. carry out temperature dependence study and determine the thermodynamic parameters of the reactions, and

v. propose plausible mechanism for the reactions.

CHAPTER TWO

2.0 LITERATURE REVIEW

2.1 Chemistry of Cobalt(III) Complexes

Complexes of cobalt(III) are exceedingly numerous and have been studied extensively for long because Co(III) is substitution inert. Most of the knowledge of kinetics have been obtained from the studies of Co(III) complexes, also, the knowledge of isomerism, mode of reactions and general properties of octahedral complexes is based on the studies of Co(III) complexes. Co(III) is known to be a powerful oxidising agent in aqueous solution, as it commonly oxidises both organic molecules and metal ion complexes. Co(III) forms complexes with both monodentate and bidentate ammine ligands (Osunkwo *et al*., 2018).

In addition, cobalt(III) complexes undergo reactions relating mainly to an electron transfer reducing the Co(III) to Co(II) ion. The rate of reduction of the complexes depends significantly on the identity of the reductant and size and nature of the ligands (Tobe and Burgess, 1999; Abu-Surrah *et al.,* 2008). Majority of reactions involving these complexes have been reported to be slow which is ascribed to the high stability constant linked with Co^{3+} ions due to high magnitude of Δ_{oct} (Oyetunji *et al.,* 2006). In spite of this property that appears hostile for redox reactions, numerous researches have been carried out on their reduction by organic and inorganic reductants (McAuley and Gomwalk, 1969; Macartney and McAuley, 1982; Oyetunji *et al.,* 2006; Asemave *et al.,* 2012; Senapati, 2014; Onu *et al.,* 2016). Similarly, cobalt(III)

complexes are known to dissolve in strongly coordinating solvent such as dimethylsulphoxide, exhibiting ^{1}H-NMR signals within a diamagnetic region, which is consistent with a low-spin, diamagnetic cobalt(III) with d^6 electron configuration (Kurahashi and Fujii, 2013).

Furthermore, cobalt(III) complexes are more consistent with the outer-sphere mechanism of electron transfer following the documented fact that they usually form stable complexes, hence are substitution inert. Hence kinetically, the rate of redox reaction of cobalt(III) complexes is usually faster than the rate of ligand substitution which is consistent with the outer-sphere mechanism (Jagannadham, 2012).

The kinetics of the reduction of tris(1,10-phenanthroline)cobalt(III) complex by N-methylthiourea was studied in aqueous acidic medium. Stoichiometric result revealed 1:1 mole ratio and existence of first order with respect to the concentrations of the redox species. Results based on spectroscopic investigation, thermodynamic information from temperature dependence studies and kinetic evidences from Michaelis–Menten's plot and interaction with added ions suggested an outer–sphere mechanism for the reaction (Osunkwo *et al.,* 2018).

Mohanty *et al.* (2014) carried out the kinetic study of the oxidation of glutathione by cis-(diaqua)-bis-(ethylenediamine)cobalt(III) ion where an outer-sphere mechanistic pathway was rationalised based on the kinetic and spectroscopic results. Also, kinetics of redox reaction of oxygenated $[Co_2(O_2)(NH_3)_{10}]^{5+}$ complex by thiourea in aqueous perchloric acid medium was investigated (Osunlaja *et al.,* 2013). The stoichiometry established for the reaction conforms to the overall (equation 2.1).

$$(NH_3)_5Co(O_2)Co(NH_3)_5^{5+} + (NH_2)_2C{=}S + 5H_2O \rightarrow 2Co^{2+} + (NH_2)_2C{=}O + 2H^{+} + 10NH_3 + SO_4^{2-} \qquad (2.1)$$

Based on the absence of both kinetic and spectroscopic evidence of complex formation, an outer-sphere mechanism was proposed.

2.2 Reactions of L-cysteine

L-cysteine (hereafter referred to as LSH) is also known as 2-amino-3-mercaptopropanoic acid, it is one of the ten most essential amino acids.

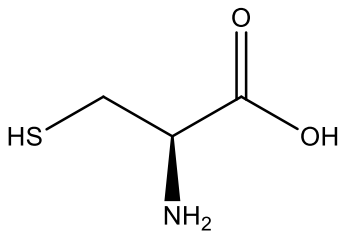


Figure 2.1: Structure of L-cysteine

It plays structural roles in proteins and can likewise partake in electron transfer reactions with its sulphydryl group, thiolate (RS^-) stabilised in a particular environment. However, the sulphydryl group of free L-cysteine is somewhat inert for redox reaction in physiological conditions. Thiolate is a relatively more potent nucleophilic agent than its protonated structure. As such, reactive L-cysteine exists in its anionic structure mostly in proteins. In addition, L-cysteine is significant for numerous protein functions; the molecule is toxic to cells in both prokaryotes and eukaryotes even at low concentrations (Özkan *et al.*, 2002; El-Hag and Dahab, 2016).

Thiol-containing compounds play important role in some biological phenomena because they are easily susceptible to oxidation (Iyun *et al.*, 1996) and numerous kinetic investigations have been carried out on their redox reactions with a view to understanding the roles of enzymes containing L-cysteine group in electron transfer reactions (Ayoko and Olatunji, 1983; Read *et*

al., 2000; Adari *et al.,* 2006; Sami *et al.,* 2009; Chakraborty *et al.,* 2012; Chakraborty *et al.,* 2013).

The stoichiometry and kinetics of the reaction of 12-tungstocobaltate(III) with L-cysteine, was investigated in aqueous perchloric acid solution over a concentration range of 0.02 to 0.1 C^2 mol dm^{-3} and at an ionic strength of 1.0 C^2 mol dm^{-3} ($NaClO_4$). One mole each of the thiols is required to reduce 12-tungstocobaltate(III) to 12-tungstocobaltate(II) ions, with formation of disulphides as one of the products. No evidence was found for the formation of an intermediate complex of significant stability that occur prior to electron transfer step. The reaction was interpreted in terms of an outer-sphere mechanism (Ayoko and Olatunji, 1983).

Chakraborty *et al.* (2012) studied the mechanistic studies on the oxidation of a series of thiols, viz. 2-mercaptoethanol (RSH), thioglycolic acid (TSH) and L-cysteine (LSH), a paradigm for aliphatic thiols, by a tetranuclear Mn oxidant, $[Mn_4(\mu\text{-}O)_6(bipy)_6]^{4+}$ (bipy = 2,2-bipyridine), in weakly acidic aqueous media (pH 2.0 – 4.0) in the presence of added bipy. The thiols were quantitatively oxidised to their respective disulphides and the Mn^{IV} species was reduced to Mn^{II}. The stoichiometric equation is shown in equation 2.2, where GSH represents the thiols.

$$[Mn_4O_6(bipy)_6]^{4+} + 8GSH + 4H^+ \rightarrow 4Mn^{2+} + 6bipy + 4GSSG + 6H_2O \qquad (2.2)$$

Kinetic studies on the oxidation of L-cysteine and 2-mercaptoethanol by a trinuclear Mn(IV) species in aqueous acidic media were studied by Chakraborty *et al.* (2013). The trinuclear Mn^{IV} complex, $[Mn^{IV}{}_3(\mu\text{-}O)_4(phen)_4(H_2O)_2]^{4+}$ (phen = 1,10-phenanthroline) behaves like a monobasic acid, equilibrates with its deprotonated conjugate base, pKa = 4.00 ± 0.15 at 25.0 ºC, μ = 1.0 mol dm^{-3}, maintained with $NaNO_3$. An aqueous solution of $[Mn^{IV}{}_3(\mu\text{-}O)_4(phen)_4(H_2O)_2]^{4+}$ in the pH range 2.2 – 4.0 smoothly oxidises 2-mercaptoethanol (RSH) and L-cysteine (LSH) to their respective disulfides; itself being reduced to $[Mn(phen)_3]^{2+}$ in presence

of excess 1,10-phenanthroline which also masks Cu^{2+}, if any, present in the reaction media as impurity as well as acting as a buffer that controls pH range during the reaction.

Reduction of heteropoly-11-tungstophosphovanadate(V), ($[PV^{V}W_{11}O_{40}]^{4-}$) by L-cysteine and thioglycolic acid were measured spectrophotometrically in aqueous acid medium. The $[PV^{V}W_{11}O_{40}]^{4-}$ oxidises cysteine to cystine and thioglycolic acid to dithioglycolic acid and gets reduced to heteropoly blue, $[PV^{IV}W_{11}O_{40}]^{5-}$. The order of the reaction with respect to oxidant is one, whereas the reaction shows second order dependence on the substrates (Sami *et al.*, 2009). Based on the experimental results, observed 1:1 stoichiometry, product identification as disulphide and absent of intermediate complex formation, outer-sphere mechanism was proposed.

The kinetics of the reaction of L-cysteine with potassium ferrate was investigated under pseudo and non-pseudo-first order conditions (Read *et al.*, 2000). Under pseudo first order conditions, L-cysteine was oxidised within 300 s to form sulfenic acid with subsequent formation of a ferric–cysteine complex in excess cysteine. The rate law involved two pathways, one being first order in the hydrogen ion, the cysteine and the ferrate ion concentrations above a pH of 8.2, and independent of the hydrogen ion concentration below this pH, and the other being first order in only cysteine and the ferrate ion concentrations. The proposed mechanism (equations 2.3 – 2.6) involves the equilibrium between the protonated and deprotonated ferrate ions, followed by the rate-determining steps of reaction between both the protonated and deprotonated forms and L-cysteine.

$$HFeO_4^- \underset{}{\overset{K}{\rightleftharpoons}} H^+ + FeO_4^{2-} \qquad (2.3)$$

$$HFeO_4^- + CE \xrightarrow{k_H} Fe(IV) + CE(O) \qquad (2.4)$$

$$FeO_4^{2-} + CE \xrightarrow{k_D} Fe(IV) + CE(O) \quad (2.5)$$

$$Fe(IV) + CE(O) \longrightarrow Fe(II) + CE(O)_2 \quad (2.6)$$

where $CE(O)_2$ is the sulphinic acid, and Fe(IV) represents an unstable active complex ion which is rapidly reduced to Fe(II). The result is consistent with the one obtained for other metal ions and thiol reductant (Nkole *et al.,* 2018a).

The kinetics of oxidation of L-cysteine by pyridinium chlorochromate (PCC) was studied at 0.1 - 0.3 mol dm^{-3} $HClO_4$ in the range 25 – 40 ºC (Adari *et al.,* 2006). The reaction exhibited first order dependence with respect to [PCC] and fractional order in [cysteine]. The increase in the oxidation rate with acidity suggests the involvement of a protonated chromium(VI) species at the rate determining step. Cysteic acid was identified as the product of the oxidation with the following stoichiometric equation 2.7.

$$HSCH_2CH(\overset{+}{N}H_3)COOH + 2Cr(VI)(PCC) \xrightarrow{H_2O} HO_3SCH_2CH(NH_3)COOH + 2Cr(III) \quad (2.7)$$

2.3 Reactions of Thioglycol



Figure 2.2: Structure of thioglycol

Thiols are the sulphur analogue of alcohols (that is, sulfur takes the place of oxygen in the hydroxyl group of an alcohol), and the word is a blend of "thio-" with "alcohol. The S−H bond in thiols is weak compared to the O−H bond in alcohols. They show little association by hydrogen bonding, both with water molecules and among themselves. Hence, they have lower boiling points and are less soluble in water and other polar solvents than alcohols of

similar molecular weight. They have strong odors resembling that of garlic. The odors of thiols, particularly those of low molecular weight, are often strong and repulsive (Roy, 2005).

Aliphatic thiols like thioglycol (2-mercaptoethanol) are of biological importance. The thiol/disulphide couple acts as a buffer in modulating activity of biological sites (Aitken, *et al.*, 2008). The change in the redox potential of the thiol/disulphide couple can usher change in protein conformation, enzymatic activity and transport activity (Nkole *et al.,* 2018a).

Thioglycol undergoes redox processes due to its ability to lose one electron and deprotonate in basic media. Its applicability in averting oxidation of protein, ribonucleases denature and protein reduction is insightful (Nelson *et al.,* 2005; Yeh, 2009; Nkole *et al.,* 2018a).

Shanmugaprabha *et al.* (2016) studied the kinetics of oxidation of 2-mercaptoethanol (RSH) by the heteropoly 11-tungsto-1-vanadophosphate anion, $[PV^{V}W_{11}O_{40}]^{4-}$, spectrophotometrically in aqueous perchloric acid at 25 ºC. Electron paramagnetic resonance (EPR) and optical studies showed that $[PV^{V}W_{11}O_{40}]^{4-}$ was reduced to the one-electron heteropoly blue, $[PV^{IV}W_{11}O_{40}]^{5-}$, whilst the thiols were oxidised to the corresponding disulphides, RSSR. Spectrophotometric titrations showed that the stoichiometry of both reactions was 1:1 as shown in equation 2.8.

$$2[PV^{V}W_{11}O_{40}]^{4-} + 2RSH \rightarrow 2[PV^{IV}W_{11}O_{40}]^{5-} + RSSR + 2H^{+} \qquad (2.8)$$

At constant pH, the reactions showed simple second order kinetics with first order dependence of rate on both [oxidant] and [thiol]. At constant [thiol], the rate of the reaction increased with increasing pH. Plots of $k_{obs}/[thiol]_t$ versus $1/[H^+]$ were linear with finite intercepts, showing that both the undissociated thiol (RSH) and thiolate ion (RS^-) are reactive species.

The kinetics of reduction of N-(2-hydroxyethyl)ethylenediaminetriacetatoiron(III) complex (hereafter [Fe(III)HEDTAOH_2]) by thioglycol was studied spectrophotometrically in a

bicarbonate buffer medium. The study was carried out under pseudo-first order conditions of an excess of thioglycol concentration at 28 ± 1℃, μ = 0.44 C^2 mol dm^{-3} (KNO_3) and λ_{max} = 490 nm. The reaction was first order in [Fe(III)HEDTAOH_2] and half order in [RSH] and a stoichiometric mole ratio of [Fe(III)HEDTAOH_2]: RSH is 2:1. Reaction rates increased with increase in ionic strength (μ) and dielectric constant (D) of the reaction medium of the reaction. The reaction displayed positive primary salt effect and test for possibility of an intermediate complex formation was negative. Based on the findings, outer-sphere mechanism was proposed for the reaction (Nkole *et al.,* 2018a).

2.4 Reactions of Thioglycolic Acid

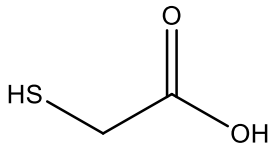


Figure 2.3: Structure of thioglycolic acid

Thioglycolic acid (TSH) also known as mercaptoacetic acid, is an organic compound with molecular formula $HSCH_2COOH$, containing both a thiol (SH) and carboxylic acid functional group (COOH). It is used for chemical depilation in leather processing, as an acid indicator and as precursor for the manufacturing of thioglycolates. The studies of thiols are of enormous importance especially in biochemistry. They are an active ingredient found in body cells and can change to disulphide on oxidation from thiols (Idris, 2005; Nkole *et al.,* 2018b). Thiols oxidation to disulphides have been reported to occur either via the transfer of electron by the realisation of stable intermediate complex or by a simple transfer of electron without any complex formation (Ayoko and Olatunji, 1983; Nkole *et al.,* 2018b).

The kinetics of interaction between di-μ-hydroxobis(1,10-phenanthroline)dipalladium(II) perchlorate and thioglycolic acid was studied spectrophotometrically in aqueous medium as a

function of the complex concentration as well as the ligand concentrations, pH, and temperature at constant ionic strength. The observed pseudo-first order rate constants, k_1 (s^{-1}) obeyed the first order equation. At pH = 6.5, the interaction with thioglycolic acid showed two distinct consecutive steps and both steps were dependent on the concentration of thioglycolic acid. The association equilibrium constant for the outer-sphere complex formation has been evaluated together with the rate constants for the two subsequent steps. On the basis of the kinetic observations and evaluated activation parameters, plausible associative mechanism was proposed for the interaction process (Ghosh *et al.*, 2013).

Saha *et al.* (2002) reported that in aqueous media at 25 °C, $[Mo(CN)_8]^{3-}$ was reduced by thioglycolic acid ($HSCH_2COOH$), and the reaction was strongly accelerated by the presence of trace amounts of copper ions. Dipicolinic acid (dipic) is an effective inhibitor of the copper catalysis. Both with and without dipic, the reaction has the stoichiometry of 1:1 with disulphide derived from formal oxidative dimerisation of TSH. The reaction was first order with respect to both [reactants].

The kinetic approach of the reduction of ethylenediaminetetraacetatoferrate(III) complex (hereafter $[Fe(III)EDTA]^-$) by thioglycolic acid in bicarbonate buffer medium was studied at 470 nm (λ_{max}), T = 28 ± 1ºC, ionic strength (μ = 0.2 C^2 mol dm^{-3}), and pH = 7.5. The stoichiometric study revealed 1:1 and the reaction rate was found to varied linearly to the first power of the concentrations of the oxidant and reductant and displayed dependence on pH of the reaction medium. The reaction was sensitive to the change in ionic strength of the medium suggesting an interaction of charged species at the activated complex. The Michaelis-Menten's plot of $1/k_1$ versus 1/[TSH] was linear with zero intercept which suggested absence of intermediate complex

formation. The reaction was rationalised in terms of outer-sphere mechanism (Nkole and Osunkwo, 2019).

2.5 Reactions of Thiosemicarbazide

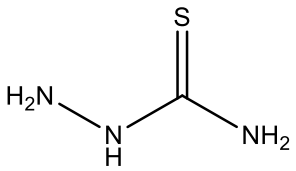


Figure 2.4: Sturcture of thiosemicarbazide

Thiosemicarbazide (hereafter referred to as TSCZ) and its derivatives are class of compounds that are useful in the treatment of various ailments such as influenza, smallpox, protozoa, and tumors. Closely related thiosemicarbazides gave convulsant and anticonvulsant effects, and it is difficult to determine which effect will dominate. They have also been shown to have pesticidal and fungicidal effects (Pandeya *et al.*, 2012). The compounds have been used as chelating agents in the analysis of metals and also in the qualitative analysis of aldehydes, ketones, and polysaccharides (Bitziou *et al.,* 2013). The major products of oxidation of thiosemicarbazide are carbon dioxide, nitrogen gas and sulphate ion except in case of ferricyanide where disulphide was reported (Llewellyn, 2014). The mechanism of oxidation by a metal ion generally involves formation of a coordination complex which further decomposes in a rate determining step to give the final product (Sherigara *et al.,* 1994). The coordination

chemistry of thiosemicarbazide has also received considerable attention as some of the coordination complexes are found to have biological activity (López-Torres and Dilworth, 2009).

Previous mechanistic studies on the oxidation of thiosemicarbazides by bromate was carried out in mixed solvents and in the presence of excess thiosemicarbazide. Under these conditions, the reactions exhibited fractional orders in thiosemicarbazide (Gowda *et al.,* 1988). The final products also depend on the oxidant: reductant mole ratio. In all cases, the final sulphur-containing species was found to be sulphate. Unsubstituted thiosemicarbazide reacted with bromate in a 3:4 ratio to produce cyanogen and hydrazine as the final nitrogen containing species (Jonnalagadda *et al.,* 2002).

Kinetics of oxidation of thiosemicarbazide by Waugh-type polyoxometalate, 9-molybdomanganate(IV), was investigated under pseudo-first order condition in aqueous perchloric acid. The stoichiometry was found to be 1 mole of $[Mn^{IV}Mo_9O_{32}]^{6-}$ per two moles of thiosemicarbazide indicating thioperoxy dicarbonimidic dihydrazide as the product. The rate of reaction increased with increase in hydrogen ion, 9-molybdomanganate(IV) and thiosemicarbazide concentrations. The protonated forms of both the oxidant and thiosemicarbazide were active species. The thiosemicarbazide in its protonated form is converted into a tautomeric form, with a negative charge on the sulfur atom which interact with the active form of the oxidant, thereby forming a precursor complex. The precursor complex formed decomposes with the formation of sulfenic acid as an intermediate. The results of effects of ionic strength, solvent polarity and the temperature also supported the proposed mechanism (More *et al.,* 2018).

Kinetics of oxidation of thiosemicarbazide (TSC) in the pure state and in its zinc metal complex by chloramine T (CAT) and bromamine T (BAT) in aqueous perchloric acid medium

and by dichloramine T (DCT) in 1:1 (v/v) water-methanol medium were studied. The rate followed first order kinetics in [oxidant] and fractional order in [TSC] in both the pure state and in the metal complex with all the oxidants. With chloramine T, the rate had an inverse first-order and inverse fractional order dependence in $[H^+]$. The rate had inverse fractional and inverse first order dependence in $[H^+]$ with BAT and DCT respectively. Addition of the reduced product of the oxidants (toluene-p-sulphonamide) had no significant effect on the rate with all the oxidants. But the increase in ionic strength of the medium decreased the rate, and decrease of dielectric constant of the reaction medium by adding methanol increased the rate indicating positive ion-dipole interactions in the rate-limiting steps (Gowda *et al.,* 1988).

Kinetics of the interaction of thiosemicarbazide with cis-$[Ru(bipy)_2(H_2O)_2]^{2+}$ (bipy = bipyridyl) was studied spectrophotometrically as a function of $[Ru(bipy)_2(H_2O)_2^{2+}]$, [bipyridyl] and temperature, at a particular pH (4.8), where the substrate complex exists predominantly as the diaqua species and thiosemicarbazide as the neutral ligand. The reaction proceeded via an outer-sphere association complex formation, followed by two slow consecutive steps. The first was the conversion of the aforementioned complex into the inner-sphere complex, and the second step involved the entrance of another thiosemicarbazide molecule in the coordination zone of Ru(II) whereby, in each step, an aqua ligand was replaced. The association equilibrium constant for the outer-sphere complex formation was evaluated together with rate constants for the two subsequent steps (Goswami and De, 2005).

Kinetics of oxidation of the zinc metal complex of thiosemicarbazide (TSC) and hydrazones by N-chlorobenzamide (NCB) were investigated in water-methanol (1: 1, v/v) medium in the presence of perchloric acid. The hydrazones studied were benzaldehyde, propionaldehyde, acetone and acetophenone thiosemicarbazones. The reactions showed first

order kinetics in [NCB], a fractional order dependence in [substrate] and an inverse fractional to inverse first order in [H^+]. Addition of benzamide had no significant effect on the rates of oxidations. Variation in the ionic strength of the medium had little effect on the rates of reactions, but a decrease in the dielectric constant of the medium by increasing the methanol concentration in the solvent increased the rates. The rate limiting steps were identified in all cases and the rate coefficients of these steps and the related activation parameters were also evaluated (Nayak and Gowda, 1992).

2.6 Reactions of 1,5-diphenylcarbazide

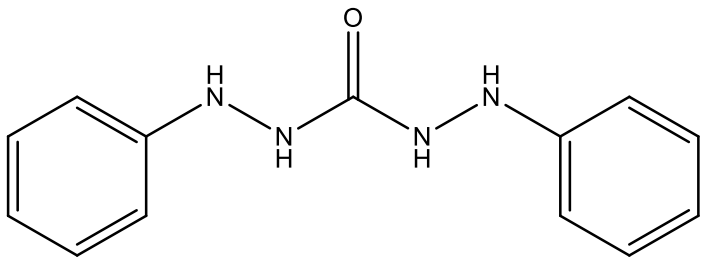


Figure 2.5: Structure of 1,5-diphenylcarbazide

Carbazides are functional group with the general formula RNH-NH(C=O)NH-NHR. They can be derived from the condensation of carbonic acid with a hydrazine forming carbohydrazide which is the simplest carbazide, with another common carbazide being diphenylcarbazide, that is used as an analytical reagent (Ashoor *et al.,* 2013).

Diphenylcarbazide (hereafter referred to as DPCI) is one of the group of chemicals derived from hydrazine, used for determination of various metals in acid media. It reacts with osmium to form a blue violet complex, which shows an absorption maximum at 560 nm. Three different methods have been reported for determination of osmium in a weakly acid solution by using DPCI to form complex with ratio 1:1 (Os: DPCI) (Moustafa *et al.,* 2016).

In order to find out about the chemical behaviour of the diphenylcarbazide (DPCI) in water, kinetic and thermodynamic studies were carried out using UV-Vis spectrophotometry within the 0 - 12 pH range. The kinetic parameters and acidity constant were then determined, and the results showed a pseudo-first order reaction rate during hydroxilation, while the reaction rate was also observed to increase with the pH (Ramírez *et al.*, 1996) .

Ashoor *et al.* (2013) carried out kinetic studies of oxidation of the cobalt(II) complex, [Co^{II}ArNNCONNAr] by N-chloro-p-toluenesulphonamide (chloramine-T) to cobalt(III) at 25 ºC. The reaction was consecutive first order with respect to both [cobalt(II) complex] and [chloramine-T]. The order of the reaction in [H^+] was fractional and the rate constant was unaffected by the ionic strength. Rate law of the suggested mechanism including all factors affecting the rate of reaction was derived.

2.7 Reactions of Acetaldehyde

Acetaldehydes are compounds containing carbonyl functional (C=O) with the carbon atom bonded to hydrogen and to any generic alkyl or side chain R group. The functional group itself (without the "R" side chain) is known as an aldehyde or formyl group. They are generally created by removing a hydrogen from an alcohol and the most well-known is formaldehyde. As they are frequently strongly scented, many fragrances are or contain aldehydes (Kohlpaintner *et al*., 2008; Chen *et al*., 2014).

Acetaldehyde is an organic compound with the formula CH_3CHO. It is one of the most important aldehydes, occurring widely in nature and being produced on a large scale in industry. It occurs naturally in coffee, bread, and ripe fruit, and is produced by plants. It is also produced by the partial oxidation of ethanol by the liver enzyme alcohol dehydrogenase and is a contributing cause of hangover after alcohol consumption (Uebelacker and Lachenmeier, 2011).

Kinetics of the oxidation of acetaldehyde by acid permanganate was studied. The reaction was of first order with respect to the aldehyde, the oxidant and hydrogen ion concentrations individually. The oxidation does not induce polymerisation of acrylonitrile and the activation parameters for the oxidation and enolisation reactions were evaluated. The rate of enolisation, under similar conditions, was less than that of oxidation. A mechanism involving the transfer of a hydride ion from the aldehyde hydrate to the oxidant was suggested (Banerji, 1972).

Kinetics of oxidation of aliphatic aldehyde, to the corresponding carboxylic acid, by bis(2,2'-bipyridyl)copper(II) permanganate (BBCP) was studied. The reaction was first order with respect to [BBCP]. The formation constants for the aldehyde-BBCP complexes and the rates of their decomposition, at different temperatures, were evaluated. Thermodynamic parameters for the complex formation and the activation parameters for their decomposition have also been determined. The reaction was catalysed by hydrogen ions. The role of aldehyde hydrate in the oxidation process was discussed. A mechanism involving formation of permanganate ester and its slow decomposition was proposed to be outer-sphere (Kothari *et al.*, 1992).

2.8 Reactions of Formaldehyde

Formaldehyde (CH_2O) is a key combustion intermediate in hydrocarbon combustion. Its oxidation leads to the formation of CO_2 with the release of a large amount of chemical energy. CH_2O and phenyl radicals coexist in the combustion of benzene; they may coexist in the initial stage of soot formation.

Kinetics for the phenyl radical and CH_2O reaction was investigated by the cavity ringdown spectrometric (CRDS) and pulsed laser photolysis/mass spectrometric (PLP/MS) methods at temperatures between 298 and 1083 K. With the CRDS method, the rate constant was

measured by monitoring the decay times of injected probing photons in the absence (tc^0) and presence (tc) of the phenyl radical. In the PLP/MS experiment at higher temperatures, the rate constant was determined by kinetic modeling of the absolute yields of C_6H_6. The values of the rate constants obtained by the two different methods agree closely (Choi *et al.,* 2000).

The stoichiometry of the reaction of plasma albumin and formaldehyde was determined by spectrophotometric method. Measurements were made at pseudo–first order condition of formaldehyde using the method of continuous variation (Job's method) and the mole ratio method at varying concentrations of formaldehyde and plasma albumin at their respective determined λ_{max} and at constant conditions. The ionic strength of the reactants, was kept constant at 0.5 C^2 mol

dm^{-3} (NaCl), and at constant temperature of 37 ºC. The results showed a stoichiometric ratio of 1:2 of plasma albumin to that of formaldehyde in aqueous medium (Ugye *et al.,* 2013).

2.9 Reactions of Iodide Ion

Iodide ion (I^-) is the most commonly encountered ion as a component of iodised salt. It is one of the largest monatomic anions and is assigned a radius of around 206 picometers. For comparison, the lighter halides are considerably smaller: bromide (196 pm), chloride (181 pm), and fluoride (133 pm). In fact, because of its size, iodide ion forms relatively weak bonds with most elements (Pillar *et al.,* 2013).

The oxidation of iodide ion by chlorine dioxide was studied by stopped-flow techniques at μ = 1.0 C^2 mol dm^{-3} ($NaClO_4$). The following two-term rate law was confirmed for the reaction (equation 2.9):

$$-d[ClO_2]/dt = k_1[ClO_2][I^-] + k_2[ClO_2][I^-]^2 \quad (2.9)$$

Both the second and third order paths were interpreted in terms of an outer-sphere electron-transfer mechanism (Fa´bia´n and Gordon, 1997).

The oxidation of potassium iodide by perborate catalysed by Keggin type $[Co(II)W_{12}O_{40}]^{6-}$ was studied in sulphuric acid medium. The reaction proceeded by the oxidation of $[Co(II)W_{12}O_{40}]^{6-}$ to $[Co(III)W_{12}O_{40}]^{5-}$ by hydrogen peroxide, generated by the decomposition of perborate, which then oxidises potassium iodide in a rate determining step. The reaction was found to be independent of $[H^+]$. Decreasing the relative permittivity of the medium increased the rate of the reaction, which is attributed to the formation of an outer-sphere complex between the catalyst and active oxidant. The activation parameters were also determined and the values supported the proposed mechanism (Rajmane and Gokavi, 2014).

Nkole and Osunkwo (2019) studied the kinetics of the reduction of ethylenediaminetetraacetatoferrate(III) complex by iodide spectrophotometrically in an aqueous acidic medium. The study was carried out under pseudo-first order conditions of an excess of iodide ion concentration at 28 ± 1℃, ionic strength (μ) = 0.43 C^2 mol dm^{-3} (KNO_3) and $[H^+]$ = 5.0 × 10^{-2} mol dm^{-3}. The rate of the reaction was first order in oxidant and reductant concentrations, and displayed positive Brønsted-Debye salt effect. On the basis of catalysis by added cation, Michaelis-Menten's plot and the absence of intermediates, the outer-sphere electron transfer mechanism was proposed for the reaction.

2.10 Reactions of L-ascorbicAcid

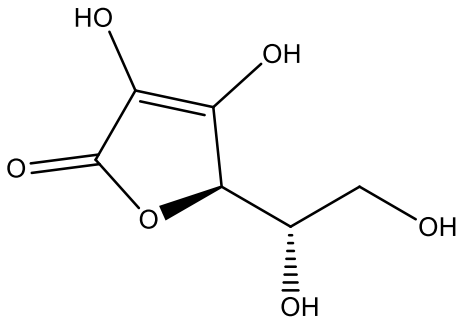


Figure 2.6: Structure of L-ascorbicacid

L-ascorbicacid (herein referred to as H_2A) is well known for its reducing properties in aqueous solutions. It can be oxidised by one electron to a radical state or doubly oxidised to the stable form called dehydroascorbic acid. Vitamin C is the term frequently used to refer to L-ascorbicacid in a nutritional context and it also encompasses the oxidation product, dehydroascorbic acid. (Jattinagoudar *et al.,* 2013). It has also been well-established as an antioxidant and a reliable redox reagent and has therefore, attracted great interest in the field of life and physical sciences. This multifunction of H_2A aroused series of investigations on transition metal complexes oxidation, particularly trivalent state (Salem and Gemeay, 1996).

The redox products of ascorbic acid could be protonated ascorbate radical, ascorbate radical or dehydroascorbic acid. A further factor in this area is that H_2A is a weak acid while the radical, $HA^{\bullet}$, is a strong acid. The vast majority of the reduction reactions of metal ions by ascorbic acid have been carried out in pH range 2 - 8. A one electron oxidation will produce either $HA^{\bullet}$ or $A^{\bullet-}$ and a two-electron oxidation will produce dehydroascorbic acid. The majority of studies of L-ascorbicacid by metal ions have proposed the formation of ascorbate free radical at the rate determining step. In all the cases, the overall product was confirmed to be dehydroascorbic acid (Jattinagoudar *et al.,* 2013; Ukoha *et al.,* 2018).

Kinetics of the reduction of iron(III) dimer, [(Fe(saloph))$_2$-μ-dicarpy] by L-ascorbicacid (H_2A), in perchloric acid was studied spectrophotometrically at λ_{max} = 424 nm. The stoichiometric studies showed that 1 mole of H_2A was oxidised for every mole of [(Fe(saloph))$_2$-μ-dicarpy] reduced. Under pseudo-first order conditions of concentrations of [H_2A] >> [(Fe(saloph))$_2$-μ-dicarpy], the order with respect to [(Fe(saloph))$_2$- μ-dicarpy] was unity and half-order with respect to [H_2A]. Second order rate constants (k_2) determined as the ratio of k_{obs} to [H_2A] and were found to be fairly constant. Reaction rate was inversely dependent on acid concentration and rate increased with increase in ionic strength of reaction system. The reduction of [(Fe(saloph))$_2$-μ-dicarpy] by H_2A was rationalised in terms of ion-pair complex formation with outer-sphere character (Ukoha *et al.,* 2018).

Alioke *et al.* (2012) have studied the reduction of the iron(III) complex ion, $[FeSalen(H_2O)_2]^+$, by L-ascorbicacid in aqueous perchloric acid medium at 28.5 ± 0.3 ºC. The kinetic data was obtained by monitoring the rate of decay of the complex at 515 nm. Under pseudo-first order conditions of concentration of L-ascorbicacid, the rate of reaction increased with increase in the concentration of ascorbic acid. Added CH_3COO^- and Cl^- ions did not affect the rate of reaction, as such, the reaction was rationalised on the basis of a plausible inner-sphere mechanism and equation 2.10 represents the stoichiometry of the reaction.

$$H_2A + 2[Fesalen(H_2O)_2]^+ \rightarrow 2[Fesalen(H_2O)_2] + A + 2H^+ \qquad (2.10)$$

The oxidation of ascorbic acid (H_2A) by hexacyanoferrate(III) (HCF) in aqueous perchloric acid medium at a constant ionic strength of 0.6 C^2 mol dm^{-3} was studied spectrophometrically at 25 ºC. The kinetic studies were carried out under pseudo-first order conditions with [ascorbic acid] in excess of the oxidant. The reaction exhibited 2:1 (reductant: oxidant) stoichiometry. The reaction was first order with respect to hexacyanoferrate(III) and

ascorbic acid concentrations. The order with respect to acid concentration was less than unity. The observed enthalpy of activation and relatively low entropy of activation and higher rate constant of slow step indicated that oxidation presumably occurred by an inner-sphere mechanism (Jattinagoudar *et al.,* 2013).

Kinetics of the copper(II) catalysed reduction of ethylenediaminetetraacetatocobaltate(III) ion ($[Co(III)EDTA]^{-}$) by H_2A was investigated spectrophotometrically in aqueous acidic medium at λ_{max} = 535 nm. The reaction followed a stoichiometry of 1:2 (H_2A: $[Co(III)EDTA]^{-}$). The order of reaction was first order with respect to both $[H_2A]$ and $[Co(III)EDTA^{-}]$ and a second order rate constant, k_2, value of (9.88 ± 0.065) × 10^{-3} dm^3 mol^{-1} s^{-1}. A negative kinetic salt effect was noticed with increase in ionic strength (Na_2SO_4). Activated parameters were obtained as $\Delta H^{\ddagger}$ = 61.85 $kJmol^{-1}$ and $\Delta S^{\ddagger}$ = −77.09 J K^{-1} mol^{-1}. Based on the results obtained, outer-sphere mechanistic pathway was proposed for the reaction (Abiti *et al.,* 2018).

2.11 Reactions of Thiodiglycol

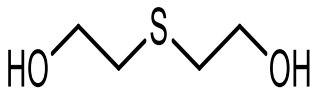


Figure 2.7: Structure of thiodiglycol

Thiodiglycol ($S(R)_2$), $[(HOC_2H_4)_2S]$ is a refractory and primary hydrolysis product of sulphur mustard $[(ClC_2H_4)_2S]$, which is a chemical warfare agent (Munro *et al.,* 1999). ($S(R)_2$) is not only a degradation product of sulphur mustard (HD) but also used as a solvent in antifreeze

solutions, a dyestuff for printing and in textile industry, an antioxidant, a vulcanising agent, an intermediate for other commodities, and a co-stabiliser in the production of polyvinyl chloride (Veriansyah *et al.,* 2005). Although it has a similar structure and physical properties with respect to those of sulphur mustard, it is also used as a model organic sulphur compound and chemical agent simulant. Also, ($S(R)_2$) has the same carbon-sulfur (C-S) bond arrangement as does sulphur mustard and a similar density, but it is more soluble in room water than is HD, which greatly facilitates its feed preparation for laboratory studies. Given the widespread use of ($S(R)_2$), the finding that it is a common environmental contaminant is not surprising (Veriansyah *et al.,* 2005).

The sulphoxidation of thiodiglycolic acid with iron(III)- salen chloride has been studied in aqueous acetonitrile medium. A substantial red shift in the λ_{max} value of Fe^{III}-salen was observed in aqueous medium. The spectrophotometric kinetic study indicated that $[Fe^{III}(salen)]^+$ was the active oxidising species. A reaction mechanism involving electron transfer from sulfur atom of thiodiglycolic acid to the central iron atom of $[Fe^{III}(salen)]^+$ was proposed. The presence of nitrogenous bases like pyridine, imidazole and 1-methylimidazole showed a retarding effect on the reaction rate. This could be explained on the basis of binding of these ligands to the coordination sphere of $[Fe^{III}(salen)]^+$ prior to the reaction with the substrate (Subramaniam *et al.,* 2014).

Hydrolysis and oxidation of thiodiglycol [$(HOC_2H_4)_2S$] over temperatures ranging from 100 to 525°C at a pressure of approximately 250 bar were examined. Under supercritical conditions (T = 400 to 525°C and P = 250 bar), thiodiglycol degradation occurred rapidly with and without oxidant. Additional experiments were performed at subcritical temperatures from 100 to 360°C to further explore hydrolysis degradation. Reaction products identified included

carbon monoxide, carbon dioxide, hydrogen, methane, ethylene, acetaldehyde, acetic acid, formic acid, thioxane, sulphuric acid, hydrogen sulphide, and elemental sulphur (Veriansyah *et al.*, 2005).

CHAPTER THREE

3.0 MATERIALS AND METHODS

3.1 Materials

3.1.1 Reagents and Chemicals

Cobalt(II) chloride hexahydrate (BDH, 89%), Salicyaldehyde (Sigma Aldrich, 99%), 1,2-phenylenediamine (Sigma Aldrich, 96%), chloroform (BDH, 90%), ethanol (BDH, 99%), hydrogen peroxide (BDH, 30%), potassium thiocyanate (Merck, 76%), acetone (BDH, 80%), pyrrole (Merck, 7%), trichloroacetic acid (BDH, 80%) , starch solution (BDH), glacial acetic acid (BDH, 99.8%), Dragendorff reagent (Merck), diethyl ether (BDH, 99%), L-cysteine hydrochloride (BDH), L-ascorbic acid (BDH), thioglycol (BDH, 98%), thioglycolic acid (BDH, 99%), sodium iodide (BDH), diphenylcarbazide (Analar), formaldehyde (BDH, 37%), acetaldehyde (BDH, 99.5%), thiosemicarbazide (Kem light), thiodiglycol (BDH, 97%), Hydrochloric acid (BDH, 35%), sodium chloride (JHD), Magnesium chloride (BDH), calcium chloride (Merck), sodium acetate (BDH), sodium formate (Hopkin and Williams), sodium sulphate (Kermel), Perchloric acid (Sigma Aldrich, 60%), sulphuric acid (Sigma Aldrich, 98%), hydrochloric acid (BDH, 37%), acrylamide (BDH), and methanol (Merck, 99%).

3.1.2 Equipment

Sherwood Colorimeter (Model 254), Corning Colorimeter (Model 252), Grant JB1 thermostated water bath (Cambridge), digital stop watch, Sartorous analytical weighing balance AG Germany (ED224S), thermometer (Paterson 12”), UV/Visible spectrophotometer (Cary 300 Series UV-Vis Spectrophotometer, Agilent Technologies), FTIR (CARRY 630), conductivity meter (HACH Sension 5), and magnetic susceptibility meter PIMV.

3.2 Methods

3.2.1 Preparation of 0.5 mol dm^{-3} L-cysteine hydrochloride solution

Solution of L-cysteine hydrochloride ($CH_2SHCH(NH_2)CO_2H(HCl)$) was prepared by dissolving 6.0075 g of the L-cysteine hydrochloride in 20 cm^3 of distilled water. The solution

was then carefully transferred into a 50 cm^3 volumetric flask and made up to the mark with distilled water.

3.2.2 Preparation of 0.5 mol dm^{-3} L-ascorbic acid solution

Solution of L-ascorbicacid ($C_6H_8O_6$) was prepared by dissolving 4.403 g of the ascorbic acid in 20 cm^3 of distilled water. The solution was then carefully transferred into a 50 cm^3 volumetric flask and made up to the mark with distilled water.

3.2.3 Preparation of thioglycolic acid solution

Solution of thioglycolic acid ($HSCH_2CO_2H$) (molecular weight = 92.11 g mol^{-1}, percentage purity = 99 %, density = 1.32 g cm^{-3}) was prepared by diluting 5.29 cm^3 of thioglycolic acid in a 50 cm^3 volumetric flask and made up to the mark with distilled water to get a 1.5 mol dm^{-3} thioglycolic acid solution.

3.2.4 Preparation of thioglycol solution

Solution of thioglycol ($HSCH_2CH_2OH$) (molecular weight = 78.13 g mol^{-1}, percentage purity = 98 %, density = 1.14 g cm^{-3}) was prepared by diluting 1.75 cm^3 of thioglycol in a 50 cm^3 volumetric flask and made up to the mark with distilled water to get a 0.5 mol dm^{-3} thioglycol solution.

3.2.5 Preparation of 0.08 mol dm^{-3} 1,5-diphenylcarbazide solution

A stock solution of diphenylcarbazide ($C_{13}H_{14}N_4O$) was prepared by dissolving 1.938 g of the diphenylcarbazide in 50 cm^3 of distilled water in a mixed solvent (DMSO: H_2O; 1:4(v/v)). The solution was then carefully transferred into a 100 cm^3 volumetric flask and made up to the mark with distilled water.

3.2.6 Preparation of 0.5 mol dm^{-3} potassium iodide solution

Solution of potassium iodide was prepared by dissolving 4.15 g of the potassium iodide in 20 cm^3 of distilled water. The solution was then carefully transferred into a 50 cm^3 volumetric flask and made up to the mark with distilled water.

3.2.7 Preparation of 0.5 mol dm^{-3} acetaldehyde solution

Solution of acetaldehyde (CH_3CHO) (molecular weight = 44.053 g mol^{-1}, percentage purity = 99.5 %, density = 1.52 g cm^{-3}) was prepared by diluting 1.46 ml of acetaldehyde in a 100 cm^3 volumetric flask and made up to the mark with distilled water.

3.2.8 Preparation of 0.5 mol dm^{-3} formaldehyde solution

Solution of formaldehyde (HCHO) (molecular weight = 30.026 g mol^{-1}, percentage purity = 37%, density = 0.815 g cm^{-3}) was prepared by diluting 4.98 cm^3 of formaldehyde in a 100 cm^3 volumetric flask and made up to the mark with distilled water.

3.2.9 Preparation of 0.5 mol dm^{-3} thiodiglycol solution

Solution of thiodiglycol ($HO(CH_2)_2S(CH_2)_2OH$) (molecular weight = 122.19 g mol^{-1}, percentage purity = 97%, density = 1.182 g cm^{-3}) was prepared by diluting 5.33 cm^3 of thiodiglycol (BDH) in a 100 cm^3 volumetric flask and made up to the mark with distilled water.

3.2.10 Preparation of 0.5 mol dm^{-3} thiosemicarbazide solution

Solution of thiosemicarbazide (N_2H_5CS) was prepared by dissolving 2.28 g of the N_3H_5CS in 20 cm^3 of distilled water. The solution was then carefully transferred into a 50 cm^3 volumetric flask and made up to the mark with distilled water.

3.2.11 Preparation of 1.5 mol dm^{-3} sodium chloride solution

Solution of sodium chloride was prepared by dissolving 58.44 g mol^{-1} of the sodium chloride in 50 cm^3 of distilled water. The solution was then carefully transferred into a 100 cm^3 volumetric flask and made up to the mark with distilled water.

3.2.12 Preparation of 0.10 mol dm^{-3} sodium carbonate solution

A stock solution of sodium carbonate was obtained by dissolving 0.53 g of Na_2CO_3 in 50 cm^3 of distilled water. This solution was used as a primary standard for the standardisation of the HCl solution.

3.2.13 Preparation of standard solution of hydrochloric acid

Stock solution of 1.0 mol dm^{-3} hydrochloric acid was made by diluting 8.22 cm^3 HCl (molecular weight = 36.47 g mol^{-1}, percentage purity = 37 %, density = 1.2 g cm^{-3}) in 100 cm^3 standard flask then made up to the mark with distilled water. The solution was standardised volumetrically using sodium carbonate as primary standard and phenolphthalein indicator.

3.1.14 Preparation of 2.0 mol dm^{-3} solution of perchloric acid

Stock solution of 2.0 mol dm^{-3} perchloric acid was prepared by diluting 21.75 cm^3 $HClO_4$ (Sigma–Aldrich, 60 %, 1.54 specific gravity) in 100 cm^3 standard flask and made up to the mark with distilled water.

3.2.15 Preparation of 1.0 mol dm^{-3} solution of sulphuric acid

Stock solution of 1.0 mol dm^{-3} sulphuric acid was prepared by diluting 5.43 cm^3 H_2SO_4 (Sigma–Aldrich, 98 %, 1.84 specific gravity) in 100 cm^3 standard flask and made up to the mark with distilled water.

3.2.16 Preparation of Salt Solutions

Stock solutions 0,5 mol dm^{-3} sodium sulphate (142. 04 g mol^{-1}), sodium acetate (82. 03 g mol^{-1}), sodium formate (68. 01 g mol^{-1}), calcium chloride (110. 99 g mol^{-1}) and magnesium chloride (203. 30 g mol^{-1}) were prepared by dissolving 7.10 g, 4.10 g, 3.40 g, 5.55 g and 10.17 g

respectively of each salt in a 100 cm3 volumetric flask with distilled water and standardized gravimetrically.

3.2.17 Preparation of 0.1 mol dm^{-3} acrylamide solution

The stock solution was prepared by dissolving 0.177 g of acrylamide (molecular weight = 71.08 g mol^{-1}) with distilled water in a 25 cm^3 volumetric flask and made up to the mark with distilled water.

3.2.18 Preparation of 0.2 mol dm^{-3} potassium thiocyanate solution

The stock solution of potassium thiocyanate was prepared by dissolving 0.485 g of KSCN (molecular weight = 97 g mol^{-1}) with distilled water in a 25 cm^3 volumetric flask and made up to the mark.

3.2.19 Preparation of 0.5 mol dm^{-3} hydrogen peroxide solution

The stock solution of hydrogen peroxide was prepared by diluting 2.55cm^3 H_2O_2 (percentage purity = 30%, density = 1.11 gcm^{-3}, molecular weight = 34 g mol^{-1}) with distilled water in a 50 cm^3 volumetric flask and made up to the mark.

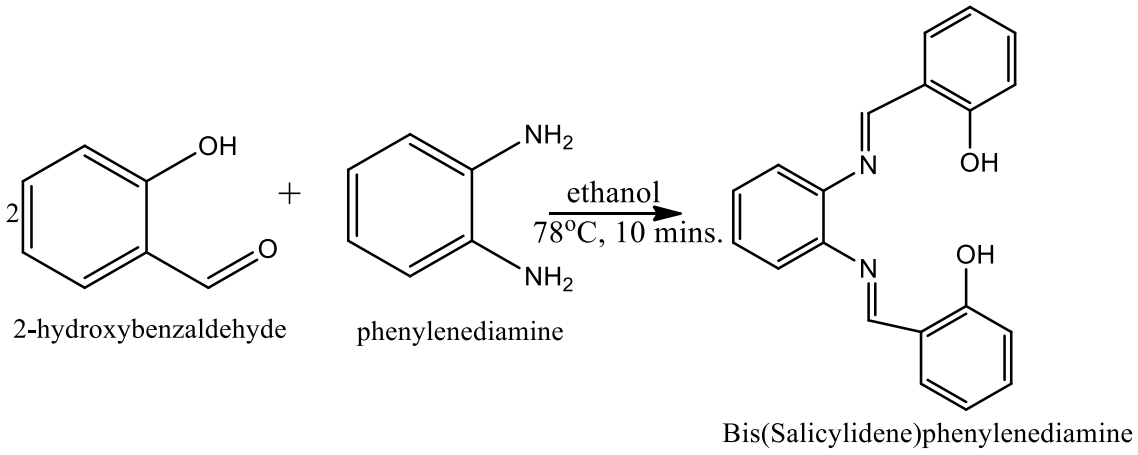
3.2.20 Synthesis and characterisation of the schiff base (ligand) and the complex

The Schiff base, bis(salicylidene)-1,2-phenylenediamine, (salophen) and the complex, *N,N'*-phenylene*bis*-(salicylideneiminato)cobalt(III), ($[Co(salophen)]^+$) were synthesised and characterised according to the reported method described in literature (Pizzolato *et al.*, 2013). The complex was characterised with FTIR (CARRY 630), Conductivity meter (HACH Sension 5) and magnetic susceptibility meter PIMV.

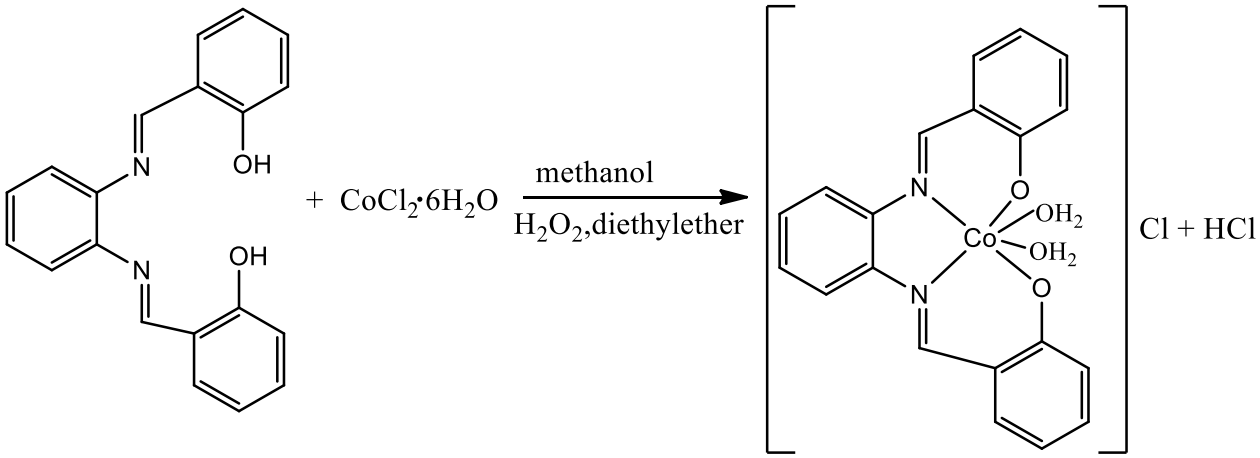
A stoichiometric amount of 1,2-phenylenediamine (1.00 g, 9.25 mmol) with salicylaldehyde (1.97 cm^3, 18.50 mmol) in ethanol (30 cm^3) was refluxed at 78 ºC for 10

minutes, and the crude was cooled to 0 ºC. The yellow precipitate was collected by filtration, washed with ethanol and dried in a desiccator.

The complex was prepared by stirring the mixture of the Schiff base (0.79 g, 2.50 mmol) with hydrated cobaltous chloride (0.63 g, 2.30 mmol) in methanol (60 cm^3) for 3 hours at room temperature followed by oxidation with H_2O_2. Diethyl ether (20 cm^3) was added to induce the formation of the precipitate. The precipitate was filtered and washed with diethyl ether and recrystallised from chloroform.



Scheme 3.1: Reaction of 2-hydroxybenzaldehyde(salicyldehyde) and O-phenylenediamine to give bis(salicylidene)phenylenediamine



Scheme 3.2: Reaction of bis(salicylidene)phenylenediamine and cobalt(II)chloride to give phenylenebis(salicylideneiminato)cobalt(III) complex

Also, the stability of the complex in dilute acids was investigated by varying the concentrations of inorganic acids such $HClO_4$, HCl and H_2SO_4 to a DMSO-H_2O solution of the $[Co(salophen)]^+$.

3.2.21 Stoichiometric studies

The stoichiometry of each system was determined by spectrophotometric titration using the mole ratio method (Ukoha and Iyun, 1999; Idris *et al.,* 2008; Onu *et al.,* 2009; Osunlaja *et al.,* 2013; Onu *et al.,* 2016). The concentration of the complex ($[Co(salophen)]^+$) was kept constant while that of the reductants were varied between the mole ratio 1:0.25 to 1:3.5 ([reductant]/ [oxidant]) as follows:

i. For $[Co(salophen)]^+$ / LSH system: $[Co(salophen)]^+ = 2.0 \times 10^{-4}$ mol dm^{-3}, [LSH] = (0.5-7.0) $\times 10^{-4}$ mol dm^{-3}, $[H^+] = 1.0 \times 10^{-3}$ mol dm^{-3}, $\mu = 0.1\ C^2$ mol dm^{-3} (NaCl), D = 74.84, λ_{max} = 470 nm, T = 300 K.

ii. For $[Co(salophen)]^+$ / RSH system: $[Co(salophen)]^+ = 3.0 \times 10^{-4}$ mol dm^{-3}, [RSH] = (0.5-7.0) $\times 10^{-4}$ mol dm^{-3}, $[H^+] = 1.4 \times 10^{-3}$ mol dm^{-3}, $\mu = 0.1\ C^2$ mol dm^{-3} (NaCl), D = 74.19, λ_{max} = 470 nm, T = 300 K.

iii. For $[Co(salophen)]^+$ / TSH system: $[Co(salophen)]^+ = 3.0 \times 10^{-4}$ mol dm^{-3}, [TSH] = (0.5-7.0) $\times 10^{-4}$ mol dm^{-3}, $\mu = 0.1\ C^2$ mol dm^{-3} (NaCl), D = 74.04, λ_{max} = 470 nm, T = 300 K.

iv. For $[Co(salophen)]^+$ / TSCZ system: $[Co(salophen)]^+ = 2.0 \times 10^{-4}$ mol dm^{-3}, [TSCZ] = (0.5-7.0) $\times 10^{-4}$ mol dm^{-3}, $[H^+] = 1.0 \times 10^{-2}$ mol dm^{-3}, $\mu = 0.1\ C^2$ mol dm^{-3} (NaCl), D = 74.41, λ_{max} = 470 nm, T = 306 K

v. For $[Co(salophen)]^+$ / DPCI system: $[Co(salophen)]^+ = 1.0 \times 10^{-4}$ mol dm^{-3}, [DPCI] = $(0.5\text{-}7.0) \times 10^{-4}$ mol dm^{-3}, $[H^+] = 0.1$ mol dm^{-3}, $\mu = 0.5\ C^2$ mol dm^{-3} (NaCl), D = 75.83, λ_{max} = 470 nm, T = 300 K

vi. For $[Co(salophen)]^+$ / CH_3CHO system: $[Co(salophen)]^+ = 3.0 \times 10^{-4}$ mol dm^{-3}, $[CH_3CHO] = (0.5\text{-}7.0) \times 10^{-4}$ mol dm^{-3}, $[H^+] = 4.0 \times 10\text{-}2$ mol dm^{-3}, $\mu = 0.2\ C^2$ mol dm^{-3} (NaCl), D = 75.67, λ_{max} = 470 nm, T = 302 K

vii. For $[Co(salophen)]^+$ / HCHO system: $[Co(salophen)]^+ = 3.0 \times 10^{-4}$ mol dm^{-3}, [HCHO] = $(0.5\text{-}7.0) \times 10^{-4}$ mol dm^{-3}, $[H^+] = 0.1$ mol dm^{-3}, $\mu = 0.2\ C^2$ mol dm^{-3} (NaCl), D = 74.78, λ_{max} = 470 nm, T = 299 K.

viii. For $[Co(salophen)]^+$ / I^- system: $[Co(salophen)]^+ = 2.0 \times 10^{-4}$ mol dm^{-3}, $[I^-] = (0.5\text{-}7.0) \times 10^{-4}$ mol dm^{-3}, $[H^+] = 0.4$ mol dm^{-3}, $\mu = 0.6\ C^2$ mol dm^{-3} (NaCl), D = 78.43, λ_{max} = 470 nm, T = 301 K.

ix. For $[Co(salophen)]^+$ / H_2A system: $[Co(salophen)]^+ = 3.0 \times 10^{-4}$ mol dm^{-3}, $[H_2A] = (0.5\text{-}7.0) \times 10^{-4}$ mol dm^{-3}, $[H^+] = 2.0 \times 10^{-3}$ mol dm^{-3}, $\mu = 0.1\ C^2$ mol dm^{-3} (NaCl), D = 74.11, λ_{max} = 470 nm, T = 306 K.

x. For $[Co(salophen)]^+$ / $S(R_2)$ system: $[Co(salophen)]^+ = 2.0 \times 10^{-4}$ mol dm^{-3}, $[S(R_2)] = (0.5\text{-}7.0) \times 10^{-4}$ mol dm^{-3}, $[H^+] = 5.0 \times 10^{-2}$ mol dm^{-3}, $\mu = 0.2\ C^2$ mol dm^{-3} (NaCl), D = 77.42, λ_{max} = 470 nm, T = 305 K.

The reactions were allowed to go to completion and the absorbances of the completely reacted mixtures (A_∞) were monitored at 470 nm (the λ_{max} of $[Co(salophen)]^+$) using Sherwood Colorimeter Model 254. The absorbances obtained were plotted against the mole ratios of the reactants. Points of sharp breaks in these plots gave the stoichiometries of these reactions.

3.2.22 Product analysis

The products of the reaction were analysed using qualitative and instrumental means.

Qualitative tests:

a. Completely reacted solutions were analysed where possible for the type of products formed. Co^{2+} product was determined by adding potassium thiocyanate (KSCN) in excess acetone to the reaction product as described by Osunlaja and his co-workers (Osunlaja *et al.,* 2013).

b. For the reactions where thiols (LSH, RSH, TSH and TSCZ) were used as reductants, test for the presence of disulphide was carried out according to literature (Idris *et al.,* 2005; Nkole *et al.,* 2018). The presence of disulphide, was ascertained by comparing the reaction mixture's spectrum after the completion of the reaction with the spectrum obtained when thiols were treated with H_2O_2 which is known to oxidise thiols to disulphides (Idris, 2005). The thiols were also reacted with the oxidant in acid medium and ionic strength of reaction. At the completion of the reaction, the mixture was extracted six times with diethyl ether. The combined ether extracts were left overnight to dry (Nkole *et al.*, 2018a).

c. Where aldehydes were used as reductants, the presence or absence of carboxylic acid was tested by adding a pinch of solid sodium carbonate to a small portion of the reaction product in a test tube (Vogel, 1996).

d. The method of Abiti *et al*. (2018) was used to check for the presence of dehydroascorbic acid as a possible product of H_2A oxidation, this involved reacting the final reaction product with pyrrole in excess trichloroacetic acid at 50 ºC.

e. The product of the oxidation of iodide ion, iodine, was confirmed by the addition of starch solution to the reaction product (Ukoha and Iyun, 1999).

f. For the reaction involving thiodiglycol, test was carried out to determine the presence of sulphoxide, 2 ml of the reaction product in glacial acetic acid was transferred to a filter paper, and after drying by a stream of hot air, the paper was sprayed with dragendorff reagent (Suchomelova *et al.,* 1965).

Instrumental test:

FTIR and UV/Vis spectroscopic techniques were used to test for the possible products involved in the reaction of $[Co(salophen)]^+$ and diphenylcarbazides (Willems and De Ranter, 1974; Ramírez *et al.,* 1996).

3.2.23 Kinetic measurements

The rates of reactions of $[Co(salophen)]^+$ with the reductants were studied by monitoring the decrease in absorbance of the reaction mixture at a λ_{max} of 470 nm using Sherwood Colorimeter Model 254. All kinetic measurements were carried out under pseudo-first order conditions with respective reductant concentrations in excess of the oxidant concentration (at least 10-fold) at the temperature 301 K. Ionic strength of the reaction medium as well as $[H^+]$ were maintained constant for each system unless otherwise stated (Hamza *et al.,* 2012; Idris *et al.,* 2015; Ukoha *et al.,* 2018).

The pseudo-first order plots of log $(A_\infty - A_t)$ against time were made and the slopes of the plots gave the pseudo-first order rate constants, k_1. The second order rate constants, k_2, were determined from k_1 as k_1/ [reductant] (Kim *et al.,* 2005; Adetoro *et al.,* 2011; Anweting, 2012).

3.2.24 Determination of the effect of $[H^+]$ on the reaction rates

The effect of $[H^+]$ on the rate of the reactions was investigated by keeping the concentration of all other reactants constant while varying the $[H^+]$. The following experimental conditions were maintained for the ten systems:

a. For $[Co(salophen)]^+$- LSH system: [LSH] = 12.0×10^{-3} mol dm^{-3}, $[H^+]$ = $(1.0 – 18.0) \times 10^{-3}$ mol dm^{-3}, $\mu = 0.1$ C^2 mol dm^{-3}, D = 74.84, T = 300 K, and λ_{max} = 470 nm

b. For $[Co(salophen)]^+$- RSH system: [RSH] = 15.0×10^{-3} mol dm^{-3}, $[H^+]$ = $(1.4 – 2.4) \times 10^{-3}$ mol dm^{-3}, $\mu = 0.1$ C^2 mol dm^{-3}, D = 74.19, T = 300 K, and λ_{max} = 470 nm

c. For $[Co(salophen)]^+$- TSH system: TSH = 7.50 mol dm^{-3}, $[H^+]$ = $(1.0 – 7.0) \times 10^{-3}$ mol dm^{-3} $\mu = 0.1$ C^2 mol dm^{-3}, D = 74.04, T = 300 K and λ_{max} = 470 nm

d. For $[Co(salophen)]^+$- TSCZ system: [TSCZ] = 8.0×10^{-2} mol dm^{-3}, $[H^+]$ = $(1.0 – 8.0) \times 10^{-2}$ mol dm^{-3}, $\mu = 0.1$ C^2 mol dm^{-3}, D = 74.41, T = 306 K and λ_{max} = 470 nm

e. For $[Co(salophen)]^+$- DPCI system: DPCI = 25.0×10^{-3} mol dm^{-3}, $[H^+]$ = (0.10 – 0.40) mol dm^{-3}, $\mu = 0.5$ C^2 mol dm^{-3}, D = 75.83, T = 300 K and λ_{max} = 470 nm

f. For $[Co(salophen)]^+$- CH_3CHO system: $[CH_3CHO]$ = 18.0×10^{-3} mol dm^{-3}, $[H^+]$ = $(2.0 - 14) \times 10^{-2}$ mol dm^{-3}, $\mu = 0.2$ C^2 mol dm^{-3}, D = 75.67, T = 302 K and λ_{max} = 470 nm

g. For $[Co(salophen)]^+$- HCHO system: [HCHO] = 18.0×10^{-3} mol dm^{-3}, $[H^+]$ = $(2.0 - 14.0) \times 10^{-2}$ mol dm^{-3}, $\mu = 0.2$ C^2 mol dm^{-3}, D = 74.78, T = 299 K and λ_{max} = 470 nm

h. For $[Co(salophen)]^+$- I^- system: $[I^-]$ = 16.0×10^{-2} mol dm^{-3} , $[H^+]$ = (0.10 – 0.45) mol dm^{-3} $\mu = 0.6$ C^2 mol dm^{-3}, D = 78.43, T = 301 K and λ_{max} = 470 nm

i. For $[Co(salophen)]^+$- H_2A system: $[H_2A]$ = 12.0×10^{-3} mol dm^{-3}, $[H^+]$ = $(2.0 – 9.0) \times 10^{-3}$ mol dm^{-3}, $\mu = 0.1$ C^2 mol dm^{-3}, D = 74.11, T = 306 K and λ_{max} = 470 nm

j. For $[Co(salophen)]^+$- $S(R)_2$ system: $[S(R)_2] = 16.0 \times 10^{-2}$ mol dm^{-3}, $[H^+] = (1.0 – 8.0) \times 10^{-2}$ mol dm^{-3}, $\mu = 0.9$ C^2 mol dm^{-3}, D = 77.42, T = 305 K and λ_{max} = 470 nm.

The order of reaction with respect to acid concentration was obtained as the slope of the plot of log k_1 against log $[H^+]$. Variation of acid dependent second order rate constant, $k_2(H^+)$ with $[H^+]$ was obtained by plotting $k_2(H^+)$ against $[H^+]$.

3.2.25 Determination of the effect of change in ionic strength of reaction medium on the rate of reactions

The ionic strength, μ, of the reaction mixtures was varied by using NaCl in the range (0.1 - 0.8) C^2 mol dm^{-3} for RSH, I^-, CH_3CHO, HCHO and TSCZ, 0.04 - 0.16 C^2 mol dm^{-3} for LSH, H_2A and TSH, 0.4 - 0.80 C^2 mol dm^{-3} for DPCI, and 0.1 - 0.9 C^2 mol dm^{-3} for $S(R)_2$ systems respectively while maintaining the concentrations of the oxidant, reductant and hydrogen ion constant at reaction temperature 301 K. The linearised form of Bronsted-Debye equation 3.1 was used to obtain the relationship between the rate constant and ionic strength.

$$\log k_2 = \log k_0 + 1.04 Z_A Z_B \sqrt{\mu} \quad (3.1)$$

where k_2, k_o, $Z_A Z_B$ and μ are the second order rate, rate constant at zero ionic strength, charges of the reactant species, and ionic strength of the reaction medium respectively.

3.2.26 Determination of the effect of change in dielectric constant of reaction medium on rate of reactions

The effect of change in dielectric constant, D, on the rate of reactions was investigated by carrying out the reactions in medium of varying dielectric constants. The medium dielectric constants were varied using a binary solvent mixture of distilled water and DMSO while keeping

all other experimental conditions constant. The dielectric constant was calculated as shown in equation 3.2:

$$D_{mixture} = \frac{(V(cm^3) \text{ of DMSO} \times D \text{ of DMSO}) + (V(cm^3) \text{ of water} \times D \text{ of water})}{\text{Total volume of solution}} \quad (3.2)$$

The relationships between the second order rates constant and the dielectric constant (D) were obtained from the plots of log k_2 against 1/D, using equation 3.3.

$$\log k_2 = \log k_0 - \frac{Z_A Z_B e^2}{DTr_+} \quad (3.3)$$

where k_2 is the second order rate constant, k_0 is the rate constant in a medium of infinite dielectric constant, Z_AZ_A are the charges of the reactants species, e is electron charge, D is the dielectric constant of the medium, T is the temperature, and r_+ is the radius of the activated complex.

3.2.27 Determination of the effect of added ions on the rate of reactions

The effect of added ions on the reaction rate was obtained by the addition of various concentrations of ions (Mg^{2+}, Ca^{2+}, SO_4^{2-}, CH_3COO^-, and $HCOO^-$) while maintaining the [oxidant], [reductant], [H^+] and ionic strength constant at stated experimental conditions.

3.2.28 Determination of the effect of change in temperature on the reaction rates

The temperature for the reactions were varied in their range 300 – 325 K for LSH, RSH, TSH and DPCI systems, 303 – 328 K, 299 – 325 K, 301- 325 K, 306 – 333 K, 307 – 337 K, and 305 – 330 K for CH_3CHO, HCHO, I^-, H_2A, TSCZ and $S(R)_2$ systems respectively. All other experimental conditions were maintained constant. Plots of ln(k_2/T) versus 1/T were made using equation 3.3 and from the slopes and intercepts of the graph, the activated parameters ($\Delta H^‡$, $\Delta S^‡$, $\Delta G^‡$ and Ea) were estimated (equation 3.4).

$$\ln\left(\frac{k_2}{T}\right) = \ln\left(\frac{K_b}{h}\right) + \frac{\Delta S^‡}{R} - \frac{\Delta H^‡}{RT} \quad (3.4)$$

where k_2 is the second order rate constant ($dm^3\ mol^{-1}\ s^{-1}$), K_b is the Boltzmann's constant (1.381×10^{-23} J K^{-1}), T is the absolute temperature (K), h is Planck's constant (6.626×10^{-34} Js), R is the gas constant (8.3144598 J $mol^{-1}K^{-1}$), $\Delta S^{\ddagger}$ is the entropy of activation (J mol^{-1} K^{-1}) and $\Delta H^{\ddagger}$ is the enthalpy of activation (kJ mol^{-1}).

3.2.29 Test for the participation of free radicals in the reaction

Test for participation of free radicals in the reaction was carried out by adding 0.1 cm^3 of acrylamide solution to a partially oxidised reaction mixture containing various concentrations of oxidant, reductant and H^+ for each system. Methanol was then added in drops and in excess. Control experiment was carried out by adding acrylamide solution to the solutions of oxidant and reductant separately at the same conditions of $[H^+]$, μ and temperature.

3.2.30 Test for formation of intermediate complex prior to electron transfer

Test for the presence of stable, detectable intermediate complexes as each of the reaction was progressing was carried out by recording the electronic spectra of partially reacted mixture at various time intervals depending on the speed of the reaction. A shift in λ_{max} and/ or enhancement of peak as the reaction progressed was determined. Furthermore, Michaelis–Menten plots of $1/ k_1$ versus 1/[reductant] was made for all the systems studied to ascertain the participation of a stable and detectable intermediate complex during the course of the reaction.

CHAPTER FOUR

4.0 RESULTS

4.1 Characterisation and Stability of the Complex

Monitoring the absorbance of the DMSO-H_2O solution of the complex ($[Co(salophen)]^+$) after one week showed no change in the absorbance at 470 nm. Similarly, the stability test showed the complex to be stable as observed from the absorbance of the complex at its λ_{max} (470 nm) which remained constant for several days in 0.002, 0.03, 0.5 and 1.0 mol dm^{-3} solutions of the acids.

With the aid of HACH Sension 5 conductivity meter at stable room temperature, the measurement of molar conductivity of the complex in DMSO-H_2O (1:4 v/v) was determined as 122 S cm^2 mol^{-1} with a specific conductance of 12.2×10^{-6} S cm^{-1}, indicating electrolyte of ratio 1:1. The FTIR result of the complex showed the complexation of the ligand with the cobalt(III) by a slight shift of peak due to the imine (ν(C=N)) bond from 1620 cm^{-1} to 1612 cm^{-1}. Peaks around 547 cm^{-1} and 462 cm^{-1} was assigned to v(Co-O) and v(Co-N) respectively (Appendice I and II). Magnetic susceptibility measurement showed that the cobalt(III) complex synthesised is of low spin inner orbital with a magnetic moment (μ_{eff}) of 0.2 BM. This value indicates the oxidation of Co(II) to Co(III) during the preparation of the complex. From the UV/Visible analysis, a λ_{max} of 470 nm was obtained for the complex (Appendix III).

4.2 Stoichiometric Studies

The result obtained from stoichiometric studies showed that one mole of the complex ($[Co(salophen)]^+$) consumed one mole each of thiols, carbazides and iodide ion, two moles of the $[Co(salophen)]^+$ consumed one mole of aldehydes (formaldehyde and acetaldehyde) while two

moles of the $[Co(salophen)]^+$ consumed three moles of ascorbic acid. The titration curves from which the stoichiometries were determined are presented in Figures 4.1 - 4.10. On the basis of the

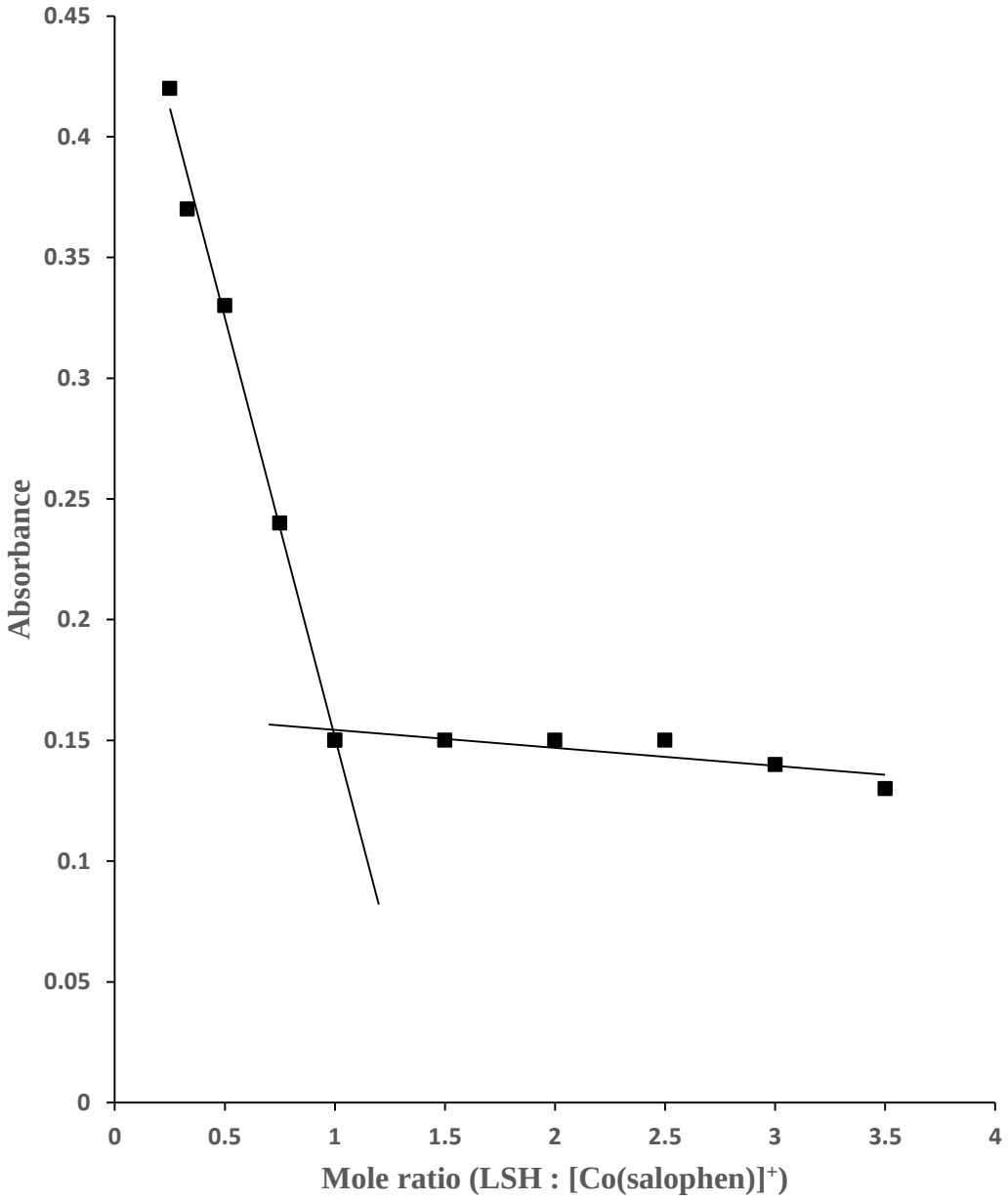


Figure 4.1: Plot of absorbance versus mole ratio for the redox reaction of $[Co(salophen)]^+$ and LSH at $[Co(salophen)^+] = 2.0 \times 10^{-4}$ mol dm^{-3}, $[H^+] = 1.0 \times 10^{-3}$ mol dm^{-3}, $\mu = 0.1$ C^2 mol dm^{-3}, D = 74.84, [LSH] = (0.5 - 7.0) $\times 10^{-4}$ mol dm^{-3}, T = 300 K and λ_{max} = 470 nm

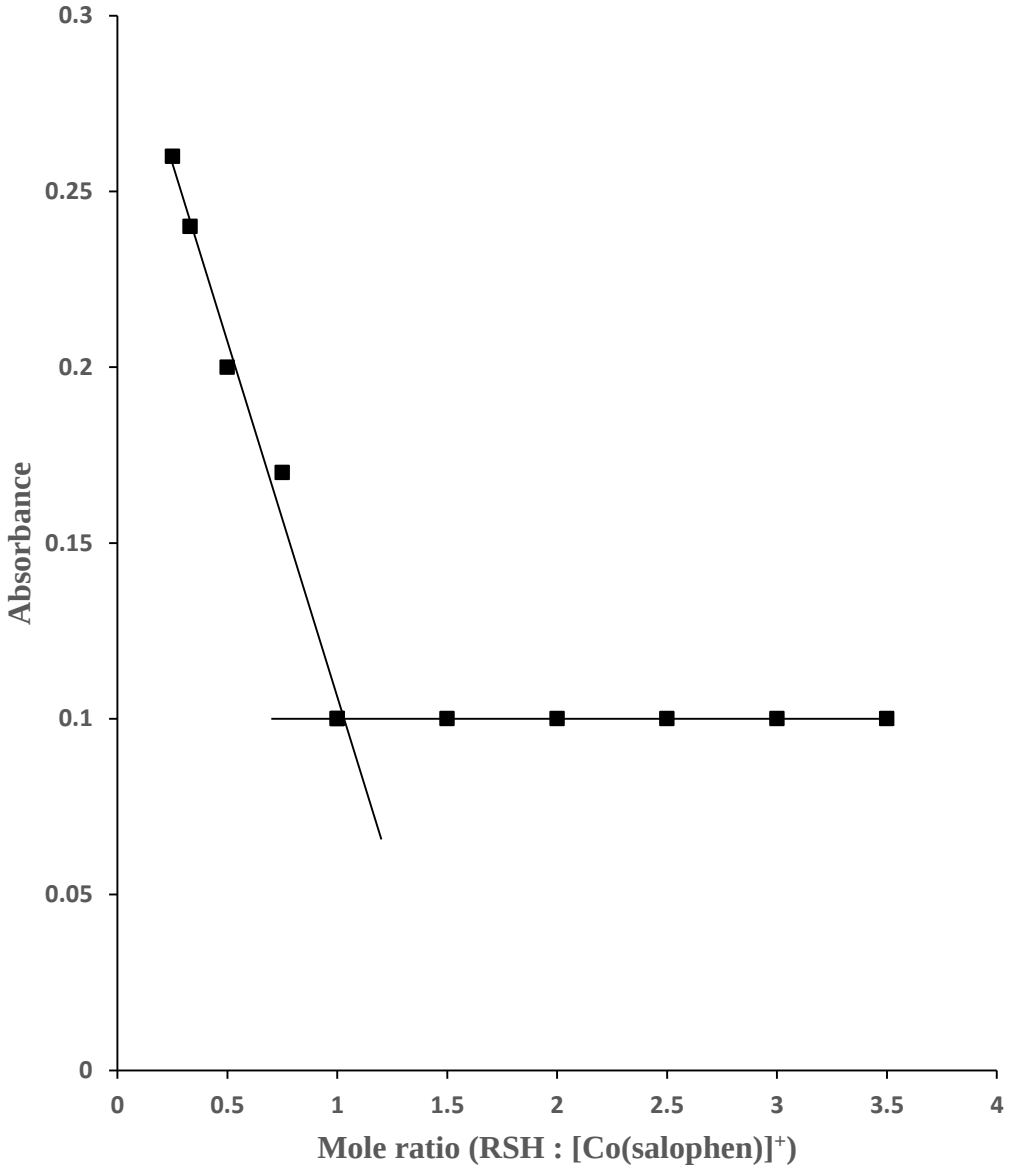


Figure 4.2: Plot of absorbance versus mole ratio for the redox reaction of $[Co(salophen)]^+$ and RSH at $[Co(salophen)^+] = 3.0 \times 10^{-4}$ mol dm^{-3}, $[H^+] = 1.4 \times 10^{-3}$ mol dm^{-3}, $\mu = 0.1\ C^2$ mol dm^{-3}, D = 74.19, [RSH] = $(0.75 - 10.5) \times 10^{-4}$ mol dm^{-3}, T = 300 K and λ_{max} = 470 nm

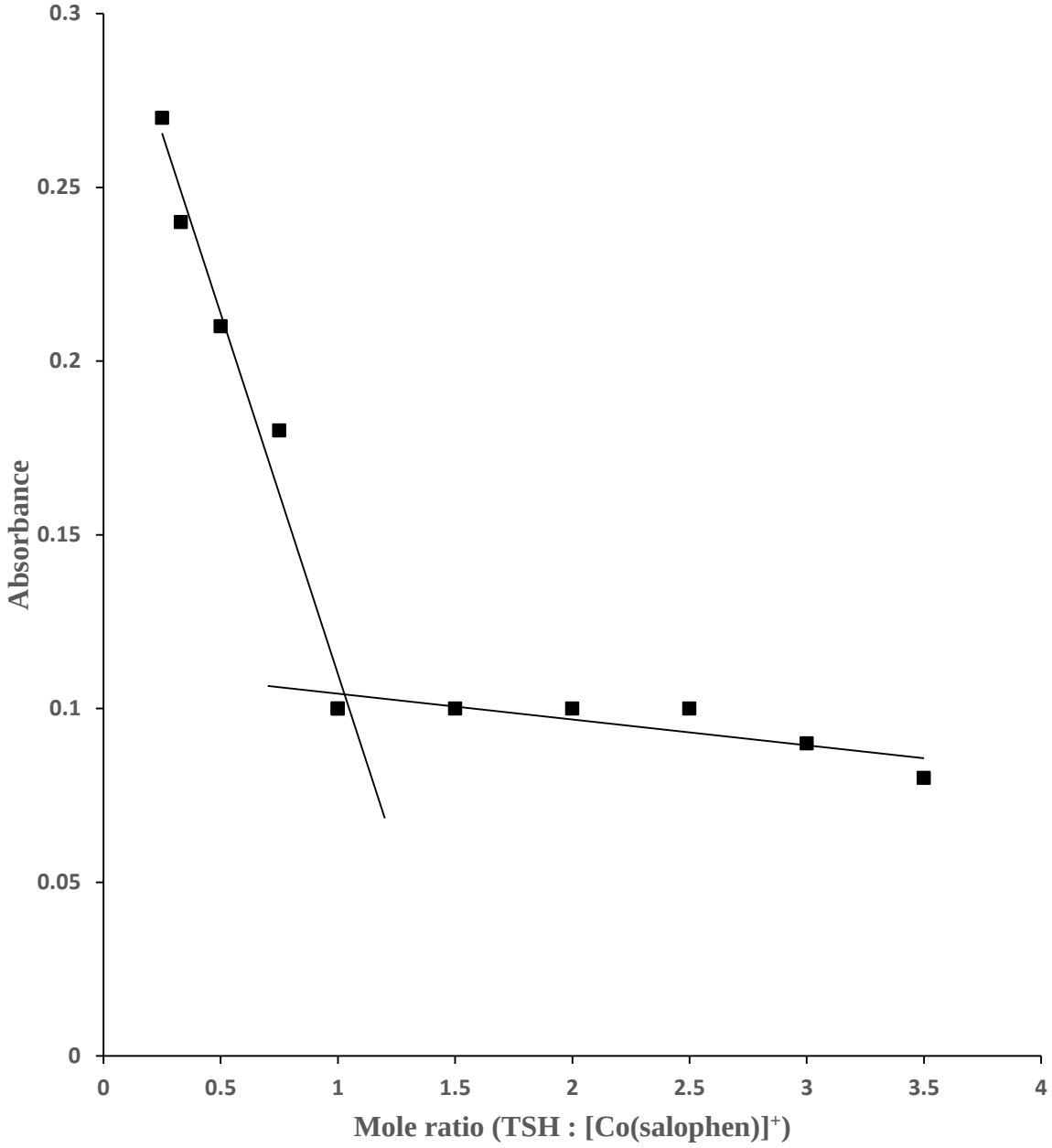


Figure 4.3: Plot of absorbance versus mole ratio for the redox reaction of $[Co(salophen)]^+$ and TSH at $[Co(salophen)^+] = 3.0 \times 10^{-4}$ mol dm^{-3}, $\mu = 0.1$ C^2 mol dm^{-3}, D = 74.04, [TSH] = $(0.75 - 10.5) \times 10^{-4}$ mol dm^{-3}, T = 300 K and λ_{max} = 470 nm

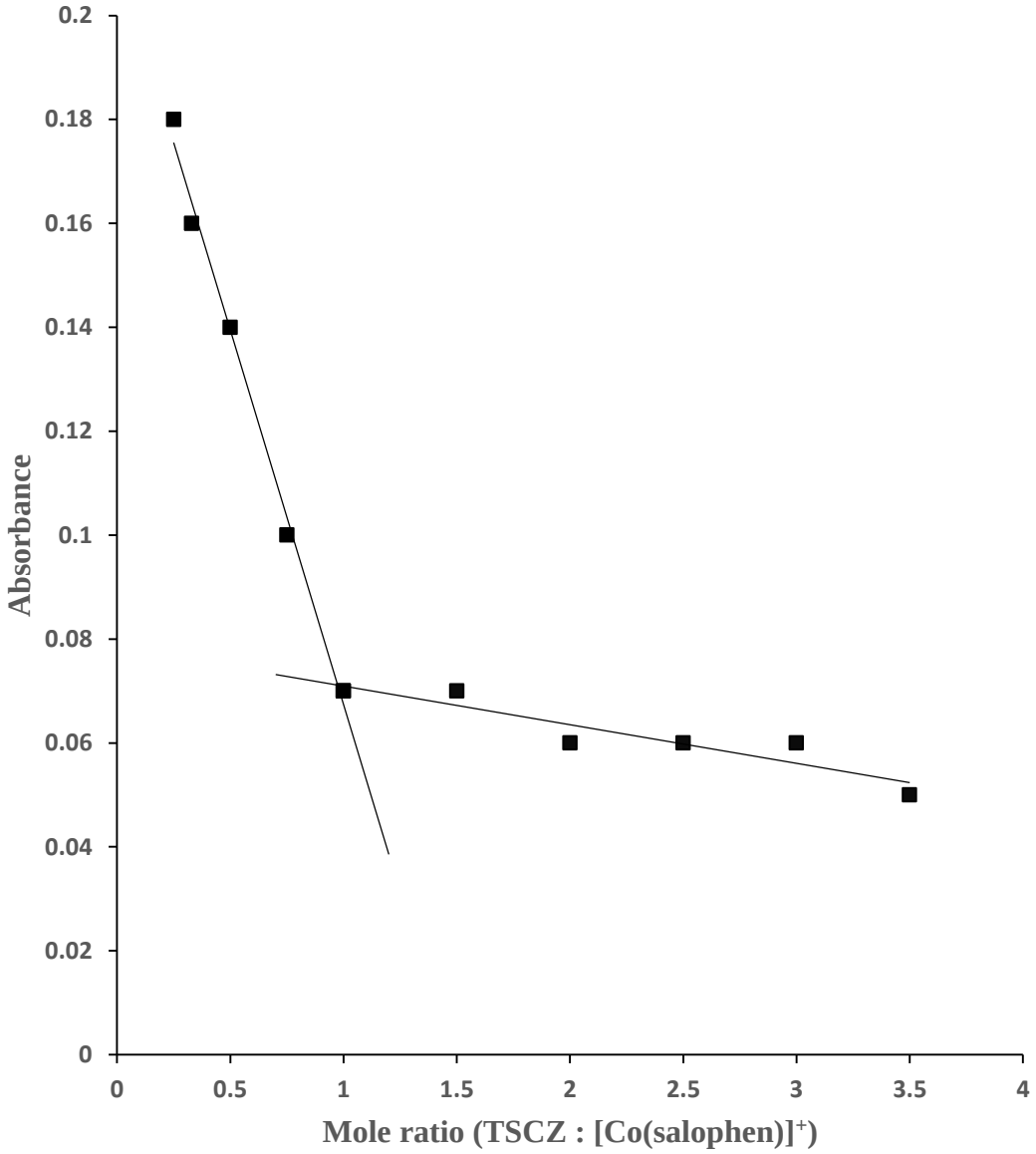


Figure 4.4: Plot of absorbance versus mole ratio for the redox reaction of $[Co(salophen)]^{+}$ and TSCZ at $[Co(salophen)^{+}] = 2.0 \times 10^{-4}$ mol dm^{-3}, $[H^{+}] = 1.0 \times 10^{-2}$ mol dm^{-3}, μ = 0.1 C^2 mol dm^{-3}, D = 74.41, [TSCZ] = (0.5 - 7.0) $\times 10^{-4}$ mol dm^{-3}, T = 306 K and λ_{max} = 470 nm

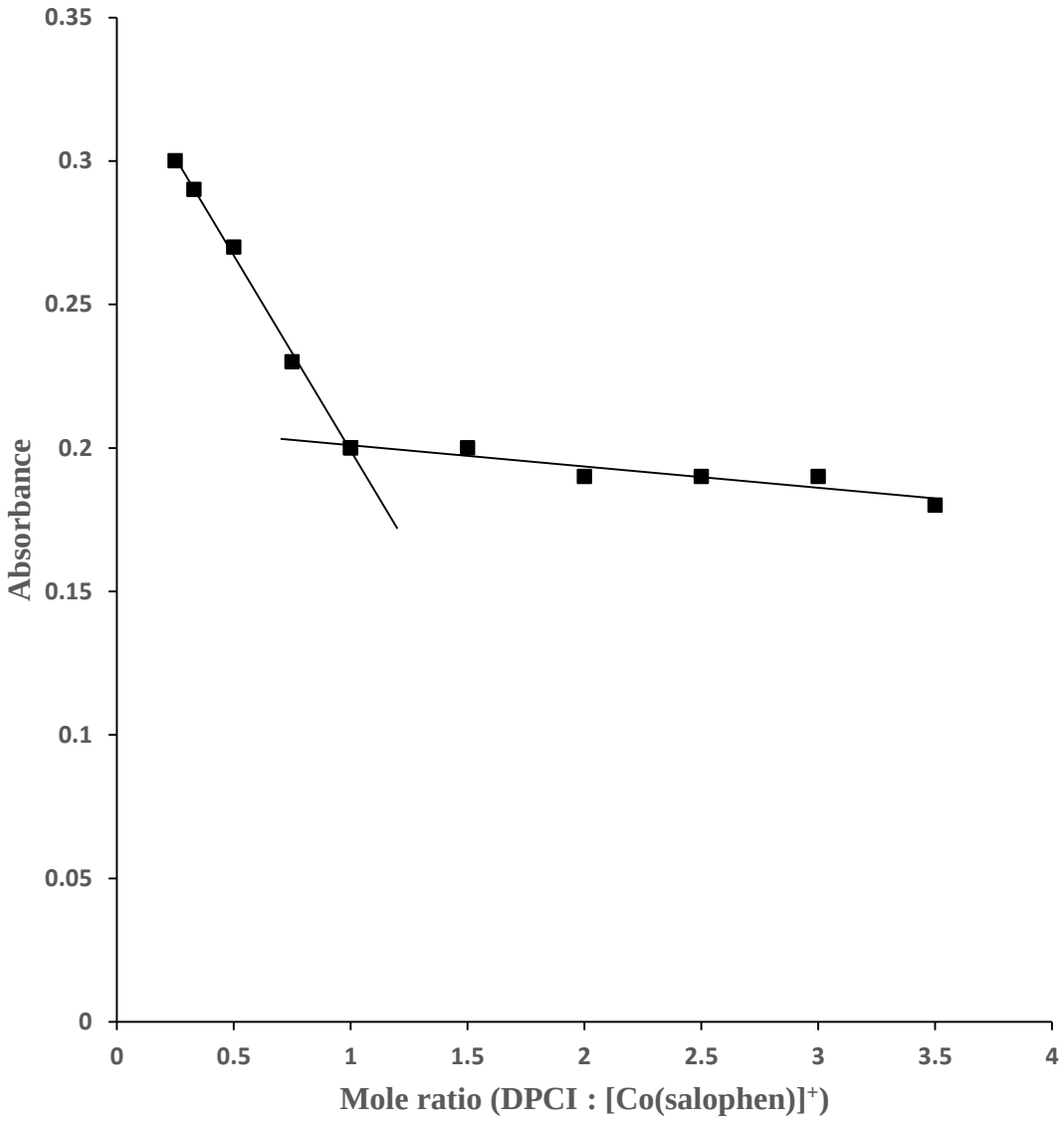


Figure 4.5: Plot of absorbance versus mole ratio for the redox reaction of $[Co(salophen)]^+$ and DPCI at $[Co(salophen)^+] = 1.0 \times 10^{-4}$ mol dm^{-3}, $[H^+] = 0.1$ mol dm^{-3}, $\mu = 0.5$ C^2 mol dm^{-3}, D = 75.83, [DPCI] = $(0.25 - 3.5) \times 10^{-4}$ mol dm^{-3}, T = 300 K and λ_{max} = 470 nm

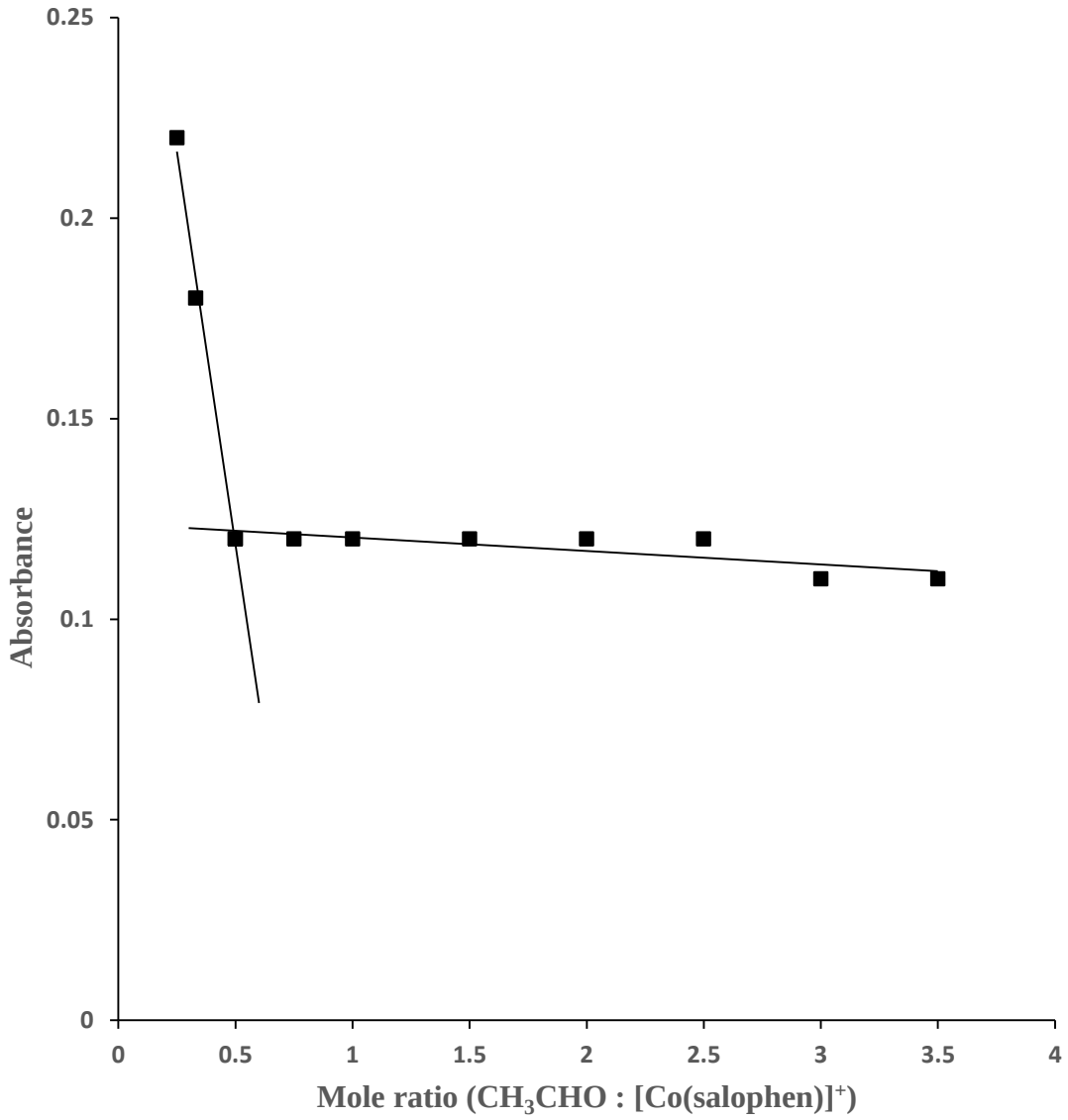


Figure 4.6: Plot of absorbance versus mole ratio for the redox reaction of $[Co(salophen)]^+$ and CH_3CHO at $[Co(salophen)^+] = 3.0 \times 10^{-4}$ mol dm^{-3}, $[H^+] = 4.0 \times 10^{-2}$ mol dm^{-3}, $\mu = 0.2$ C^2 mol dm^{-3}, D = 75.67, $[CH_3CHO] = (0.75 - 10.5) \times 10^{-4}$ mol dm^{-3}, T = 302 K and λ_{max} = 470 nm

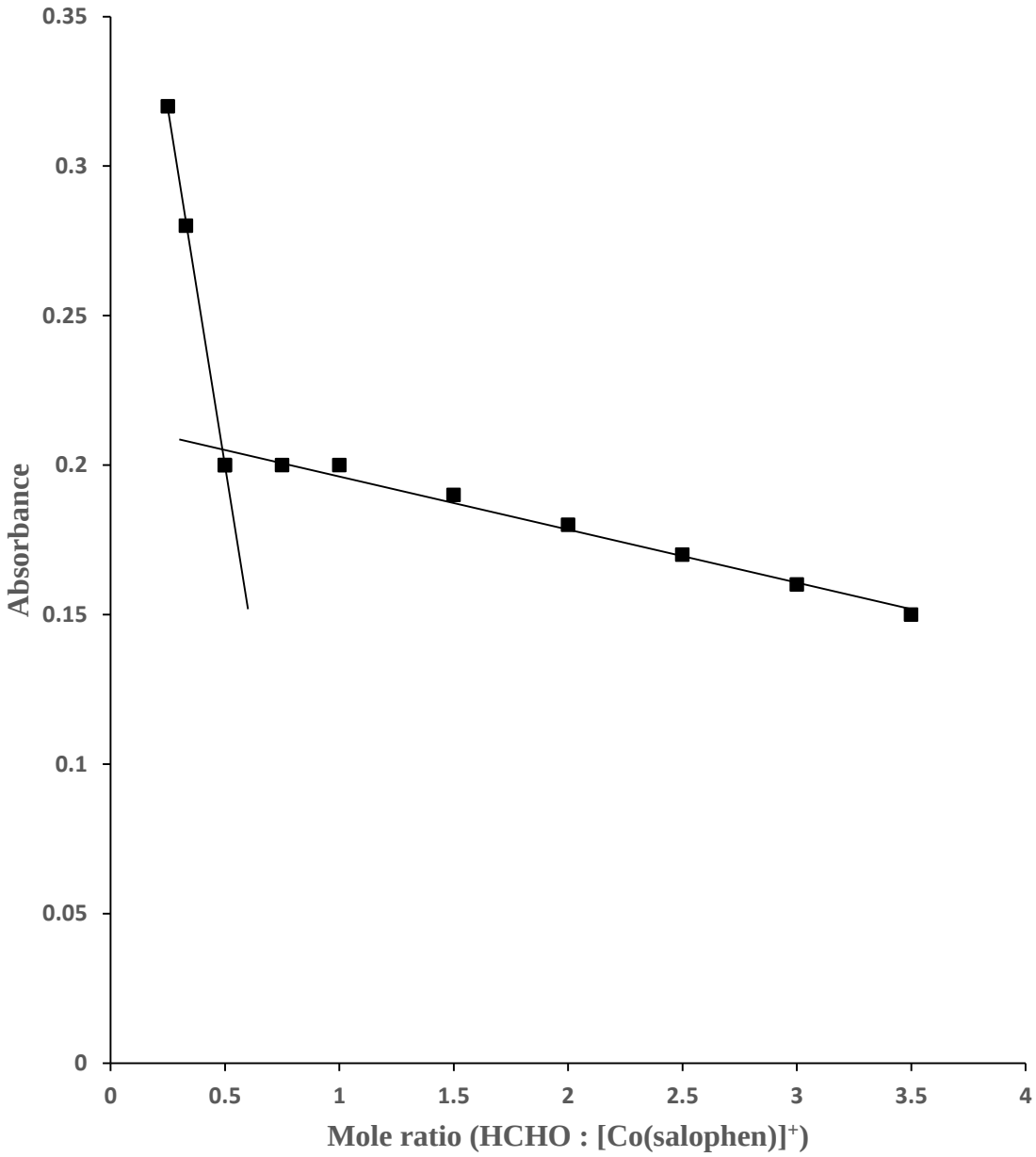


Figure 4.7: Plot of absorbance versus mole ratio for the redox reaction of $[Co(salophen)]^+$ and HCHO at $[Co(salophen)^+] = 3.0 \times 10^{-4}$ mol dm^{-3}, $[H^+] = 0.1$ mol dm^{-3}, $\mu = 0.2$ C^2 mol dm^{-3}, D = 74.78, $[HCHO] = (0.75 - 10.5) \times 10^{-4}$ mol dm^{-3}, T = 299 K and λ_{max} = 470 nm

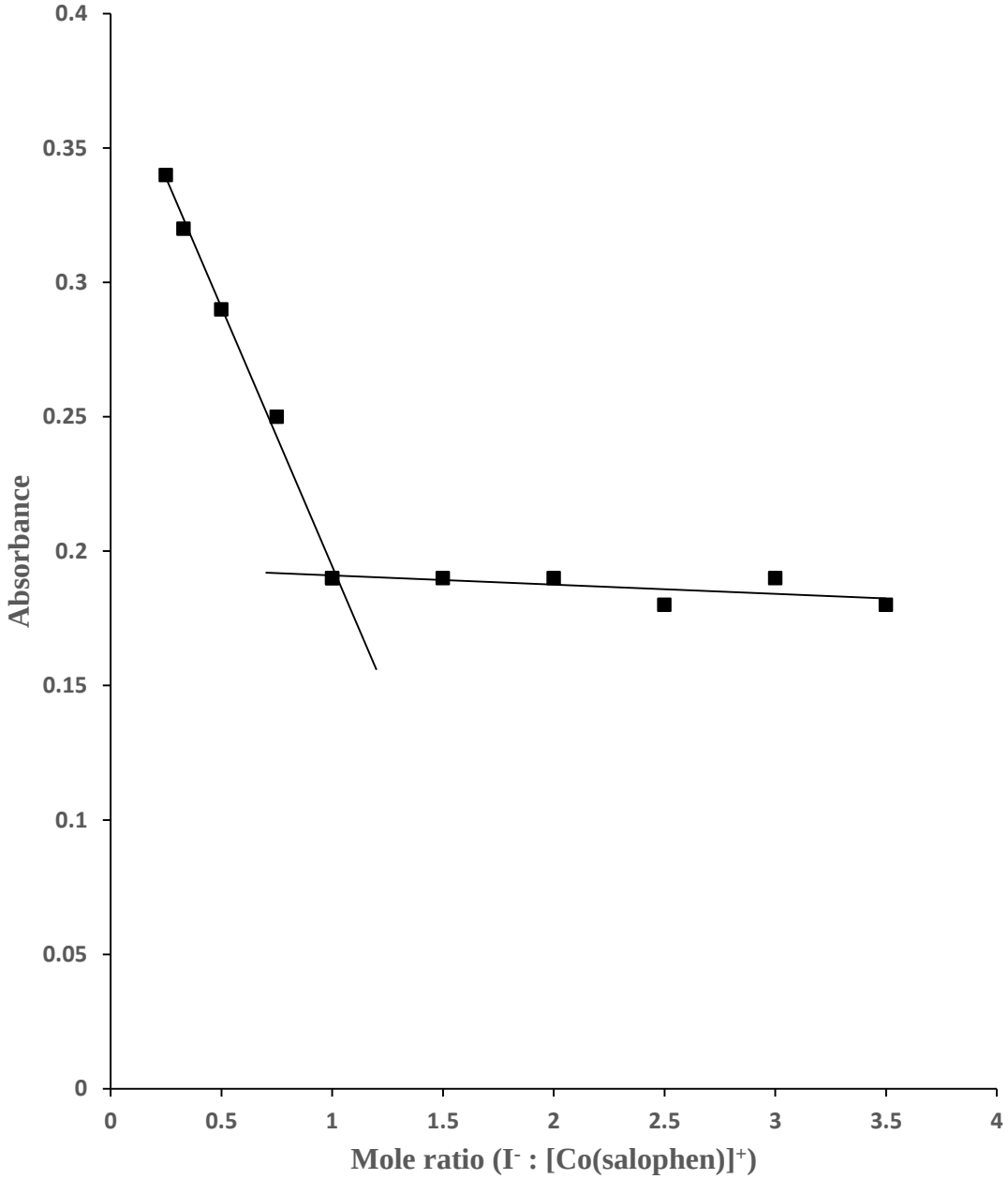


Figure 4.8: Plot of absorbance versus mole ratio for the redox reaction of $[Co(salophen)]^+$ and I^- at $[Co(salophen)^+] = 2.0 \times 10^{-4}$ mol dm^{-3}, $[H^+] = 0.40$ mol dm^{-3}, $\mu = 0.6$ C^2 mol dm^{-3}, D = 78.43, $[I^-] = (0.5 – 7.0) \times 10^{-4}$ mol dm^{-3}, T = 301 K and λ_{max} = 470 nm

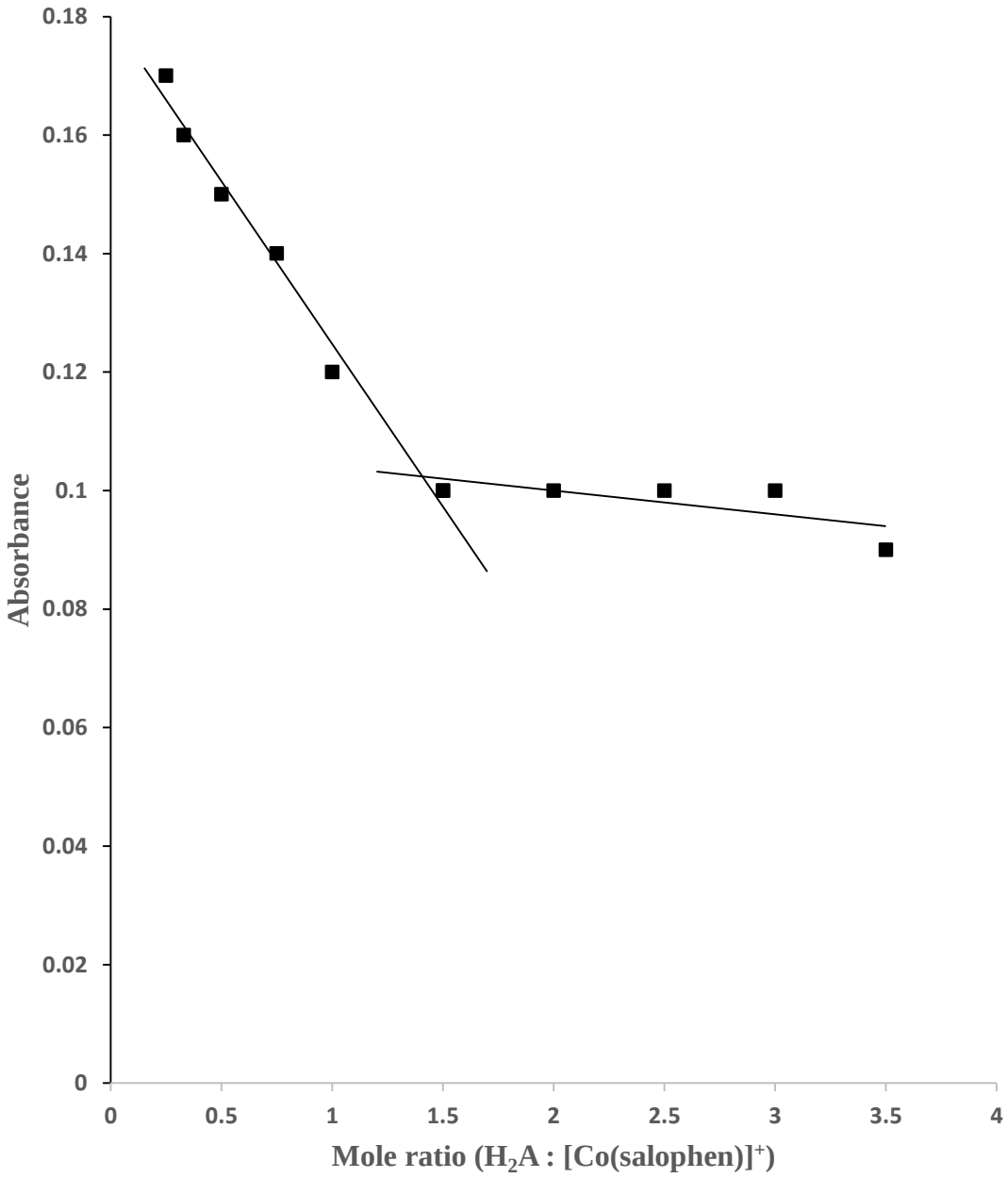


Figure 4.9: Plot of absorbance versus mole ratio for the redox reaction of $[Co(salophen)]^+$ and H_2A at $[Co(salophen)^+] = 3.0 \times 10^{-4}$ mol dm^{-3}, $[H^+] = 2.0 \times 10^{-3}$ mol dm^{-3}, $\mu = 0.1$ C^2 mol dm^{-3}, D = 74.11, $[H_2A] = (0.75 - 10.5) \times 10^{-4}$ mol dm^{-3}, T = 306 K and λ_{max} = 470 nm

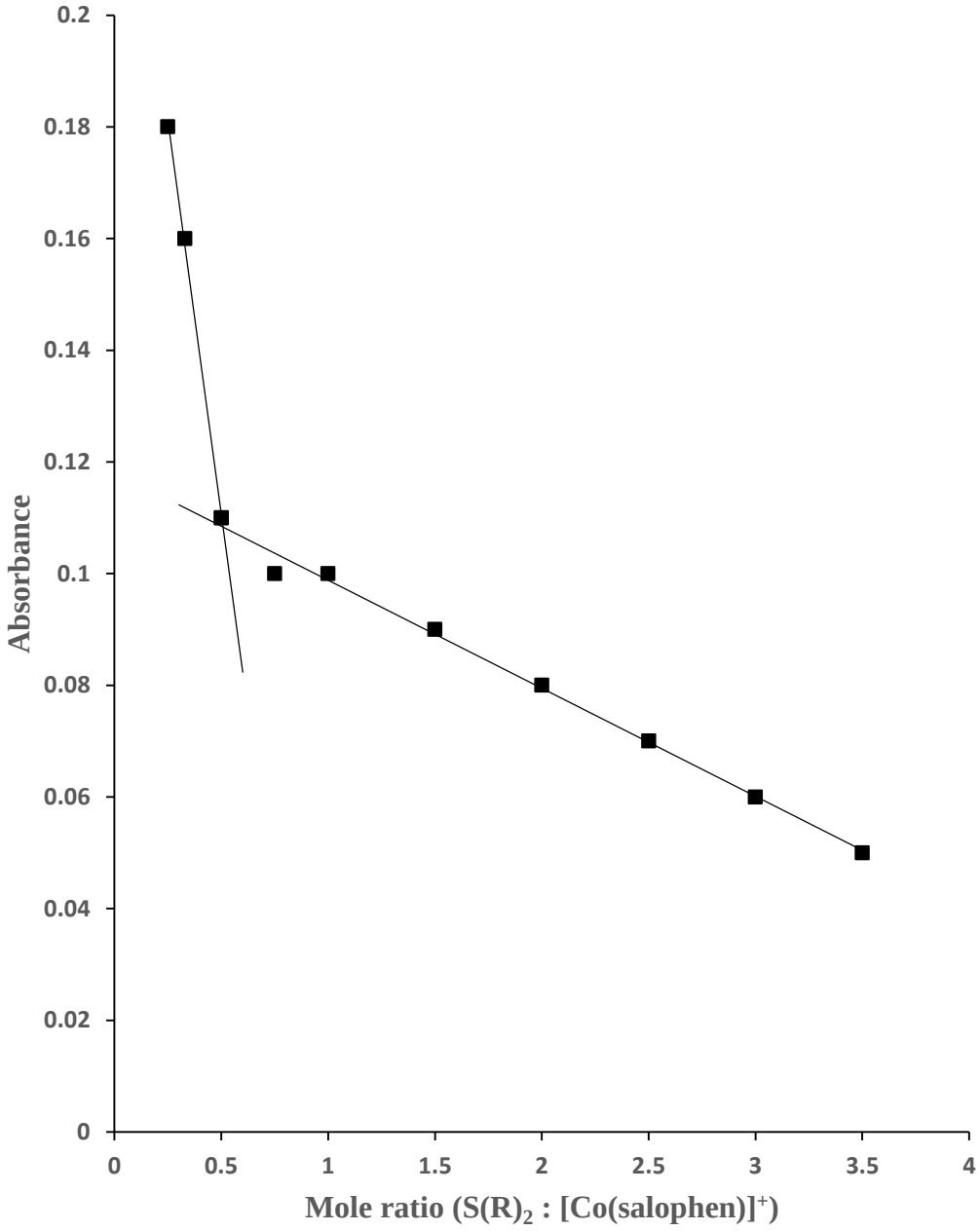
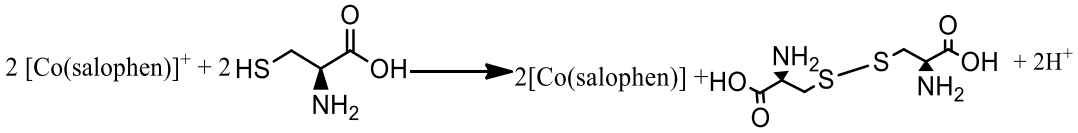
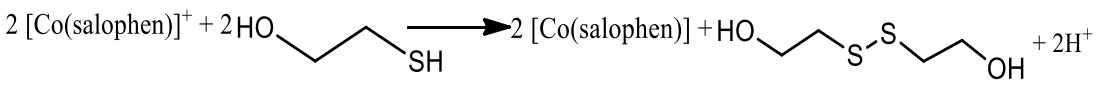


Figure 4.10: Plot of Absorbance versus mole ratio for the redox reaction of $[Co(salophen)]^{+}$ and $S(R)_2$ at $[Co(salophen)^{+}] = 2.0 \times 10^{-4}$ mol dm^{-3}, $[H^{+}] = 5.0 \times 10^{-2}$ mol dm^{-3}, $\mu = 0.2$ C^2 mol dm^{-3}, D = 77.42, $[S(R)_2] = (0.5 - 7.0) \times 10^{-4}$ mol dm^{-3}, T = 305 K and $\lambda_{max} = 470$ nm

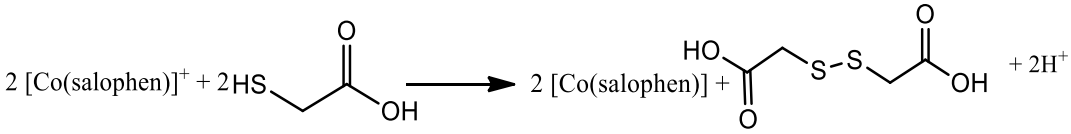
stoichiometries determined, the overall equations of the reactions are represented by equations 4.1 – 4.10.



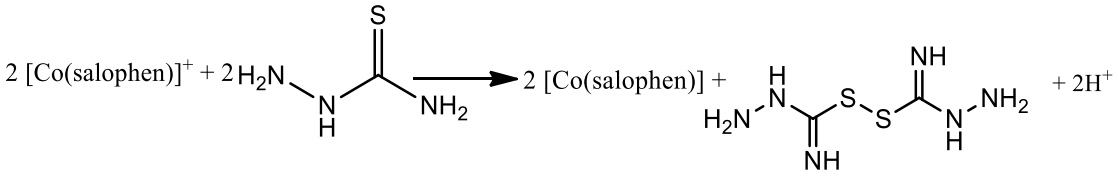
(4.1)



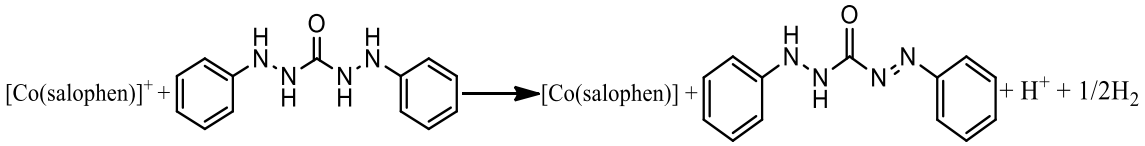
(4.2)



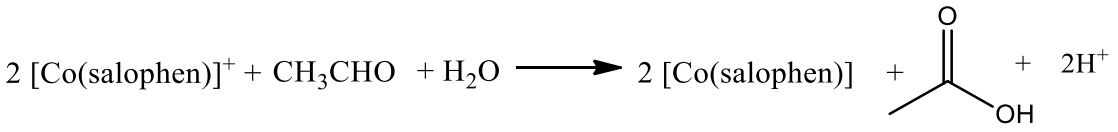
(4.3)



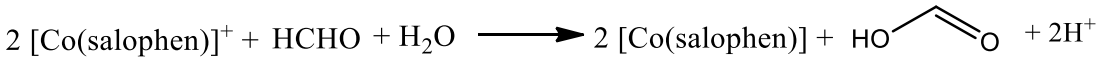
(4.4)



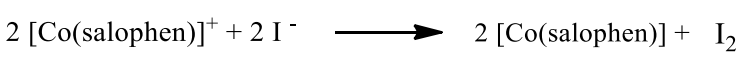
(4.5)



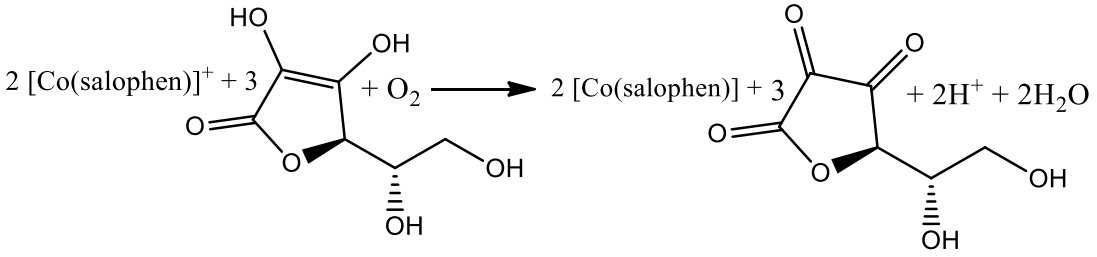
(4.6)



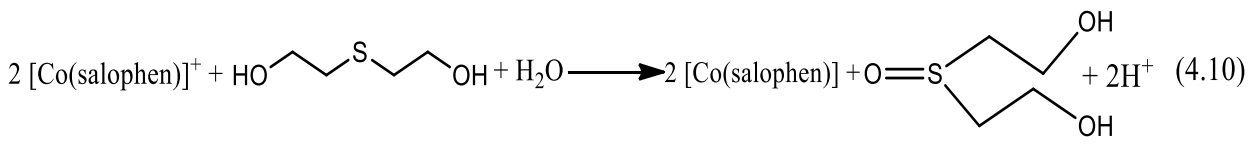
(4.7)



(4.8)



(4.9)



(4.10)

4.3 Product Analyses

The products formed in each of the systems as represented in equations 4.1 – 4.10 at the completion of the reaction are as follows:

a. A blue solution was formed in the separated aqueous layer of the product mixture when 1 cm^3 of potassium thiocyanate (KSCN) in excess acetone was added to all the reacted mixtures of the ten systems which showed the presence of Co(II) (Osunlaja *et al.,* 2013; Osunkwo *et al.,* 2018).

b. The formation of disulphides as the only organic products in the reactions of $[Co(salophen)]^+$/LSH, $[Co(salophen)]^+$/RSH, $[Co(salophen)]^+$/TSH and $[Co(salophen)]^+$/TSCZ were ascertained by comparing the spectra of the reaction mixture after the completion of the reactions with the spectra obtained when the thiols were treated with hydrogen peroxide (Appendices IV - VII) which is known to oxidise thiols to disulphides (Idris *et al.,* 2005).

   Also, formation of disulphides was further confirmed by the appearance of crystals in the diethyl ether extracts (organic layer) left overnight to dry (Mohammed, 2015; Nkole *et al.,* 2018).

c. The oxidation of diphenylcarbazide to diphenylcarbazone was determined by comparing the spectrum of the reactant ($[Co(salophen)]^+$/DPCI) with that of the reaction product. The wavelength of maximum absorption (λ_{max}) of 280 nm which is the characteristic peak of the diphenylcarbazide shifted to 305 nm which is the peak for diphenylcarbazone (Willems and De Ranter, 1974; Ramírez *et al.,* 1996). The spectra are presented as

Appendices VIII and IX. FTIR spectroscopic analysis carried out on the diphenylcarbazide and the reaction product showed a carbonyl peak (C=O) at 1654 and 1666 cm^{-1} respectively (Appendices X and XI).

d. A white precipitate observed which turned lime water milky due the evolution of carbon dioxide gas, confirmed the presence of carboxylic acid for the reactions of $[Co(salophen)]^{+}/CH_3CHO$ and $[Co(salophen)]^{+}/HCHO$ (Vogel, 1996).

e. The formation of iodine was confirmed by its characteristic bluish-black colour when the reaction product was mixed with starch solution for the $[Co(salophen)]^{+}/I^{-}$ reaction (Ukoha and Iyun, 1999).

f. After mixing the reaction mixture with pyrrole in excess trichloroacetic acid, blue-green colour was observed. This confirmed the oxidation of ascorbic acid to dehydroascorbic acid (Abiti *et al.,* 2018).

g. The formation of an orange-coloured spot confirmed the presence of sulphoxide for the reaction of $[Co(salophen)]^{+}/S(R)_2$ (Suchomelova *et al.,* 1965).

4.4 Pseudo-first Order and Second Order Rate Constants and Order of Reactions

The graphs of log ($A_t - A_\infty$) versus time (where A_t and A_∞ are the absorbances of the reaction at time t, and at the end of the reaction respectively) for all the systems obtained under pseudo-first order conditions were linear suggesting the reactions to be first order with respect to each of the oxidant (complex). Pseudo-first order rate constants, k_1, were obtained from the slopes of the graphs of log ($A_t - A_\infty$) versus time. Typical plots are shown in Figures 4.11 – 4.20.

The order of the reactions with respect to [reductants] for each of the system studied was determined from the slopes of the graphs of log k_1 versus log [reductant] (Figures 4.21 - 4.30).

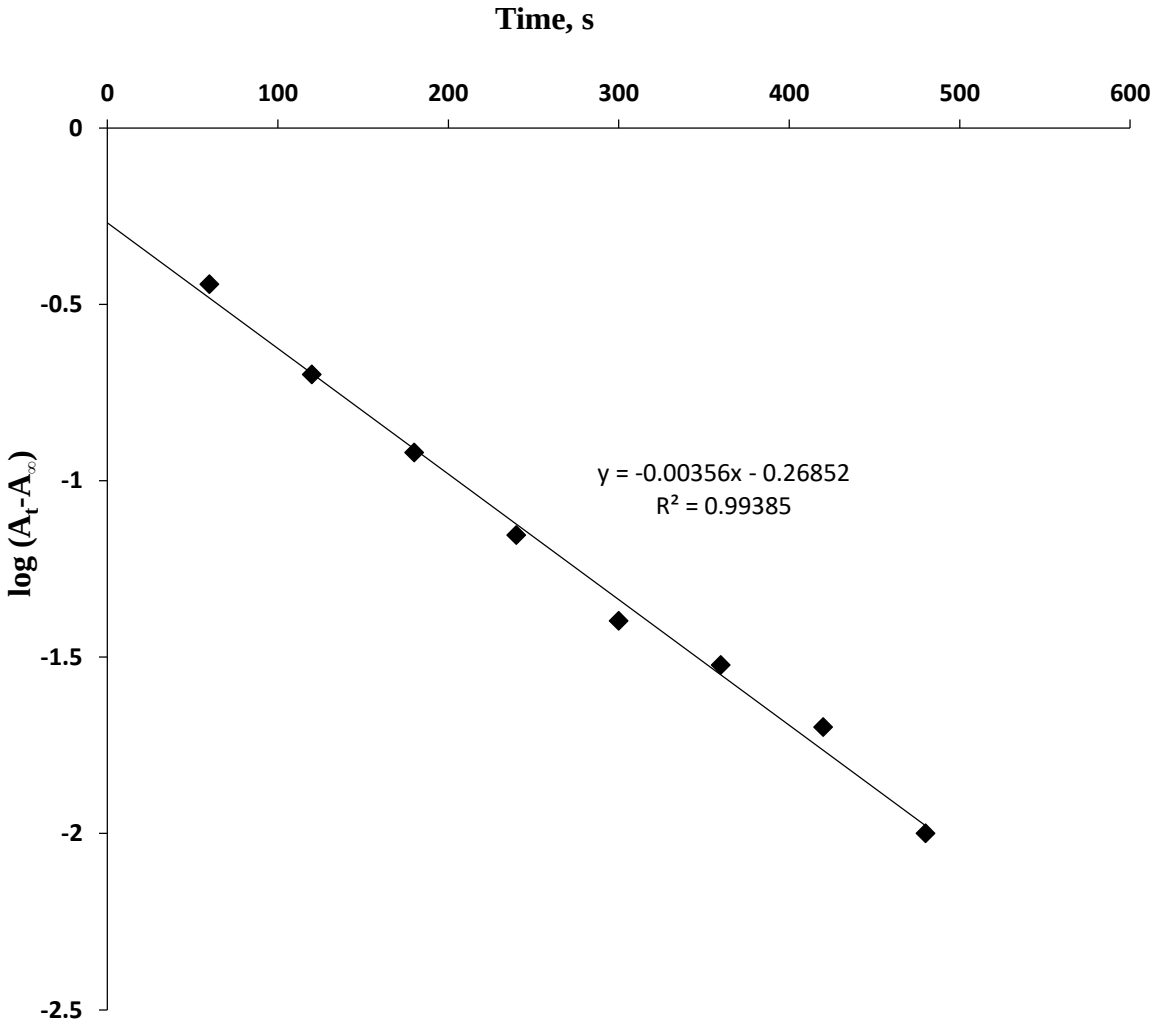


Figure 4.11: Typical pseudo-first order plot for the redox reaction of $[Co(salophen)]^+$ and LSH at $[Co(salophen)^+] = 2.0 \times 10^{-4}$ mol dm^{-3}, [LSH] = 12.0×10^{-3} mol dm^{-3}, $[H^+] = 1.0 \times 10^{-3}$ mol dm^{-3}, $\mu = 0.1$ C^2 mol dm^{-3}, D = 74.84, T = 300 K and λ_{max} = 470 nm

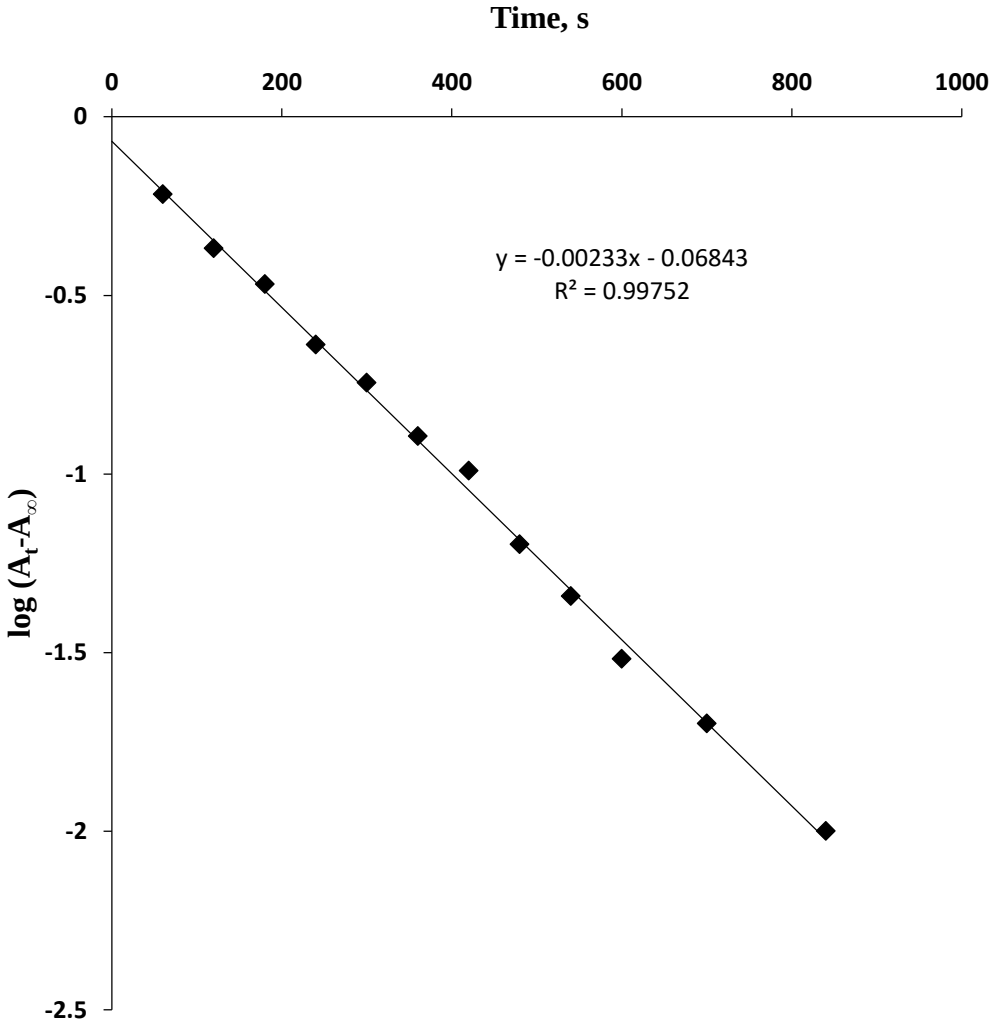


Figure 4.12: Typical pseudo-first order plot for the redox reaction of $[Co(salophen)]^+$ and RSH at $[Co(salophen)^+] = 3.0 \times 10^{-4}$ mol dm^{-3}, $[RSH] = 15.0 \times 10^{-3}$ mol dm^{-3}, $[H^+] = 1.4 \times 10^{-3}$ mol dm^{-3}, $\mu = 0.1$ C^2 mol dm^{-3}, D = 74.19, T = 300 K and λ_{max} = 470 nm

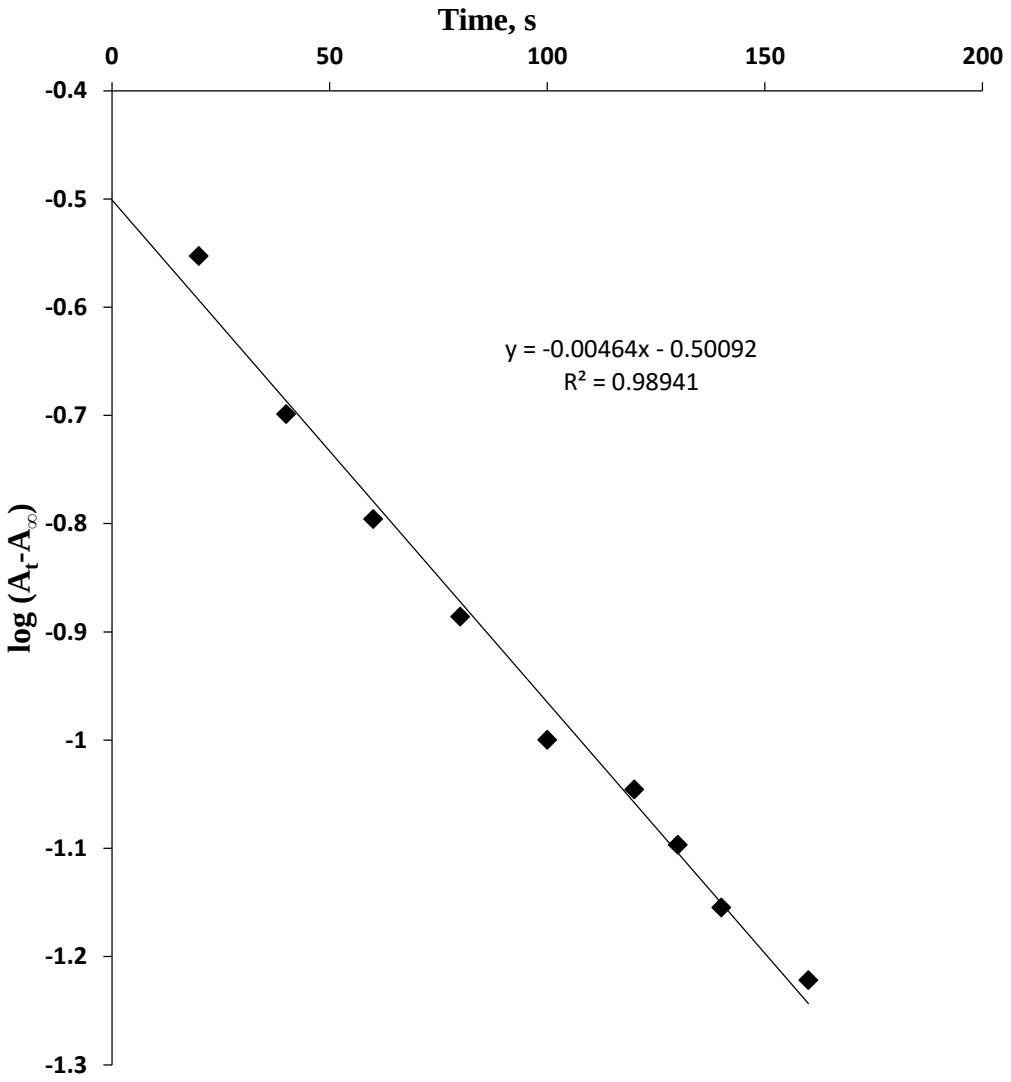


Figure 4.13: Typical pseudo-first order plot for the redox reaction of $[Co(salophen)]^{+}$ and TSH at $[Co(salophen)^{+}] = 3.0 \times 10^{-4}$ mol dm^{-3}, $[TSH] = 7.5 \times 10^{-3}$ mol dm^{-3}, $\mu = 0.1$ C^2 mol dm^{-3}, D = 74.04, T = 300 K and $\lambda_{max} = 470$ nm

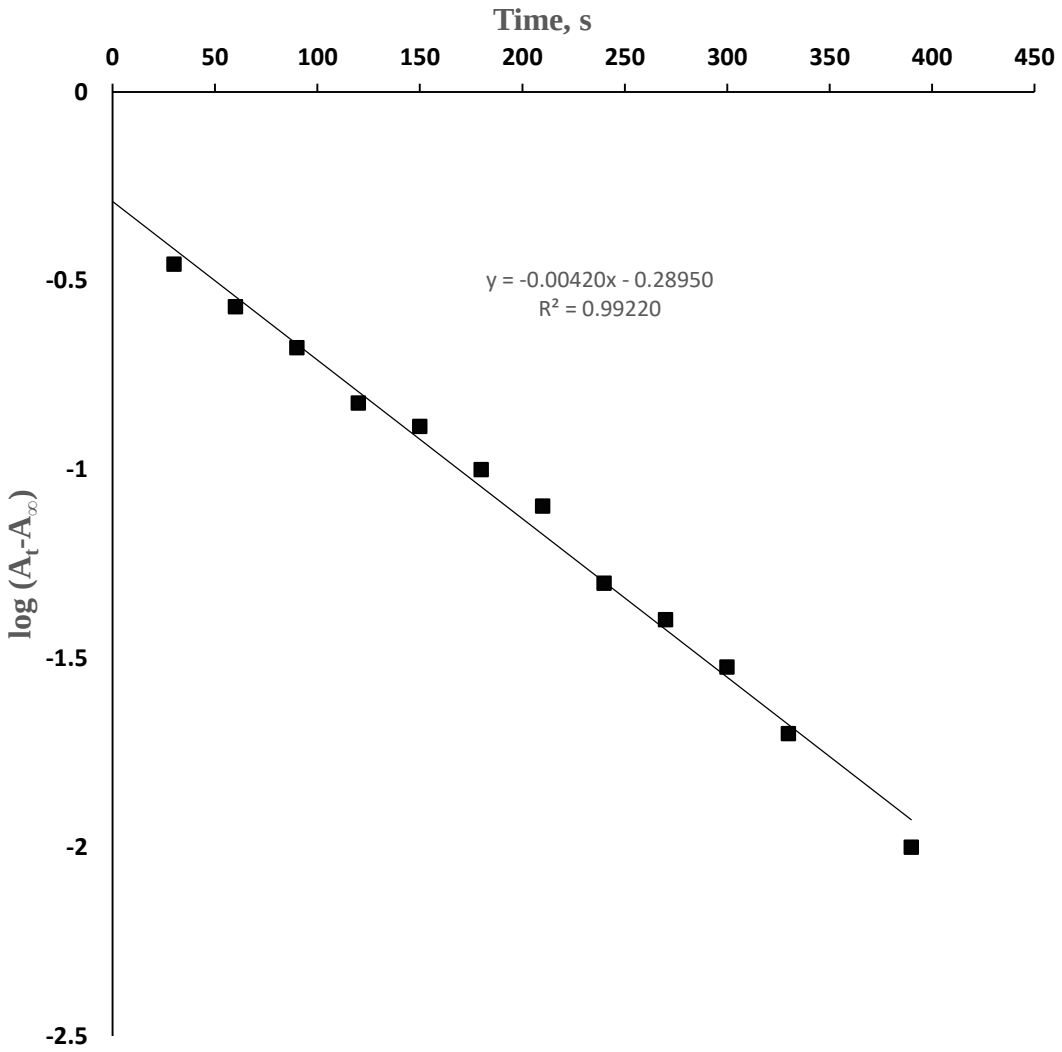


Figure 4.14: Typical pseudo-first order plot for the redox reaction of $[Co(salophen)]^{+}$ and TSCZ at $[Co(salophen)^{+}] = 2.0 \times 10^{-4}$ mol dm^{-3}, $[TSCZ] = 8.0 \times 10^{-2}$ mol dm^{-3}, $[H^{+}] = 1.0 \times 10^{2}$ mol dm^{-3}, $\mu = 0.1$ C^2 mol dm^{-3}, D = 74.41, T = 306 K and λ_{max} = 470 nm

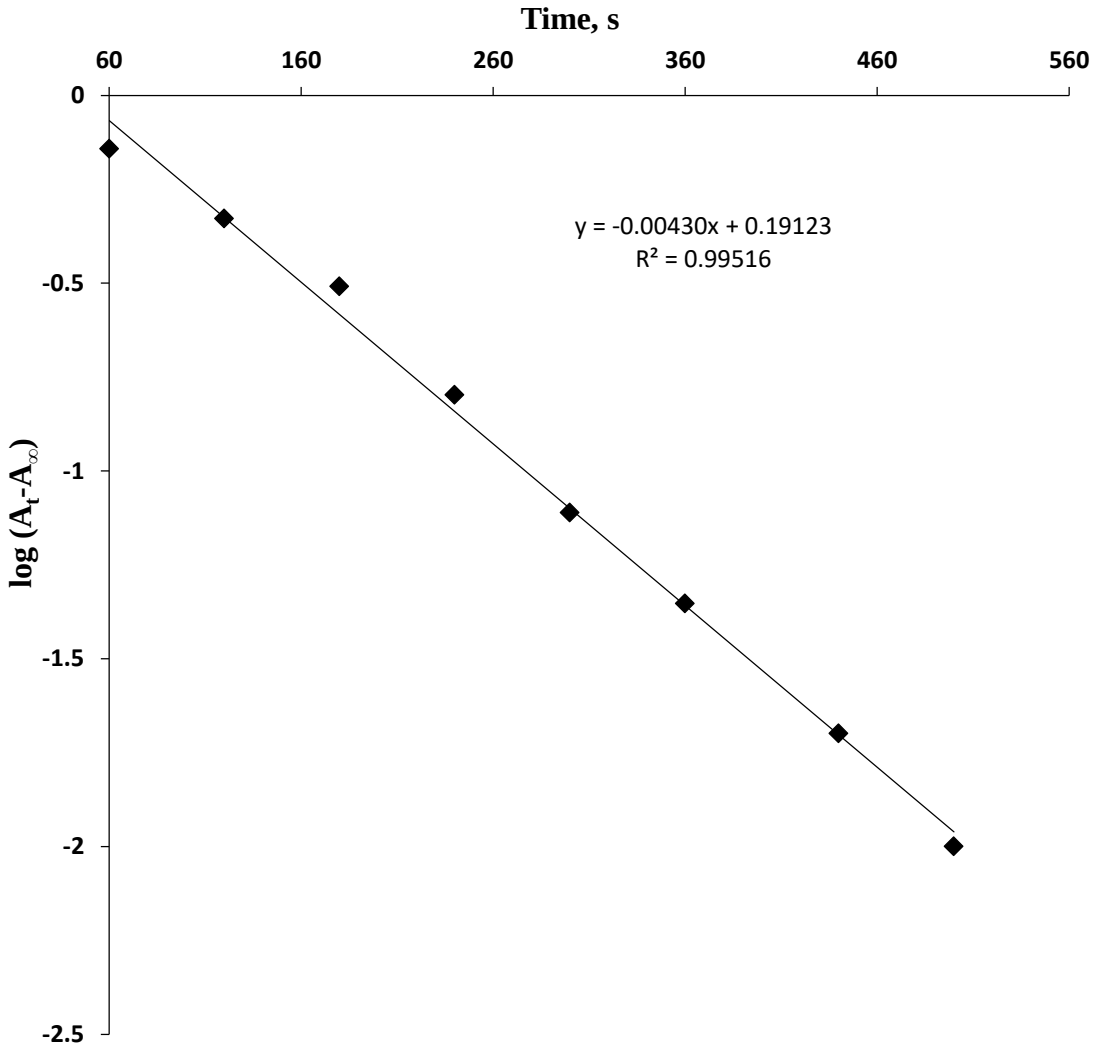


Figure 4.15: Typical pseudo-first order plot for the redox reaction of $[Co(salophen)]^{+}$ and DPCI at $[Co(salophen)^{+}] = 1.0 \times 10^{-4}$ mol dm^{-3}, [DPCI] = 25.0×10^{-3} mol dm^{-3}, $[H^{+}] = 0.1$ mol dm^{-3}, $\mu = 0.5$ C^2 mol dm^{-3}, D = 75.83, T = 300 K and λ_{max} = 470 nm

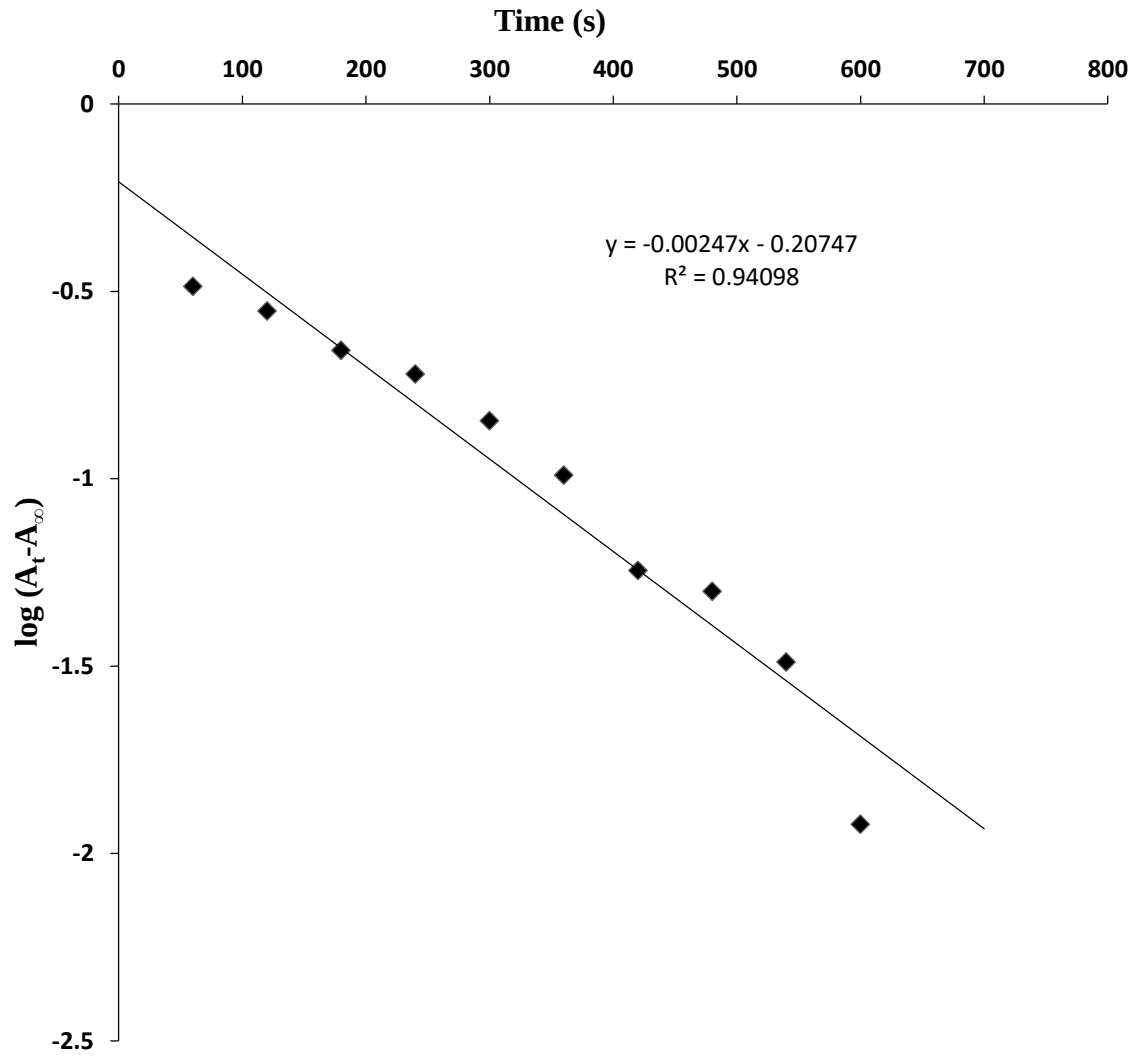


Figure 4.16: Typical pseudo-first order plot for the redox reaction of $[Co(salophen)]^{+}$ and CH_3CHO at $[Co(salophen)^{+}] = 3.0 \times 10^{-4}$ mol dm^{-3}, $[CH_3CHO] = 13.5 \times 10^{-2}$ mol dm^{-3}, $[H^{+}] = 4.0 \times 10^{-2}$ mol dm^{-3}, $\mu = 0.2$ C^2 mol dm^{-3}, D = 75.67, T = 302 K and $\lambda_{max} = 470$ nm

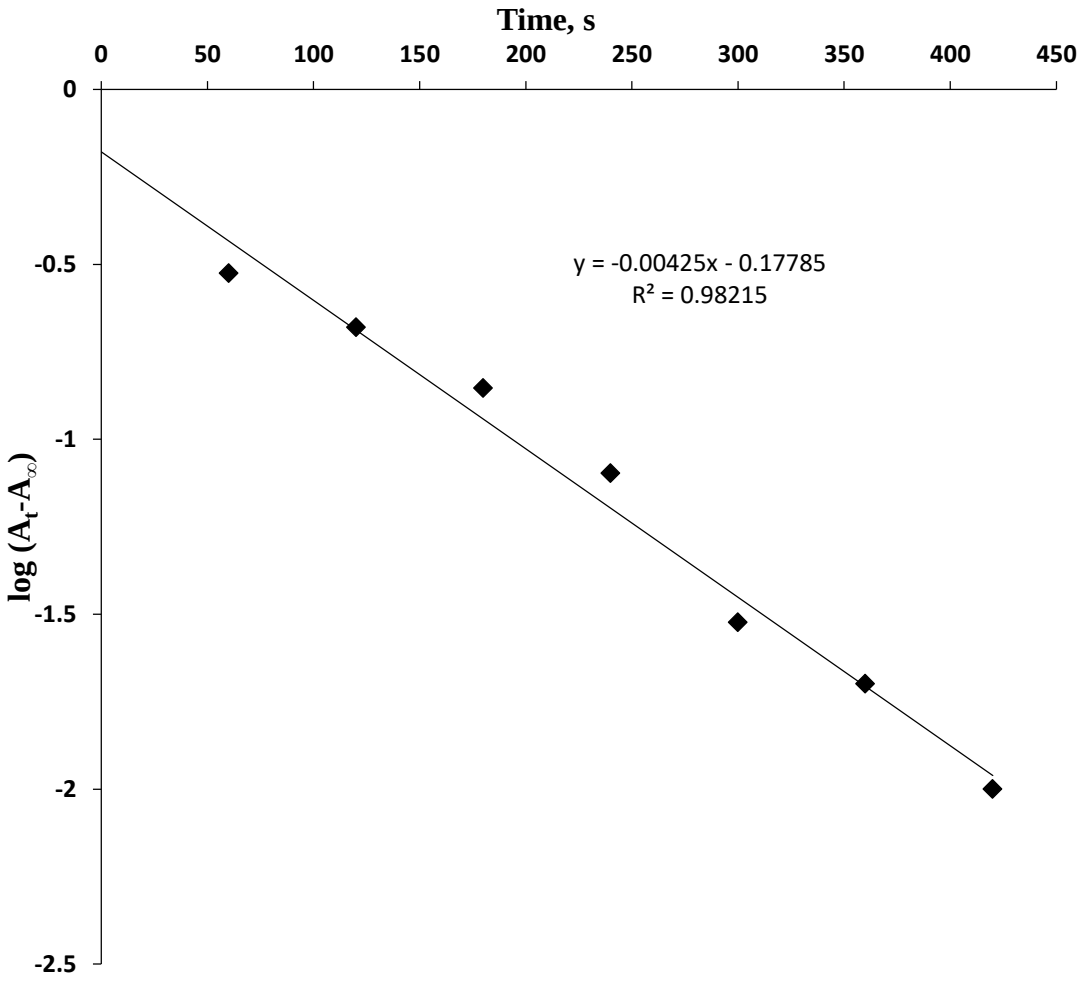


Figure 4.17: Typical pseudo-first order plot for the redox reaction of $[Co(salophen)]^+$ and HCHO at $[Co(salophen)^+] = 3.0 \times 10^{-4}$ mol dm^{-3}, $[HCHO] = 18 \times 10^{-4}$ mol dm^{-3}, $[H^+] = 0.1$ mol dm^{-3}, $\mu = 0.2$ C^2 mol dm^{-3}, D = 74.78, T = 299 K and λ_{max} = 470 nm

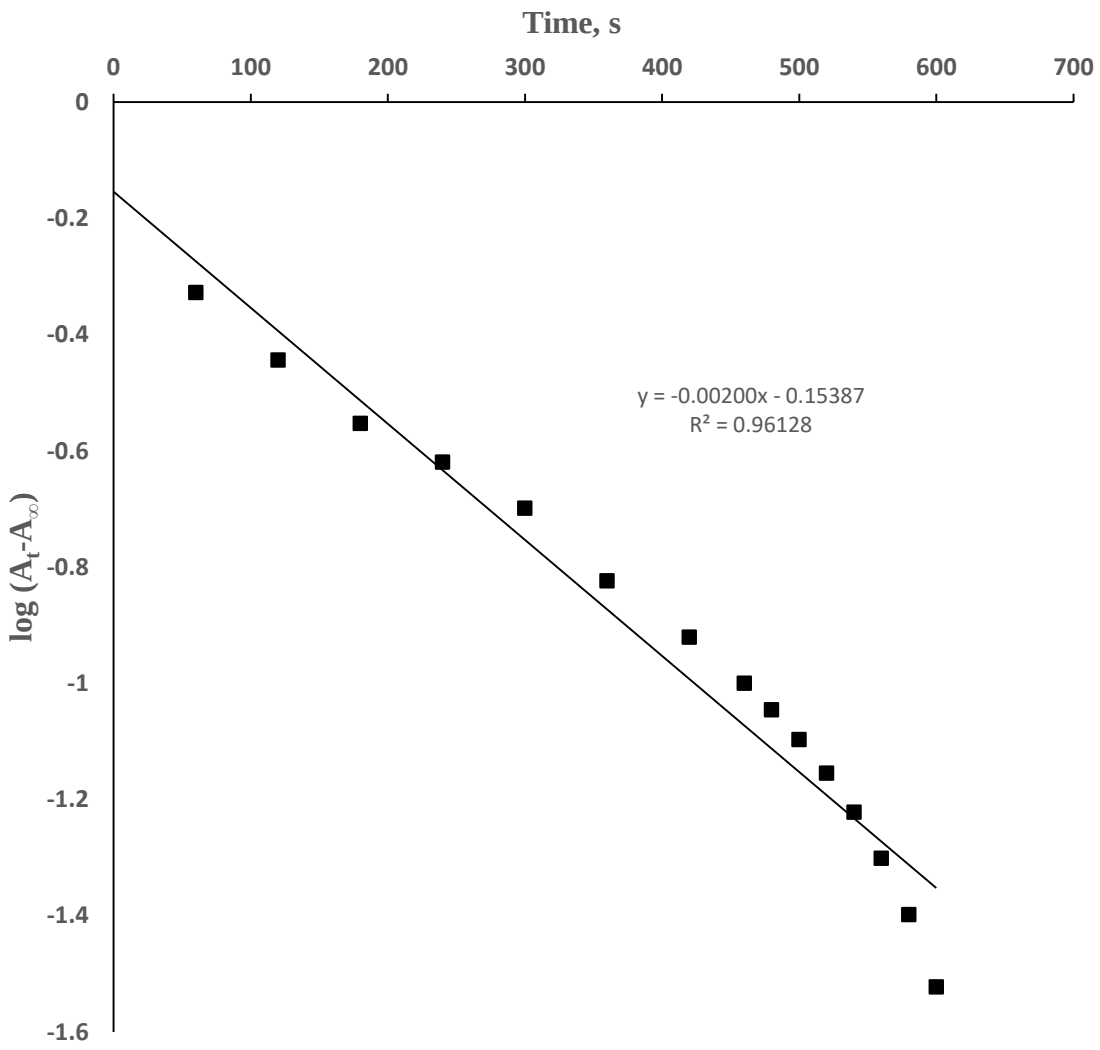


Figure 4.18: Typical pseudo-first order plot for the redox reaction of $[Co(salophen)]^{+}$ and I^{-} at $[Co(salophen)^{+}] = 2.0 \times 10^{-4}$ mol dm^{-3}, $[I^{-}] = 16.0 \times 10^{-2}$ mol dm^{-3} $[H^{+}] = 0.40$ mol dm^{-3}, $\mu = 0.6$ C^2 mol dm^{-3}, D = 78.43, T = 301 K and $\lambda_{max} = 470$ nm

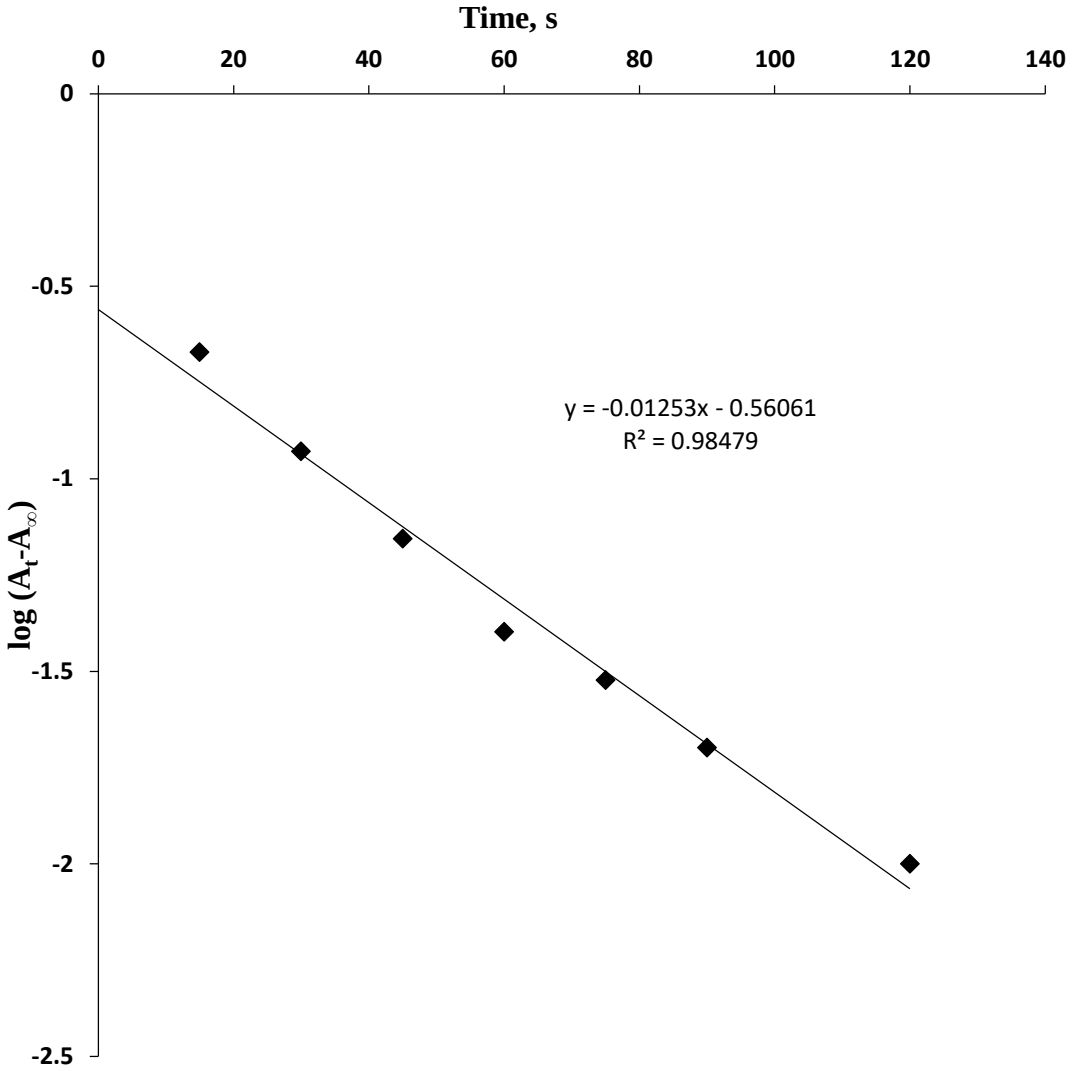


Figure 4.19: Typical pseudo-first order plot for the redox reaction of $[Co(salophen)]^{+}$ and H_2A at $[Co(salophen)^{+}] = 3.0 \times 10^{-4}$ mol dm^{-3}, $[H_2A] = 12.0 \times 10^{-3}$ mol dm^{-3}, $[H^{+}] = 2.0 \times 10^{-3}$ mol dm^{-3}, $\mu = 0.1$ C^2 mol dm^{-3}, D = 74.11, T = 306 K and λ_{max} = 470 nm

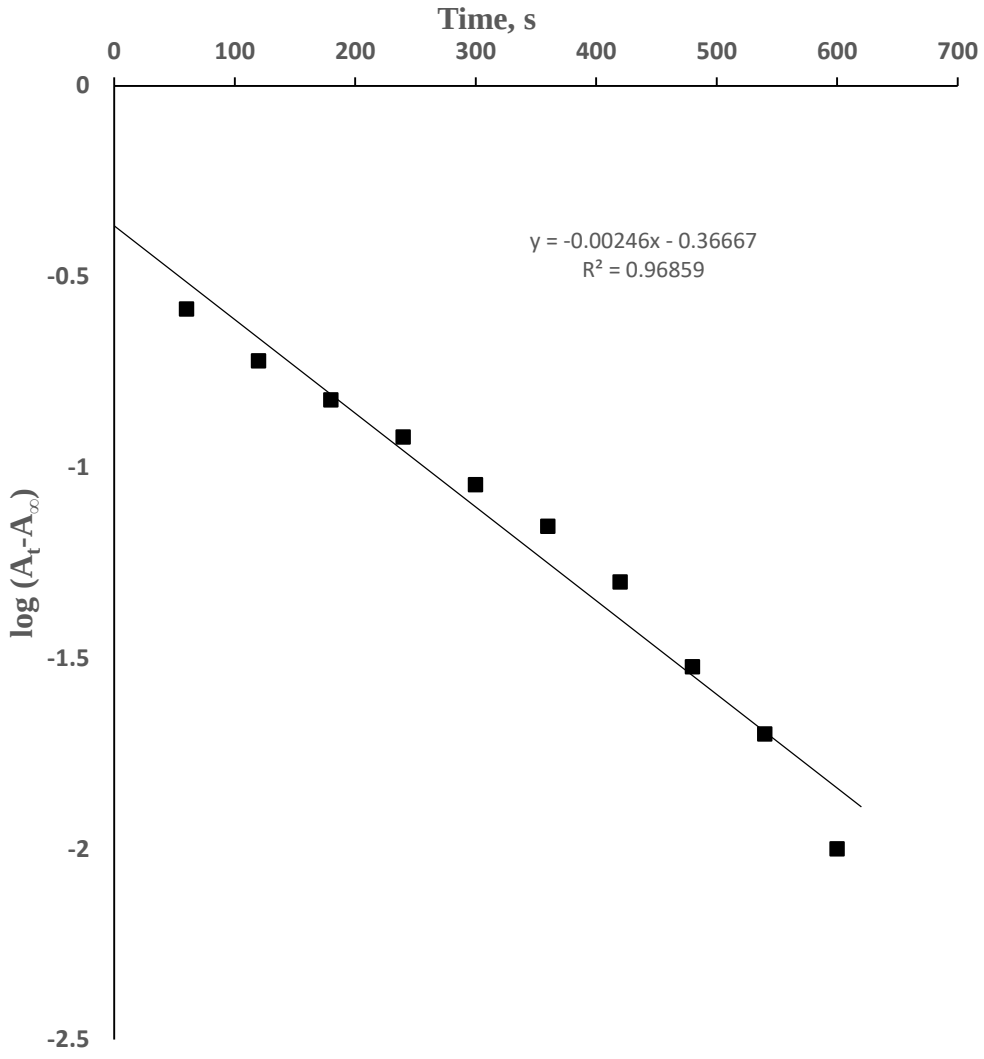


Figure 4.20: Typical pseudo-first order plot for the redox reaction of $[Co(salophen)]^+$ and $S(R)_2$ at $[Co(salophen)^+] = 2.0 \times 10^{-4}$ mol dm^{-3}, $[S(R)_2] = 16.0 \times 10^{-2}$ mol dm^{-3}, $[H^+] = 5.0 \times 10^{-2}$ mol dm^{-3}, $\mu = 0.2$ C^2 mol dm^{-3}, D = 77.42, T = 305 K and λ_{max} = 470 nm

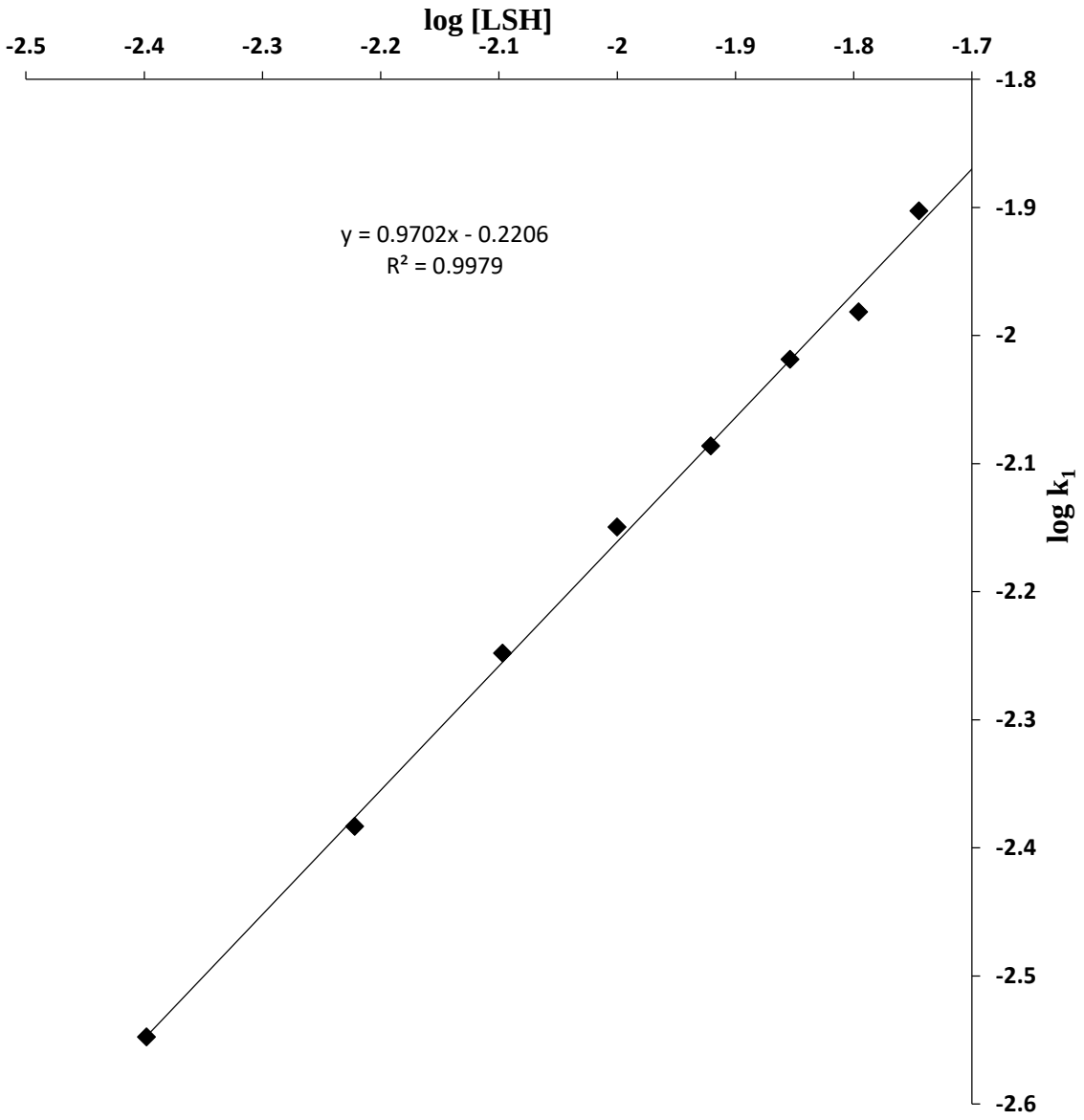


Figure 4.21: Plot of log k_1 versus log [LSH] for the redox reaction of $[Co(salophen)]^+$ and LSH at $[Co(salophen)^+] = 2.0 \times 10^{-4}$ mol dm^{-3}, [LSH] = (4.0 – 18.0) $\times 10^{-3}$ mol dm^{-3}, $[H^+] = 1.0 \times 10^{-3}$ mol dm^{-3}, $\mu = 0.1$ C^2 mol dm^{-3}, D = 74.84, T = 300 K and λ_{max} = 470 nm

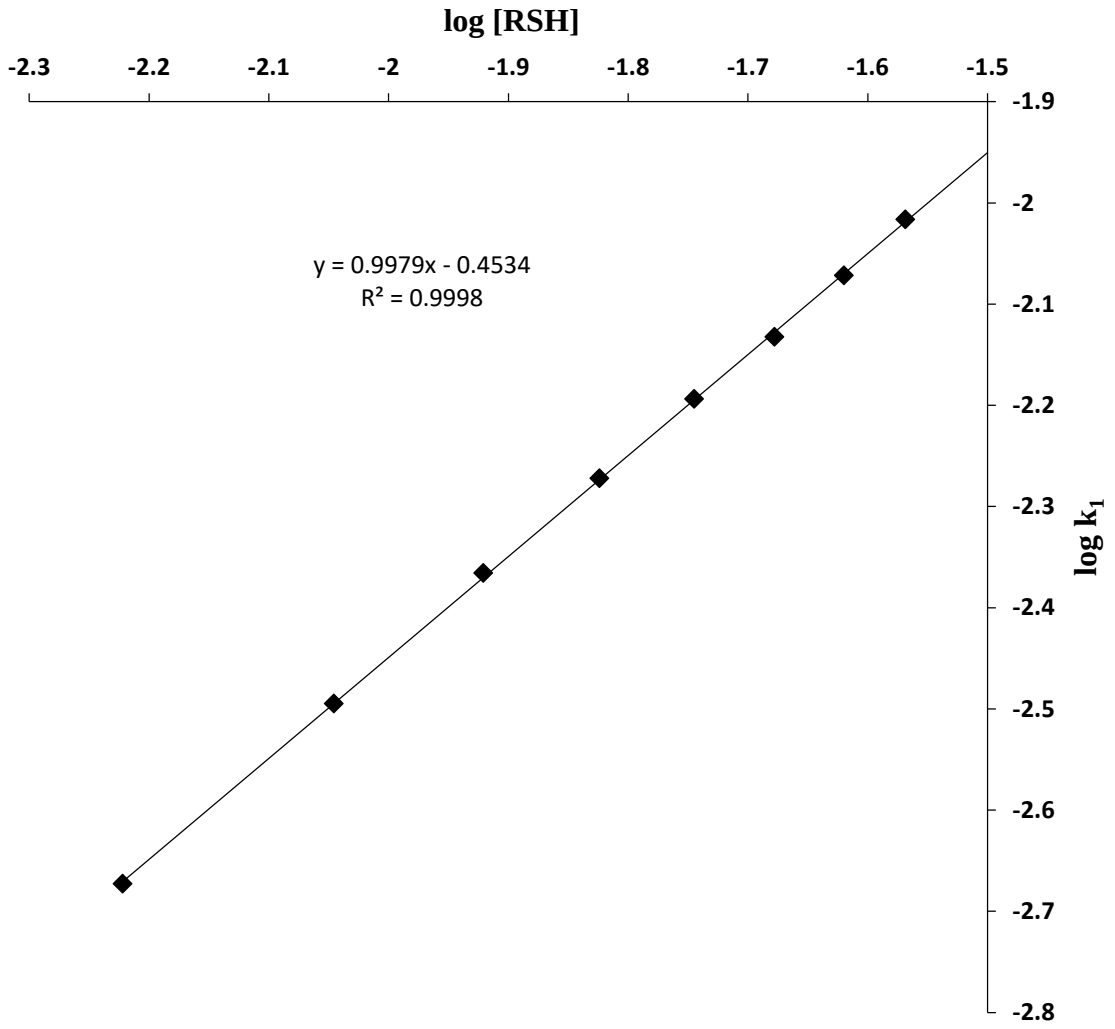


Figure 4.22: Plot of logk_1 versus log [RSH] for the redox reaction of $[Co(salophen)]^+$ and RSH at $[Co(salophen)^+] = 3.0 \times 10^{-4}$ mol dm^{-3}, [RSH] = (6.0 – 27.0) $\times 10^{-3}$ mol dm^{-3}, $[H^+] = 1.4 \times 10^{-3}$ mol dm^{-3}, $\mu = 0.1$ C^2 mol dm^{-3}, D = 74.19, T = 300 K and λ_{max} = 470 nm

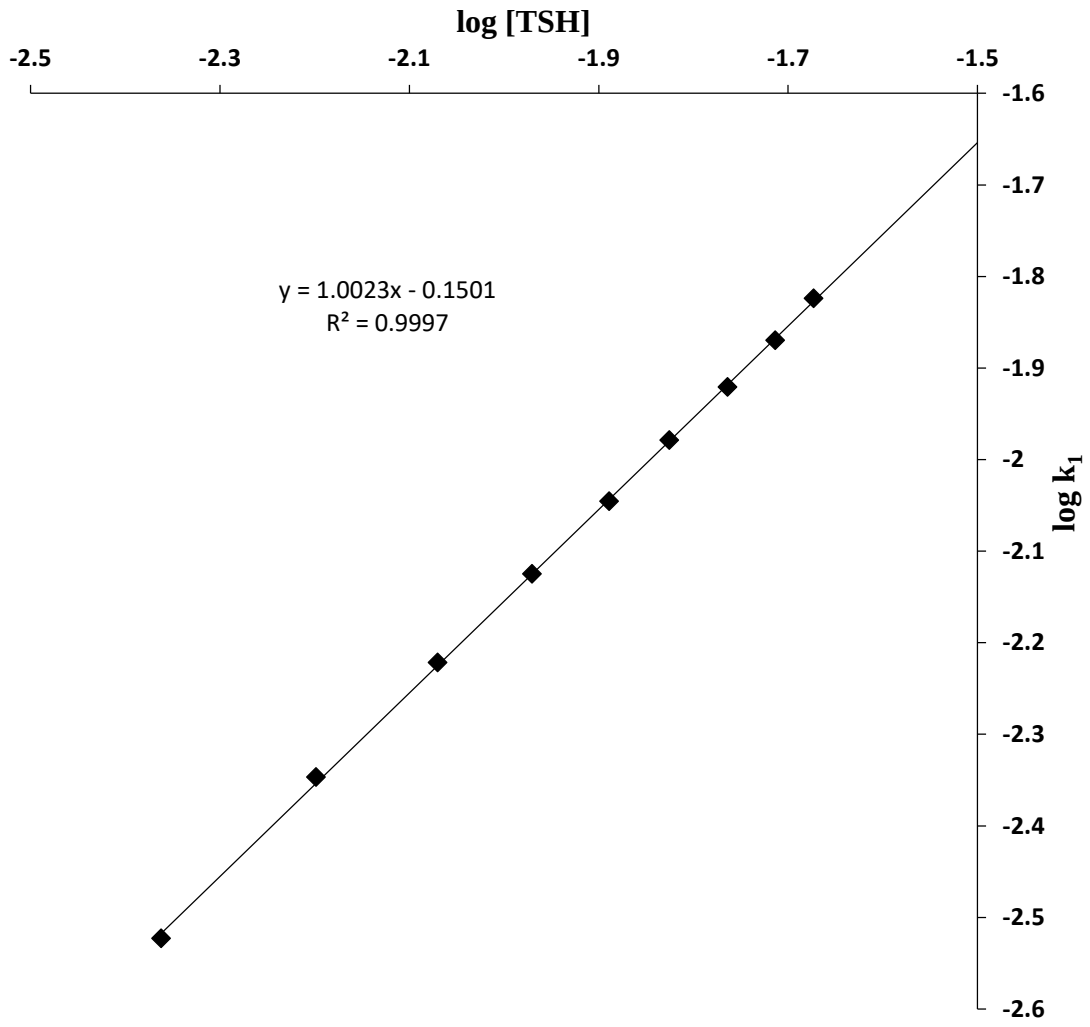


Figure 4.23: Plot of log k_1 versus log [TSH] for the redox reaction of $[Co(salophen)]^+$ and TSH at $[Co(salophen)^+] = 3.0 \times 10^{-4}$ mol dm^{-3}, [TSH] = $(3.0 – 15.0) \times 10^{-3}$ mol dm^{-3}, $\mu = 0.1$ C^2 mol dm^{-3}, D = 74.04, T = 300 K and λ_{max} = 470 nm

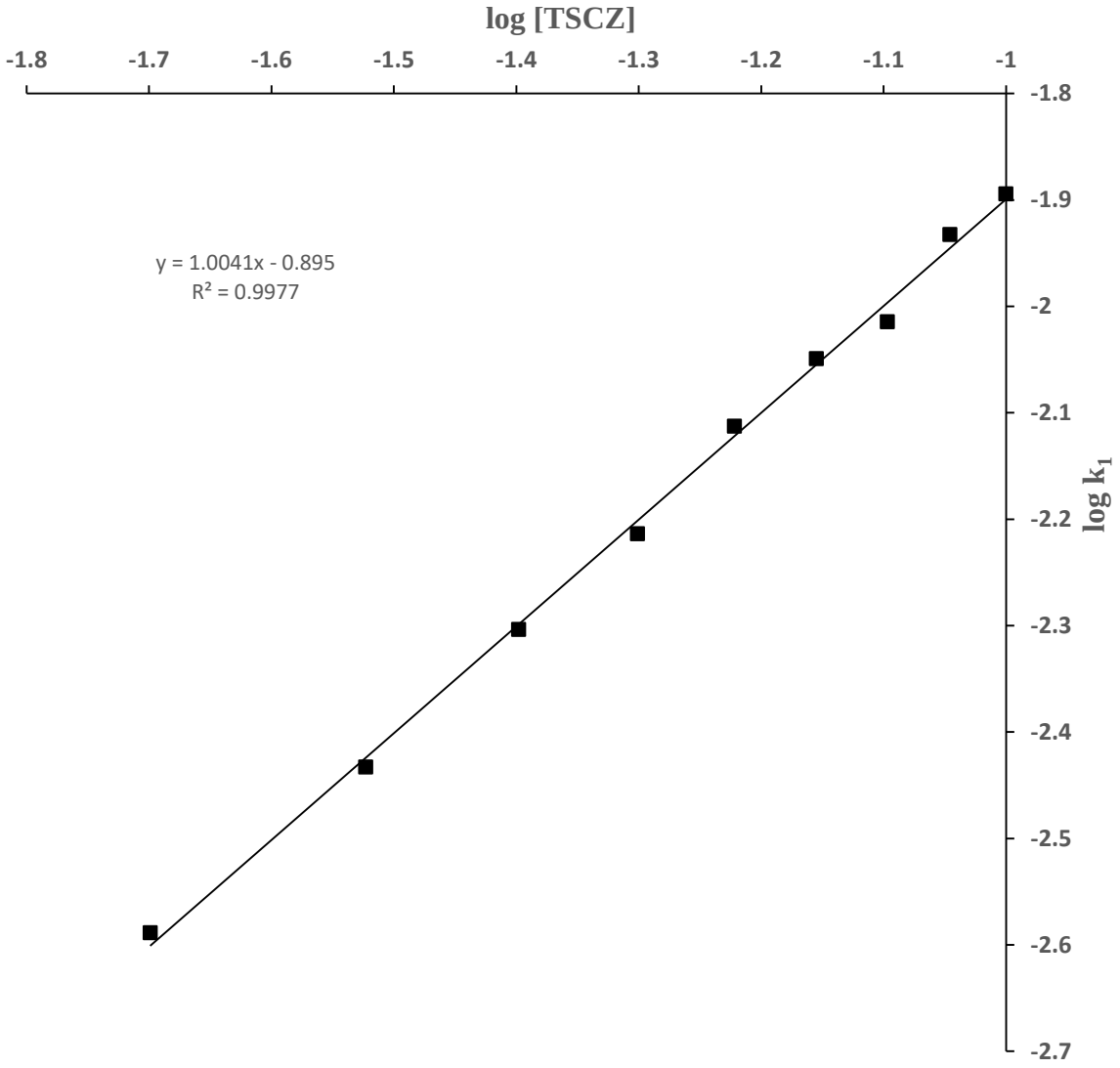


Figure 4.24: Plot of log k_1 versus log [TSCZ] for the redox reaction of $[Co(salophen)]^+$ and TSCZ at $[Co(salophen)^+] = 2.0 \times 10^{-4}$ mol dm^{-3}, [TSCZ] = (2.0 - 10.0) × 10^{-2} mol dm^{-3}, $[H^+] = 1.0 \times 10^{-2}$ mol dm^{-3}, $\mu = 0.1$ C^2 mol dm^{-3}, D = 74.41, T = 306 K and λ_{max} = 470 nm

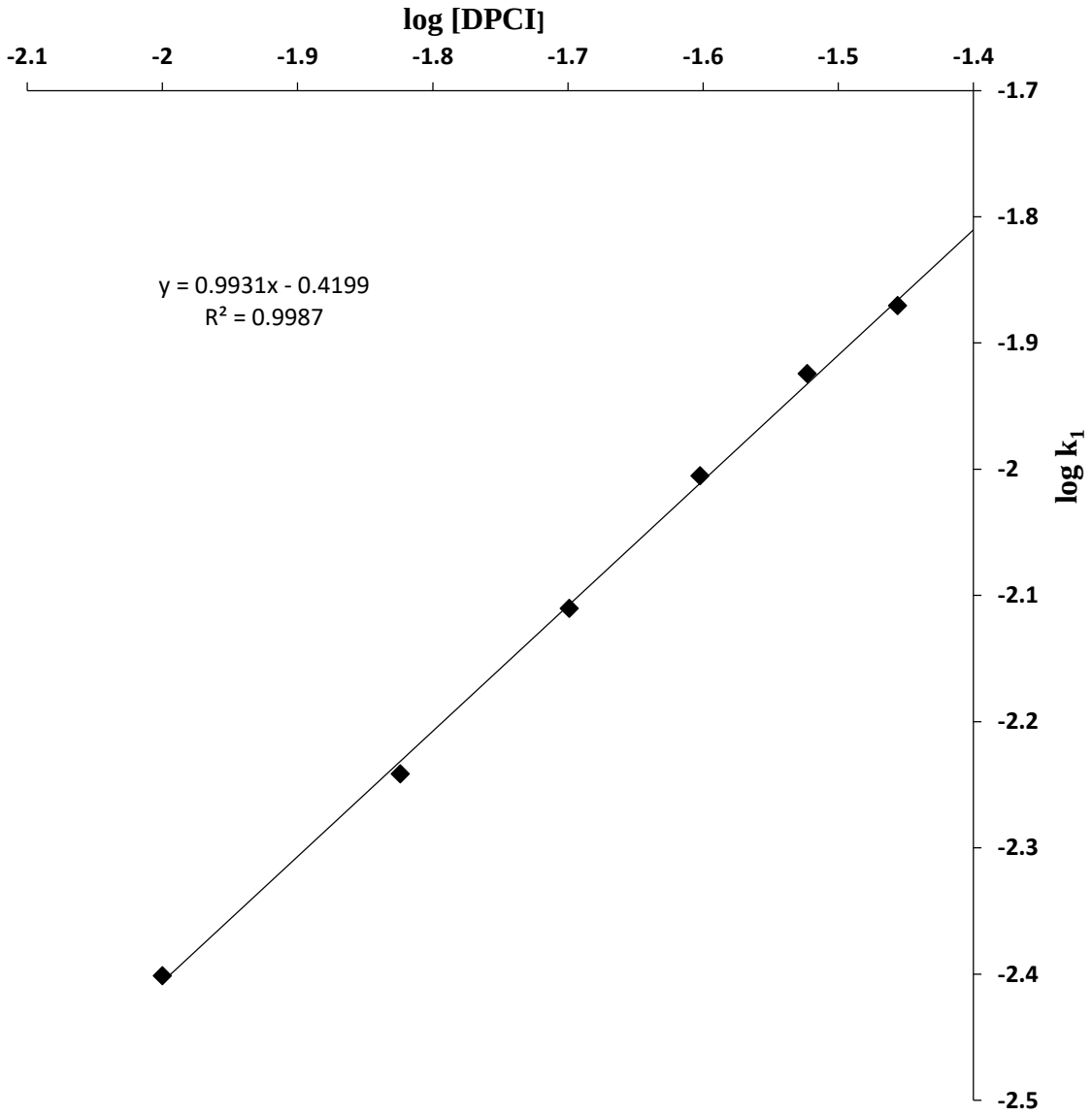


Figure 4.25: Plot of log k_1 versus log [DPCI] for the redox reaction of $[Co(salophen)]^+$ and DPCI at $[Co(salophen)^+] = 1.0 \times 10^{-4}$ mol dm^{-3}, [DPCI] = (10.0 - 45.0) × 10^{-3} mol dm^{-3} $[H^+]$ = 0.1 mol dm^{-3}, μ = 0.5 C^2 mol dm^{-3}, D = 75.83, T = 300 K and λ_{max} = 470 nm

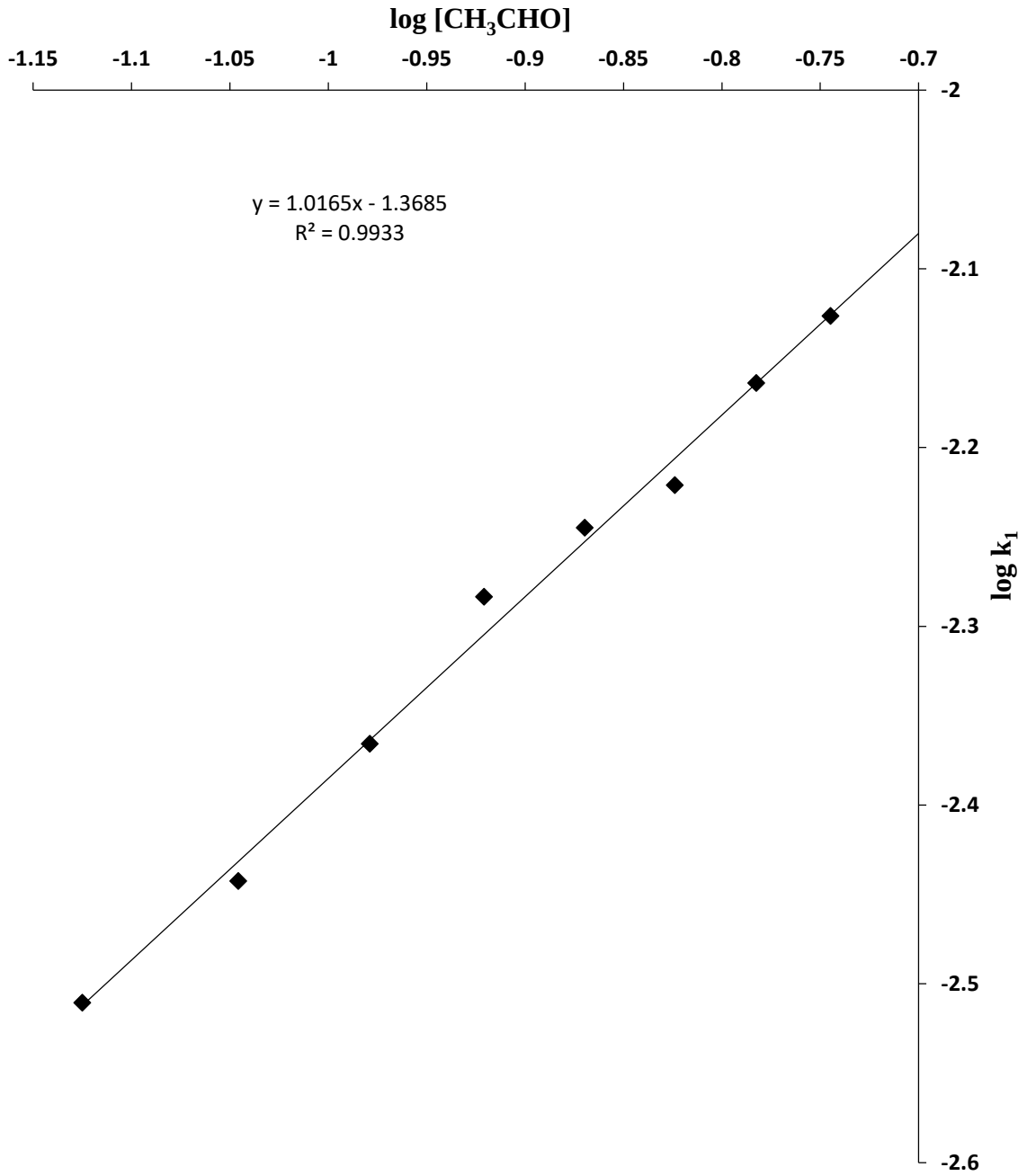


Figure 4.26: Plot of log k_1 versus log [CH_3CHO] for the redox reaction of [Co(salophen)]$^+$ and CH_3CHO at [Co(salophen)$^+$] = 3.0×10^{-4} mol dm^{-3}, [CH_3CHO] = (7.5 - 18.0) × 10^{-2} mol dm^{-3}, [H^+] = 4.0×10^{-2} mol dm^{-3}, μ = 0.2 C^2 mol dm^{-3}, D = 75.67, T = 302 K and λ_{max} = 470 nm

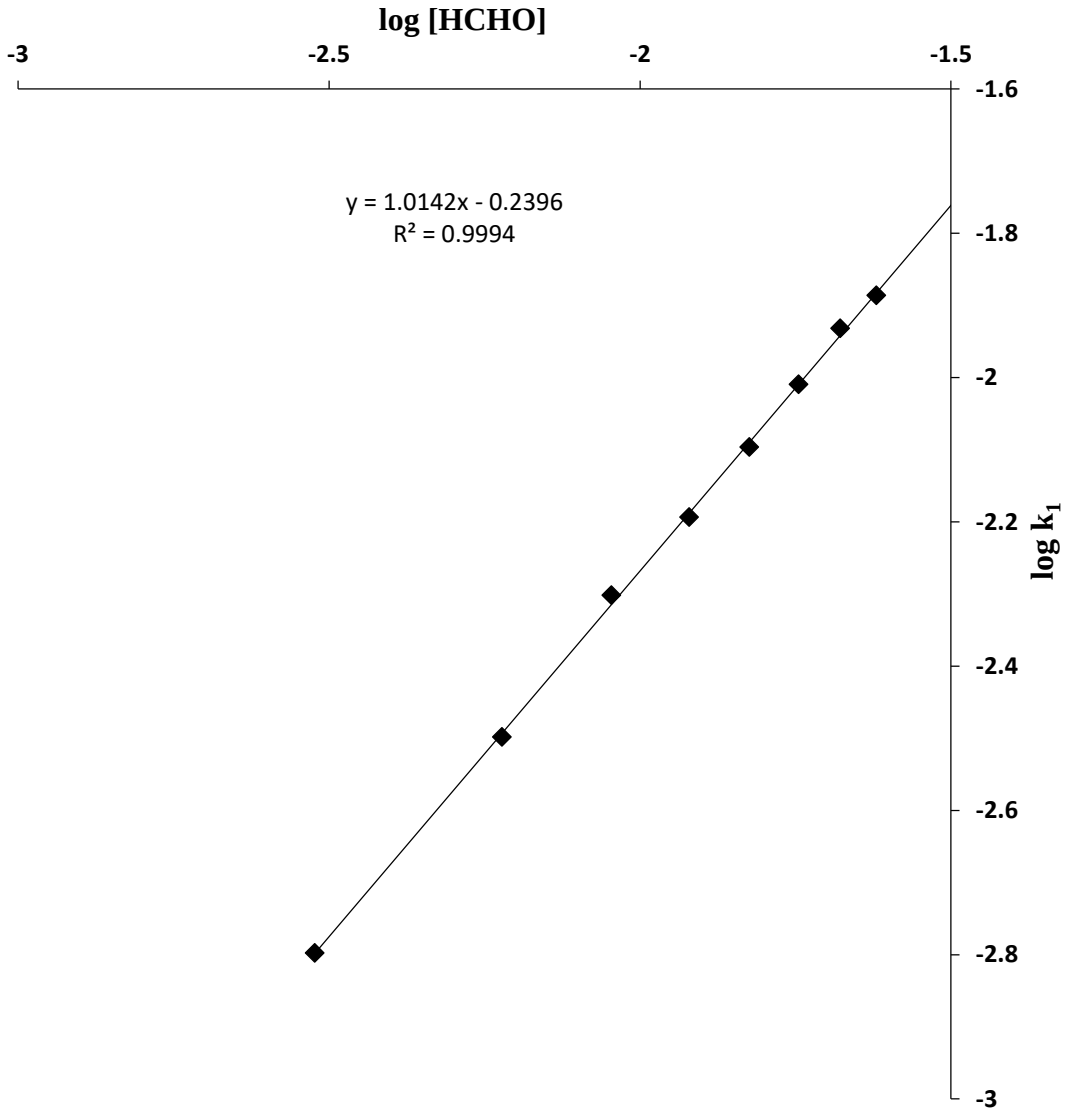


Figure 4.27: Plot of log k_1 versus log [HCHO] for the redox reaction of $[Co(salophen)]^+$ and HCHO at $[Co(salophen)^+] = 3.0 \times 10^{-4}$ mol dm^{-3}, [HCHO] = (3.0 - 24.0) × 10^{-3} mol dm^{-3}, $[H^+]$ = 0.1 mol dm^{-3}, μ = 0.2 C^2 mol dm^{-3}, D = 74.78, T = 299 K and λ_{max} = 470 nm

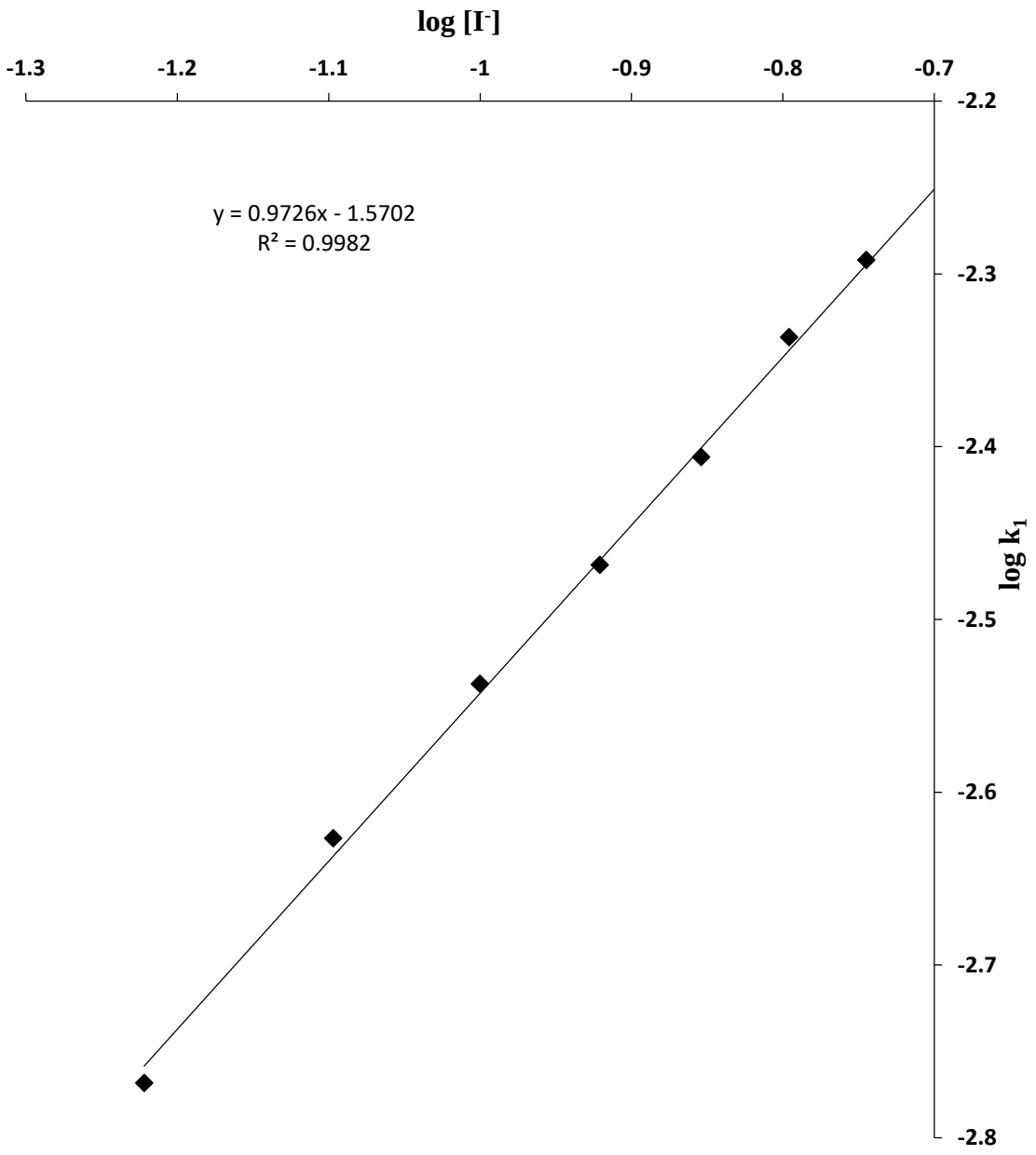


Figure 4.28: Plot of log k_1 versus log [I^-] for the redox reaction of $[Co(salophen)]^+$ and I^- at $[Co(salophen)^+] = 2.0 \times 10^{-4}$ mol dm^{-3}, $[I^-] = (6.0 – 20.0) \times 10^{-2}$ mol dm^{-3} $[H^+] =$ 0.40 mol dm^{-3}, $\mu = 0.6$ C^2 mol dm^{-3}, D = 78.43, T = 301 K and λ_{max} = 470 nm

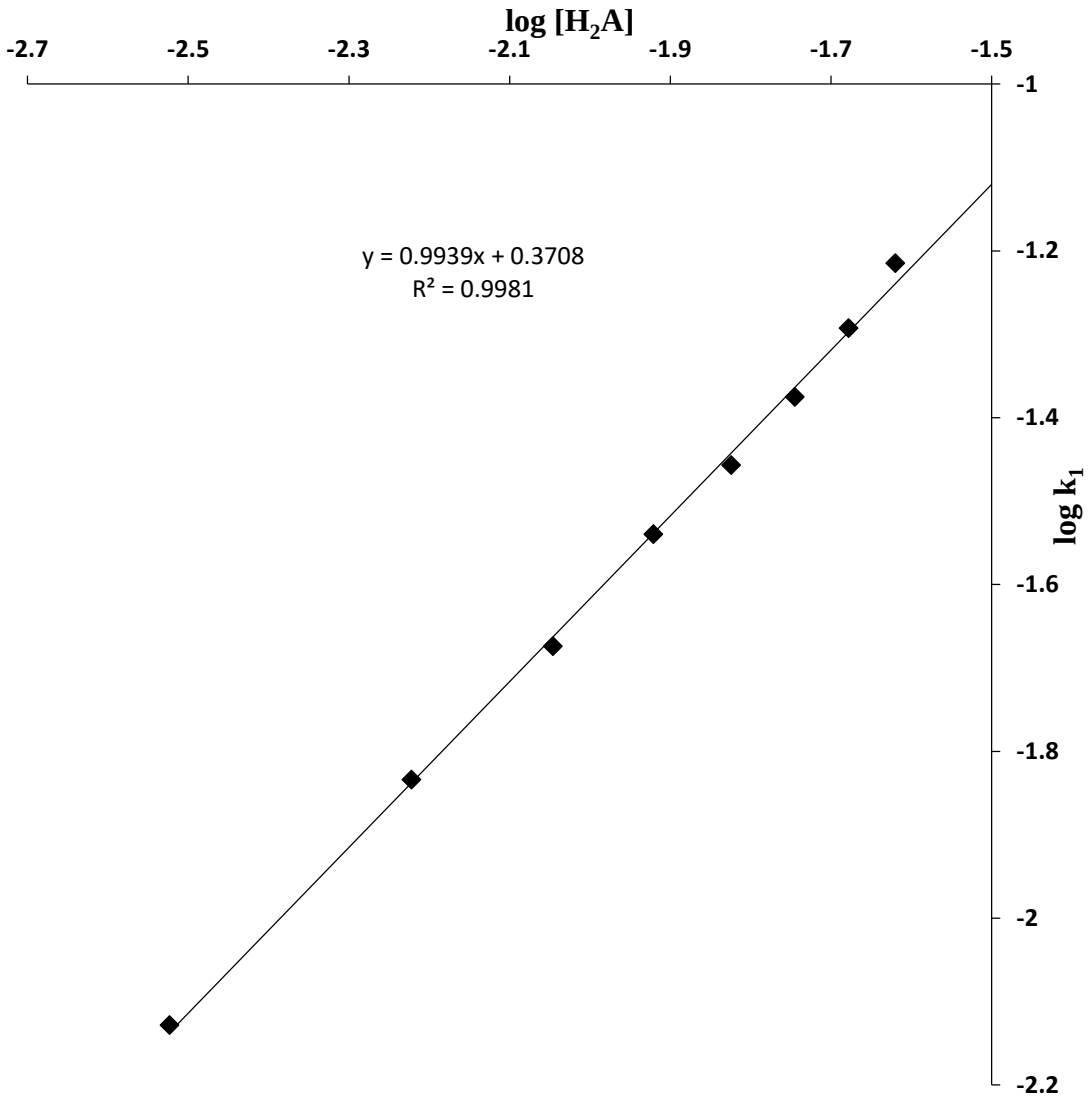


Figure 4.29: Plot of log k_1 versus log [H_2A] for the redox reaction of [Co(salophen)]$^+$ and H_2A at [Co(salophen)$^+$] = 3.0×10^{-4} mol dm^{-3}, [H_2A] = $(3.0 – 24.0) \times 10^{-3}$ mol dm^{-3}, [H^+] = 2.0×10^{-3} mol dm^{-3}, μ = 0.1 C^2 mol dm^{-3}, D = 74.11, T = 306 K and λ_{max} = 470 nm

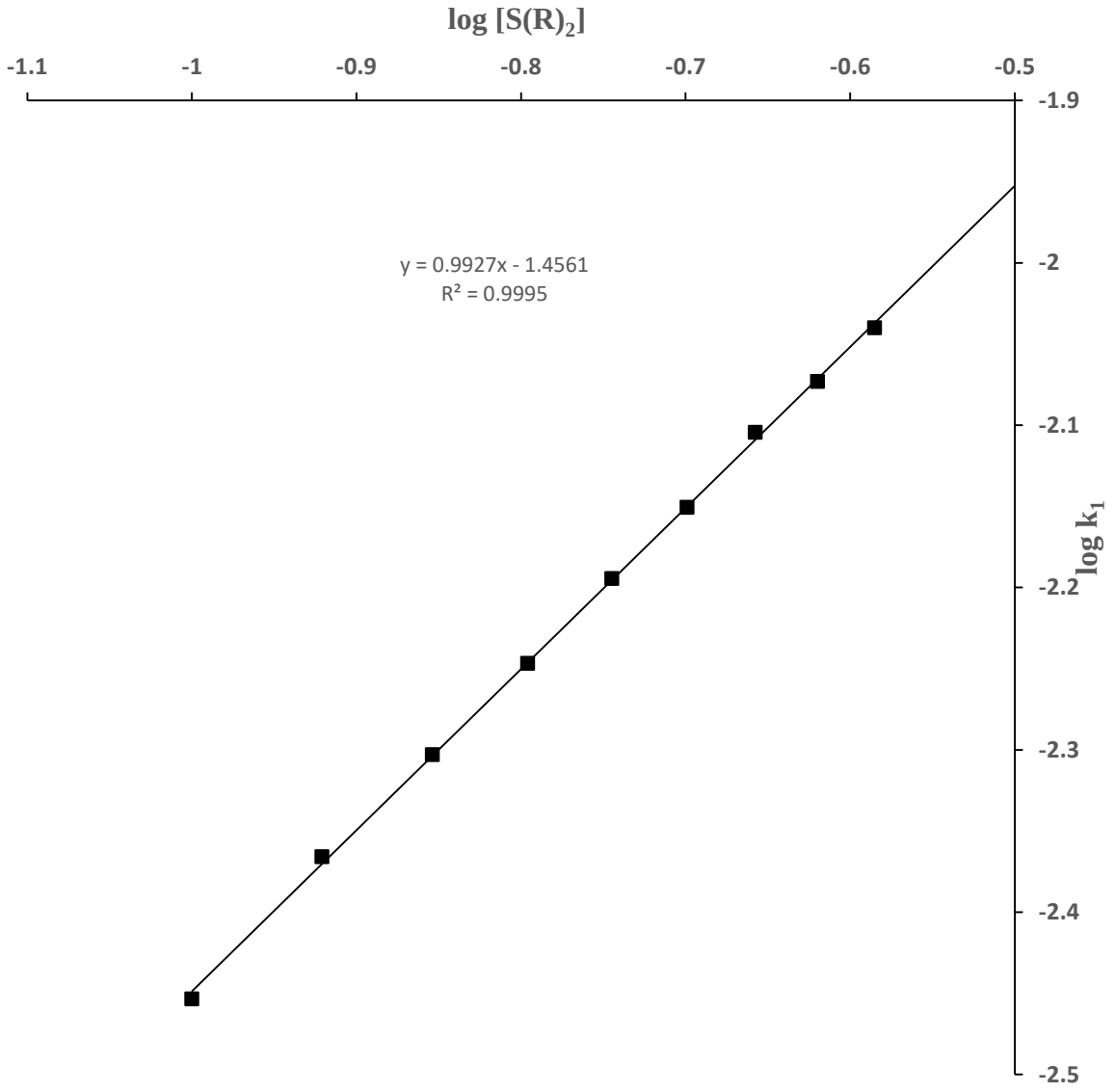


Figure 4.30: Plot of log k_1 versus log $[S(R)_2]$ for the redox reaction of $[Co(salophen)]^+$ and $S(R)_2$ at $[Co(salophen)^+] = 2.0 \times 10^{-4}$ mol dm^{-3}, $[S(R)_2] = (10.0 - 24.0) \times 10^{-2}$ mol dm^{-3}, $[H^+] = 5.0 \times 10^{-2}$ mol dm^{-3}, $\mu = 0.2$ C^2 mol dm^{-3}, D = 77.42, T = 305 K and λ_{max} = 470 nm

The slopes obtained were 0.97 ($Co(salophen)^+$ / LSH), 0.99 ($Co(salophen)^+$ / RSH), 1.00 ($Co(salophen)^+$ / TSH), 1.00 ($Co(salophen)^+$ / TSCZ), 0.99 ($Co(salophen)^+$ / DPCI), 1.02 ($Co(salophen)^+$ / CH_3CHO), 1.01 ($Co(salophen)^+$ / HCHO), 0.97 ($Co(salophen)^+$ / I^-), 0.99 ($Co(salophen)^+$ / H_2A) and 0.99 ($Co(salophen)^+$ / $S(R)_2$) systems. The second order rate constants (k_2) determined from the ratio of k_1 to [reductants] are fairly constant (Tables 4.1 – 4.10). From these results, the rate laws are represented by equations 4.11 – 4.20.

$$-\frac{d}{dt}[Co(salophen)^+] = k_2[Co(salophen)^+][LSH] \quad (4.11)$$

where $k_2 = (6.91 \pm 0.19) \times 10^{-1}\ dm^3\ mol^{-1}\ s^{-1}$

$$-\frac{d}{dt}[Co(salophen)^+] = k_2[Co(salophen)^+][RSH] \quad (4.12)$$

where $k_2 = (3.55 \pm 0.02) \times 10^{-1}\ dm^3\ mol^{-1}\ s^{-1}$

$$-\frac{d}{dt}[Co(salophen)^+] = k_2[Co(salophen)^+][TSH] \quad (4.13)$$

where $k_2 = (14.27 \pm 0.12) \times 10^{-1}\ dm^3\ mol^{-1}\ s^{-1}$

$$-\frac{d}{dt}[Co(salophen)^+] = k_2[Co(salophen)^+][TSCZ] \quad (4.14)$$

where $k_2 = (1.26 \pm 0.03) \times 10^{-1}\ dm^3\ mol^{-1}\ s^{-1}$

$$-\frac{d}{dt}[Co(salophen)^+] = k_2[Co(salophen)^+][DPCI] \quad (4.15)$$

where $k_2 = (3.90 \pm 0.07) \times 10^{-1}\ dm^3\ mol^{-1}\ s^{-1}$

$$-\frac{1}{2}\frac{d}{dt}[Co(salophen)^+] = k_2[Co(salophen)^+][CH_3CHO] \quad (4.16)$$

where $k_2 = (4.14 \pm 0.11) \times 10^{-2}\ dm^3\ mol^{-1}\ s^{-1}$

$$-\frac{1}{2}\frac{d}{dt}[Co(salophen)^+] = k_2[Co(salophen)^+][HCHO] \quad (4.17)$$

where $k_2 = (5.41 \pm 0.11) \times 10^{-1}\ dm^3\ mol^{-1}\ s^{-1}$

Table 4.1: The pseudo-first order and second order rate constants for the redox reaction of $[Co(salophen)]^+$ and LSH at $[Co(salophen)^+] = 2.0 \times 10^{-4}$ mol dm^{-3}, D = 74.84, T = 300 K and λ_{max} = 470 nm

10^3[LSH], mol dm^{-3}	10^3H^+, mol dm^{-3}	μ, C^2 mol dm^{-3}	10^3k_1, s^{-1}	k_2, dm^3 mol^{-1} s^{-1}
4.00	1.00	0.10	2.83	0.71
6.00	1.00	0.10	4.14	0.69
8.00	1.00	0.10	5.65	0.71
10.00	1.00	0.10	7.09	0.71
12.00	1.00	0.10	8.20	0.68
14.00	1.00	0.10	9.58	0.68
16.00	1.00	0.10	10.43	0.65
18.00	1.00	0.10	12.51	0.69
12.00	1.00	0.04	5.97	0.49
12.00	1.00	0.06	6.89	0.57
12.00	1.00	0.08	7.58	0.63
12.00	1.00	0.10	8.24	0.69
12.00	1.00	0.12	8.77	0.73
12.00	1.00	0.14	9.53	0.79
12.00	1.00	0.16	10.20	0.85
12.00	1.00	0.18	11.01	0.92
12.00	1.00	0.10	8.20	0.68
12.00	3.00	0.10	18.10	1.51
12.00	6.00	0.10	31.10	2.59
12.00	9.00	0.10	54.10	4.54
12.00	12.00	0.10	70.20	5.85
12.00	15.00	0.10	89.60	7.47
12.00	18.00	0.10	97.80	8.15

Table 4.2: The pseudo-first order and second order rate constants for the redox reaction of $[Co(salophen)]^+$ and RSH at $[Co(salophen)^+] = 3.0 \times 10^{-4}$ mol dm^{-3}, D = 74.19, T = 300 K and λ_{max} = 470 nm

10^3[RSH], mol dm^{-3}	10^3H^+, mol dm^{-3}	μ, C^2 mol dm^{-3}	10^3k_1, s^{-1}	k_2, dm^3 mol^{-1} s^{-1}
6.00	1.40	0.10	2.12	0.35
9.00	1.40	0.10	3.20	0.36
12.00	1.40	0.10	4.31	0.36
15.00	1.40	0.10	5.34	0.36
18.00	1.40	0.10	6.40	0.36
21.00	1.40	0.10	7.37	0.35
24.00	1.40	0.10	8.48	0.35
27.00	1.40	0.10	9.63	0.36
15.00	1.40	0.10	5.34	0.36
15.00	1.40	0.20	6.20	0.41
15.00	1.40	0.30	7.09	0.47
15.00	1.40	0.40	8.48	0.57
15.00	1.40	0.50	8.96	0.59
15.00	1.40	0.60	10.76	0.72
15.00	1.40	0.70	12.34	0.82
15.00	1.40	0.80	13.89	0.93
15.00	1.40	0.10	5.34	0.36
15.00	1.60	0.10	6.02	0.40
15.00	1.80	0.10	6.64	0.44
15.00	2.00	0.10	7.24	0.48
15.00	2.20	0.10	7.85	0.52
15.00	2.40	0.10	8.44	0.56

Table 4.3: The pseudo-first order and second order rate constants for the redox reaction of $[Co(salophen)]^+$ and TSH at $[Co(salophen)^+] = 3.0 \times 10^{-4}$ mol dm^{-3}, D = 74.04, T = 300 K and λ_{max} = 470 nm

10^3[TSH], mol dm^{-3}	**μ, C^2 mol dm^{-3}**	**$10^3 k_1$, s^{-1}**	**k_2, dm^3 mol^{-1} s^{-1}**
3.00	0.10	4.35	1.45
4.50	0.10	6.33	1.41
6.00	0.10	8.51	1.42
7.50	0.10	10.71	1.43
9.00	0.10	12.92	1.44
10.50	0.10	14.95	1.42
12.00	0.10	17.23	1.44
13.50	0.10	19.34	1.43
15.00	0.10	21.24	1.42
7.50	0.04	14.39	1.92
7.50	0.06	13.04	1.74
7.50	0.08	11.84	1.58
7.50	0.10	10.73	1.43
7.50	0.12	9.72	1.30
7.50	0.14	8.68	1.16
7.50	0.16	8.18	1.09

Table 4.4: The pseudo-first order and second order rate constants for the redox reaction of $[Co(salophen)]^+$ and TSCZ at $[Co(salophen)^+] = 2.0 \times 10^{-4}$ mol dm^{-3}, D = 74.41, T = 306 K and λ_{max} = 470 nm

10^2[TSCZ], mol dm^{-3}	10^2H^+, mol dm^{-3}	μ, C^2 mol dm^{-3}	10^3k_1, s^{-1}	k_2, dm^3 mol^{-1} s^{-1}
2.00	1.00	0.10	2.58	0.13
3.00	1.00	0.10	3.69	0.12
4.00	1.00	0.10	4.97	0.12
5.00	1.00	0.10	6.11	0.12
6.00	1.00	0.10	7.71	0.13
7.00	1.00	0.10	8.93	0.13
8.00	1.00	0.10	9.67	0.12
9.00	1.00	0.10	11.68	0.13
10.00	1.00	0.10	12.76	0.13
8.00	1.00	0.10	9.70	0.12
8.00	1.00	0.20	9.68	0.12
8.00	1.00	0.30	9.86	0.13
8.00	1.00	0.40	9.75	0.12
8.00	1.00	0.50	9.75	0.12
8.00	1.00	0.60	9.87	0.12
8.00	1.00	0.70	9.80	0.12
8.00	1.00	0.10	9.70	0.12
8.00	2.00	0.10	9.72	0.12
8.00	3.00	0.10	9.67	0.12
8.00	4.00	0.10	9.76	0.12
8.00	5.00	0.10	9.72	0.12
8.00	6.00	0.10	9.72	0.12
8.00	7.00	0.10	9.74	0.12
8.00	8.00	0.10	9.86	0.12

Table 4.5: The pseudo-first order and second order rate constants for the reaction of $[Co(salophen)]^+$ and DPCI at $[Co(salophen)^+] = 1.0 \times 10^{-4}$ mol dm^{-3}, D = 75.83, T = 300 K and λ_{max} = 470 nm

10^3[DPCI], mol dm^{-3}	**$[H^+]$, mol dm^{-3}**	**μ, C^2 mol dm^{-3}**	**10^3k_1, s^{-1}**	**k_2, dm^3 mol^{-1} s^{-1}**
10.00	0.10	0.50	3.97	0.39
15.00	0.10	0.50	5.74	0.38
20.00	0.10	0.50	7.76	0.39
25.00	0.10	0.50	9.88	0.39
30.00	0.10	0.50	11.90	0.39
35.00	0.10	0.50	13.47	0.39
40.00	0.10	0.50	15.89	0.39
45.00	0.10	0.50	17.09	0.38
25.00	0.10	0.40	9.90	0.39
25.00	0.10	0.45	9.71	0.39
25.00	0.10	0.50	9.88	0.39
25.00	0.10	0.55	9.93	0.39
25.00	0.10	0.60	9.87	0.39
25.00	0.10	0.65	9.53	0.38
25.00	0.10	0.70	9.57	0.38
25.00	0.10	0.80	9.78	0.39
25.00	0.10	0.50	9.88	0.39
25.00	0.15	0.50	9.90	30.9
25.00	0.20	0.50	9.97	0.39
25.00	0.25	0.50	9.88	0.39
25.00	0.30	0.50	9.97	0.39
25.00	0.35	0.50	9.90	30.9
25.00	0.40	0.50	9.88	0.39

Table 4.6: The pseudo-first order and second order rate constants for the redox reaction of $[Co(salophen)]^+$ and CH_3CHO at $[Co(salophen)^+] = 3.0 \times 10^{-4}$ mol dm^{-3}, D = 75.67, T = 302 K and λ_{max} = 470 nm

$10^2[CH_3CHO]$, mol dm^{-3}	10^2H^+, mol dm^{-3}	μ, C^2 mol dm^{-3}	10^3k_1, s^{-1}	$10^2 k_2$, $dm^3 mol^{-1} s^{-1}$
7.50	4.00	0.20	3.09	4.11
9.00	4.00	0.20	3.61	4.01
10.50	4.00	0.20	4.31	4.10
12.00	4.00	0.20	5.21	4.34
13.50	4.00	0.20	5.69	4.21
15.00	4.00	0.20	6.01	4.01
16.50	4.00	0.20	6.86	4.15
18.00	4.00	0.20	7.48	4.15
13.50	4.00	0.10	5.65	4.19
13.50	4.00	0.20	5.69	4.21
13.50	4.00	0.30	5.57	4.13
13.50	4.00	0.40	5.58	4.14
13.50	4.00	0.50	5.59	4.14
13.50	4.00	0.60	5.66	4.19
13.50	4.00	0.70	5.73	4.24
13.50	4.00	0.80	5.57	4.12
13.50	2.00	0.20	5.94	4.40
13.50	4.00	0.20	5.73	4.25
13.50	6.00	0.20	5.57	4.13
13.50	8.00	0.20	5.64	4.18
13.50	10.00	0.20	5.69	4.21
13.50	12.00	0.20	5.48	4.06
13.50	14.00	0.20	5.62	4.16

Table 4.7: The pseudo-first order and second order rate constants for the reaction of $[Co(salophen)]^+$ and HCHO at $[Co(salophen)^+] = 3.0 \times 10^{-4}$ mol dm^{-3}, D = 74.78, T = 299 K and λ_{max} = 470 nm

10^3[HCHO], mol dm^{-3}	10^1H^+, mol dm^{-3}	μ, C^2 mol dm^{-3}	10^3k_1, s^{-1}	k_2, dm^3 mol^{-1} s^{-1}
3.00	1.00	0.20	1.59	0.53
6.00	1.00	0.20	3.17	0.53
9.00	1.00	0.20	4.99	0.55
12.00	1.00	0.20	6.40	50.3
15.00	1.00	0.20	8.01	0.53
18.00	1.00	0.20	9.79	0.54
21.00	1.00	0.20	11.69	0.56
24.00	1.00	0.20	12.99	0.54
18.00	1.00	0.10	9.78	0.54
18.00	1.00	0.20	9.81	0.55
18.00	1.00	0.30	9.72	0.54
18.00	1.00	0.40	9.79	0.54
18.00	1.00	0.50	9.67	0.54
18.00	1.00	0.60	9.74	0.54
18.00	1.00	0.70	9.79	0.54
18.00	1.00	0.80	9.83	0.55
18.00	0.20	0.20	9.72	0.54
18.00	0.40	0.20	9.81	0.55
18.00	0.60	0.20	9.76	0.54
18.00	0.80	0.20	9.72	0.54
18.00	1.00	0.20	9.79	0.54
18.00	1.20	0.20	10.02	0.56
18.00	1.40	0.20	9.79	0.54

Table 4.8: The pseudo-first order and second order rate constants for the reaction of $[Co(salophen)]^+$ and I^- at $[Co(salophen)^+] = 2.0 \times 10^{-4}$ mol dm^{-3}, D = 78.43, T = 301 K and λ_{max} = 470 nm

$10^2[I^-]$, mol dm^{-3}	10^1H^+, mol dm^{-3}	μ, C^2 mol dm^{-3}	10^3k_1, s^{-1}	$10^2 k_2$, dm^3 mol^{-1} s^{-1}
6.00	4.00	0.60	1.71	2.84
8.00	4.00	0.60	2.36	2.95
10.00	4.00	0.60	2.90	2.90
12.00	4.00	0.60	3.40	2.83
14.00	4.00	0.60	3.93	2.80
16.00	4.00	0.60	4.61	2.88
18.00	4.00	0.60	5.10	2.84
20.00	4.00	0.60	5.53	2.76
16.00	1.00	0.60	4.51	2.82
16.00	1.50	0.60	4.69	2.94
16.00	2.00	0.60	4.58	2.84
16.00	2.50	0.60	4.56	2.85
16.00	3.00	0.60	4.86	3.04
16.00	3.50	0.60	4.54	2.84
16.00	4.00	0.60	4.61	2.88
16.00	4.50	0.60	4.65	2.91
16.00	4.00	0.10	4.58	2.85
16.00	4.00	0.20	4.57	2.84
16.00	4.00	0.30	4.56	2.83
16.00	4.00	0.40	4.61	2.88
16.00	4.00	0.50	4.63	2.90
16.00	4.00	0.60	4.60	2.87
16.00	4.00	0.70	4.61	2.88

Table 4.9: The pseudo-first order and second order rate constants for the redox reaction of $[Co(salophen)]^+$ and H_2A at $[Co(salophen)^+] = 3.0 \times 10^{-4}$ mol dm^{-3}, D = 74.11, T = 306 K and λ_{max} = 470 nm

$10^3[H_2A]$, mol dm^{-3}	10^3H^+, mol dm^{-3}	μ, C^2 mol dm^{-3}	10^3k_1, s^{-1}	k_2, dm^3 mol^{-1} s^{-1}
3.00	2.00	0.10	7.44	2.48
6.00	2.00	0.10	14.66	2.44
9.00	2.00	0.10	21.18	2.35
12.00	2.00	0.10	28.86	2.40
15.00	2.00	0.10	34.91	2.33
18.00	2.00	0.10	42.13	2.34
21.50	2.00	0.10	50.96	2.43
24.00	2.00	0.10	60.98	2.54
12.00	2.00	0.04	38.88	3.24
12.00	2.00	0.06	33.39	2.78
12.00	2.00	0.08	31.48	2.62
12.00	2.00	0.10	28.95	2.41
12.00	2.00	0.12	27.48	2.29
12.00	2.00	0.14	26.39	2.20
12.00	2.00	0.16	23.56	1.96
12.00	2.00	0.18	21.42	1.78
12.00	1.00	0.10	46.81	3.90
12.00	2.00	0.10	28.86	2.40
12.00	3.00	0.10	25.86	2.16
12.00	4.00	0.10	19.80	1.65
12.00	5.00	0.10	15.94	1.33
12.00	6.00	0.10	14.33	1.19
12.00	7.00	0.10	13.40	1.12
12.00	8.00	0.10	12.01	1.00
12.00	9.00	0.10	11.06	0.92

Table 4.10: The pseudo-first order and second order rate constants for the redox reaction of $[Co(salophen)]^+$ and $S(R)_2$ at $[Co(salophen)^+] = 2.0 \times 10^{-4}$ mol dm^{-3}, D = 77.42, T = 305 K and λ_{max} = 470 nm

$10^2[S(R)_2]$, mol dm^{-3}	10^2H^+, mol dm^{-3}	μ, C^2 mol dm^{-3}	10^3k_1, s^{-1}	$10^2 k_2$, dm^3 mol^{-1} s^{-1}
10.00	5.00	0.20	3.52	3.52
12.00	5.00	0.20	4.31	3.59
14.00	5.00	0.20	4.98	3.55
16.00	5.00	0.20	5.67	3.54
18.00	5.00	0.20	6.39	3.55
20.00	5.00	0.20	7.07	3.54
22.00	5.00	0.20	7.86	3.57
24.00	5.00	0.20	8.45	3.52
16.00	1.00	0.20	5.67	3.54
16.00	2.00	0.20	5.58	3.49
16.00	3.00	0.20	5.64	3.53
16.00	4.00	0.20	5.72	3.57
12.00	5.00	0.20	5.67	3.54
12.00	6.00	0.20	5.71	3.57
12.00	7.00	0.20	5.57	3.48
12.00	8.00	0.20	5.62	3.51
12.00	0.50	0.10	5.60	3.50
12.00	0.50	0.20	5.55	3.47
12.00	0.50	0.30	5.60	3.50
12.00	0.50	0.40	5.67	3.54
12.00	0.50	0.50	5.73	3.58
12.00	0.50	0.60	5.64	3.53
12.00	0.50	0.70	5.67	3.54

$$-\frac{d}{dt}[Co(salophen)^+] = k_2[Co(salophen)^+][I^-] \quad (4.18)$$

where $k_2 = (2.85 \pm 0.06) \times 10^{-2}\ dm^3\ mol^{-1}\ s^{-1}$

$$-\frac{3}{2}\frac{d}{dt}[Co(salophen)^+] = k_2[Co(salophen)^+][H_2A] \quad (4.19)$$

where $k_2 = (24.1 \pm 0.74) \times 10^{-1}\ dm^3\ mol^{-1}\ s^{-1}$

$$-\frac{d}{dt}[Co(salophen)^+] = k_2[Co(salophen)^+][S(R)_2] \quad (4.20)$$

where $k_2 = (3.54 \pm 0.03) \times 10^{-2}\ dm^3\ mol^{-1}\ s^{-1}$

4.5 Effect of Hydrogen Ion Concentration on the Rate of Reaction

The acid dependent rate constants shown in Tables 4.1 and 4.2 indicated that the rate of the reactions increased with increase in $[H^+]$. The plots of log k_1 versus log $[H^+]$ for $Co(salophen)^+$/LSH and $Co(salophen)^+$/RSH (Figures 4.31 and 4.32) gave a straight line with slopes of 0.89 and 0.84 respectively. The plot of hydrogen ion dependence second order rate constants $k_2(H^+)$ versus $[H^+]$ was linear with positive intercept for $Co(salophen)^+$/LSH and $Co(salophen)^+$/RSH (Figures 4.35 and 4.36). In $Co(salophen)^+$/TSH and $Co(salophen)^+/H_2A$ systems, plots of log k_1 versus log $[H^+]^{-1}$ (Figures 4.33 and 4.34) gave the slopes of 0.77 and 0.66 respectively. For $Co(salophen)^+$/TSH and $Co(salophen)^+/H_2A$ systems as depicted in Tables 4.9 and 4.11, the rate of the reaction was found to decrease with increase in $[H^+]$ within the range investigated. The least square plots of $k_2(H^+)$ versus $1/[H^+]$ was linear with positive intercept (Figures 4.37 and 4.38). Whereas for the rest of the systems investigated (DPCI, TSCZ, RCHO, HCHO, I^- and $S(R)_2$), the rate of the reaction was found to be independent on acid concentrations within the range of $[H^+]$ investigated.

Table 4.11: Acid dependence effect on the rate of reaction of $[Co(salophen)]^+$ and TSH at $[Co(salophen)]^+ = 3.0 \times 10^{-4}$ mol dm^{-3}, [TSH] = 7.50 mol dm^{-3}, $\mu = 0.1$ C^2 mol dm^{-3}, D = 74.04, T = 300 K and λ_{max} = 470 nm

10^3 $[H^+]$, mol dm^{-3}	**10^3 k_1, s^{-1}**	**k_2, dm^3 mol^{-1} s^{-1}**
0.0	10.71	1.43
1.0	10.37	1.38
2.0	6.13	0.82
3.0	4.63	0.62
4.0	3.70	0.49
5.0	3.04	0.41
6.0	2.61	0.35
7.0	2.29	0.30

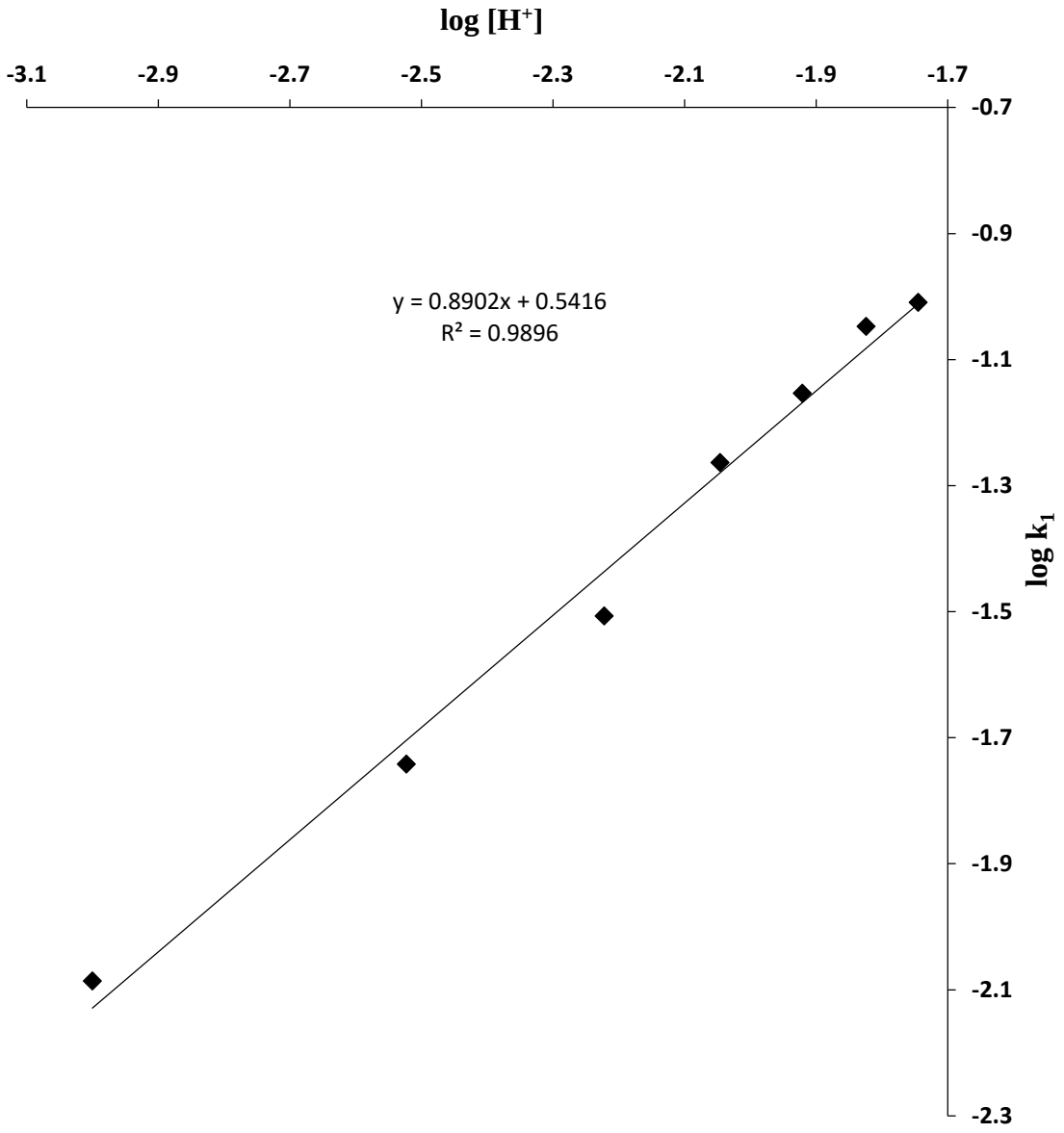


Figure 4.31: Plot of log k_1 versus log $[H^+]$ for the redox reaction of $[Co(salophen)]^+$ and LSH at $[Co(salophen)^+] = 2.0 \times 10^{-4}$ mol dm^{-3}, [LSH] = 12.0×10^{-3} mol dm^{-3}, $[H^+] = (1.0 – 18.0) \times 10^{-3}$ mol dm^{-3}, $\mu = 0.1$ C^2 mol dm^{-3}, D = 74.84, T = 300 K, and λ_{max} = 470 nm

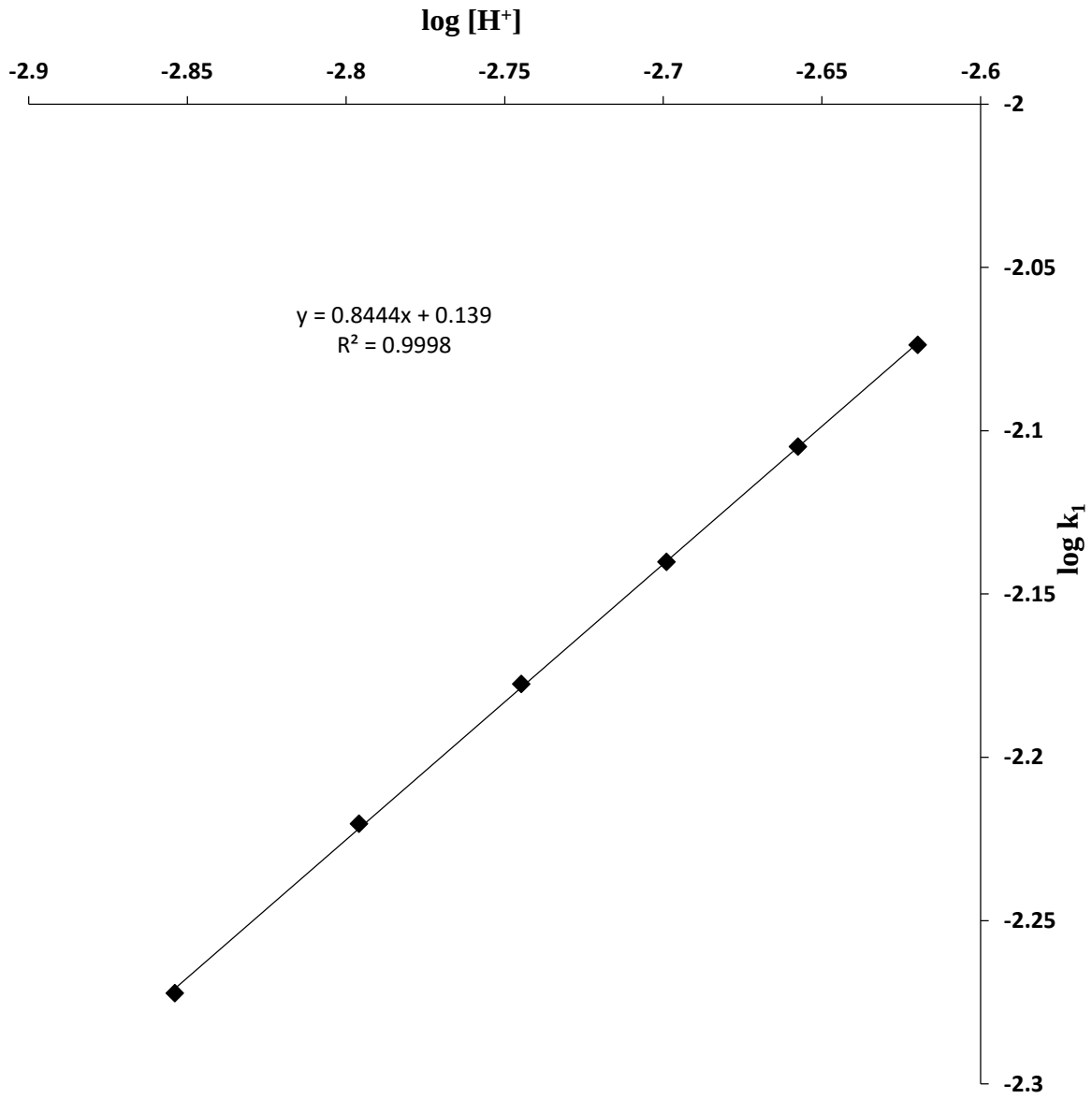


Figure 4.32: Plot of log k_1 versus log $[H^+]$ for the redox reaction of $[Co(salophen)]^+$ and RSH at $[Co(salophen)^+] = 3.0 \times 10^{-4}$ mol dm^{-3}, [RSH] = 15.0×10^{-3} mol dm^{-3}, $[H^+] = (1.4 – 2.4) \times 10^{-3}$ mol dm^{-3}, $\mu = 0.1$ C^2 mol dm^{-3}, D = 74.19, T = 300 K, and λ_{max} = 470 nm

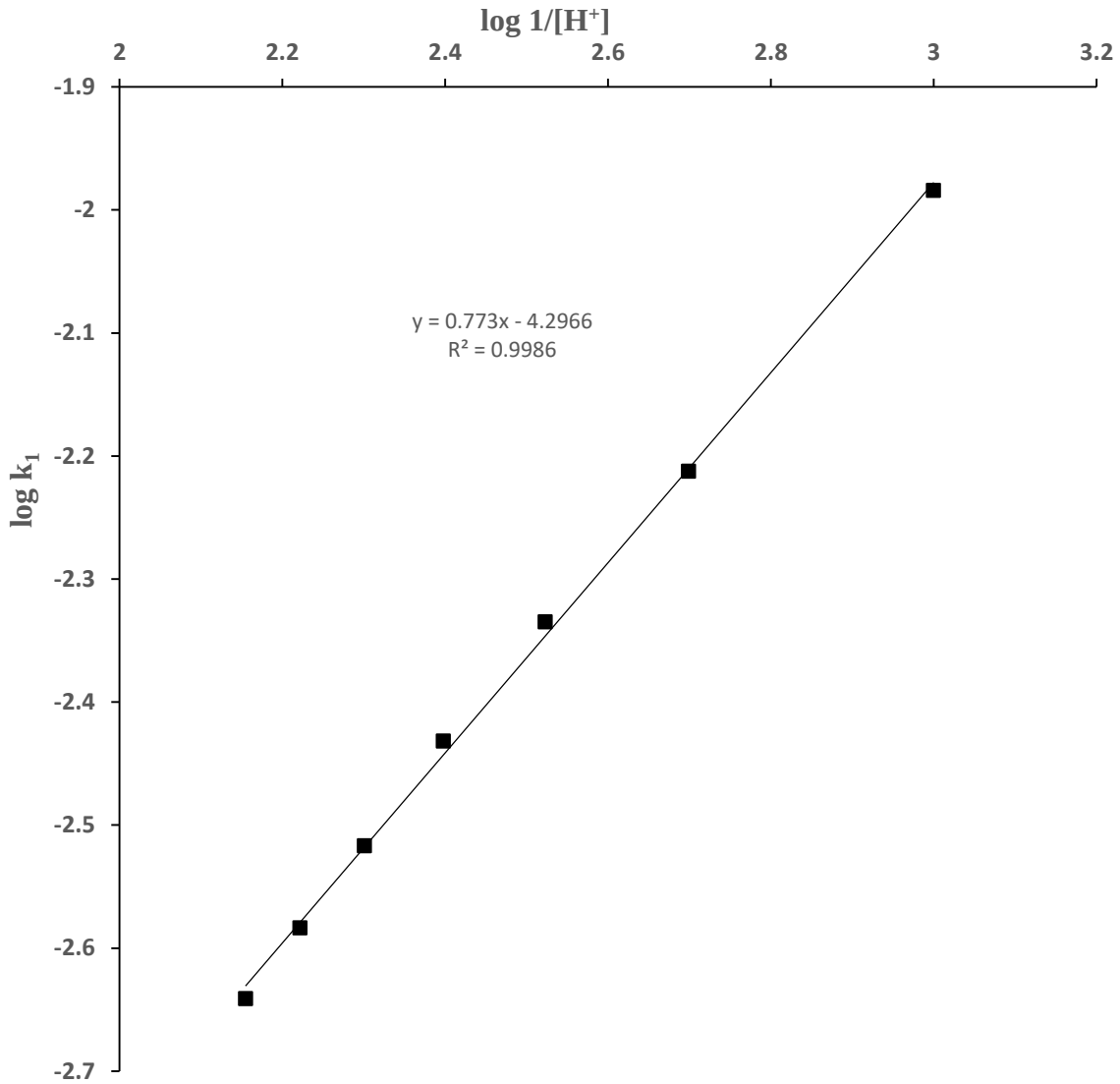


Figure 4.33: Plot of log k_1 versus log $1/[H^+]$ for the redox reaction of $[Co(salophen)]^+$ and TSH at $[Co(salophen)^+] = 3.0 \times 10^{-4}$ mol dm^{-3}, [TSH] = 7.5×10^{-3} mol dm^{-3}, $[H^+] = (1.0 – 7.0) \times 10^{-3}$ mol dm^{-3}, $\mu = 0.1$ C^2 mol dm^{-3}, D = 74.04, T = 300 K, and λ_{max} = 470 nm

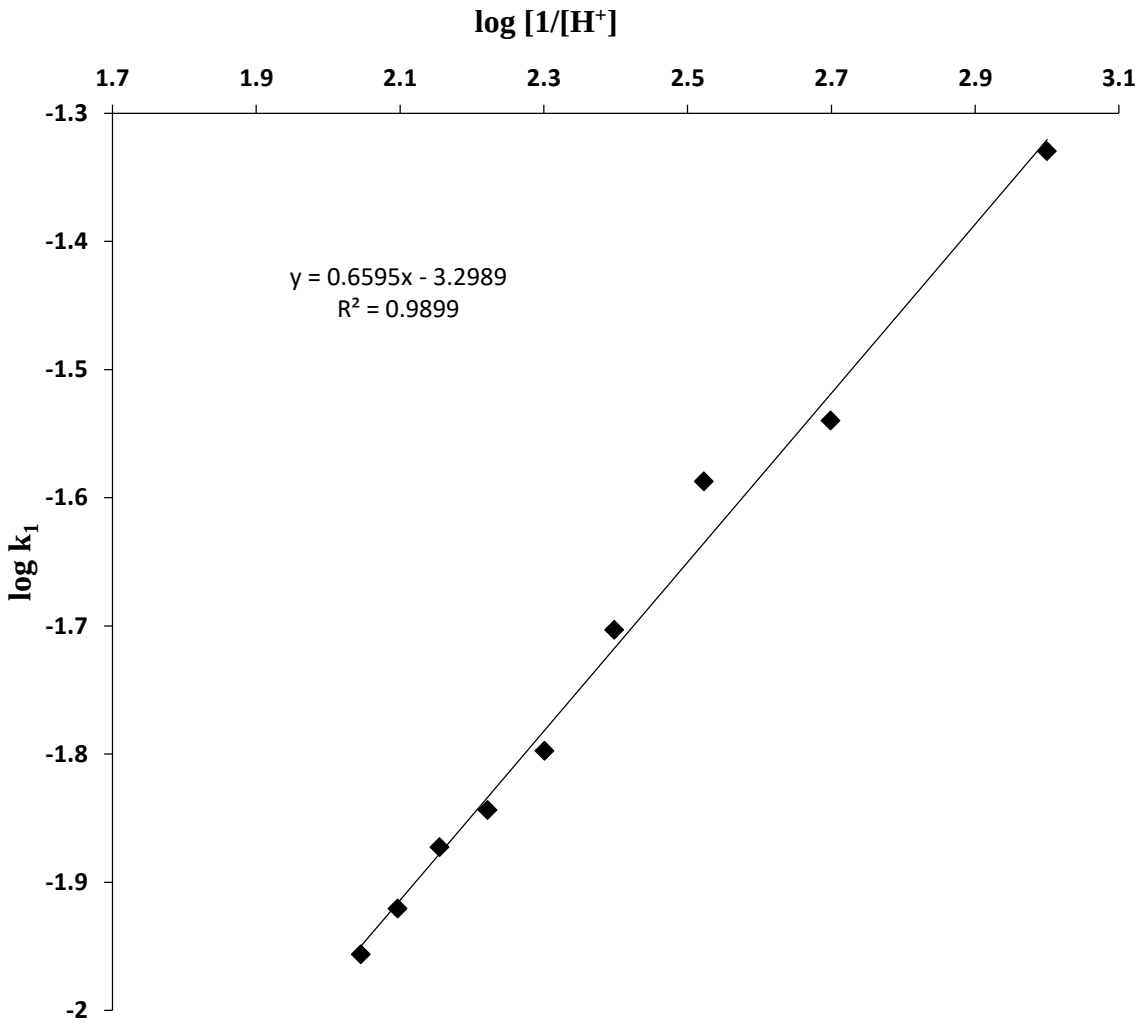


Figure 4.34: Plot of log k_1 versus log $[H^+]^{-1}$ for the redox reaction of $[Co(salophen)]^+$ and H_2A at $[Co(salophen)^+] = 3.0 \times 10^{-4}$ mol dm^{-3}, $[H_2A] = 12.0 \times 10^{-3}$ mol dm^{-3}, $[H^+] = (1.0 – 9.0) \times 10^{-3}$ mol dm^{-3}, $\mu = 0.1$ C^2 mol dm^{-3}, D = 74.11, T = 306 K, and λ_{max} = 470 nm

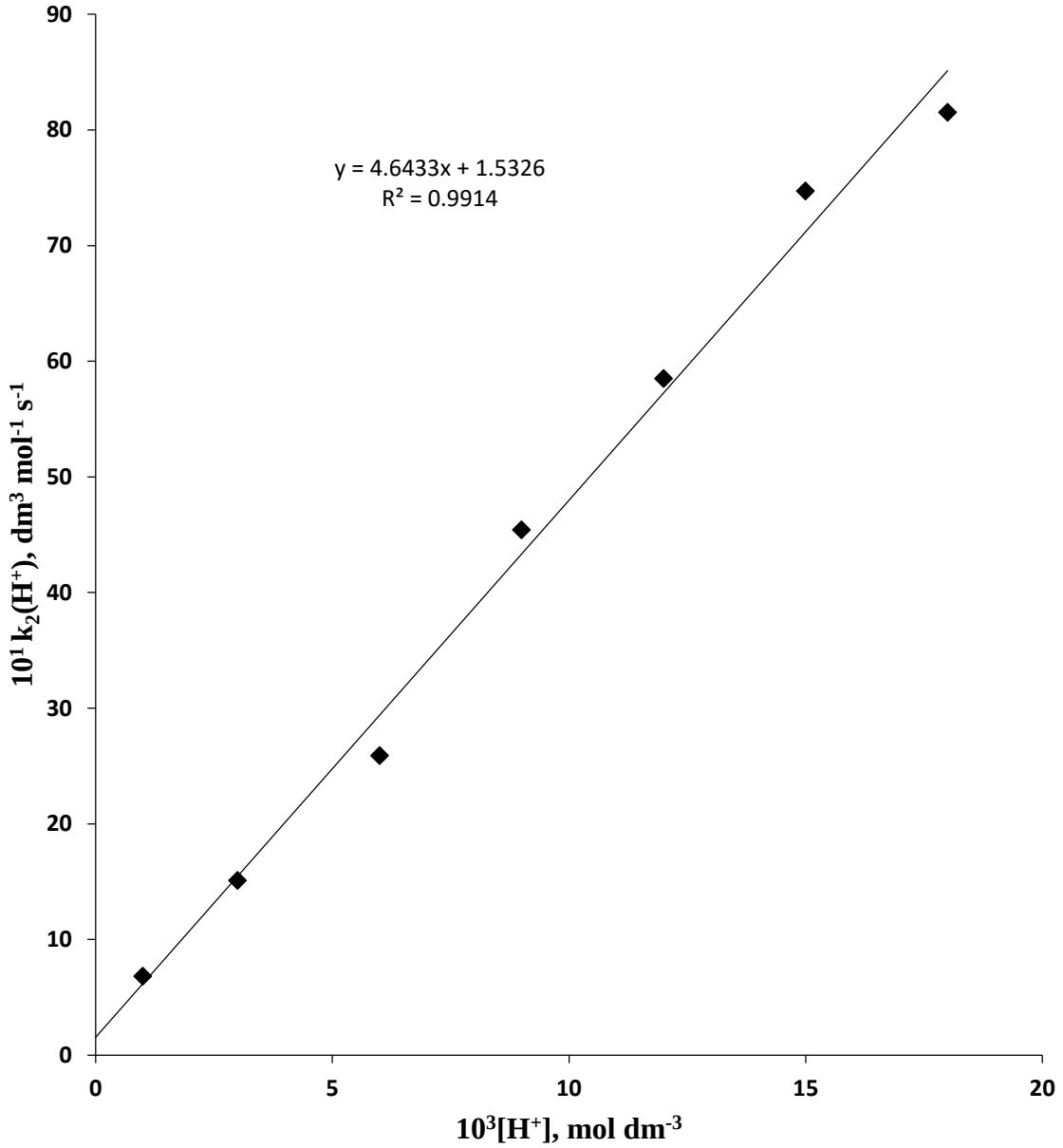


Figure 4.35: Plot of k_2 versus $[H^+]$ for the redox reaction of $[Co(salophen)]^+$ and LSH at $[Co(salophen)^+] = 2.0 \times 10^{-4}$ mol dm^{-3}, $[LSH] = 12.0 \times 10^{-3}$ mol dm^{-3}, $[H^+] = (1.0 – 18.0) \times 10^{-3}$ mol dm^{-3}, $\mu = 0.1$ C^2 mol dm^{-3}, D = 74.84, T = 300 K, and λ_{max} = 470 nm

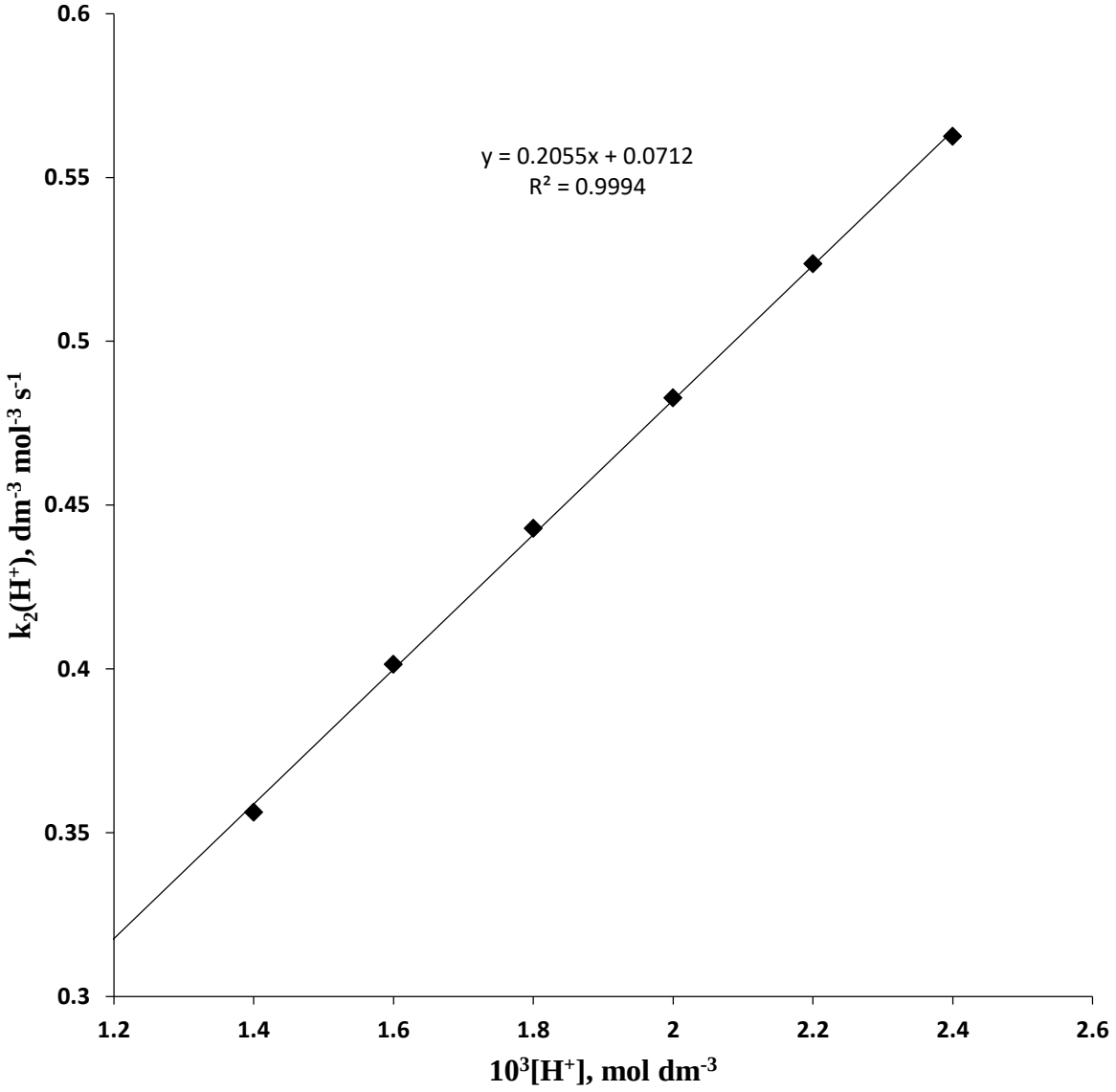


Figure 4.36: Plot of k_2 versus $[H^+]$ for the redox reaction of $[Co(salophen)]^+$ and RSH at $[Co(salophen)^+] = 3.0 \times 10^{-4}$ mol dm^{-3}, [RSH] = 15.0×10^{-3} mol dm^{-3}, $[H^+] = (1.4 – 2.4) \times 10^{-3}$ mol dm^{-3}, $\mu = 0.1$ C^2 mol dm^{-3}, D = 74.19, T = 300 K, and λ_{max} = 470 nm

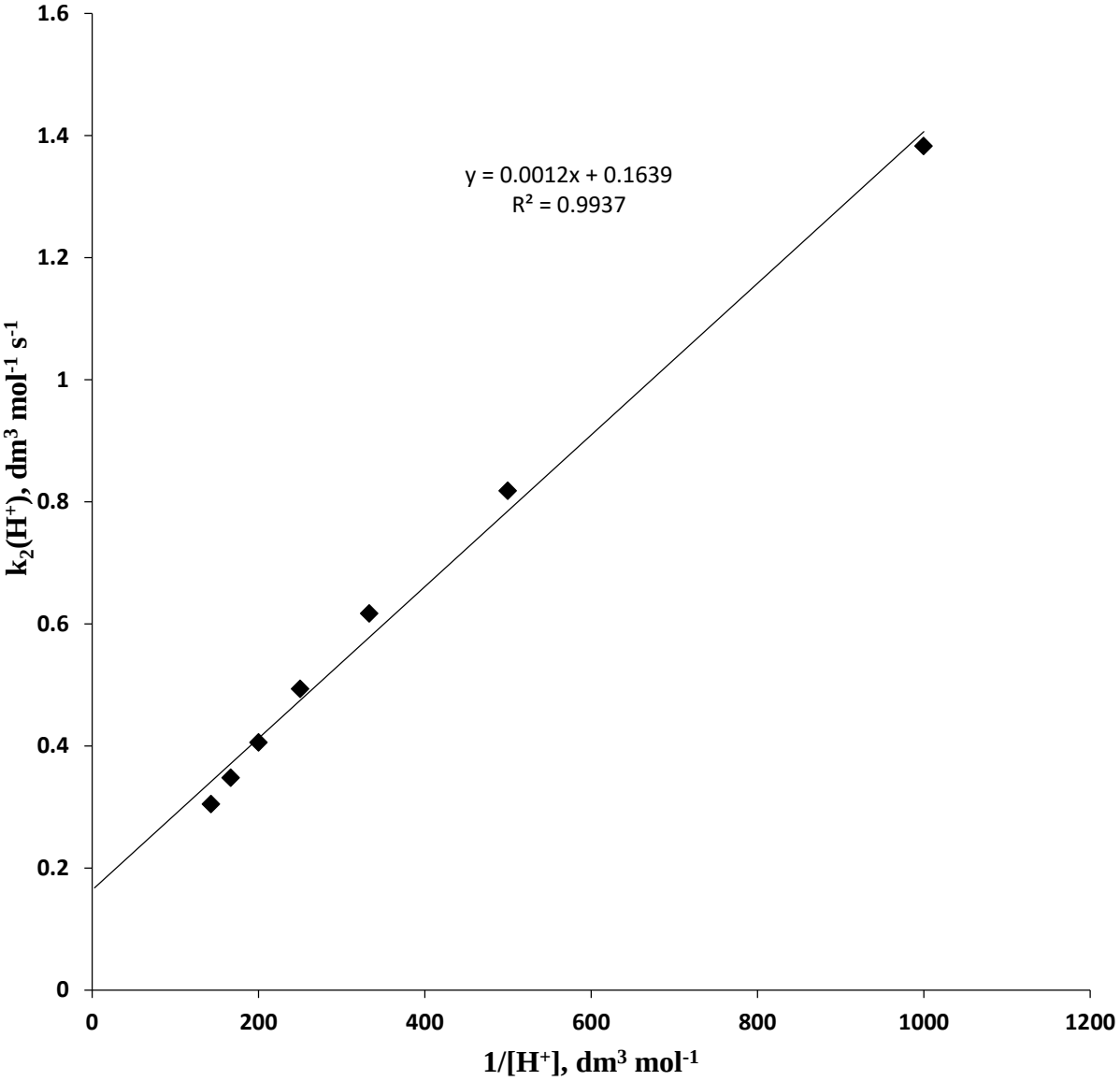


Figure 4.37: Plot of k_2 versus $1/[H^+]$ for the redox reaction of $[Co(salophen)]^+$ and TSH at $[Co(salophen)]^+ = 3.0 \times 10^{-4}$ mol dm^{-3}, [TSH] = 7.50 mol dm^{-3}, $\mu = 0.1$ C^2 mol dm^{-3}, $[H^+] = (1.0 – 7.0) \times 10^{-3}$ mol dm^{-3}, D = 74.04, T = 300 K and λ_{max} = 470 nm

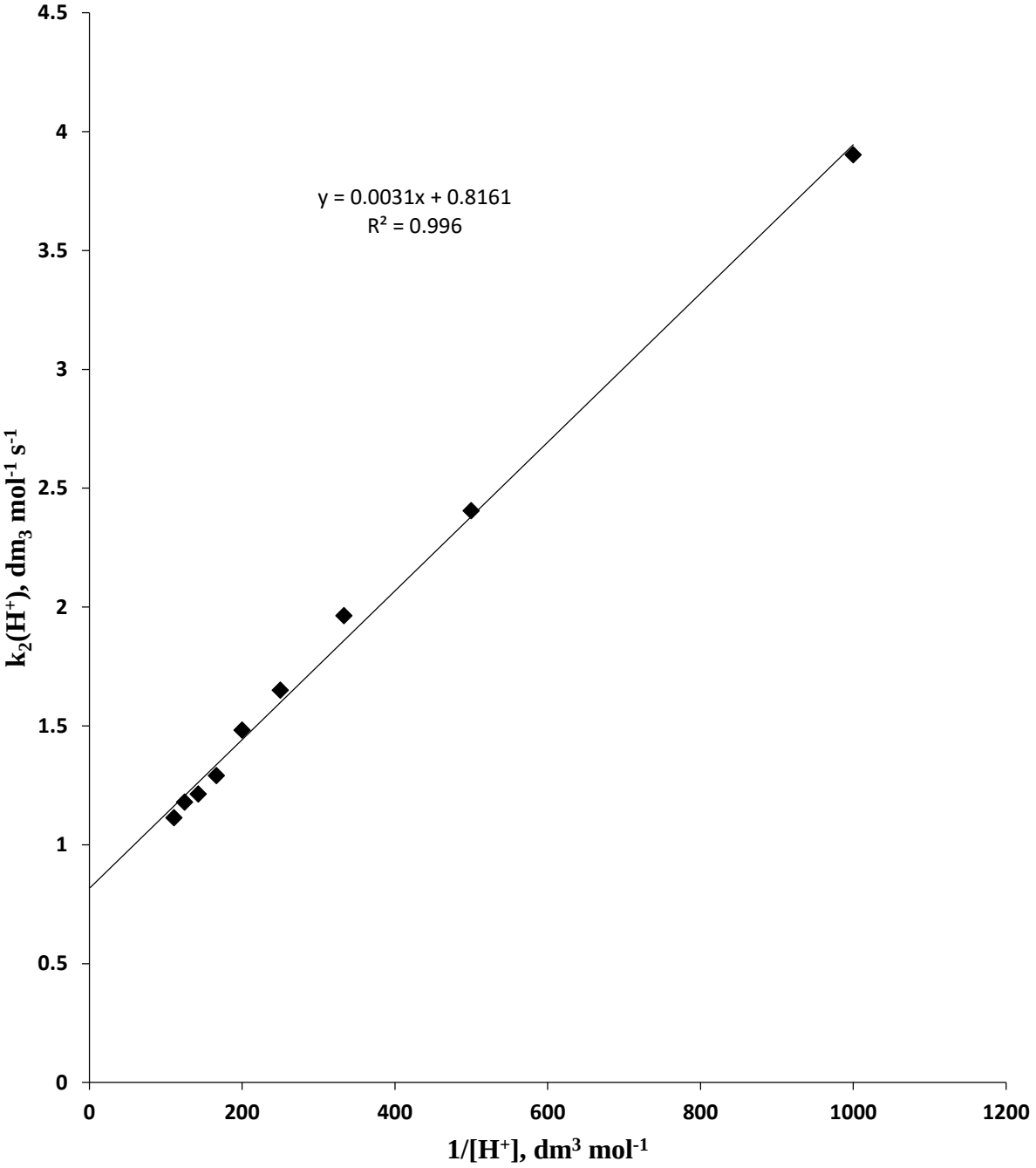


Figure 4.38: Plot of k_2 versus $1/[H^+]$ for the redox reaction of $[Co(salophen)]^+$ and H_2A at $[Co(salophen)^+] = 3.0 \times 10^{-4}$ mol dm^{-3}, $[H_2A] = 12.0 \times 10^{-3}$ mol dm^{-3}, $[H^+] = (1.0 – 9.0) \times 10^{-3}$ mol dm^{-3}, $\mu = 0.1$ C^2 mol dm^{-3}, D = 74.11, T = 306 K, and λ_{max} = 470 nm

From the plots, the acid-dependent rates constant are represented in equations 4.21 and 4.22 for the $Co(salophen)^+$ / LSH and $Co(salophen)^+$ / RSH reactions, and equations 4.23 and 4.24 for $Co(salophen)^+$ / TSH and $Co(salophen)^+$ / H_2A reactions respectively.

$$k_2(H^+) = a + b[H^+] \quad (4.21)$$

where $a = 0.16\ dm^3\ mol^{-1}\ s^{-1}$ and $b = 464.16\ dm^6\ mol^{-2}\ s^{-1}$

$$k_2(H^+) = c + d[H^+] \quad (4.22)$$

where $c = 0.07\ dm^3\ mol^{-1}\ s^{-1}$ and $d = 205.45\ dm^6\ mol^{-2}\ s^{-1}$

$$k_2(H^+) = e + f[H^+]^{-1} \quad (4.23)$$

where $e = 0.16\ dm^3\ mol^{-1}\ s^{-1}$ and $f = 1.2 \times 10^{-3}\ s^{-1}$

$$k_2(H^+) = g + h[H^+]^{-1} \quad (4.24)$$

where $g = 0.82\ dm^3\ mol^{-1}\ s^{-1}$ and $h = 3.10 \times 10^{-3}\ s^{-1}$

The overall rate equations for the systems are represented in equations 4.25 (LSH and RSH) and 4.26 (TSH and H_2A) respectively.

$$-d[Co(salophen)^+]/dt = (w + x[H^+])[Co(salophen)^+][reductants] \quad (4.25)$$

$$-d[Co(salophen)^+]/dt = (y + z[H^+]^{-1})[Co(salophen)^+][reductants] \quad (4.26)$$

Where w and y are the intercepts and x and z are the slopes for the direct acid dependent and inverse acid dependent reactions respectively.

4.6 Effect of Change in Ionic Strength of Reaction Medium on the Reaction Rate

The rates of the reaction were found to increase with increase in ionic strength (μ) for the reaction of $Co(salophen)^+$ / LSH and $Co(salophen)^+$ / RSH (Tables 4.1 and 4.2), and decreased with increase in μ for $Co(salophen)^+$ / TSH and $Co(salophen)^+$ / H_2A (Tables 4.3 and 4.9). For the reactions of $Co(salophen)^+$ / TSCZ, $Co(salophen)^+$ / DPCI, $Co(salophen)^+$ / CH_3CHO, $Co(salophen)^+$ / HCHO, $Co(salophen)^+$ / I^-, and $Co(salophen)^+$ / $S(R)_2$, μ has negligible effect on the rate of reaction and the pseudo-first order, k_1, and second order rate constants, k_2, were fairly constant. The results are presented in Tables 4.4 - 4.8 and 4.10 respectively. Plots of log k_2 against $\sqrt{\mu}$ are shown in Figures 4.39 – 4.42.

4.7 Effect of Change in Dielectric Constant of Reaction Medium on the Reaction Rate

Decreasing the dielectric constant of the reaction medium decreased the rate of reaction for $Co(salophen)^+$ / LSH and $Co(salophen)^+$ / RSH, and increased the rate of reaction for $Co(salophen)^+$ / TSH and $Co(salophen)^+$ / H_2A, but had negligible effect for $Co(salophen)^+$ / TSCZ, $Co(salophen)^+$ / DPCI, $Co(salophen)^+$ / CH_3CHO, $Co(salophen)^+$ / HCHO, $Co(salophen)^+$ / I^-, and $Co(salophen)^+$ / $S(R)_2$ reactions (Tables 4.12 - 4.21).

4.8 Effect of Added Ions on the Reaction Rates

The reactions of $Co(salophen)^+$ with all the reductants under study were catalysed by added ions except in the case of $Co(salophen)^+$ / I^- reaction where added ions were found not to have effect on the reaction rate (Tables 4.22 – 4.41). The plots of the ion dependent second order rate constant, $k_2(X^{n-}$ or $Y^{m+})$, versus concentrations of the ions, $[X^{n-}]$ or $[Y^{m+}]$ are presented as Figures 4.43 - 4.75.

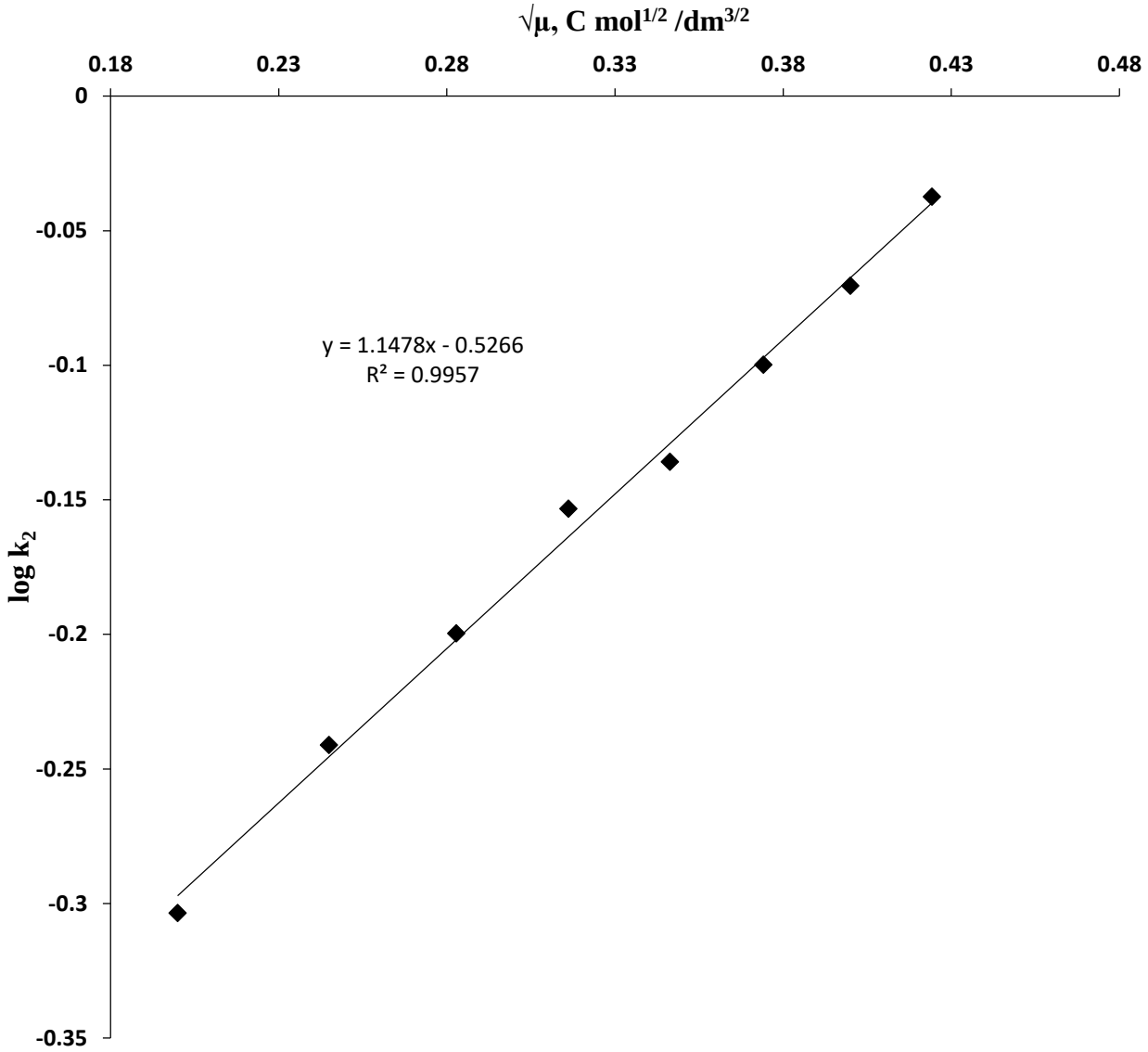


Figure 4.39: Plot of log k_2 versus √μ for the redox reaction of $[Co(salophen)]^+$ and LSH at $[Co(salophen)^+] = 2.0 \times 10^{-4}$ mol dm^{-3}, $[LSH] = 12.0 \times 10^{-3}$ mol dm^{-3}, $[H^+] = 1.0 \times 10^{-3}$ mol dm^{-3}, μ = (0.04 – 0.18) C^2 mol dm^{-3}, D = 74.84, T = 300 K, and λ_{max} = 470 nm

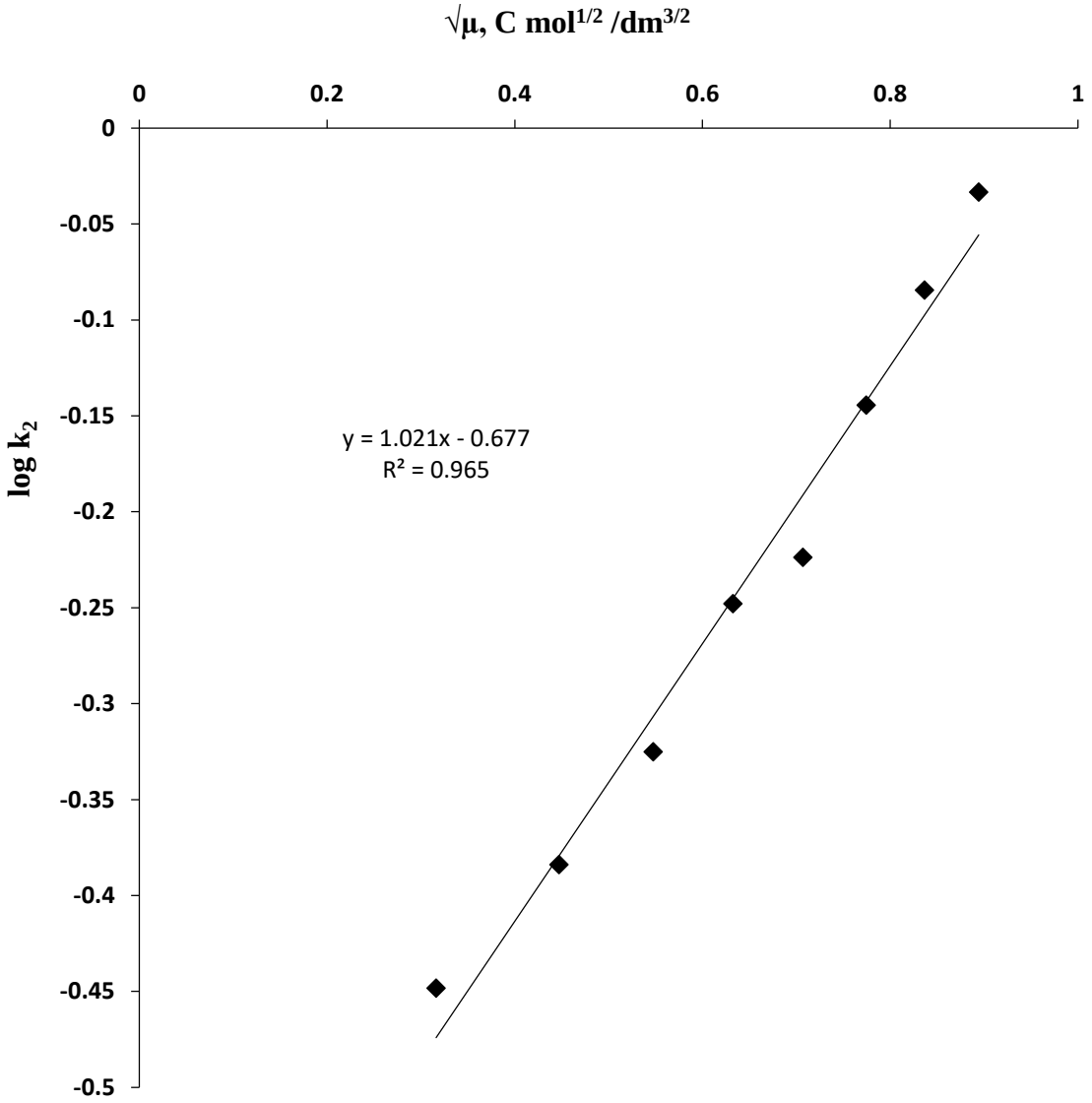


Figure 4.40: Plot of log k_2 versus √μ for the redox reaction of $[Co(salophen)]^+$ and RSH at $[Co(salophen)^+] = 3.0 \times 10^{-4}$ mol dm^{-3}, $[RSH] = 15.0 \times 10^{-3}$ mol dm^{-3}, $[H^+] = 1.4 \times 10^{-3}$ mol dm^{-3}**,** μ = (0.1 – 0.8) C^2 mol dm^{-3}, D = 74.19, T = 300 K, and λ_{max} = 470 nm

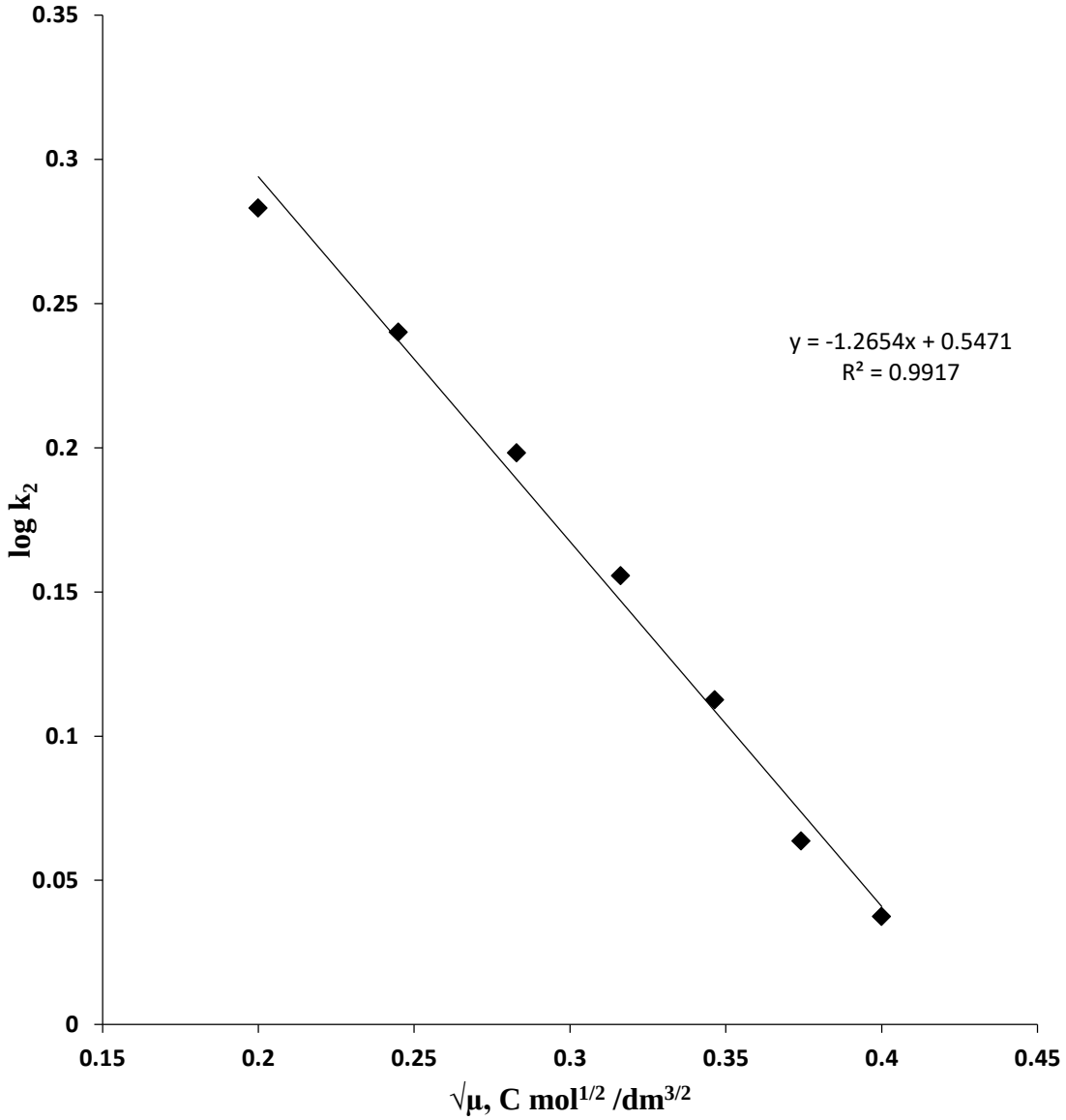


Figure 4.41: Plot of log k_2 versus $\sqrt{\mu}$ for the redox reaction of $[Co(salophen)]^+$ and TSH at $[Co(salophen)^+] = 3.0 \times 10^{-4}$ mol dm^{-3}, [TSH] = 7.50×10^{-3} mol dm^{-3}, μ = (0.04 – 0.16) C^2 mol dm^{-3}, D = 74.04, T = 300 K, and λ_{max} = 470 nm

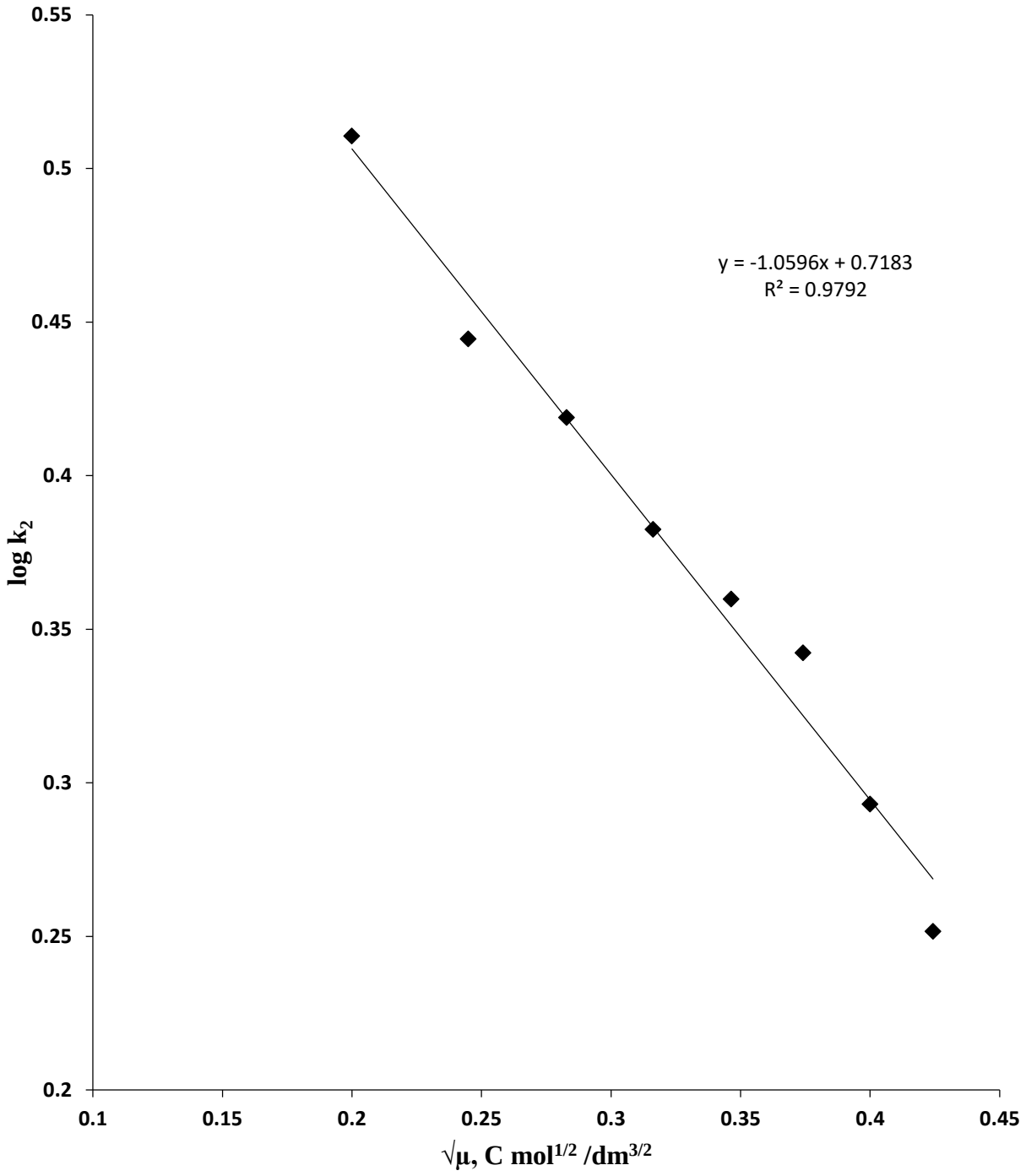


Figure 4.42: Plot of log k_2 versus $\sqrt{\mu}$ for the redox reaction of $[Co(salophen)]^+$ and H_2A at $[Co(salophen)^+] = 3.0 \times 10^{-4}$ mol dm^{-3}, $[H_2A] = 12.0 \times 10^{-3}$ mol dm^{-3}, $[H^+] = 2.0 \times 10^{-3}$ mol dm^{-3}, $\mu = (0.04 - 0.18)$ C^2 mol dm^{-3}, D = 74.11, T = 306 K, and λ_{max} = 470 nm

Table 4.12: Effect of dielectric constant on the redox reaction of $[Co(salophen)]^+$ and LSH at $[Co(salophen)^+] = 2.0 \times 10^{-4}$ mol dm^{-3}, $[LSH] = 12.0 \times 10^{-3}$ mol dm^{-3}, $[H^+] = 1.0 \times 10^{-3}$ mol dm^{-3}, $\mu = 0.1$ C^2 mol dm^{-3}, T = 300 K and λ_{max} = 470 nm

D	**$10^2$1/D**	**10^3k_1, s^{-1}**	**k_2, dm^3 mol^{-1} s^{-1}**
74.84	1.34	8.20	0.68
74.29	1.35	7.39	0.62
73.74	1.36	7.35	0.61
73.24	1.37	7.12	0.59
72.71	1.38	6.61	0.55
72.19	1.39	6.47	0.54
71.66	1.40	5.90	0.49

Table 4.13: Effect of dielectric constant on the redox reaction of $[Co(salophen)]^+$ and RSH at $[Co(salophen)^+] = 3.0 \times 10^{-4}$ mol dm^{-3}, $[RSH] = 15.0 \times 10^{-3}$ mol dm^{-3}, $[H^+] = 1.4 \times 10^{-3}$ mol dm^{-3}, $\mu = 0.1$ C^2 mol dm^{-3}, T = 300 K, and λ_{max} = 470 nm

D	**$10^2$1/D**	**10^3k_1, s^{-1}**	**k_2, dm^3 mol^{-1} s^{-1}**
74.19	1.35	5.34	0.36
73.66	1.36	5.27	0.35
73.13	1.37	5.09	0.34
72.61	1.38	5.02	0.34
72.08	1.39	3.55	0.24
71.56	1.40	2.88	0.19
71.03	1.4079	2.72	0.18

Table 4.14: Effect of dielectric constant on the redox reaction of $[Co(salophen)]^+$ and TSH at $[Co(salophen)^+] = 3.0 \times 10^{-4}$ mol dm^{-3}, $[TSH] = 7.50 \times 10^{-3}$ mol dm^{-3}, $\mu = 0.1$ C^2 mol dm^{-3}, T = 300 K, and $\lambda_{max} = 470$ nm

D	**$10^2$1/D**	**10^3k_1, s^{-1}**	**k_2, dm^3 mol^{-1} s^{-1}**
74.04	1.35	10.71	1.43
73.51	1.36	13.40	1.79
72.99	1.37	16.42	2.19
72.46	1.38	20.03	2.67
71.94	1.39	23.79	3.17
71.41	1.40	27.08	3.61
70.89	1.41	33.16	4.42

Table 4.15: Effect of dielectric constant on the redox reaction of $[Co(salophen)]^+$ and TSCZ at $[Co(salophen)^+] = 2.0 \times 10^{-4}$ mol dm^{-3}, $[TSCZ] = 8.0 \times 10^{-2}$ mol dm^{-3}, $[H^+] = 1.0 \times 10^{-2}$ mol dm^{-3}, $\mu = 0.1$ C^2 mol dm^{-3}, T = 306 K and $\lambda_{max} = 470$ nm

D	**$10^2$1/D**	**10^3k_1, s^{-1}**	**k_2, dm^3 mol^{-1} s^{-1}**
74.41	1.34	9.70	0.12
73.88	1.35	9.77	0.12
73.36	1.36	9.77	0.12
72.83	1.37	9.67	0.12
72.31	1.38	9.74	0.12
71.78	1.39	9.70	0.12
71.25	1.40	9.74	0.12

Table 4.16: Effect of dielectric constant on the rate of reaction of $[Co(salophen)]^+$ and DPCI at $[Co(salophen)^+] = 1.0 \times 10^{-4}$ mol dm^{-3}, DPCI = 25.0×10^{-3} mol dm^{-3} $[H^+] = 0.1$ mol dm^{-3}, $\mu = 0.5$ C^2 mol dm^{-3}, T = 300 K and $\lambda_{max} = 470$ nm

D	**$10^2 1/D$**	**$10^3 k_1$, s^{-1}**	**k_2, dm^3 mol^{-1} s^{-1}**
75.83	1.32	9.88	0.39
75.30	1.33	9.88	0.39
74.78	1.34	9.70	0.39
74.25	1.35	9.77	0.39
73.73	1.36	9.77	0.39
73.20	1.37	9.83	0.39
72.67	1.38	9.74	0.39

Table 4.17: Effect of dielectric constant on the redox reaction of $[Co(salophen)]^{+}$ and CH_3CHO at $[Co(salophen)^{+}] = 3.0 \times 10^{-4}$ mol dm^{-3}, $[CH_3CHO] = 13.5 \times 10^{-2}$ mol dm^{-3}, $[H^{+}] = 4.0 \times 10^{-2}$ mol dm^{-3}, $\mu = 0.2$ C^2 mol dm^{-3}, T = 302 K and λ_{max} = 470 nm

D	**$10^2$1/D**	**10^3k_1, s^{-1}**	**10^2k_2, dm^3 mol^{-1} s^{-1}**
75.67	1.32	5.67	4.20
75.14	1.33	5.71	4.23
74.62	1.34	5.73	4.25
74.09	1.35	5.57	4.13
73.57	1.36	5.55	4.11
73.04	1.37	5.69	4.21
72.52	1.38	5.74	4.25

Table 4.18: Effect of dielectric constant on the rate of reaction of $[Co(salophen)]^+$ and HCHO at $[Co(salophen)^+] = 3.0 \times 10^{-4}$ mol dm^{-3}, $[HCHO] = 18.0 \times 10^{-3}$ mol dm^{-3}, $[H^+] = 0.1$ mol dm^{-3}, $\mu = 0.2$ C^2 mol dm^{-3}, T = 299 K and $\lambda_{max} = 470$ nm

D	**$10^2 1/D$**	**$10^3 k_1$, s^{-1}**	**k_2, dm^3 mol^{-1} s^{-1}**
74.78	1.34	9.79	0.54
74.25	1.35	9.86	0.55
73.73	1.36	9.88	0.55
73.20	1.37	9.81	0.55
72.67	1.38	9.83	0.55
72.15	1.39	9.88	0.55
71.62	1.40	9.91	0.55

Table 4.19: Effect of dielectric constant on the rate of reaction of $[Co(salophen)]^+$ and I^- at $[Co(salophen)^+] = 2.0 \times 10^{-4}$ mol dm^{-3}, $[I^-] = 16.0 \times 10^{-2}$ mol dm^{-3} $[H^+] = 0.40$ mol dm^{-3}, $\mu = 0.6$ C^2 mol dm^{-3}, T = 301 K and $\lambda_{max} = 470$ nm

D	**$10^2 1/D$**	**$10^3 k_1$, s^{-1}**	**$10^2 k_2$, dm^3 mol^{-1} s^{-1}**
78.43	1.27	4.63	2.89
77.90	1.28	4.65	2.91
77.38	1.29	4.63	2.89
76.85	1.30	4.58	2.86
76.33	1.31	4.61	2.88
75.80	1.32	4.61	2.88
75.28	1.33	4.65	2.91

Table 4.20: Effect of dielectric constant on the redox reaction of reaction of $[Co(salophen)]^{+}$ and H_2A at $[Co(salophen)^{+}] = 3.0 \times 10^{-4}$ mol dm^{-3}, $[H_2A] = 12.0 \times 10^{-3}$ mol dm^{-3}, $[H^{+}] = 2.0 \times 10^{-3}$ mol dm^{-3}, $\mu = 0.1$ C^2 mol dm^{-3}, T = 306 K, and λ_{max} = 470 nm

D	**$10^2$1/D**	**10^2k_1, s^{-1}**	**k_2, dm^3 mol^{-1} s^{-1}**
74.11	1.35	2.90	2.42
73.58	1.36	3.20	2.67
73.05	1.37	3.41	2.84
72.53	1.38	3.61	3.01
72.00	1.39	3.98	3.32
71.48	1.40	4.04	3.36
70.95	1.41	4.53	3.78

Table 4.21: Effect of dielectric constant on the redox reaction of $[Co(salophen)]^{+}$ and $S(R)_2$ at $[Co(salophen)^{+}] = 2.0 \times 10^{-4}$ mol dm^{-3}, $S(R)_2 = 16.0 \times 10^{-2}$ mol dm^{-3}, $[H^{+}] = 5.0 \times 10^{-2}$ mol dm^{-3}, $\mu = 0.2$ C^2 mol dm^{-3}, T = 305 K and $\lambda_{max} = 470$ nm

D	**$10^2$1/D**	**10^3k_1, s^{-1}**	**10^2k_2, dm^3 mol^{-1} s^{-1}**
77.42	1.29	5.67	3.54
76.89	1.30	5.69	3.56
76.37	1.31	5.72	3.57
75.84	1.32	5.73	3.58
75.32	1.33	5.74	3.59
74.79	1.34	5.75	3.59
74.26	1.35	5.60	3.50

Table 4.22: Effect of added cations on the redox reaction of $[Co(salophen)]^+$ and LSH at $[Co(salophen)^+] = 2.0 \times 10^{-4}$ mol dm^{-3}, $[LSH] = 12.0 \times 10^{-3}$ mol dm^{-3}, $[H^+] = 1.0 \times 10^{-3}$ mol dm^{-3}, $\mu = 0.1$ C^2 mol dm^{-3}, D = 74.84, T = 300 K, and λ_{max} = 470 nm

[Y]	**10^3 [Y], mol dm^{-3}**	**10^3 k_1, s^{-1}**	**k_2, dm^3 mol^{-1} s^{-1}**
Mg^{2+}	0.00	8.20	0.68
	3.00	7.46	0.62
	6.00	7.20	0.59
	9.00	6.92	0.58
	12.00	6.52	0.54
	15.00	5.90	0.49
	18.00	5.27	0.44
Ca^{2+}	0.00	8.20	0.68
	3.00	7.14	0.59
	6.00	5.56	0.46
	9.00	4.14	0.35
	12.00	3.48	0.29
	15.00	2.55	0.21
	18.00	0.94	0.08

Table 4.23: Effect of added anions on the redox reaction of $[Co(salophen)]^{+}$ and LSH at $[Co(salophen)^{+}] = 2.0 \times 10^{-4}$ mol dm^{-3}, $[LSH] = 12.0 \times 10^{-3}$ mol dm^{-3}, $[H^{+}] = 1.0 \times 10^{-3}$ mol dm^{-3}, $\mu = 0.1$ C^2 mol dm^{-3}, D = 74.84, T = 300 K, and λ_{max} = 470 nm

[X]	**10^3 [X], mol dm^{-3}**	**10^3 k_1, s^{-1}**	**10^1 k_2, dm^3 mol^{-1} s^{-1}**
SO_4^{2-}	0.00	8.20	0.68
	3.00	8.33	0.69
	6.00	8.43	0.70
	9.00	8.52	0.71
	12.00	8.68	0.72
	15.00	8.81	0.73
	18.00	8.89	0.74
CH_3COO^{-}	0.00	8.20	0.68
	3.00	8.39	0.69
	6.00	8.56	0.71
	9.00	8.67	0.72
	12.00	8.78	0.73
	15.00	8.95	0.75
	18.00	9.10	0.76

Table 4.24: Effect of added cations on the redox reaction of $[Co(salophen)]^{+}$ and RSH at $[Co(salophen)^{+}] = 3.0 \times 10^{-4}$ mol dm^{-3}, $[RSH] = 15.0 \times 10^{-3}$ mol dm^{-3}, $[H^{+}] = 1.4 \times 10^{-3}$ mol dm^{-3}, $\mu = 0.1$ C^2 mol dm^{-3}, D = 74.19, T = 300 K, and λ_{max} = 470 nm

[Y]	**10^3 [Y], mol dm^{-3}**	**10^3 k_1, s^{-1}**	**k_2, dm^3 mol^{-1} s^{-1}**
Mg^{2+}	0.00	5.34	0.36
	3.00	5.02	0.34
	6.00	4.77	0.32
	9.00	4.28	0.28
	12.00	4.08	0.27
	15.00	3.52	0.24
	18.00	3.25	0.22
Ca^{2+}	0.00	5.34	0.36
	3.00	5.16	0.34
	6.00	4.79	0.32
	9.00	4.42	0.29
	12.00	4.01	0.27
	15.00	3.50	0.23
	18.00	3.18	0.22

Table 4.25: Effect of added anion on the redox reaction of $[Co(salophen)]^{+}$ and RSH at $[Co(salophen)^{+}] = 3.0 \times 10^{-4}$ mol dm^{-3}, $[RSH] = 15.0 \times 10^{-3}$ mol dm^{-3}, $[H^{+}] = 1.4 \times 10^{-3}$ mol dm^{-3}, $\mu = 0.1$ C^2 mol dm^{-3}, D = 74.19, T = 300 K, and λ_{max} = 470 nm

[X]	**10^3 [X], mol dm^{-3}**	**10^3 k_1, s^{-1}**	**k_2, dm^3 mol^{-1} s^{-1}**
SO_4^{2-}	0.00	5.34	0.36
	3.00	5.50	0.37
	6.00	6.54	0.44
	9.00	6.93	0.46
	12.00	7.72	0.51
	15.00	8.08	0.54
	18.00	8.89	0.59

Table 4.26: Effect of added cations on the redox reaction of $[Co(salophen)]^{+}$ and TSH at $[Co(salophen)^{+}] = 3.0 \times 10^{-4}$ mol dm^{-3}, $[TSH] = 7.50 \times 10^{-3}$ mol dm^{-3}, $\mu = 0.1$ C^2 mol dm^{-3}, D = 74.04, T = 300 K, and λ_{max} = 470 nm

[Y]	**10^3 [Y], mol dm^{-3}**	**10^3 k_1, s^{-1}**	**k_2, dm^3 mol^{-1} s^{-1}**
Mg^{2+}	0.00	10.71	1.43
	3.00	17.92	2.39
	6.00	19.65	2.62
	9.00	22.22	2.96
	12.00	23.56	3.14
	15.00	26.14	3.49
	18.00	28.30	3.77
Ca^{2+}	0.00	10.71	1.43
	3.00	13.77	1.84
	6.00	14.58	1.94
	9.00	15.52	2.07
	12.00	16.51	2.20
	15.00	17.69	2.36
	18.00	18.56	2.47

Table 4.27: Effect of added anion on the redox reaction of $[Co(salophen)]^{+}$ and TSH at $[Co(salophen)^{+}] = 3.0 \times 10^{-4}$ mol dm^{-3}, $[TSH] = 7.50 \times 10^{-3}$ mol dm^{-3}, $\mu = 0.1$ C^2 mol dm^{-3}, D = 74.04, T = 300 K, and λ_{max} = 470 nm

[X]	**10^3 [X], mol dm^{-3}**	**10^3 k_1, s^{-1}**	**k_2, dm^3 mol^{-1} s^{-1}**
SO_4^{2-}	0.00	10.71	1.43
	3.00	11.84	1.58
	6.00	12.57	1.68
	9.00	13.61	1.81
	12.00	14.53	1.94
	15.00	15.27	2.04
	18.00	17.41	2.32

Table 4.28: Effect of added cations on the redox reaction of $[Co(salophen)]^{+}$ and TSCZ at $[Co(salophen)^{+}] = 2.0 \times 10^{-4}$ mol dm^{-3}, [TSCZ] = 8.0×10^{-2} mol dm^{-3}, $[H^{+}] = 1.0 \times 10^{-2}$ mol dm^{-3}, $\mu = 0.1$ C^2 mol dm^{-3}, D = 74.41, T = 306 K and λ_{max} = 470 nm

[Y]	**10^3 [Y], mol dm^{-3}**	**10^3 k_1, s^{-1}**	**k_2, dm^3 mol^{-1} s^{-1}**
Mg^{2+}	0.00	9.70	0.12
	2.00	10.13	0.13
	4.00	10.50	0.13
	6.00	10.69	0.13
	8.00	10.96	0.14
	10.00	11.22	0.14
	12.00	11.40	0.14
	14.00	11.72	0.15
Ca^{2+}	0.00	9.70	0.12
	2.00	10.06	0.13
	4.00	10.25	0.13
	6.00	10.43	0.13
	8.00	10.76	0.13
	10.00	10.96	0.13
	12.00	11.24	0.14
	14.00	11.49	0.14

Table 4.29: Effect of added anion on the redox reaction of $[Co(salophen)]^{+}$ and TSCZ at $Co(salophen)^{+}] = 2.0 \times 10^{-4}$ mol dm^{-3}, $[TSCZ] = 8.0 \times 10^{-2}$ mol dm^{-3}, $[H^{+}] = 1.0 \times 10^{-2}$ mol dm^{-3}, $\mu = 0.1$ C^2 mol dm^{-3}, D = 74.41, T = 306 K and λ_{max} = 470 nm

[X]	**10^3 [X], mol dm^{-3}**	**10^3 k_1, s^{-1}**	**k_2, dm^3 mol^{-1} s^{-1}**
$HCOO^{-}$	0.00	9.70	0.12
	2.00	12.30	0.15
	4.00	17.72	0.22
	6.00	20.89	0.26
	8.00	26.30	0.33
	10.00	31.18	0.39
	12.00	33.23	0.42
	14.00	36.57	0.46

Table 4.30: Effect of added cations on the rate of reaction of $[Co(salophen)]^+$ and DPCI at $[Co(salophen)^+] = 1.0 \times 10^{-4}$ mol dm^{-3}, DPCI = 25.0×10^{-3} mol dm^{-3} $[H^+] = 0.1$ mol dm^{-3}, $\mu = 0.5$ C^2 mol dm^{-3}, D = 75.83, T = 300 K and λ_{max} = 470 nm

[Y]	**10^3 [Y], mol dm^{-3}**	**10^3 k_1, s^{-1}**	**k_2, dm^3 mol^{-1} s^{-1}**
Mg^{2+}	0.00	9.88	3.95
	3.00	10.09	4.03
	6.00	10.29	4.12
	9.00	10.73	4.29
	12.00	10.92	4.37
	15.00	11.31	4.52
	18.00	11.79	4.72
Ca^{2+}	0.00	9.88	3.95
	3.00	10.32	4.13
	6.00	10.96	4.38
	9.00	11.35	4.54
	12.00	11.79	4.72
	15.00	12.29	4.92
	18.00	12.97	5.19

Table 4.31: Effect of added anions on the rate of reaction of $[Co(salophen)]^+$ and DPCI at $[Co(salophen)^+] = 1.0 \times 10^{-4}$ mol dm^{-3}, DPCI = 25.0×10^{-3} mol dm^{-3} $[H^+] = 0.1$ mol dm^{-3}, $\mu = 0.5$ C^2 mol dm^{-3}, D = 75.83, T = 300 K and λ_{max} = 470 nm

[X]	**10^3 [X], mol dm^{-3}**	**10^3 k_1, s^{-1}**	**k_2, dm^3 mol^{-1} s^{-1}**
SO_4^{2-}	0.00	9.88	3.95
	3.00	10.02	4.01
	6.00	10.20	4.08
	9.00	10.71	4.28
	12.00	10.89	4.36
	15.00	11.05	4.42
	18.00	11.31	4.52
CH_3COO^-	0.00	9.88	3.95
	3.00	10.06	4.03
	6.00	10.34	4.14
	9.00	10.69	4.27
	12.00	10.85	4.34
	15.00	11.22	4.49
	18.00	11.56	4.62

Table 4.32: Effect of added cations on the redox reaction of $[Co(salophen)]^{+}$ and CH_3CHO at $[Co(salophen)^{+}] = 3.0 \times 10^{-4}$ mol dm^{-3}, $[CH_3CHO] = 13.5 \times 10^{-2}$ mol dm^{-3}, $[H^{+}] = 4.0 \times 10^{-2}$ mol dm^{-3}, $\mu = 0.2$ C^2 mol dm^{-3}, D = 75.67, T = 302 K and λ_{max} = 470 nm

[Y]	**10^3 [Y], mol dm^{-3}**	**10^3 k_1, s^{-1}**	**10^2 k_2, dm^3 mol^{-1} s^{-1}**
Mg^{2+}	0.00	5.67	4.20
	1.00	5.34	3.96
	5.00	4.56	3.38
	10.00	3.75	2.78
	15.00	3.02	2.23
	20.00	3.51	1.86
Ca^{2+}	0.00	5.67	4.20
	1.00	5.37	3.97
	5.00	5.05	3.74
	10.00	4.20	3.11
	15.00	3.64	2.70
	20.00	3.25	2.41

Table 4.33: Effect of added anions on the redox reaction of $[Co(salophen)]^{+}$ and CH_3CHO at $[Co(salophen)^{+}] = 3.0 \times 10^{-4}$ mol dm^{-3}, $[CH_3CHO] = 13.5 \times 10^{-2}$ mol dm^{-3}, $[H^{+}] = 4.0 \times 10^{-2}$ mol dm^{-3}, $\mu = 0.2$ C^2 mol dm^{-3}, D = 75.67, T = 302 K and λ_{max} = 470 nm

[X]	**10^3 [X], mol dm^{-3}**	**10^3 k_1, s^{-1}**	**10^2 k_2, dm^3 mol^{-1} s^{-1}**
SO_4^{2-}	0.00	5.67	4.20
	1.00	5.82	4.31
	5.00	6.00	4.44
	10.00	6.25	4.63
	15.00	6.51	4.82
	20.00	6.73	4.98
CH_3COO^{-}	0.00	5.67	4.20
	1.00	5.78	4.28
	5.00	6.00	4.44
	10.00	6.24	4.62
	15.00	6.43	4.76
	20.00	6.70	4.96

Table 4.34: Effect of added cations on the rate of reaction of $[Co(salophen)]^{+}$ and HCHO at $[Co(salophen)^{+}] = 3.0 \times 10^{-4}$ mol dm^{-3}, $[HCHO] = 18.0 \times 10^{-3}$ mol dm^{-3}, $[H^{+}] = 0.1$ mol dm^{-3}, $\mu = 0.2$ C^2 mol dm^{-3}, D = 74.78, T = 299 K and λ_{max} = 470 nm

[Y]	**10^3 [Y], mol dm^{-3}**	**10^3 k_1, s^{-1}**	**10^1 k_2, dm^3 mol^{-1} s^{-1}**
Mg^{2+}	0.00	9.79	5.44
	1.00	9.35	5.19
	3.00	8.73	4.85
	6.00	7.30	4.06
	9.00	5.82	3.23
	12.0	4.93	2.74
	15.0	4.67	2.59
Ca^{2+}	0.00	9.79	5.44
	1.00	9.63	5.35
	3.00	8.96	4.98
	6.00	7.92	4.40
	9.00	6.01	3.34
	12.0	4.79	2.66
	15.0	4.35	2.42

Table 4.35: Effect of added anions on the rate of reaction of $[Co(salophen)]^+$ and HCHO at $[Co(salophen)^+] = 3.0 \times 10^{-4}$ mol dm^{-3}, $[HCHO] = 18.0 \times 10^{-3}$ mol dm^{-3}, $[H^+] = 0.1$ mol dm^{-3}, $\mu = 0.2$ C^2 mol dm^{-3}, D = 74.78, T = 299 K and $\lambda_{max} = 470$ nm

[X]	**10^3 [X], mol dm^{-3}**	**10^3 k_1, s^{-1}**	**k_2, dm^3 mol^{-1} s^{-1}**
SO_4^{2-}	0.00	9.79	0.54
	1.00	9.83	0.55
	3.00	9.90	0.55
	6.00	10.06	0.56
	9.00	10.27	0.57
	12.00	10.45	0.58
	15.00	10.61	0.59
CH_3COO^-	0.00	9.79	0.54
	1.00	9.81	0.55
	3.00	9.97	0.55
	6.00	10.25	0.57
	9.00	10.46	0.58
	12.00	10.82	0.61
	15.00	10.99	0.61

Table 4.36: Effect of added cations on the rate of reaction of $[Co(salophen)]^{+}$ and I^{-} at $[Co(salophen)^{+}] = 2.0 \times 10^{-4}$ mol dm^{-3}, $[I^{-}] = 16.0 \times 10^{-2}$ mol dm^{-3} $[H^{+}] = 0.40$ mol dm^{-3}, $\mu = 0.6\ C^2$ mol dm^{-3}, D = 78.43, T = 301 K and λ_{max} = 470 nm

[Y]	**10^3 [Y], mol dm^{-3}**	**10^3 k_1, s^{-1}**	**10^2 k_2, dm^3 mol^{-1} s^{-1}**
Mg^{2+}	0.00	4.61	2.88
	1.00	4.61	2.88
	3.00	4.56	2.85
	6.00	4.61	2.88
	9.00	4.40	2.75
	12.0	4.65	2.91
Ca^{2+}	0.00	4.61	2.88
	1.00	4.49	2.81
	3.00	4.63	2.89
	6.00	4.65	2.91
	9.00	4.51	2.82
	12.0	4.58	2.86

Table 4.37: Effect of added anions on the rate of reaction of $[Co(salophen)]^{+}$ and I^{-} at $[Co(salophen)^{+}] = 2.0 \times 10^{-4}$ mol dm^{-3}, $[I^{-}] = 16.0 \times 10^{-2}$ mol dm^{-3} $[H^{+}] = 0.40$ mol dm^{-3}, $\mu = 0.6\ C^2$ mol dm^{-3}, D = 78.43, T = 301 K and λ_{max} = 470 nm

[X]	**10^3 [X], mol dm^{-3}**	**10^3 k_1, s^{-1}**	**10^2 k_2, dm^3 mol^{-1} s^{-1}**
SO_4^{2-}	0.00	4.61	2.88
	1.00	4.63	2.89
	3.00	4.63	2.89
	6.00	4.63	2.89
	9.00	4.65	2.91
	12.0	4.65	2.91
CH_3COO^{-}	0.00	4.61	2.88
	1.00	4.74	2.97
	3.00	4.86	3.03
	6.00	4.84	3.02
	9.00	4.63	2.89
	12.0	4.61	2.88

Table 4.38: Effect of added cations on the redox reaction of $[Co(salophen)]^+$ and H_2A at $[Co(salophen)^+] = 3.0 \times 10^{-4}$ mol dm^{-3}, $[H_2A] = 12.0 \times 10^{-3}$ mol dm^{-3}, $[H^+] = 2.0 \times 10^{-3}$ mol dm^{-3}, $\mu = 0.1$ C^2 mol dm^{-3}, D = 74.11, T = 306 K, and λ_{max} = 470 nm

[Y]	**10^3 [Y], mol dm^{-3}**	**10^2 k_1, s^{-1}**	**k_2, dm^3 mol^{-1} s^{-1}**
Ca^{2+}	0.00	2.89	2.40
	3.00	3.17	2.64
	6.00	3.41	2.84
	9.00	3.71	3.10
	12.00	3.92	3.27
	15.00	4.09	3.41
	18.00	4.36	3.63
Mg^{2+}	0.00	2.89	2.40
	3.00	3.07	2.56
	6.00	3.19	2.66
	9.00	3.65	3.04
	12.00	3.74	3.11
	15.00	4.41	3.67
	18.00	4.98	4.15

Table 4.39: Effect of added anions on the redox reaction of $[Co(salophen)]^+$ and H_2A at $[Co(salophen)^+] = 3.0 \times 10^{-4}$ mol dm^{-3}, $[H_2A] = 12.0 \times 10^{-3}$ mol dm^{-3}, $[H^+] = 2.0 \times 10^{-3}$ mol dm^{-3}, $\mu = 0.1$ C^2 mol dm^{-3}, D = 74.11, T = 306 K, and λ_{max} = 470 nm

[X]	**10^3 [X], mol dm^{-3}**	**10^2 k_1, s^{-1}**	**k_2, dm^3 mol^{-1} s^{-1}**
SO_4^{2-}	0.00	2.89	2.40
	3.00	3.10	2.58
	6.00	3.38	2.82
	9.00	3.62	3.01
	12.00	3.87	3.22
	15.00	4.09	3.41
	18.00	4.35	3.62
CH_3COO^-	0.00	2.89	2.40
	3.00	3.04	2.53
	6.00	3.27	2.73
	9.00	3.45	2.88
	12.00	3.62	3.02
	15.00	3.95	3.30
	18.00	4.04	3.37

Table 4.40: Effect of added cations on the redox reaction of $[Co(salophen)]^{+}$ and $S(R)_2$ at $[Co(salophen)^{+}] = 2.0 \times 10^{-4}$ mol dm^{-3}, $[S(R)_2] = 16.0 \times 10^{-2}$ mol dm^{-3}, $[H^{+}] = 5.0 \times 10^{-2}$ mol dm^{-3}, $\mu = 0.2$ C^2 mol dm^{-3}, D = 77.42, T = 305 K and λ_{max} = 470 nm

[Y]	**10^3 [Y], mol dm^{-3}**	**10^3 k_1, s^{-1}**	**10^2 k_2, dm^3 mol^{-1} s^{-1}**
Mg^{2+}	0.00	5.67	3.54
	3.00	6.10	3.81
	6.00	6.20	3.87
	9.00	6.56	4.10
	12.00	6.79	4.25
	15.00	6.84	4.27
	18.00	7.09	4.43
	21.00	7.32	4.58
Ca^{2+}	0.00	5.67	3.54
	3.00	6.15	3.84
	6.00	6.36	3.97
	9.00	6.36	3.97
	12.00	6.61	4.13
	15.00	6.77	4.23
	18.00	7.02	4.39
	21.00	7.14	4.46

Table 4.41: Effect of added anions on the redox reaction of $[Co(salophen)]^{+}$ and $S(R)_2$ at $[Co(salophen)^{+}] = 2.0 \times 10^{-4}$ mol dm^{-3}, $[S(R)_2] = 16.0 \times 10^{-2}$ mol dm^{-3}, $[H^{+}] = 5.0 \times 10^{-2}$ mol dm^{-3}, $\mu = 0.2$ C^2 mol dm^{-3}, D = 77.42, T = 305 K and λ_{max} = 470 nm

[X]	**10^3 [X], mol dm^{-3}**	**10^3 k_1, s^{-1}**	**10^2 k_2, dm^3 mol^{-1} s^{-1}**
SO_4^{2-}	0.00	5.67	3.54
	3.00	6.06	3.79
	6.00	6.26	3.92
	9.00	6.36	3.97
	12.00	6.56	4.10
	15.00	6.70	4.19
	18.00	6.86	4.29
	21.00	7.02	4.39
CH_3COO^{-}	0.00	5.67	3.54
	3.00	6.15	3.84
	6.00	6.38	3.99
	9.00	6.66	4.16
	12.00	6.89	4.30
	15.00	6.96	4.35
	18.00	7.23	4.52
	21.00	7.45	4.65

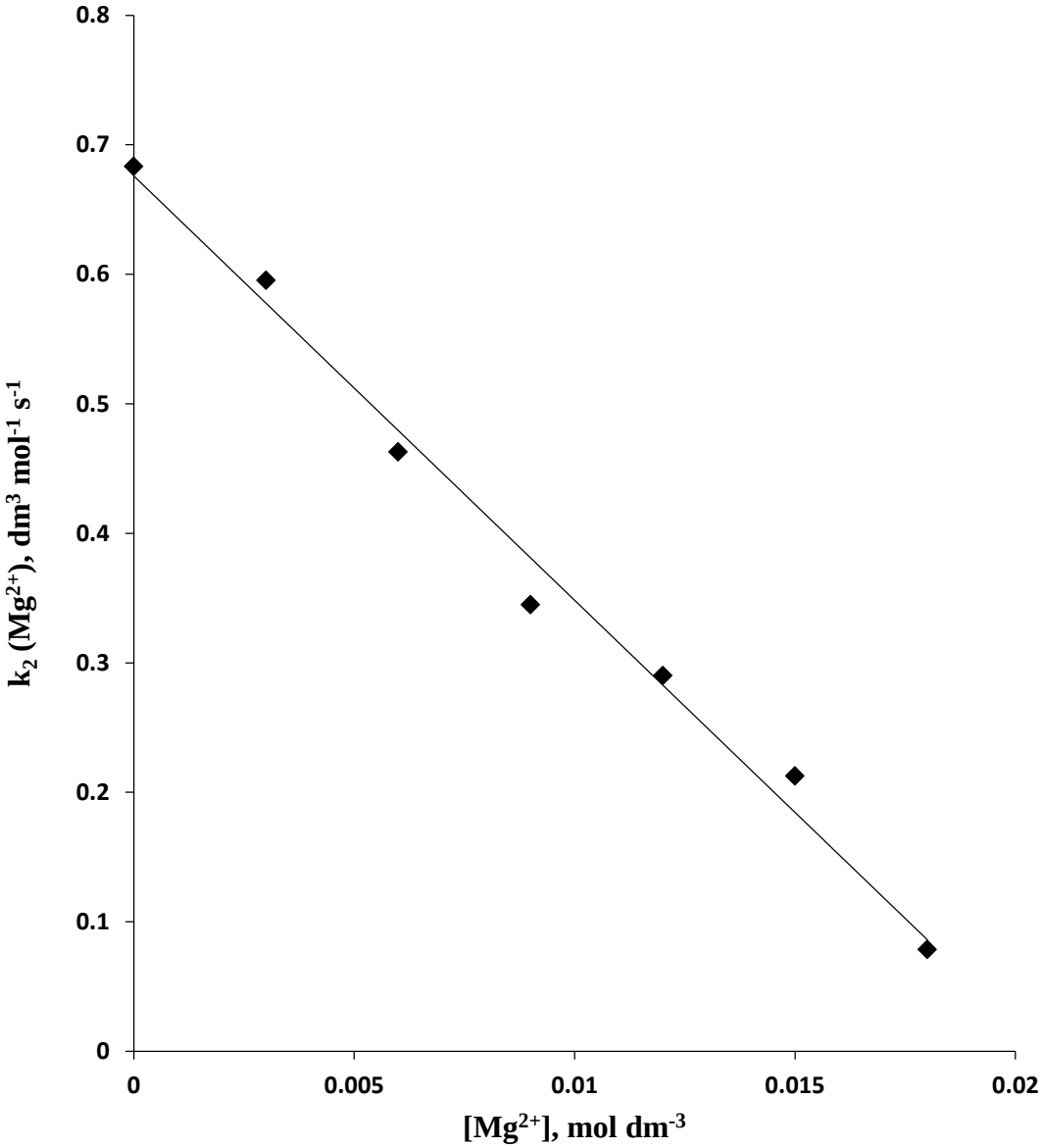


Figure 4.43: Plot of k_2 versus $[Mg^{2+}]$ for the redox reaction of $[Co(salophen)]^+$ and LSH at $[Co(salophen)^+] = 2.0 \times 10^{-4}$ mol dm^{-3}, [LSH] = 12.0×10^{-3} mol dm^{-3}, $[H^+] = 1.0 \times 10^{-3}$ mol dm^{-3} $\mu = 0.1$ C^2 mol dm^{-3}, D = 74.84, T = 300 K, and λ_{max} = 470 nm

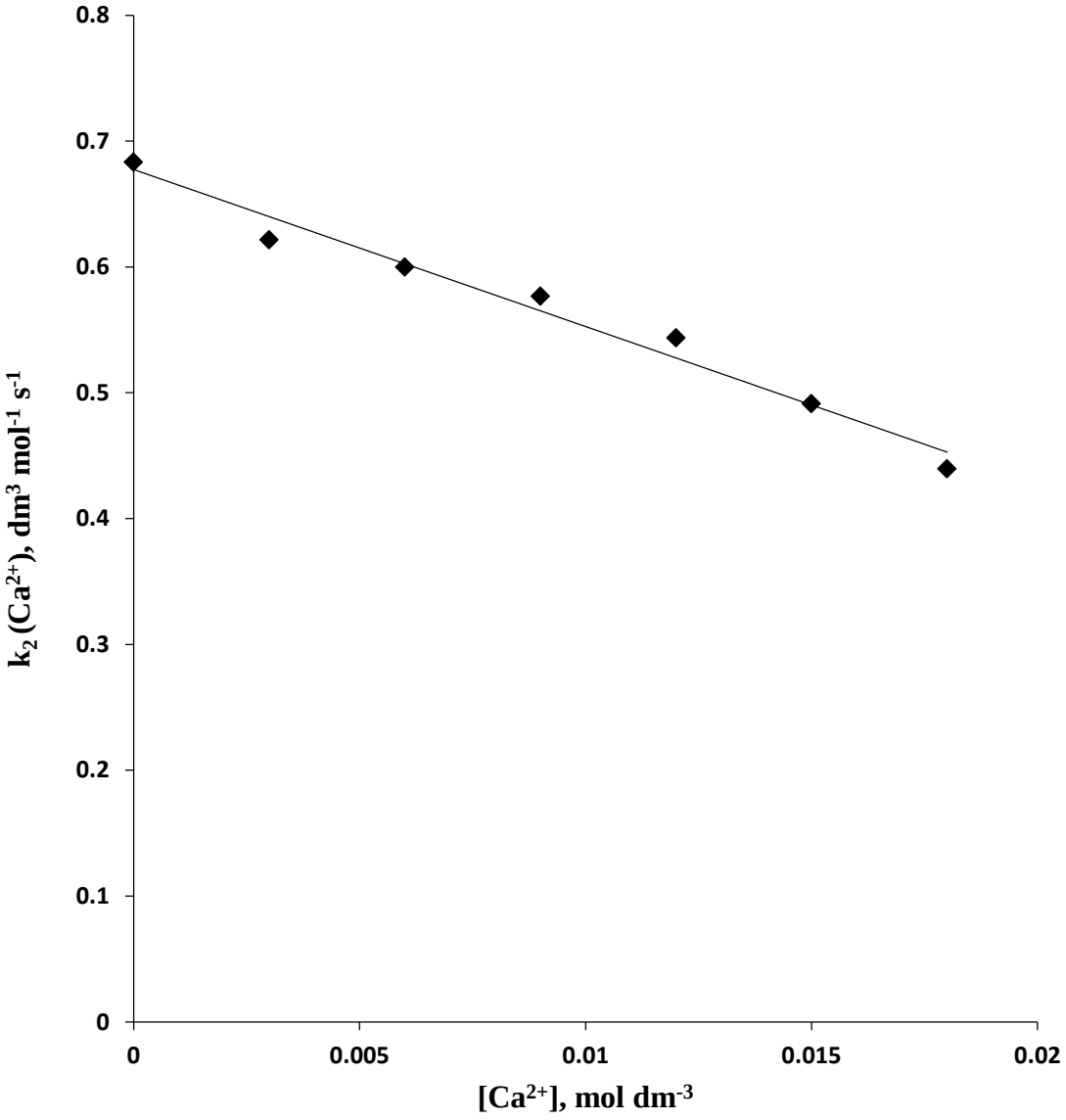


Figure 4.44: Plot of k_2 versus $[Ca^{2+}]$ for the redox reaction of $[Co(salophen)]^+$ and LSH at $[Co(salophen)^+] = 2.0 \times 10^{-4}$ mol dm^{-3}, [LSH] = 12.0×10^{-3} mol dm^{-3}, $[H^+] = 1.0 \times 10^{-3}$ mol dm^{-3} $\mu = 0.1$ C^2 mol dm^{-3}, D = 74.84, T = 300 K, and λ_{max} = 470 nm

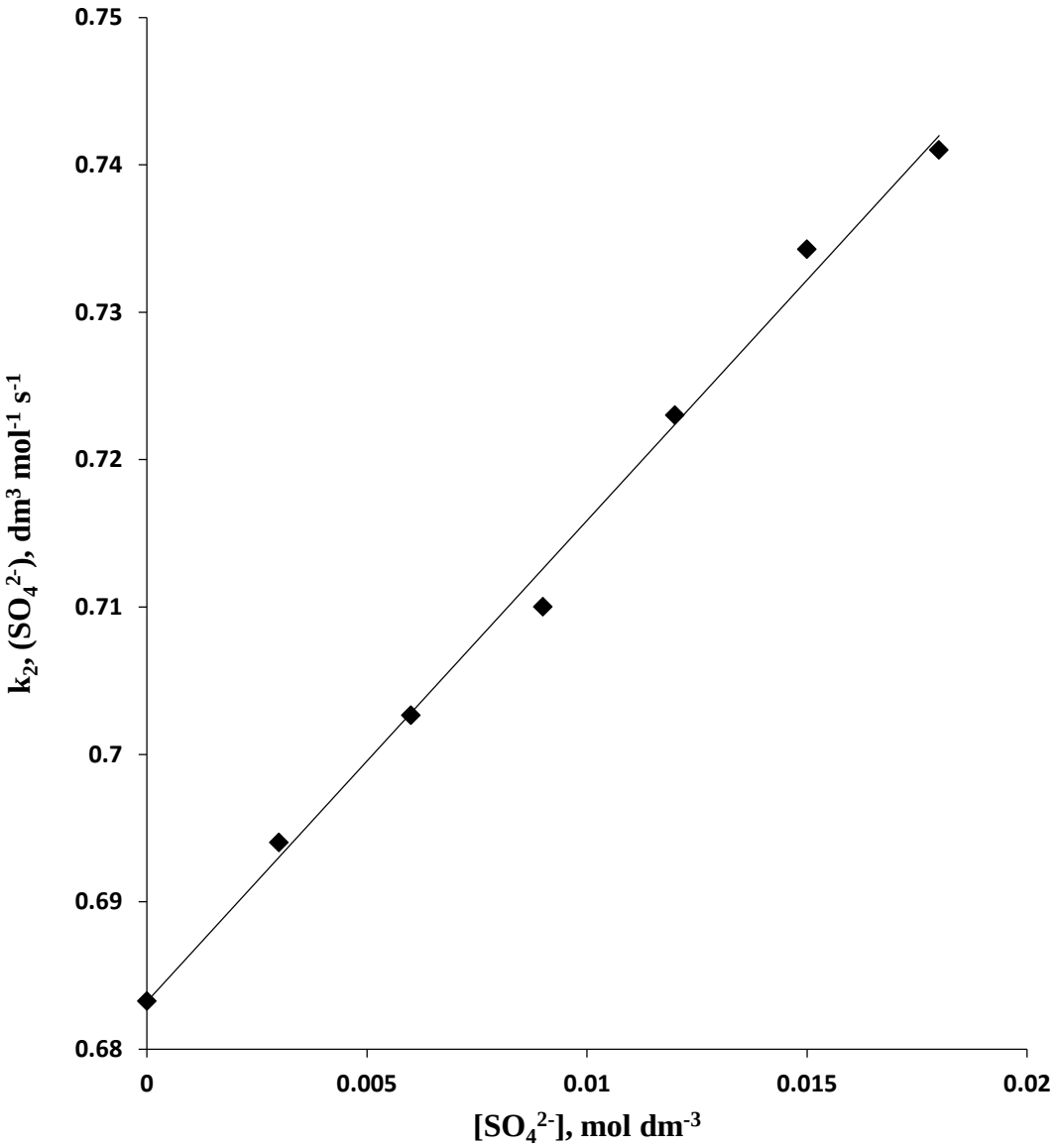


Figure 4.45: Plot of k_2 versus $[SO_4^{2-}]$ for the redox reaction of $[Co(salophen)]^+$ and LSH at $[Co(salophen)^+] = 2.0 \times 10^{-4}$ mol dm^{-3}, [LSH] = 12.0×10^{-3} mol dm^{-3}, $[H^+] = 1.0 \times 10^{-3}$ mol dm^{-3}, $\mu = 0.1$ C^2 mol dm^{-3}, D = 74.84, T = 300 K, and λ_{max} = 470 nm

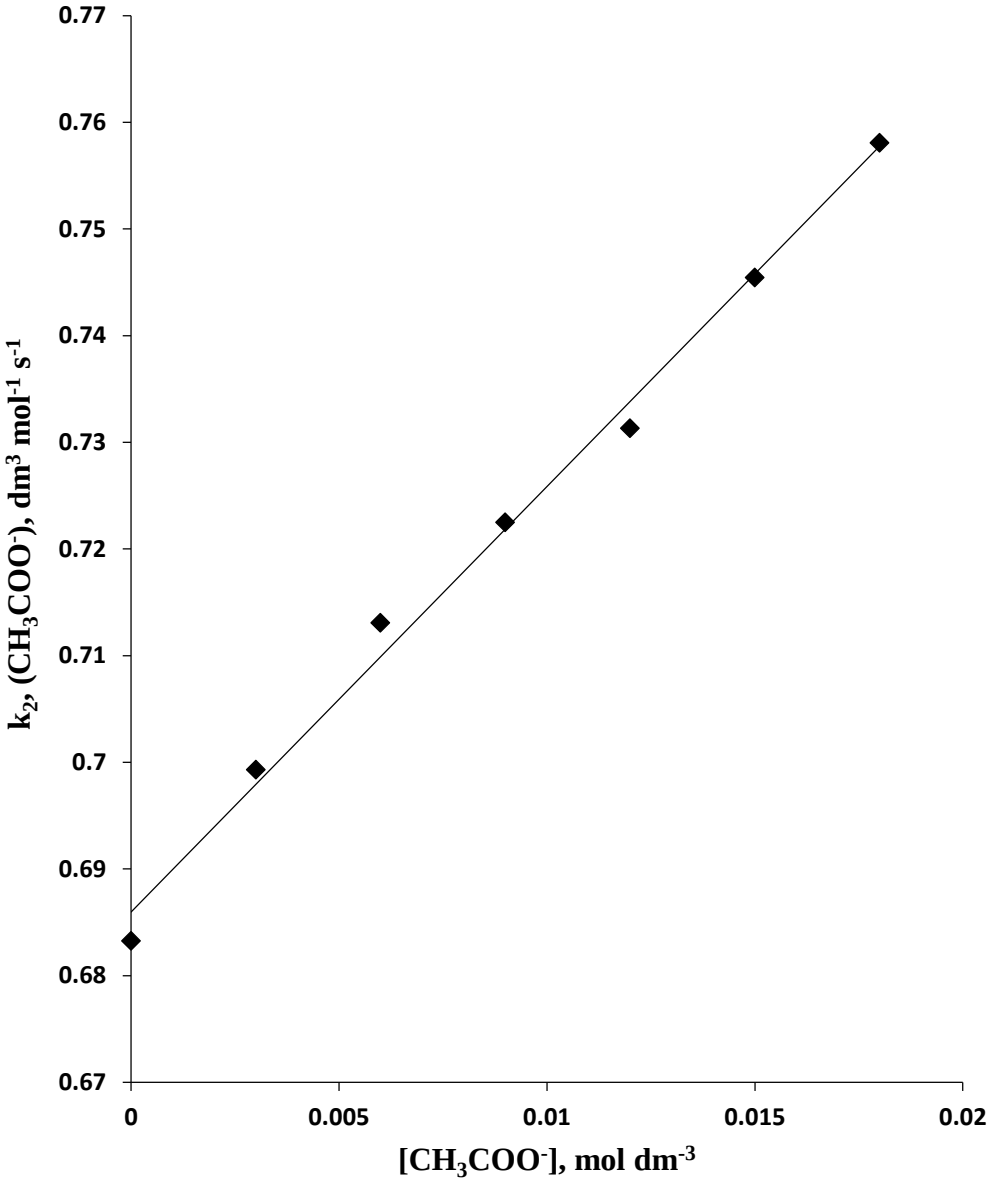


Figure 4.46: Plot of k_2 versus $[CH_3COO^-]$ for the redox reaction of $[Co(salophen)]^+$ and LSH at $[Co(salophen)^+] = 2.0 \times 10^{-4}$ mol dm^{-3}, [LSH] = 12.0×10^{-3} mol dm^{-3}, $[H^+] = 1.0 \times 10^{-3}$ mol dm^{-3}, $\mu = 0.1$ C^2 mol dm^{-3}, D = 74.84, T = 300 K, and λ_{max} = 470 nm

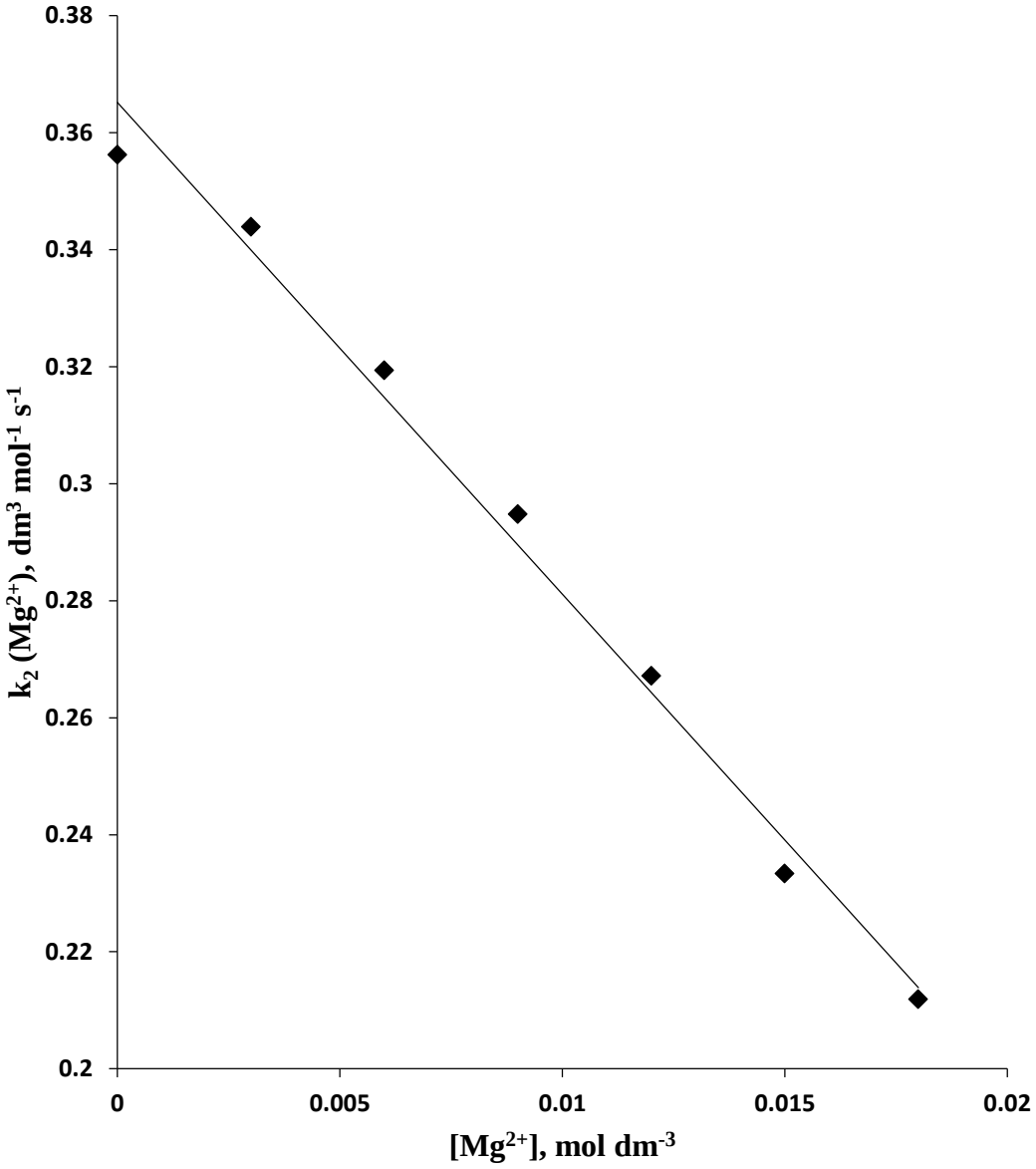


Figure 4.47: Plot of k_2 versus $[Mg^{2+}]$ for the redox reaction of $[Co(salophen)]^+$ and RSH at $[Co(salophen)^+] = 3.0 \times 10^{-4}$ mol dm^{-3}, $[RSH] = 15.0 \times 10^{-3}$ mol dm^{-3}, $[H^+] = 1.4 \times 10^{-3}$ mol dm^{-3} $\mu = 0.1$ C^2 mol dm^{-3}, D = 74.19, T = 300 K, and λ_{max} = 470 nm

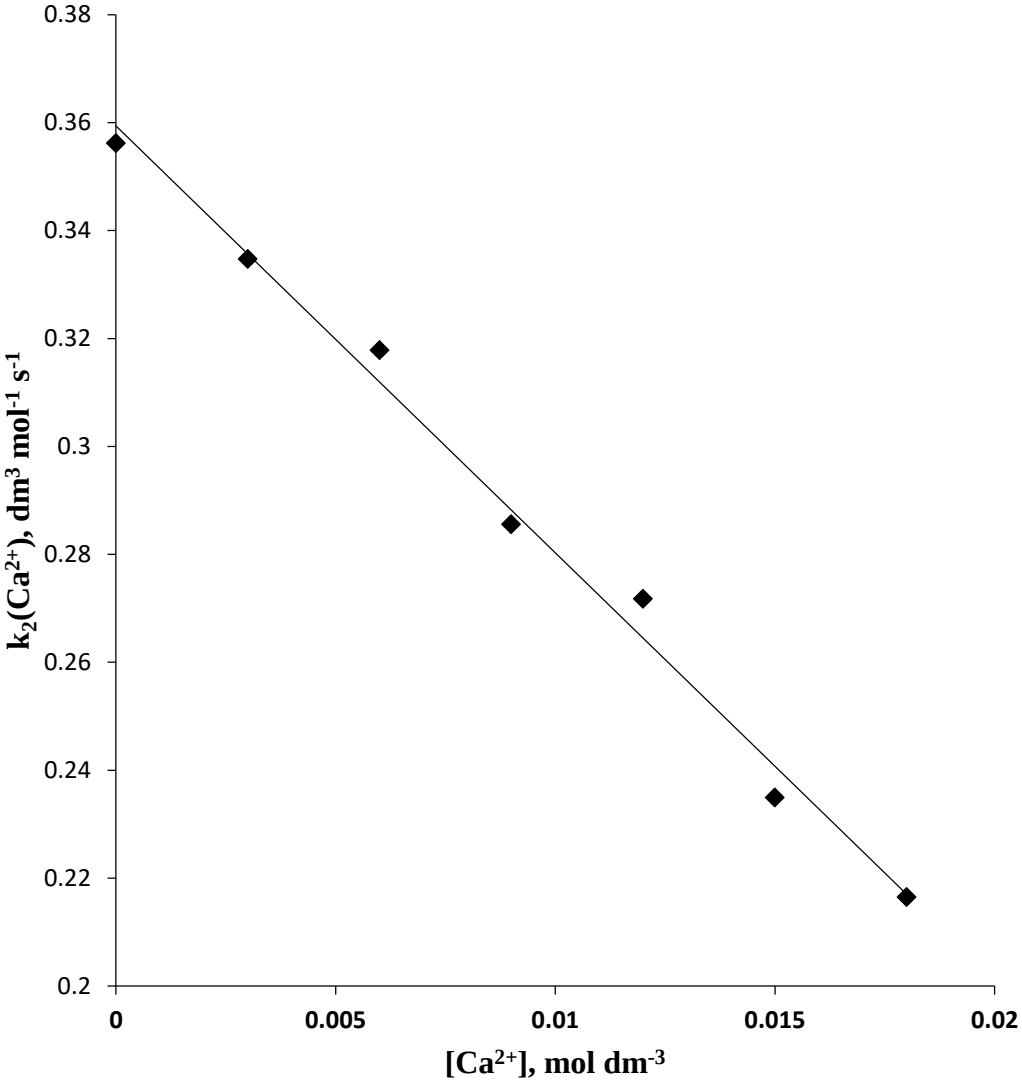


Figure 4.48: Plot of k_2 versus $[Ca^{2+}]$ for the redox reaction of $[Co(salophen)]^+$ and RSH at $[Co(salophen)^+] = 3.0 \times 10^{-4}$ mol dm^{-3}, $[RSH] = 15.0 \times 10^{-3}$ mol dm^{-3}, $[H^+] = 1.4 \times 10^{-3}$ mol dm^{-3} $\mu = 0.1$ C^2 mol dm^{-3}, D = 74.19, T = 300 K, and λ_{max} = 470 nm

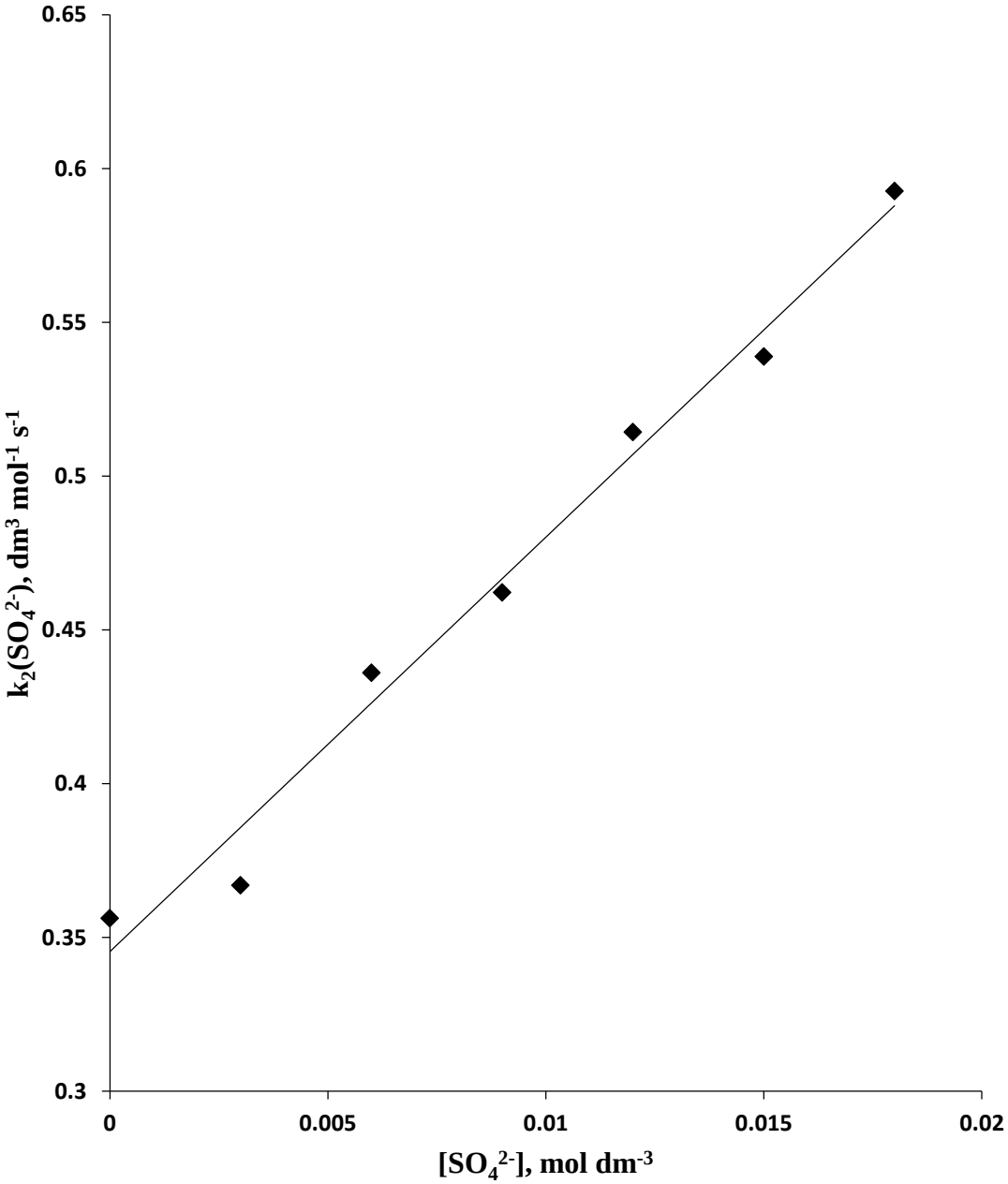


Figure 4.49: Plot of k_2 versus $[SO_4^{2-}]$ for the redox reaction of $[Co(salophen)]^+$ and RSH at $[Co(salophen)^+] = 3.0 \times 10^{-4}$ mol dm^{-3}, [RSH] = 15.0×10^{-3} mol dm^{-3}, $[H^+] = 1.4 \times 10^{-3}$ mol dm^{-3}, $\mu = 0.1$ C^2 mol dm^{-3}, D = 74.19, T = 300 K, and λ_{max} = 470 nm

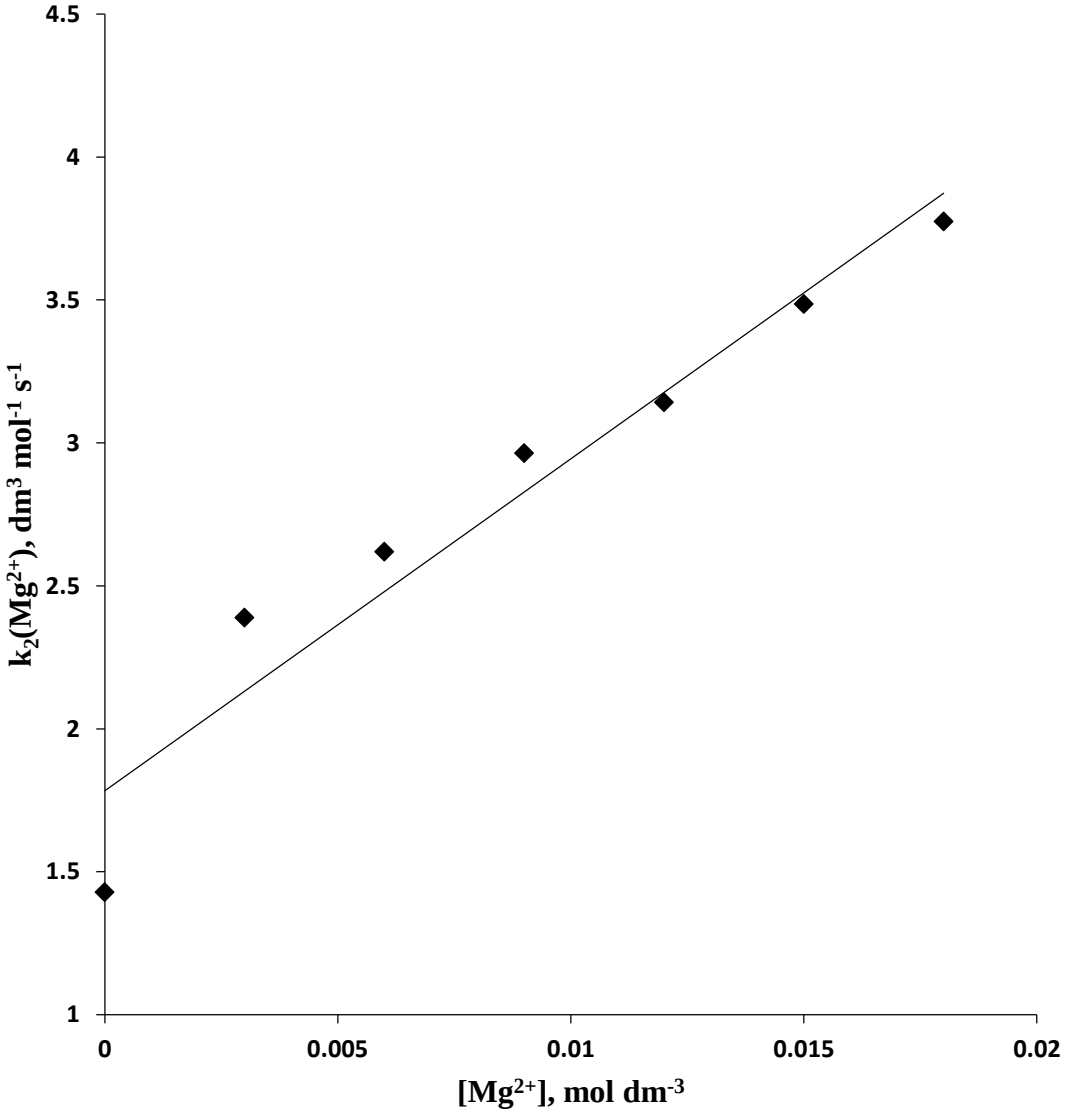


Figure 4.50: Plot of k_2 versus $[Mg^{2+}]$ for the redox reaction of $[Co(salophen)]^+$ and TSH at $[Co(salophen)^+] = 3.0 \times 10^{-4}$ mol dm^{-3}, [TSH] = 7.50×10^{-3} mol dm^{-3}, μ = 0.1 C^2 mol dm^{-3}, D = 74.04, T = 300 K, and λ_{max} = 470 nm

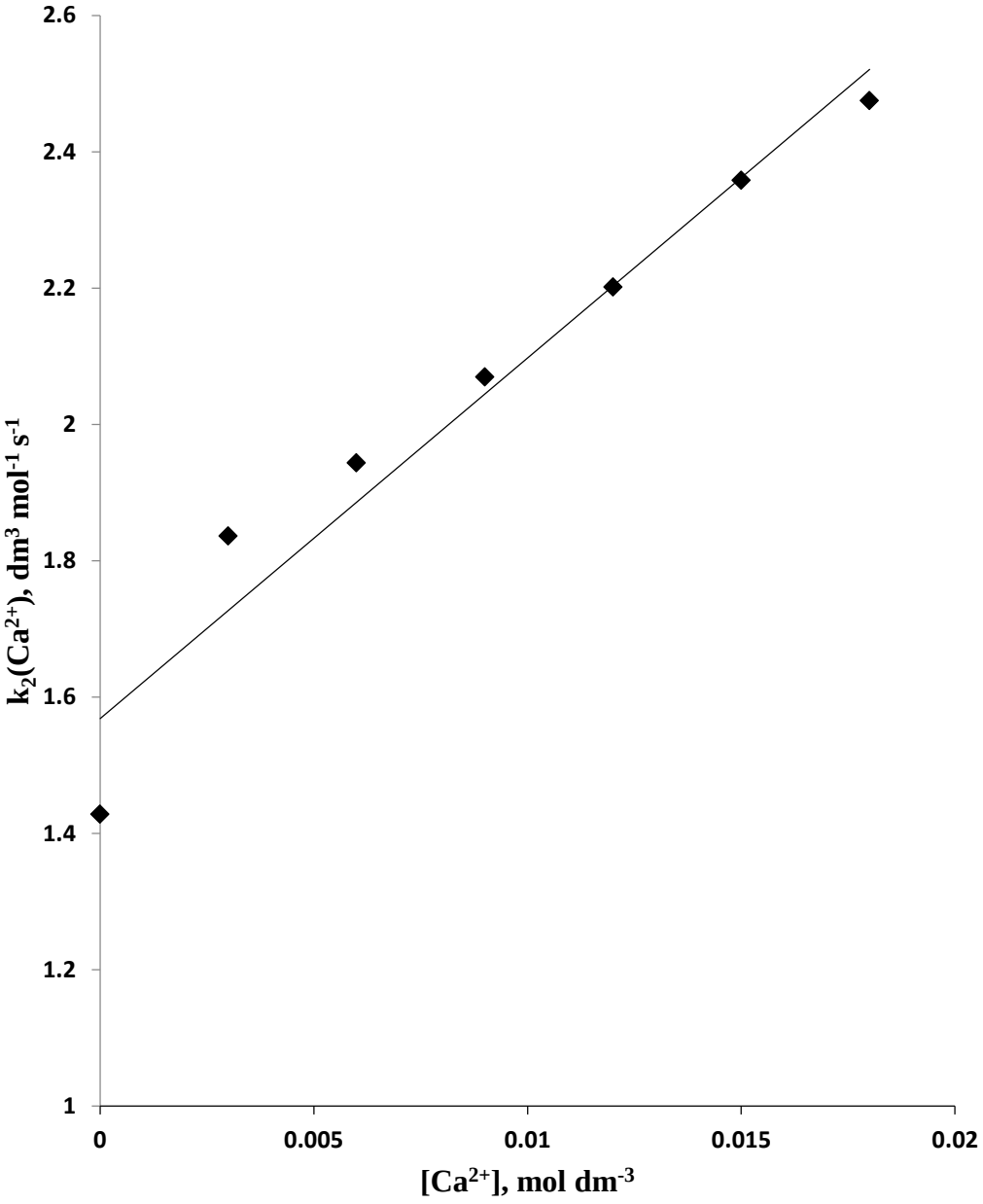


Figure 4.51: Plot of k_2 versus $[Ca^{2+}]$ for the redox reaction of $[Co(salophen)]^+$ and TSH at $[Co(salophen)^+] = 3.0 \times 10^{-4}$ mol dm^{-3}, [TSH] = 7.50×10^{-3} mol dm^{-3}, μ = 0.1 C^2 mol dm^{-3}, D = 74.04, T = 300 K, and λ_{max} = 470 nm

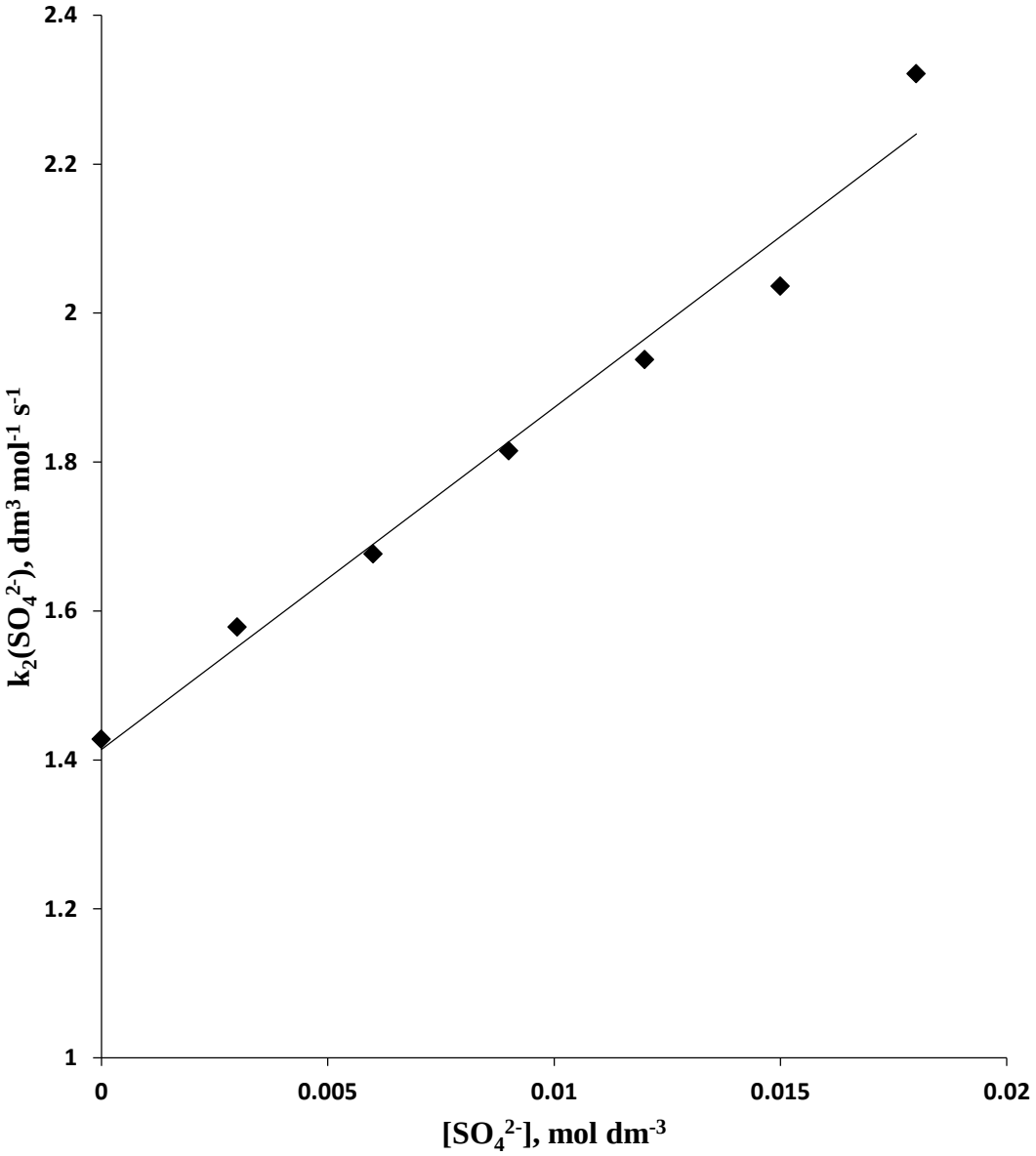


Figure 4.52: Plot of k_2 versus $[SO_4^{2-}]$ for the redox reaction of $[Co(salophen)]^+$ and TSH at $[Co(salophen)^+] = 3.0 \times 10^{-4}$ mol dm^{-3}, [TSH] = 7.50×10^{-3} mol dm^{-3}, μ = 0.1 C^2 mol dm^{-3}, D = 74.04, T = 300 K, and λ_{max} = 470 nm

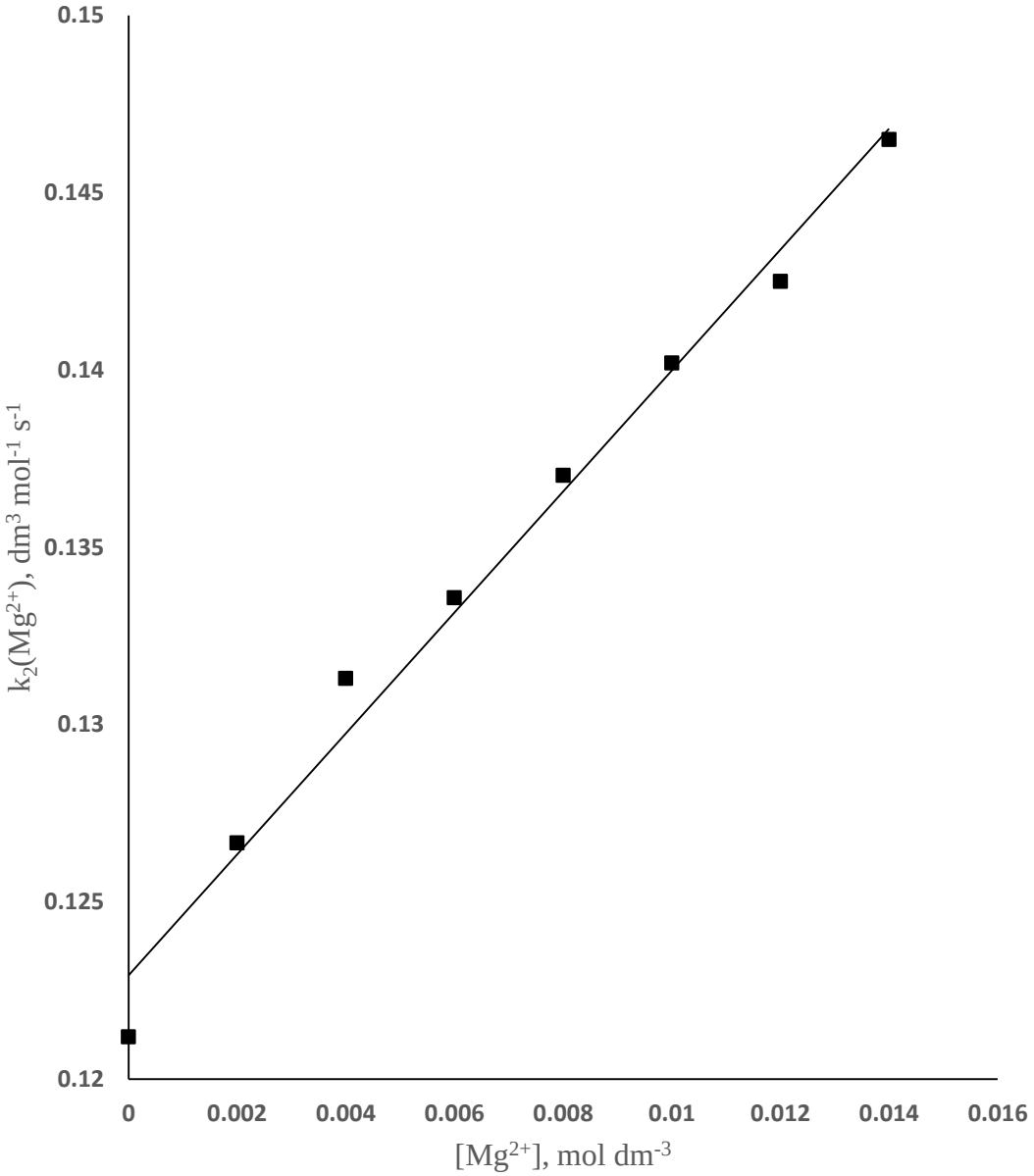


Figure 4.53: Plot of k_2 versus $[Mg^{2+}]$ for the redox reaction of $[Co(salophen)]^+$ and TSCZ at $[Co(salophen)^+] = 2.0 \times 10^{-4}$ mol dm^{-3}, $[TSCZ] = 8.0 \times 10^{-2}$ mol dm^{-3}, $[H^+] = 1.0 \times 10^{-2}$ mol dm^{-3}, $\mu = 0.1$ C^2 mol dm^{-3}, D = 74.41, T = 306 K and λ_{max} = 470 nm

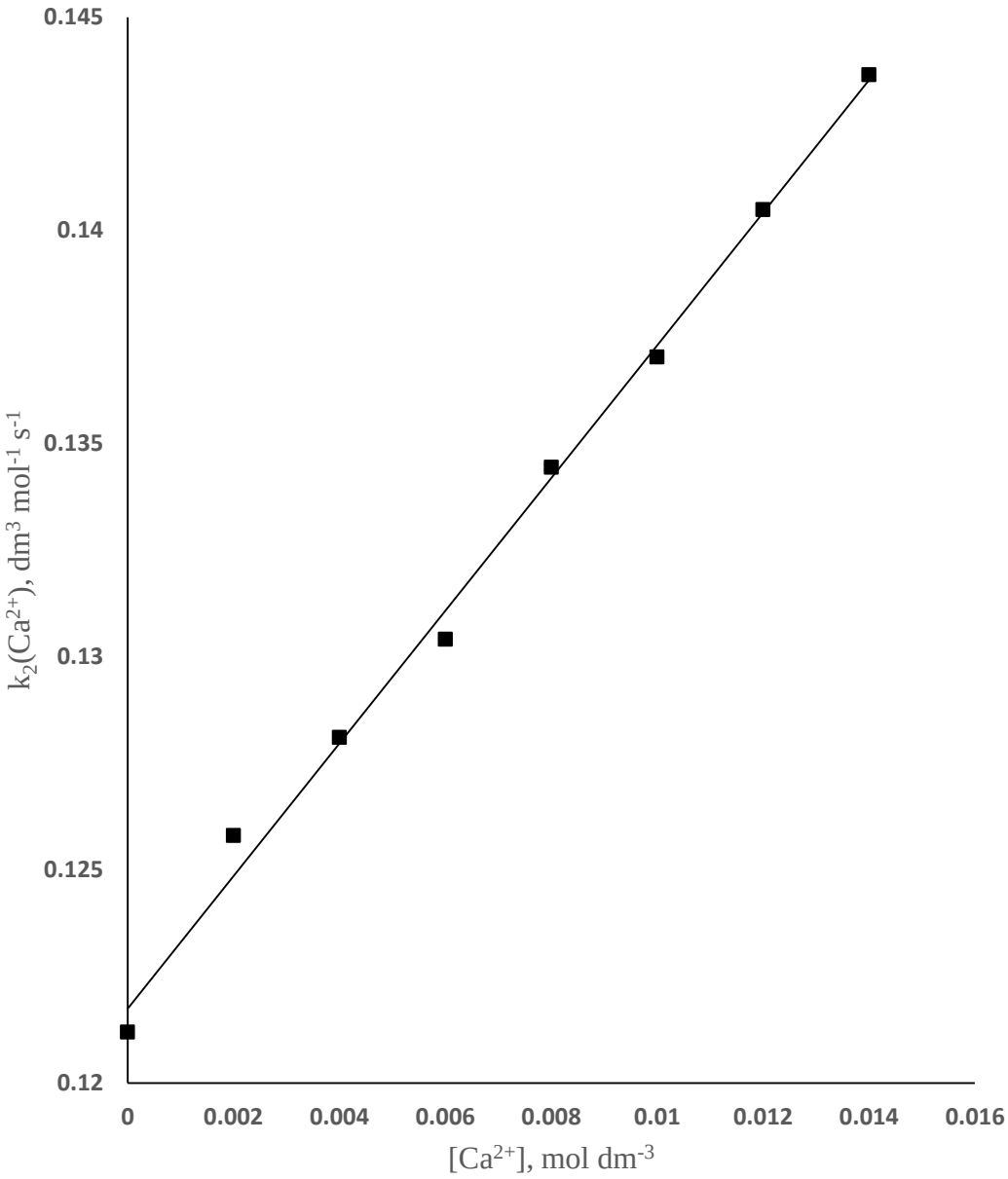


Figure 4.54: Plot of k_2 versus $[Ca^{2+}]$ for the redox reaction of $[Co(salophen)]^+$ and TSCZ at $[Co(salophen)^+] = 2.0 \times 10^{-4}$ mol dm^{-3}, $[TSCZ] = 8.0 \times 10^{-2}$ mol dm^{-3}, $[H^+] = 1.0 \times 10^{-2}$ mol dm^{-3}, $\mu = 0.1$ C^2 mol dm^{-3}, D = 74.41, T = 306 K and λ_{max} = 470 nm

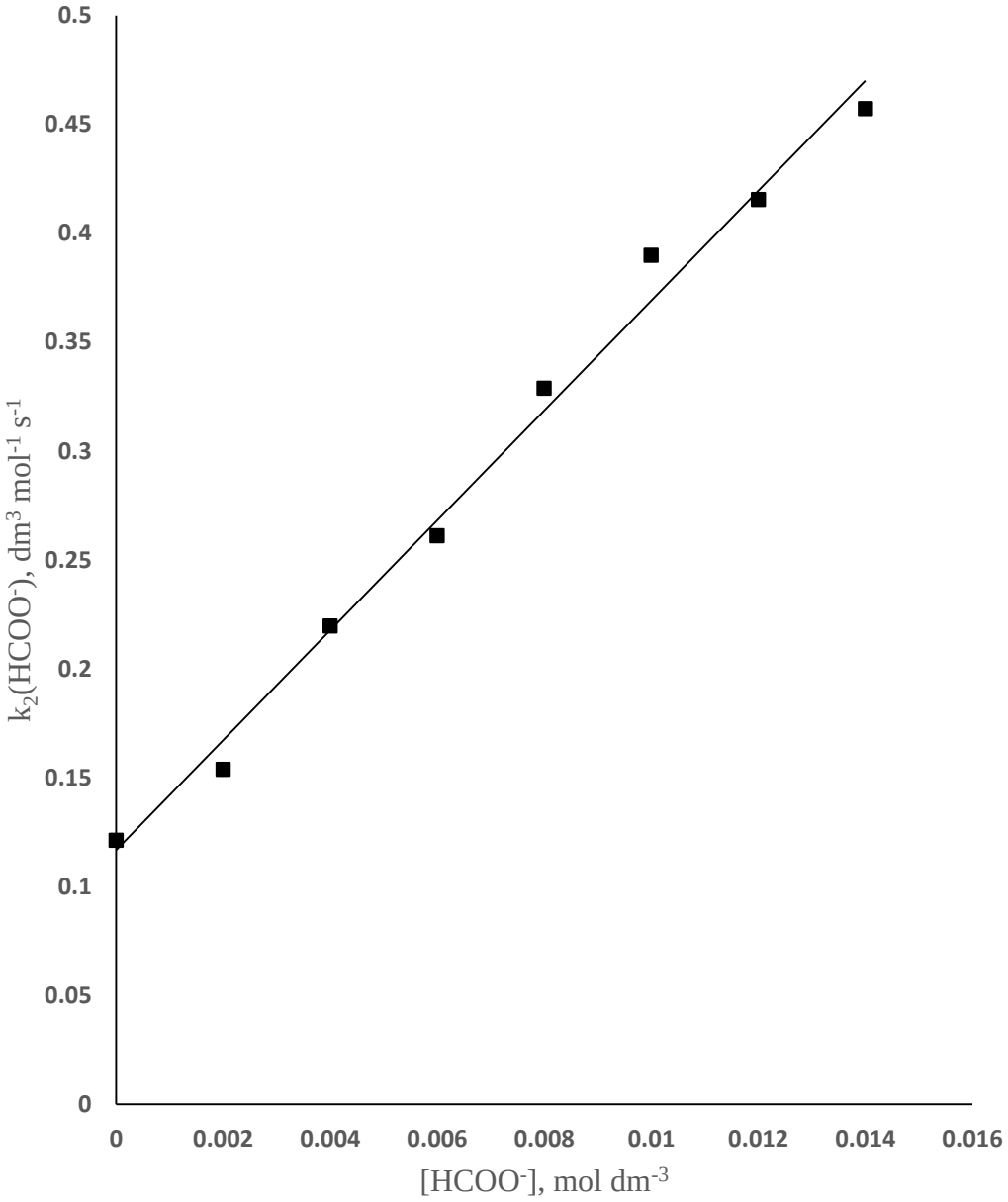


Figure 4.55: Plot of k_2 versus $[HCOO^-]$ for the redox reaction of $[Co(salophen)]^+$ and TSCZ at $[Co(salophen)^+] = 2.0 \times 10^{-4}$ mol dm^{-3}, [TSCZ] = 8.0×10^{-2} mol dm^{-3}, $[H^+] = 1.0 \times 10^{-2}$ mol dm^{-3}, $\mu = 0.1$ C^2 mol dm^{-3}, D = 74.41, T = 306 K and λ_{max} = 470 nm

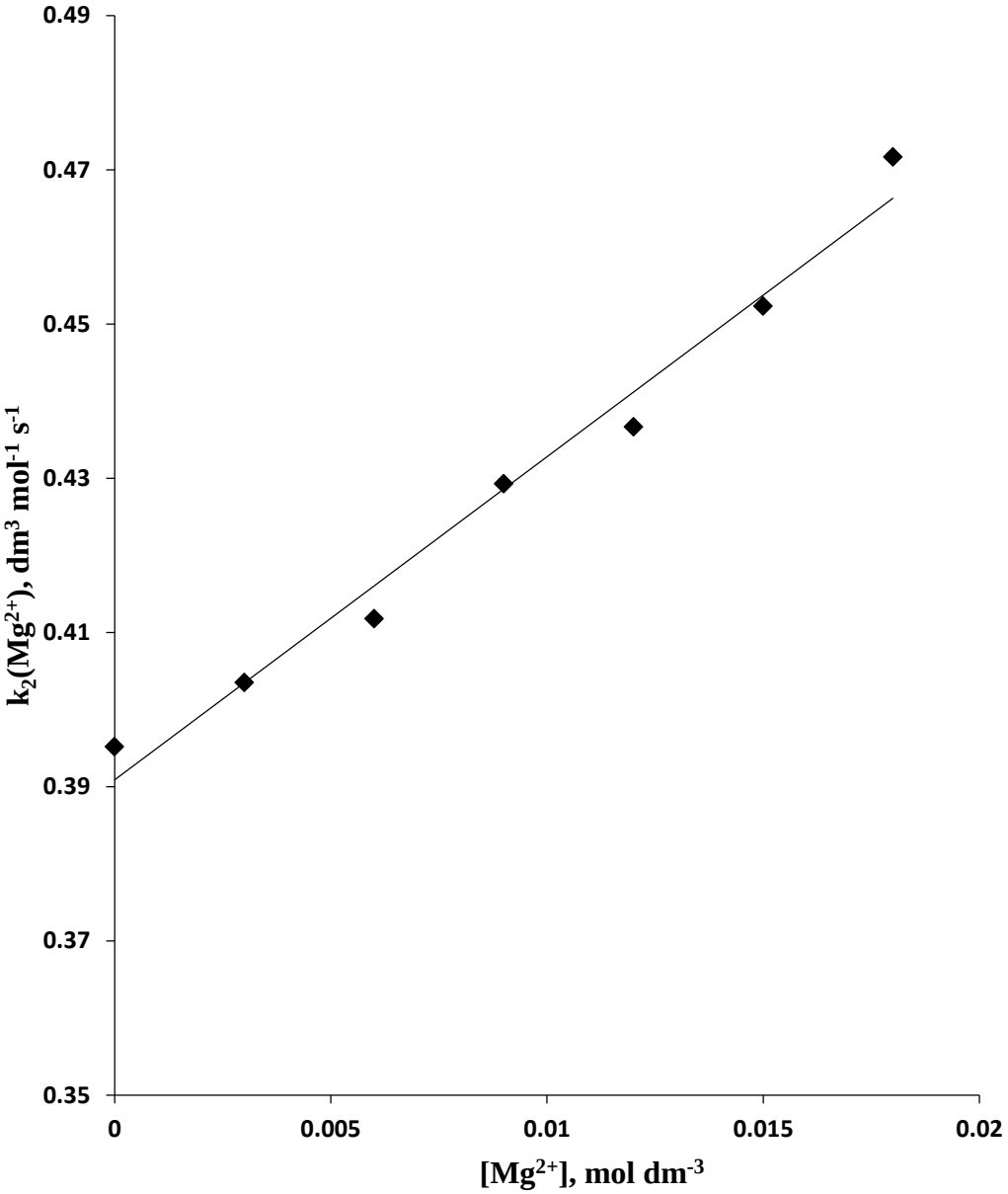


Figure 4.56: Plot of k_2 versus $[Mg^{2+}]$ for the reaction of $[Co(salophen)]^+$ and DPCI at $[Co(salophen)^+] = 1.0 \times 10^{-4}$ mol dm^{-3}, [DPCI] = 25.0×10^{-3} mol dm^{-3} $[H^+] = 0.1$ mol dm^{-3}, $\mu = 0.5$ C^2 mol dm^{-3}, D = 75.83, T = 300 K and λ_{max} = 470 nm

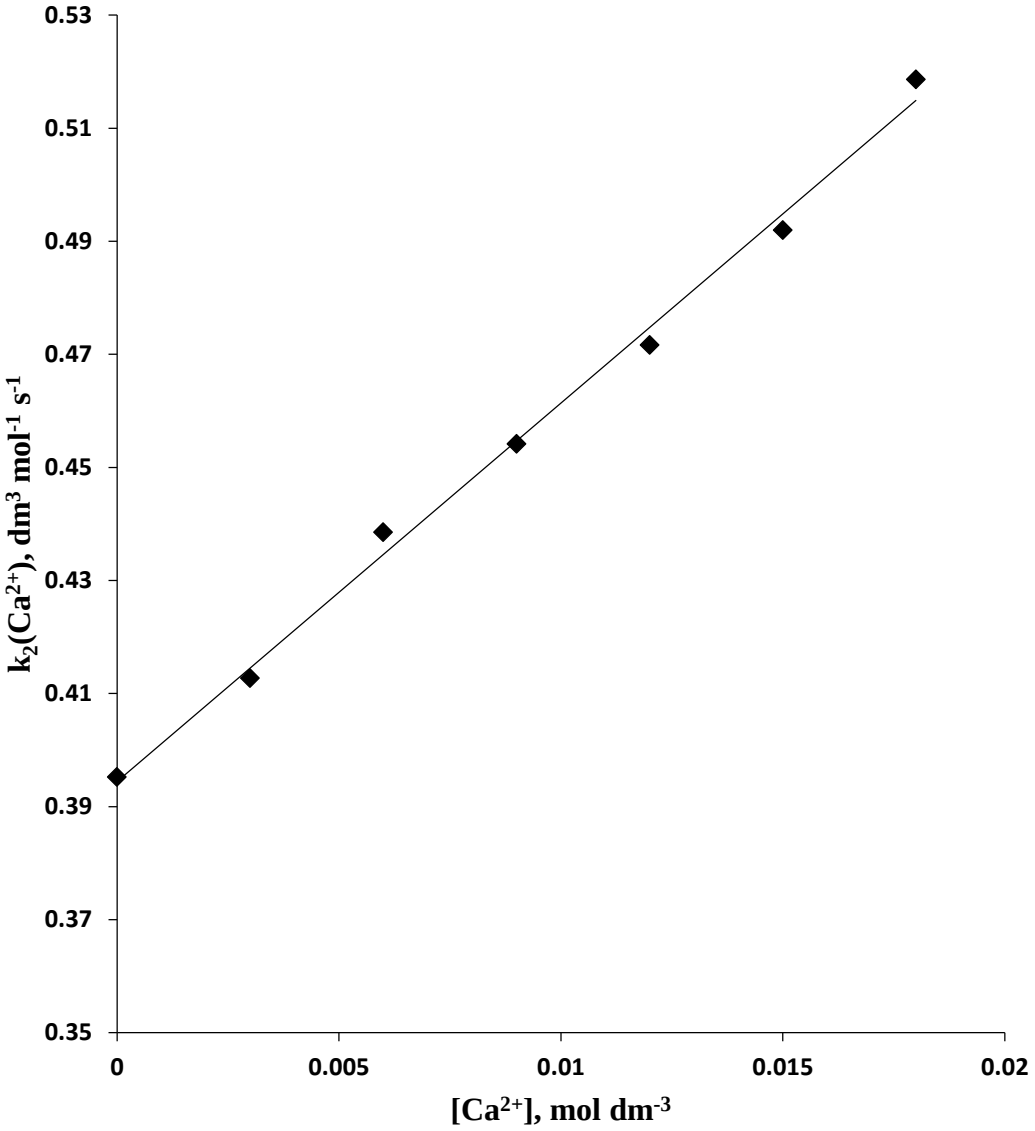


Figure 4.57: Plot of k_2 versus $[Ca^{2+}]$ for the reaction of $[Co(salophen)]^+$ and DPCI at $[Co(salophen)^+] = 1.0 \times 10^{-4}$ mol dm^{-3}, [DPCI] = 25.0×10^{-3} mol dm^{-3} $[H^+] = 0.1$ mol dm^{-3}, $\mu = 0.5$ C^2 mol dm^{-3}, D = 75.83, T = 300 K and λ_{max} = 470 nm

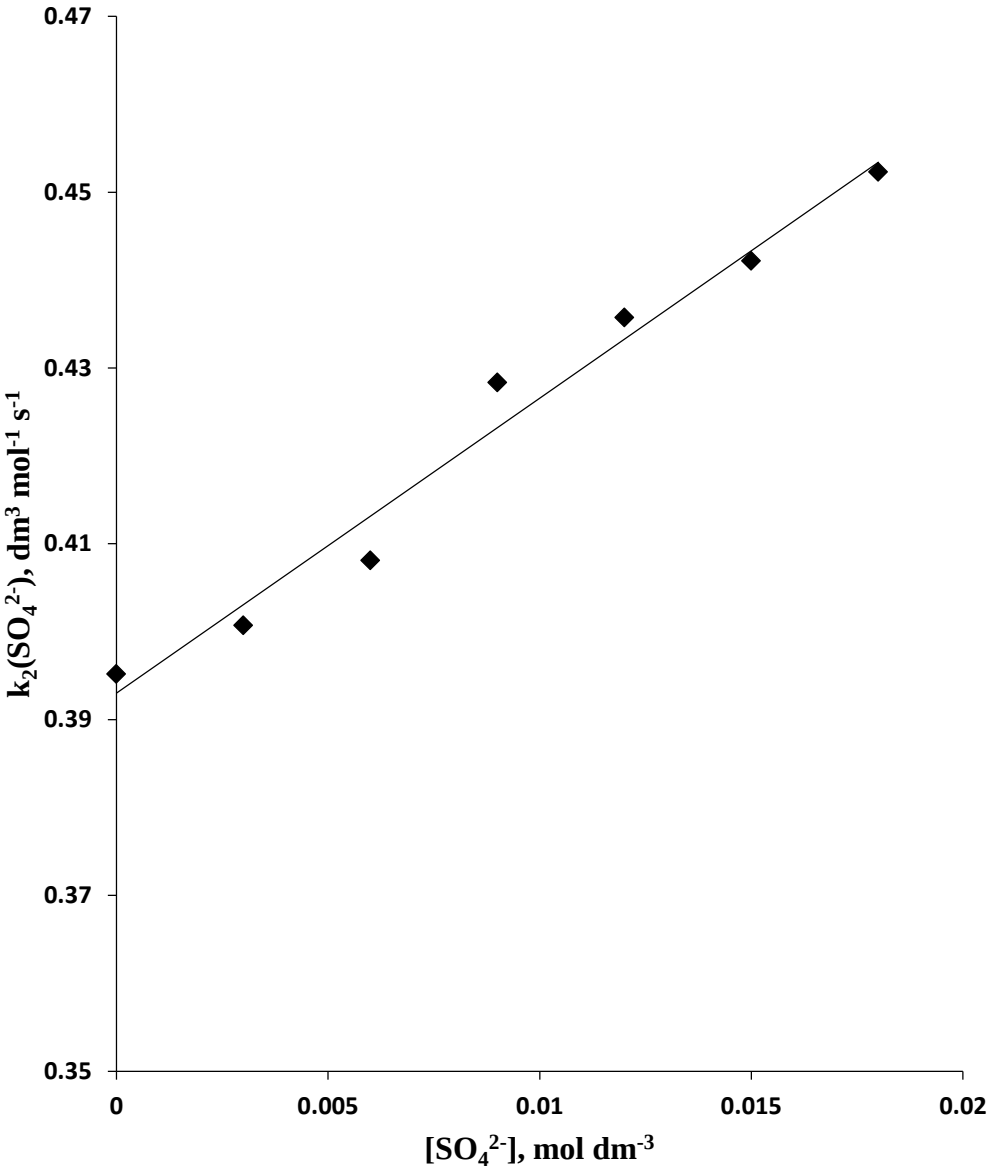


Figure 4.58: Plot of k_2 versus $[SO_4^{2-}]$ for the reaction of $[Co(salophen)]^+$ and DPCI at $[Co(salophen)^+] = 1.0 \times 10^{-4}$ mol dm^{-3}, DPCI = 25.0×10^{-3} mol dm^{-3} $[H^+] = 0.1$ mol dm^{-3}, $\mu = 0.5$ C^2 mol dm^{-3}, D = 75.83, T = 300 K and λ_{max} = 470 nm

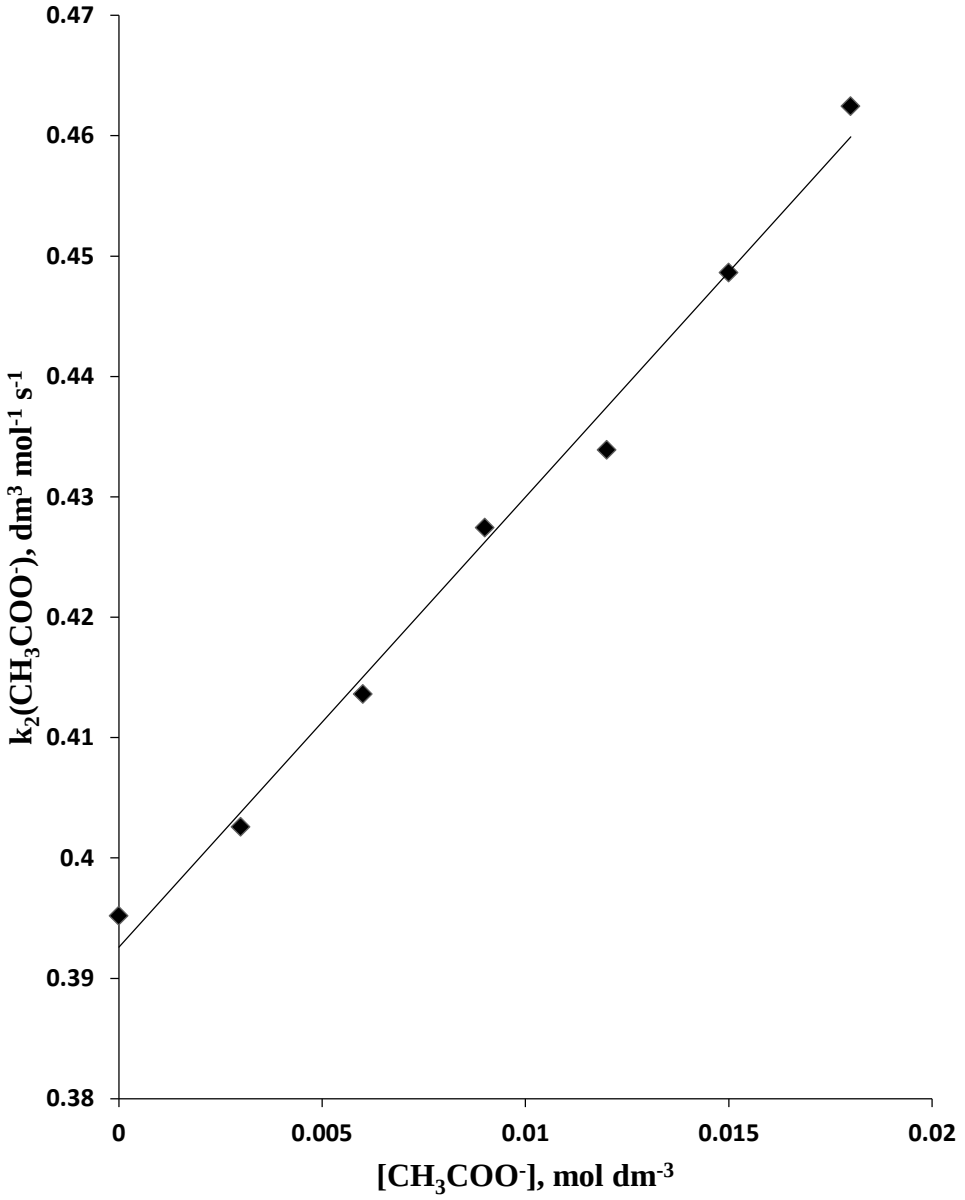


Figure 4.59: Plot of k_2 versus $[CH_3COO^-]$ for the reaction of $[Co(salophen)]^+$ and DPCI at $[Co(salophen)^+] = 1.0 \times 10^{-4}$ mol dm^{-3}, DPCI = 25.0×10^{-3} mol dm^{-3} $[H^+] = 0.1$ mol dm^{-3}, $\mu = 0.5$ C^2 mol dm^{-3}, D = 75.83, T = 300 K and λ_{max} = 470 nm

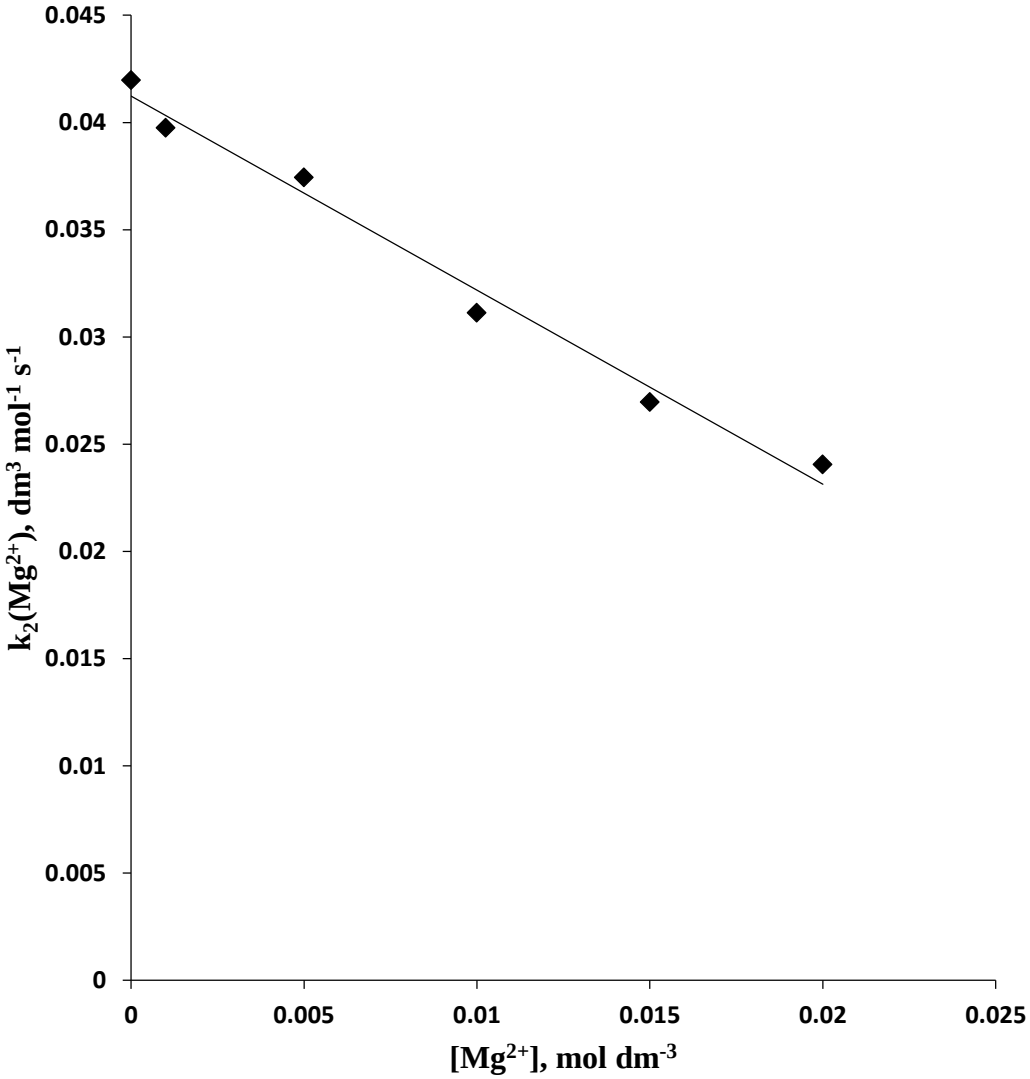


Figure 4.60: Plot of k_2 versus $[Mg^{2+}]$ for the redox reaction of $[Co(salophen)]^+$ and CH_3CHO at $[Co(salophen)^+] = 3.0 \times 10^{-4}$ mol dm^{-3}, $[CH_3CHO] = 13.5 \times 10^{-2}$ mol dm^{-3}, $[H^+] = 4.0 \times 10^{-2}$ mol dm^{-3}, $\mu = 0.2$ C^2 mol dm^{-3}, D = 75.67, T = 302 K and λ_{max} = 470 nm

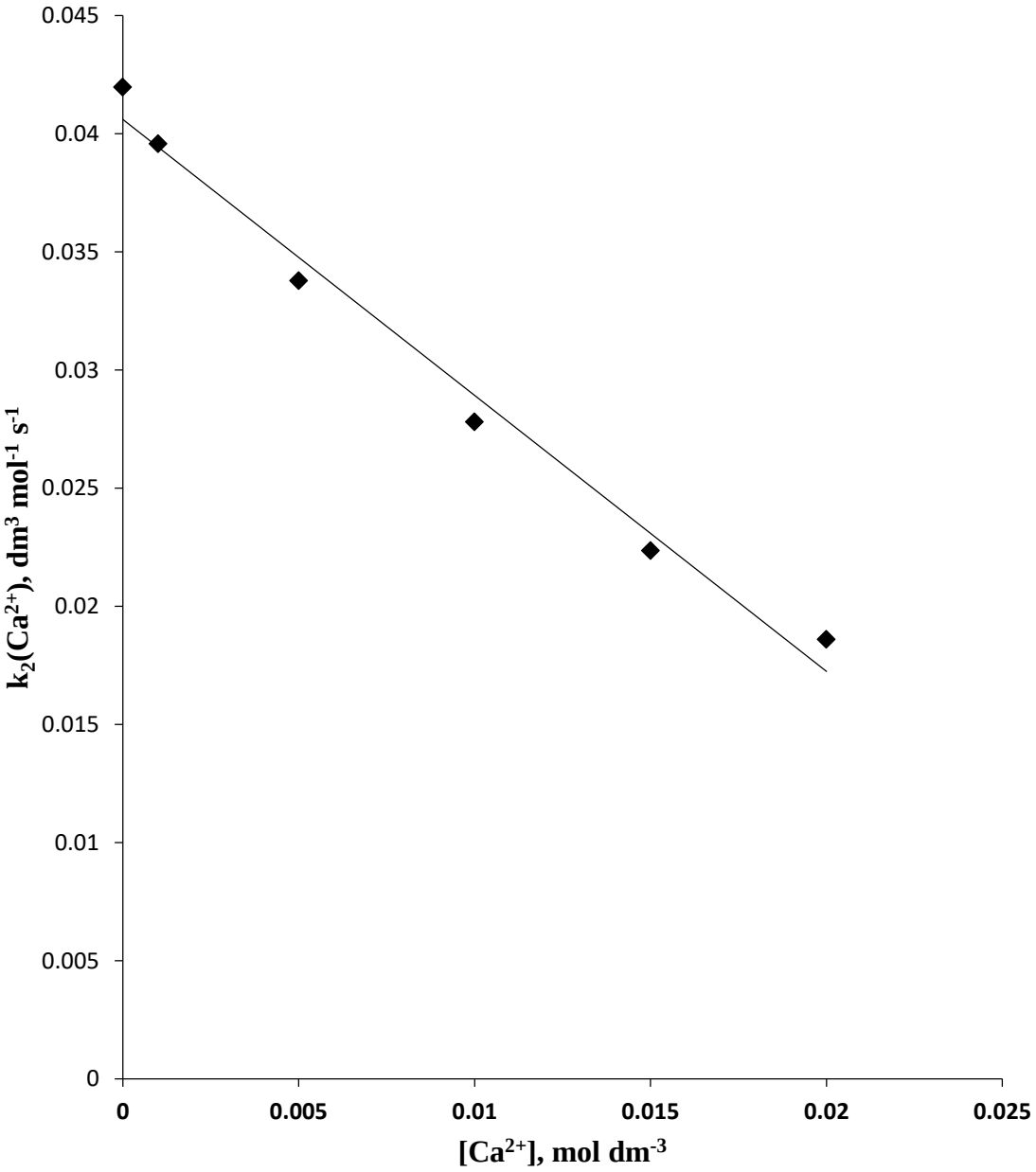


Figure 4.61: Plot of k_2 versus $[Ca^{2+}]$ for the redox reaction of $[Co(salophen)]^+$ and CH_3CHO at $[Co(salophen)^+] = 3.0 \times 10^{-4}$ mol dm^{-3}, $[CH_3CHO] = 13.5 \times 10^{-2}$ mol dm^{-3}, $[H^+] = 4.0 \times 10^{-2}$ mol dm^{-3}, $\mu = 0.2$ C^2 mol dm^{-3}, D = 75.67, T = 302 K and λ_{max} = 470 nm

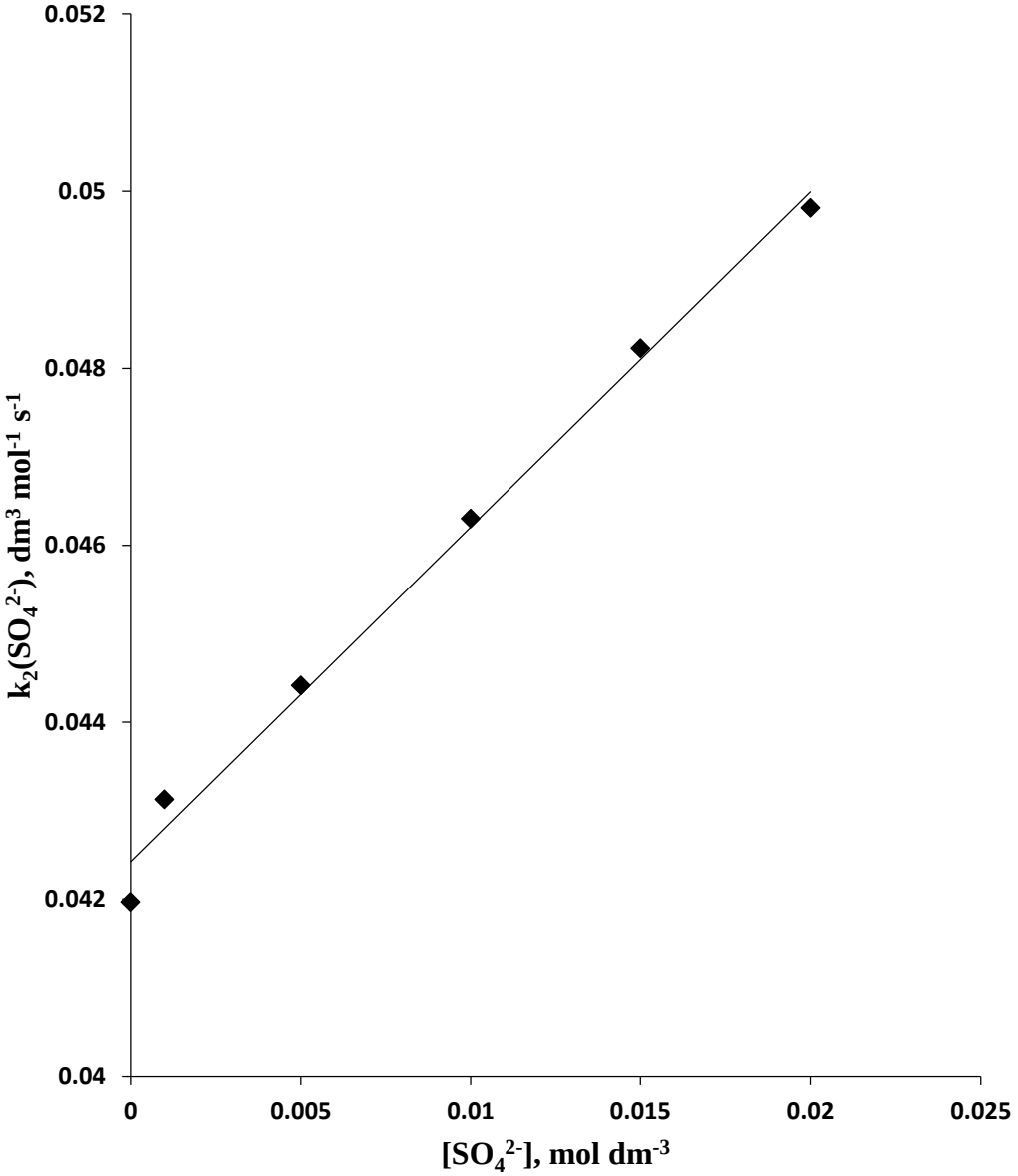


Figure 4. 62: Plot of k_2 versus $[SO_4^{2-}]$ for the redox reaction of $[Co(salophen)]^+$ and CH_3CHO at $[Co(salophen)^+] = 3.0 \times 10^{-4}$ mol dm^{-3}, $[CH_3CHO] = 13.5 \times 10^{-2}$ mol dm^{-3}, $[H^+] = 4.0 \times 10^{-2}$ mol dm^{-3}, $\mu = 0.2$ C^2 mol dm^{-3}, D = 75.67, T = 302 K and λ_{max} = 470 nm

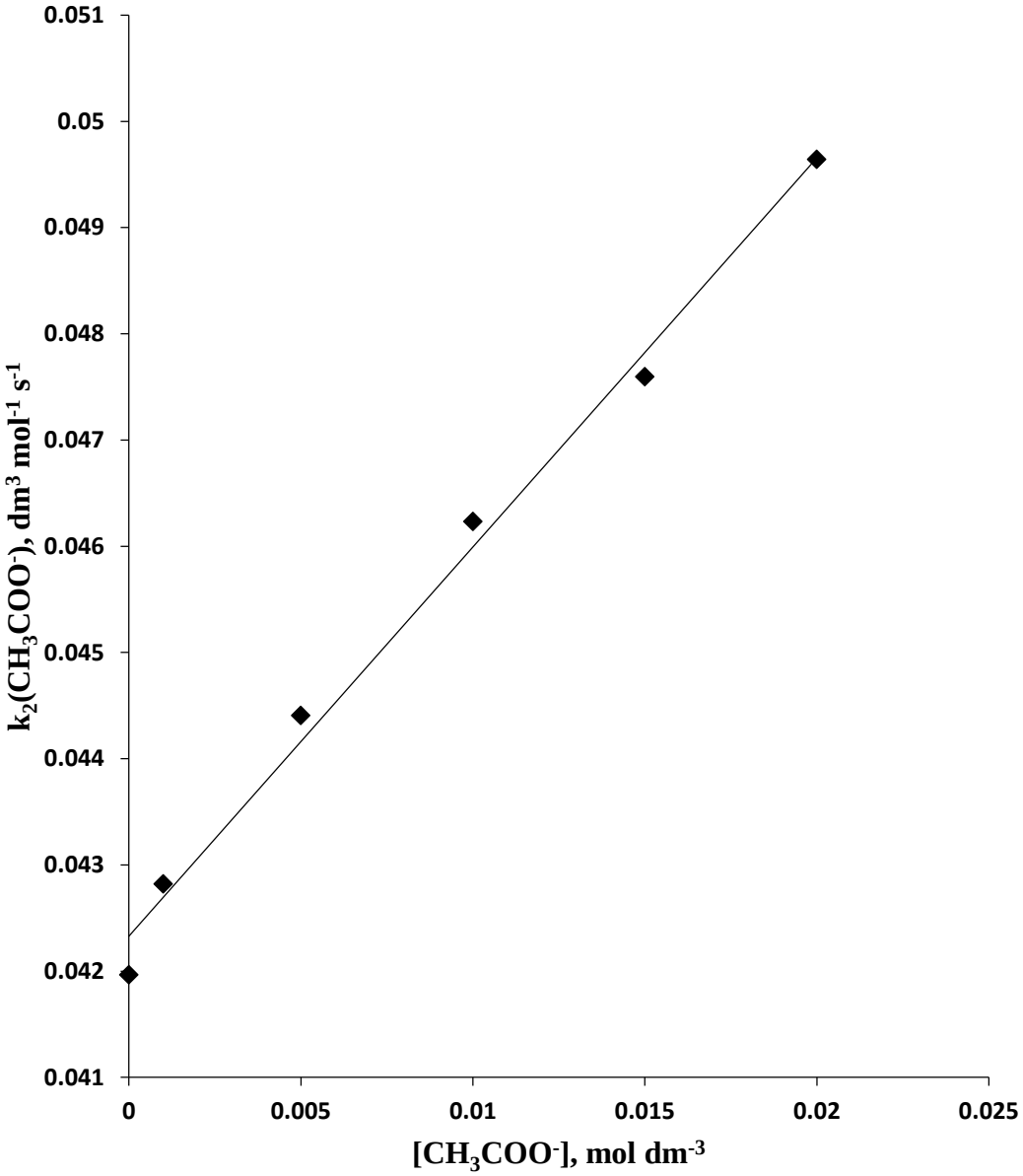


Figure 4.63: Plot of k_2 versus $[CH_3COO^-]$ for the redox reaction of $[Co(salophen)]^+$ and CH_3CHO at $[Co(salophen)^+] = 3.0 \times 10^{-4}$ mol dm^{-3}, $[CH_3CHO] = 13.5 \times 10^{-2}$ mol dm^{-3}, $[H^+] = 4.0 \times 10^{-2}$ mol dm^{-3}, $\mu = 0.2$ C^2 mol dm^{-3}, D = 75.67, T = 302 K and $\lambda_{max} = 470$ nm

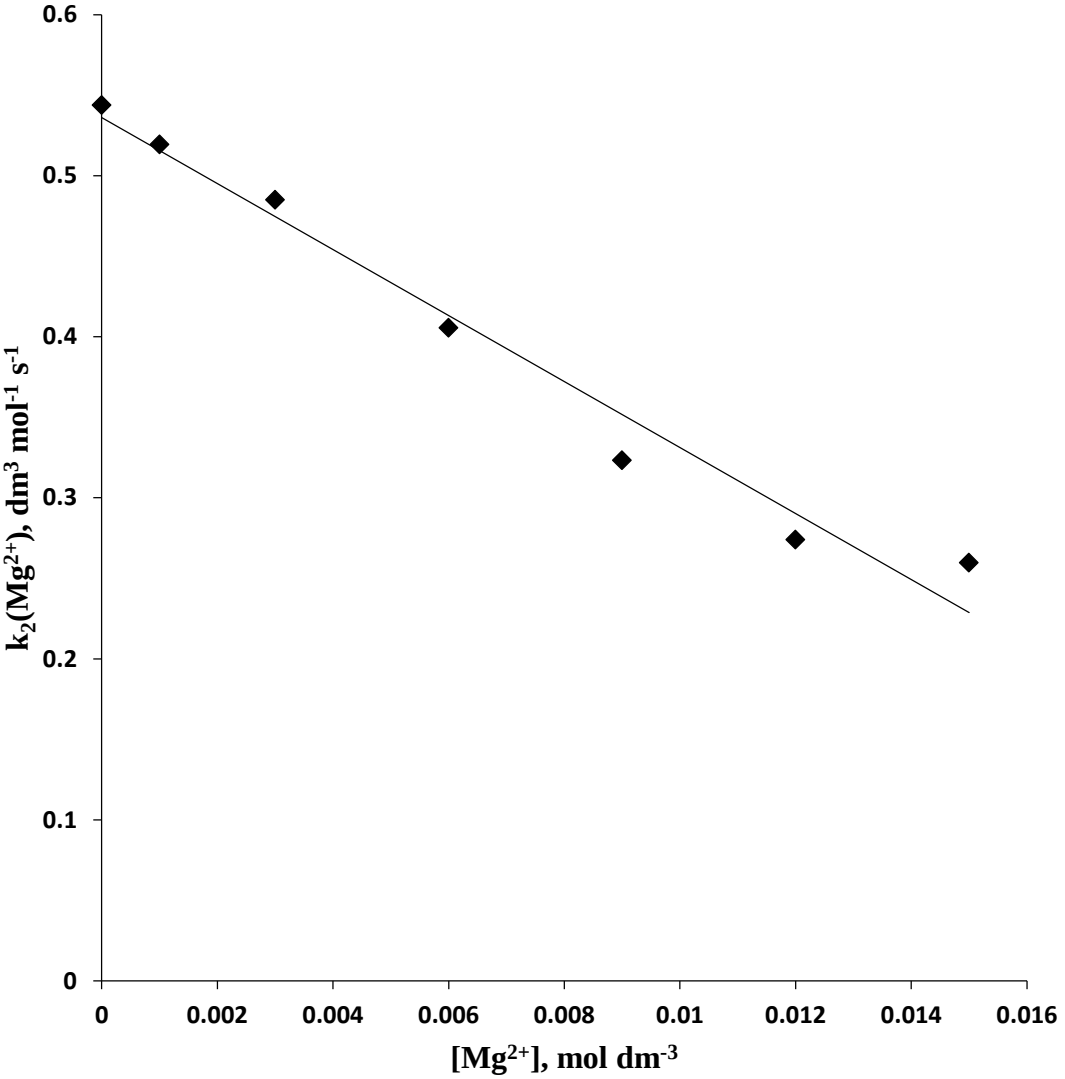


Figure 4.64: Plot of k_2 versus $[Mg^{2+}]$ for the redox reaction of $[Co(salophen)]^+$ and HCHO at $[Co(salophen)^+] = 3.0 \times 10^{-4}$ mol dm^{-3}, $[HCHO] = 18.0 \times 10^{-3}$ mol dm^{-3}, $[H^+] = 0.1$ mol dm^{-3}, $\mu = 0.2$ C^2 mol dm^{-3}, D = 74.78, T = 299 K and $\lambda_{max} = 470$ nm

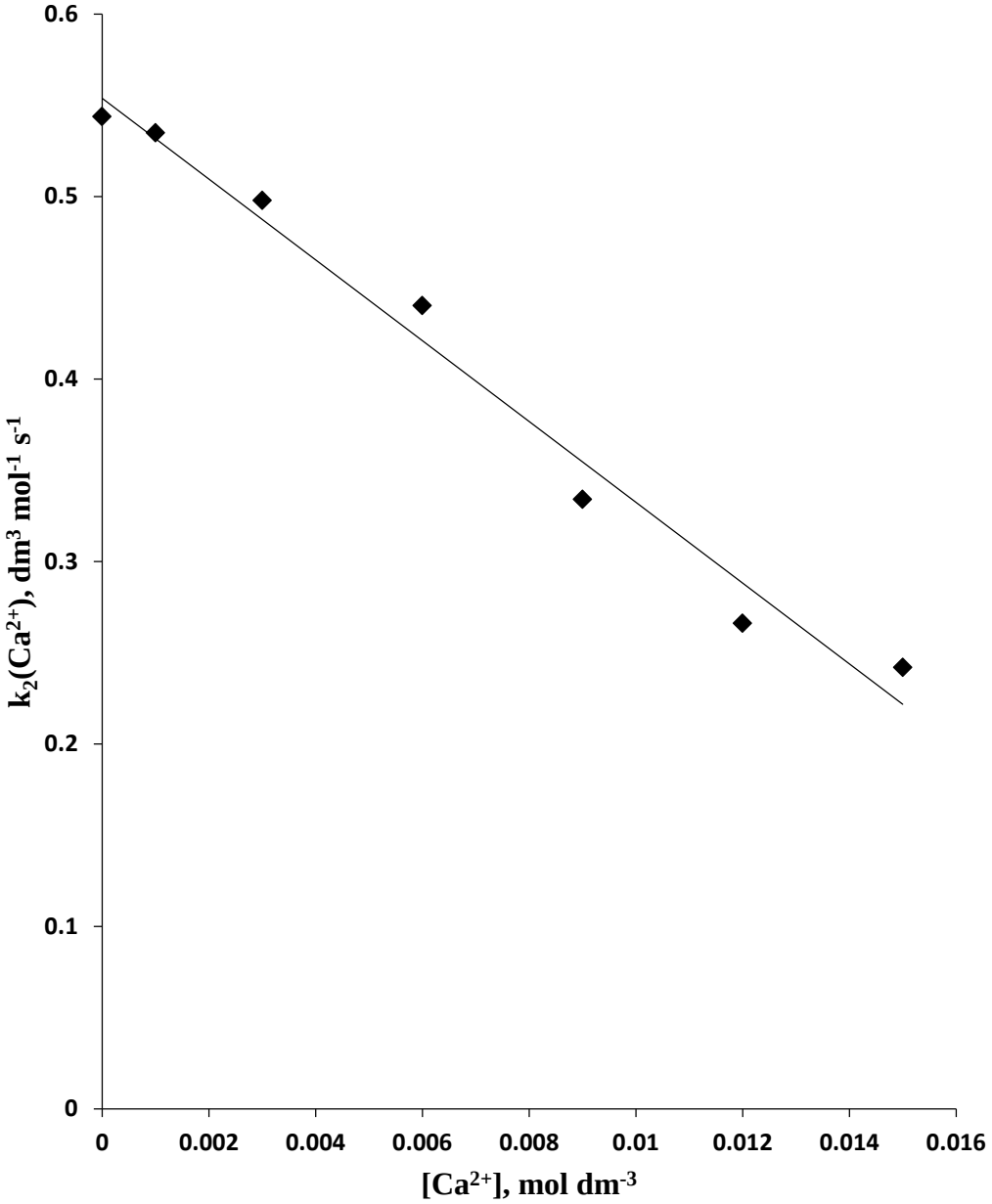


Figure 4.65: Plot of k_2 versus $[Ca^{2+}]$ for the redox reaction of $[Co(salophen)]^+$ and HCHO at $[Co(salophen)^+] = 3.0 \times 10^{-4}$ mol dm^{-3}, [HCHO] = 18.0×10^{-3} mol dm^{-3}, $[H^+]$ = 0.1 mol dm^{-3}, $\mu = 0.2$ C^2 mol dm^{-3}, D = 74.78, T = 299 K and λ_{max} = 470 nm

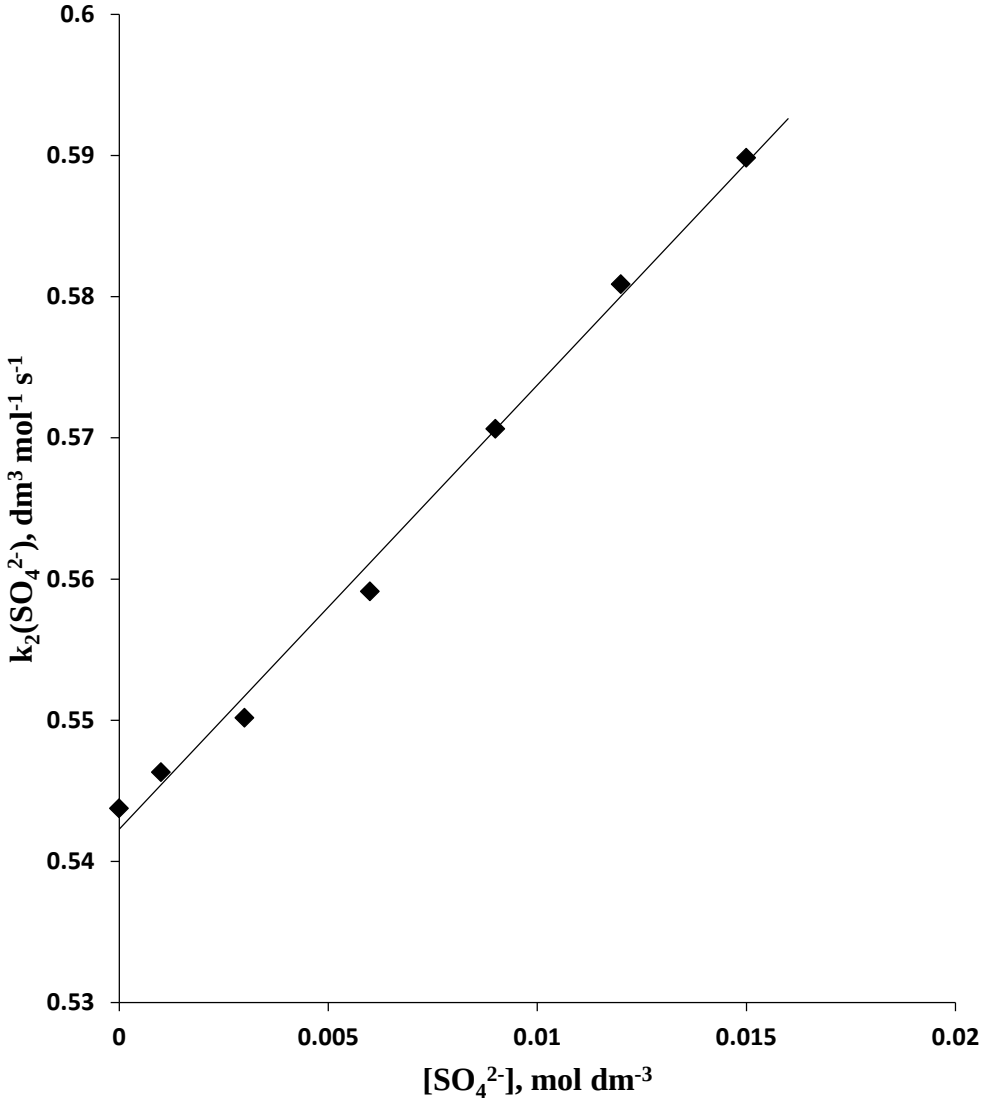


Figure 4.66: Plot of k_2 versus $[SO_4^{2-}]$ for the reaction of $[Co(salophen)]^+$ and HCHO at $[Co(salophen)^+] = 3.0 \times 10^{-4}$ mol dm^{-3}, [HCHO] = 18.0×10^{-3} mol dm^{-3}, $[H^+]$ = 0.1 mol dm^{-3}, $\mu = 0.2$ C^2 mol dm^{-3}, D = 74.78, T = 299 K and λ_{max} = 470 nm

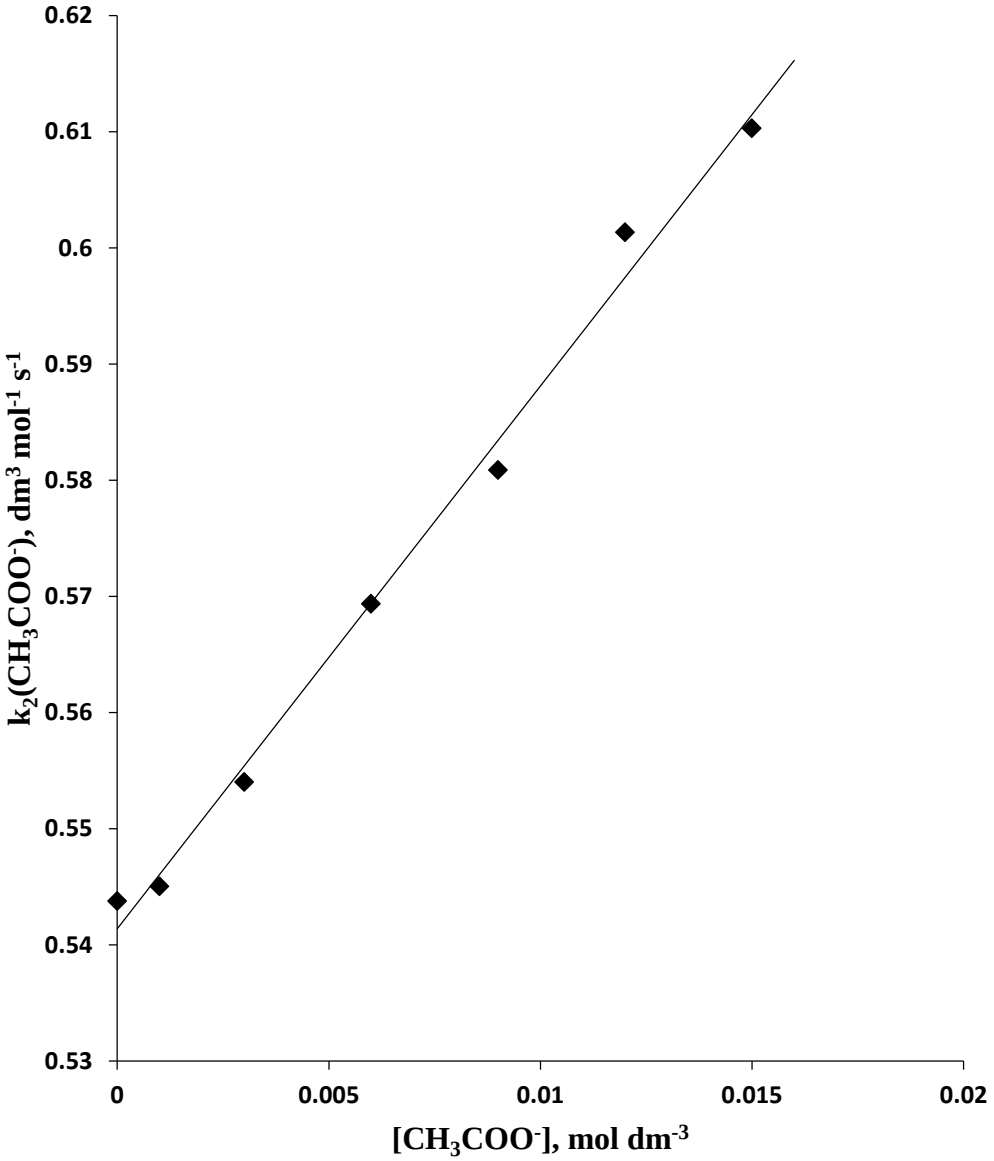


Figure 4.67: Plot of k_2 versus $[CH_3COO^-]$ for the redox reaction of $[Co(salophen)]^+$ and HCHO at $[Co(salophen)^+] = 3.0 \times 10^{-4}$ mol dm^{-3}, $[HCHO] = 18.0 \times 10^{-3}$ mol dm^{-3}, $[H^+]$ = 0.1 mol dm^{-3}, $\mu = 0.2$ C^2 mol dm^{-3}, D = 74.78, T = 299 K and λ_{max} = 470 nm

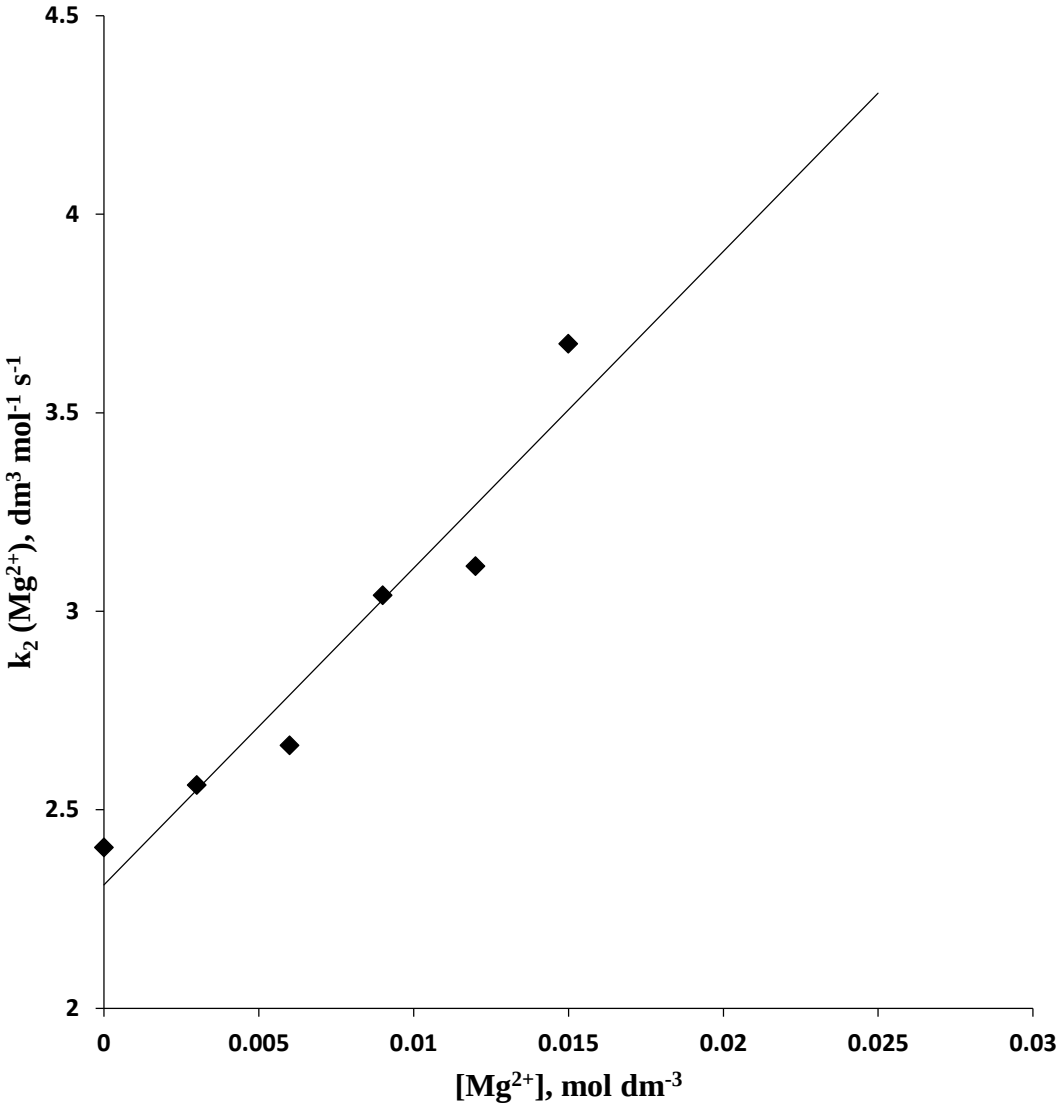


Figure 4.68: Plot of k_2 versus $[Mg^{2+}]$ for the redox reaction of $[Co(salophen)]^+$ and H_2A at $[Co(salophen)^+] = 3.0 \times 10^{-4}$ mol dm^{-3}, $[H_2A] = 12.0 \times 10^{-3}$ mol dm^{-3}, $[H^+] = 2.0 \times 10^{-3}$ mol dm^{-3} $\mu = 0.1$ C^2 mol dm^{-3}, D = 74.11, T = 306 K, and λ_{max} = 470 nm

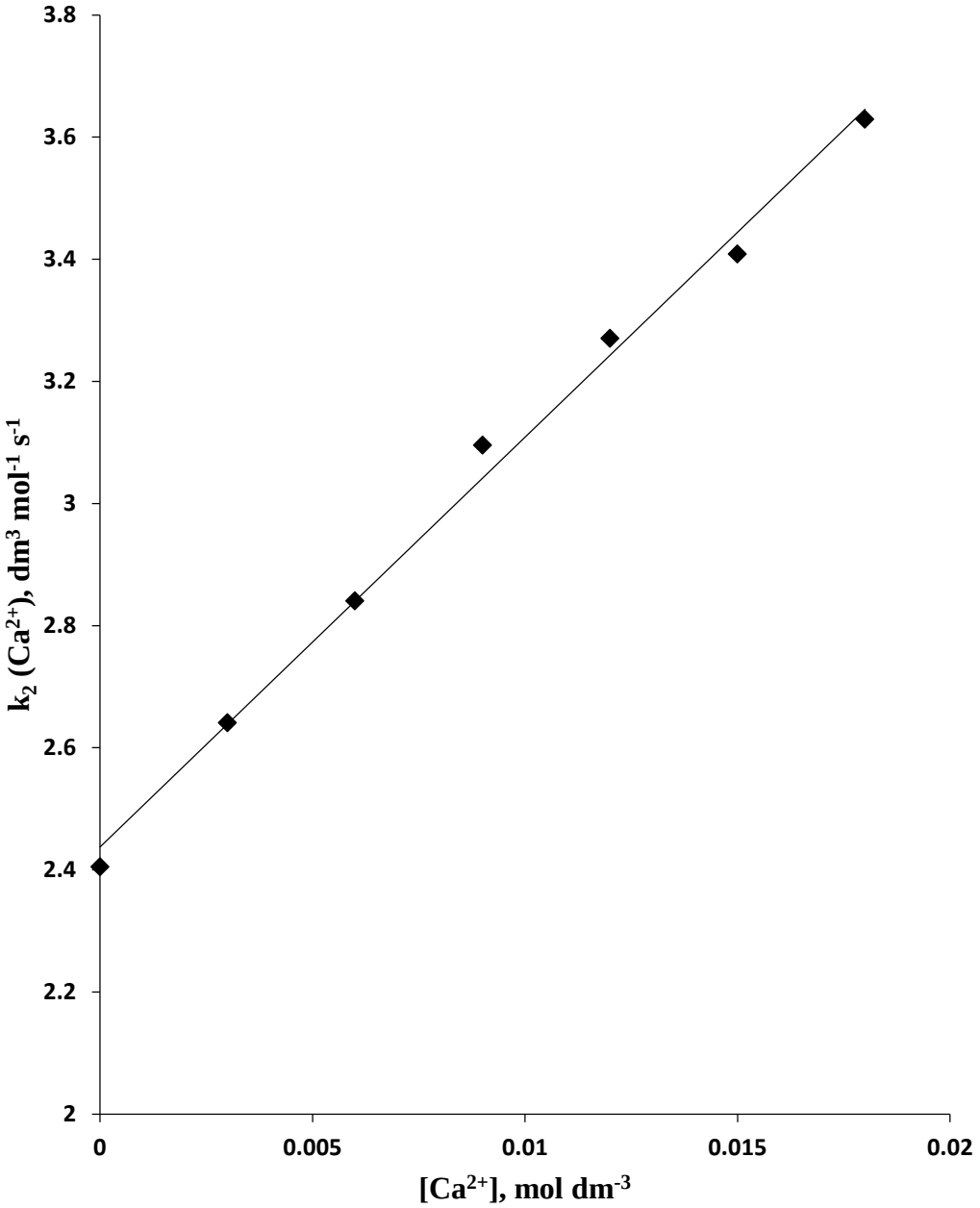


Figure 4.69: Plot of k_2 versus $[Ca^{2+}]$ for the redox reaction of $[Co(salophen)]^+$ and H_2A at $[Co(salophen)^+] = 3.0 \times 10^{-4}$ mol dm^{-3}, $[H_2A] = 12.0 \times 10^{-3}$ mol dm^{-3}, $[H^+] = 2.0 \times 10^{-3}$ mol dm^{-3} $\mu = 0.1$ C^2 mol dm^{-3}, D = 74.11, T = 306 K, and λ_{max} = 470 nm

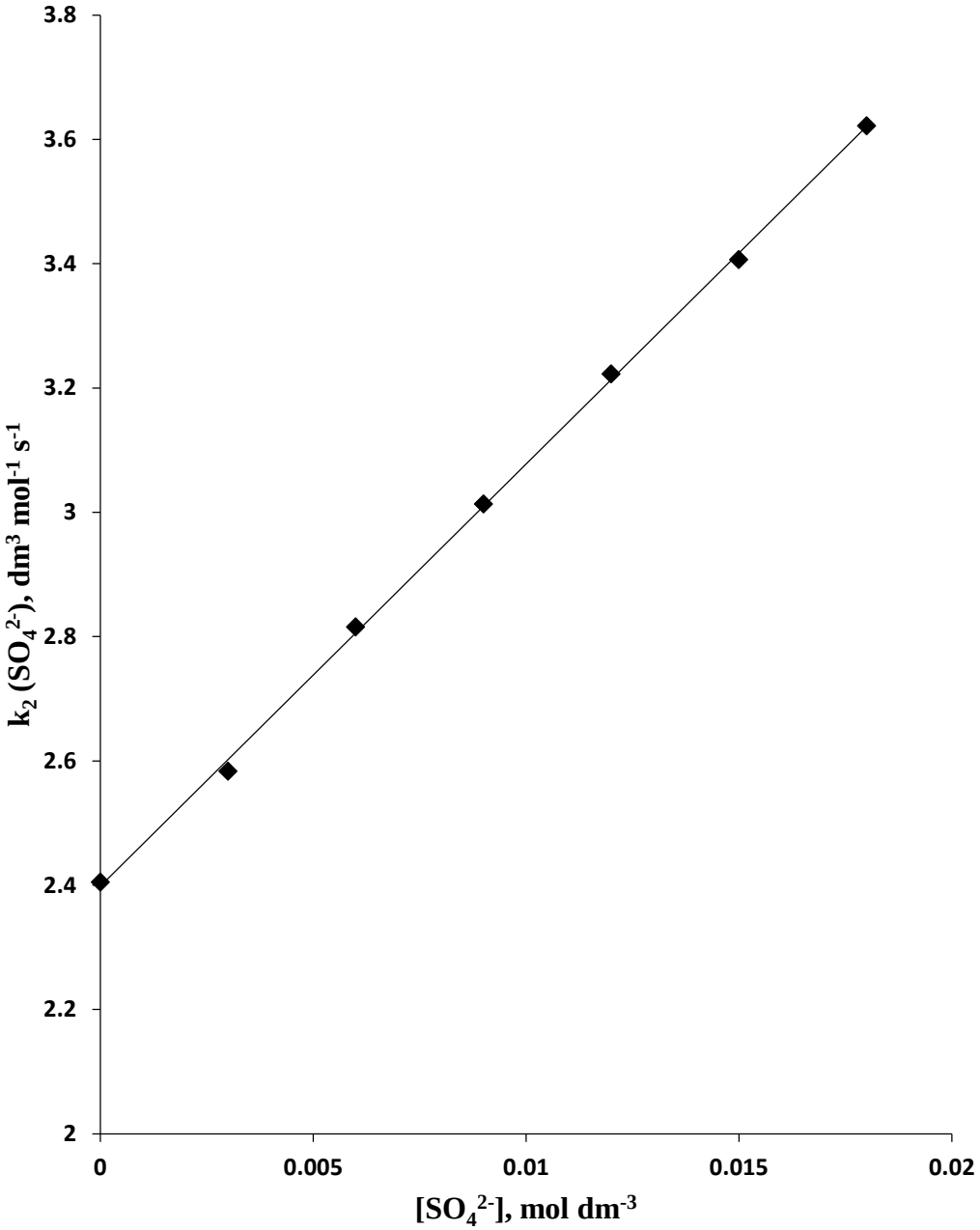


Figure 4.70: Plot of k_2 versus $[SO_4^{2-}]$ for the redox reaction of $[Co(salophen)]^+$ and H_2A at $[Co(salophen)^+] = 3.0 \times 10^{-4}$ mol dm^{-3}, $[H_2A] = 12.0 \times 10^{-3}$ mol dm^{-3}, $[H^+] = 2.0 \times 10^{-3}$ mol dm^{-3}, $\mu = 0.1$ C^2 mol dm^{-3}, D = 74.11, T = 306 K, and λ_{max} = 470 nm

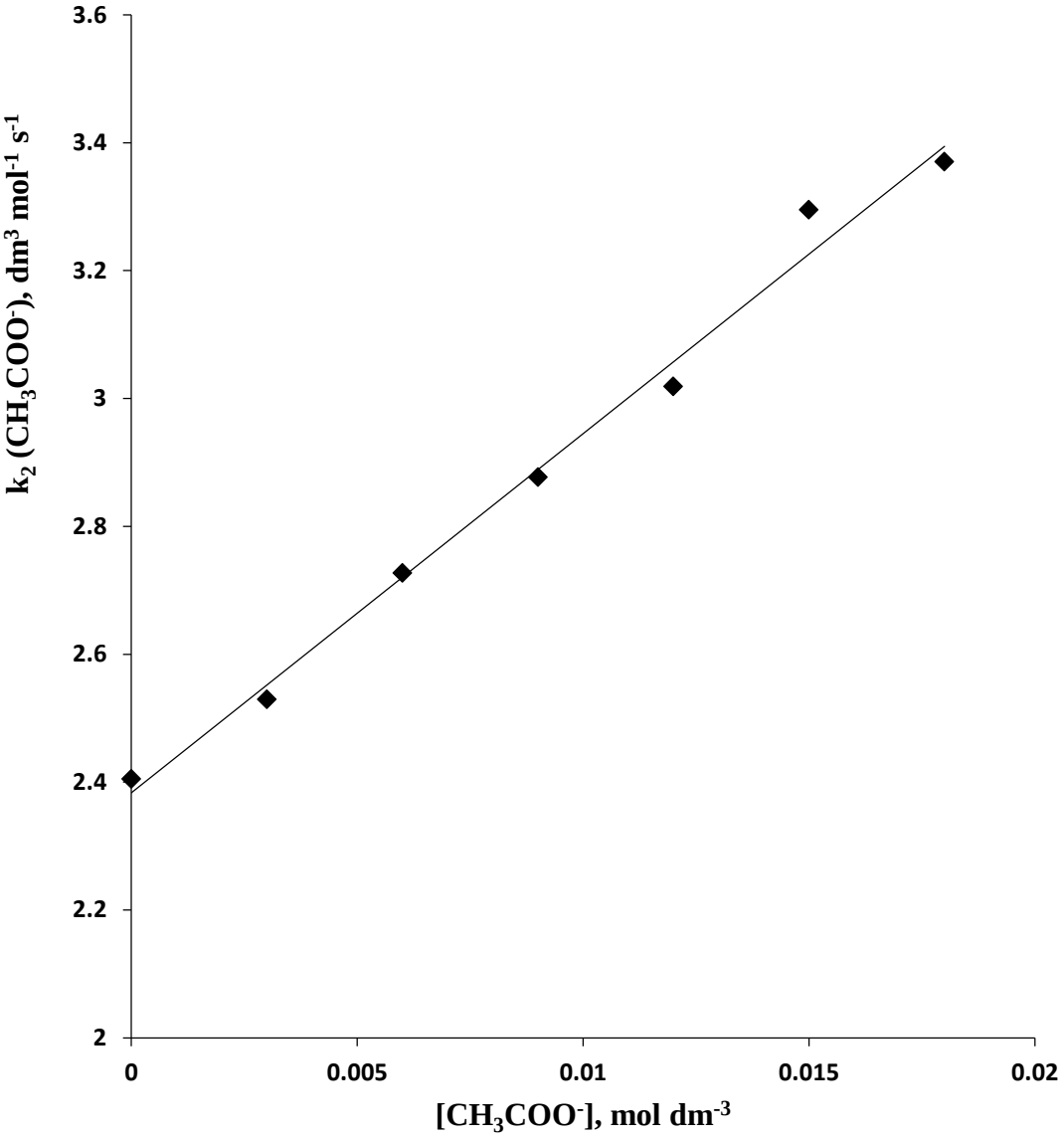


Figure 4.71: Plot of k_2 versus $[CH_3COO^-]$ for the redox reaction of $[Co(salophen)]^+$ and H_2A at $[Co(salophen)^+] = 3.0 \times 10^{-4}$ mol dm^{-3}, $[H_2A] = 12.0 \times 10^{-3}$ mol dm^{-3}, $[H^+] = 2.0 \times 10^{-3}$ mol dm^{-3}, $\mu = 0.1$ C^2 mol dm^{-3}, D = 74.11, T = 306 K, and $\lambda_{max} = 470$ nm

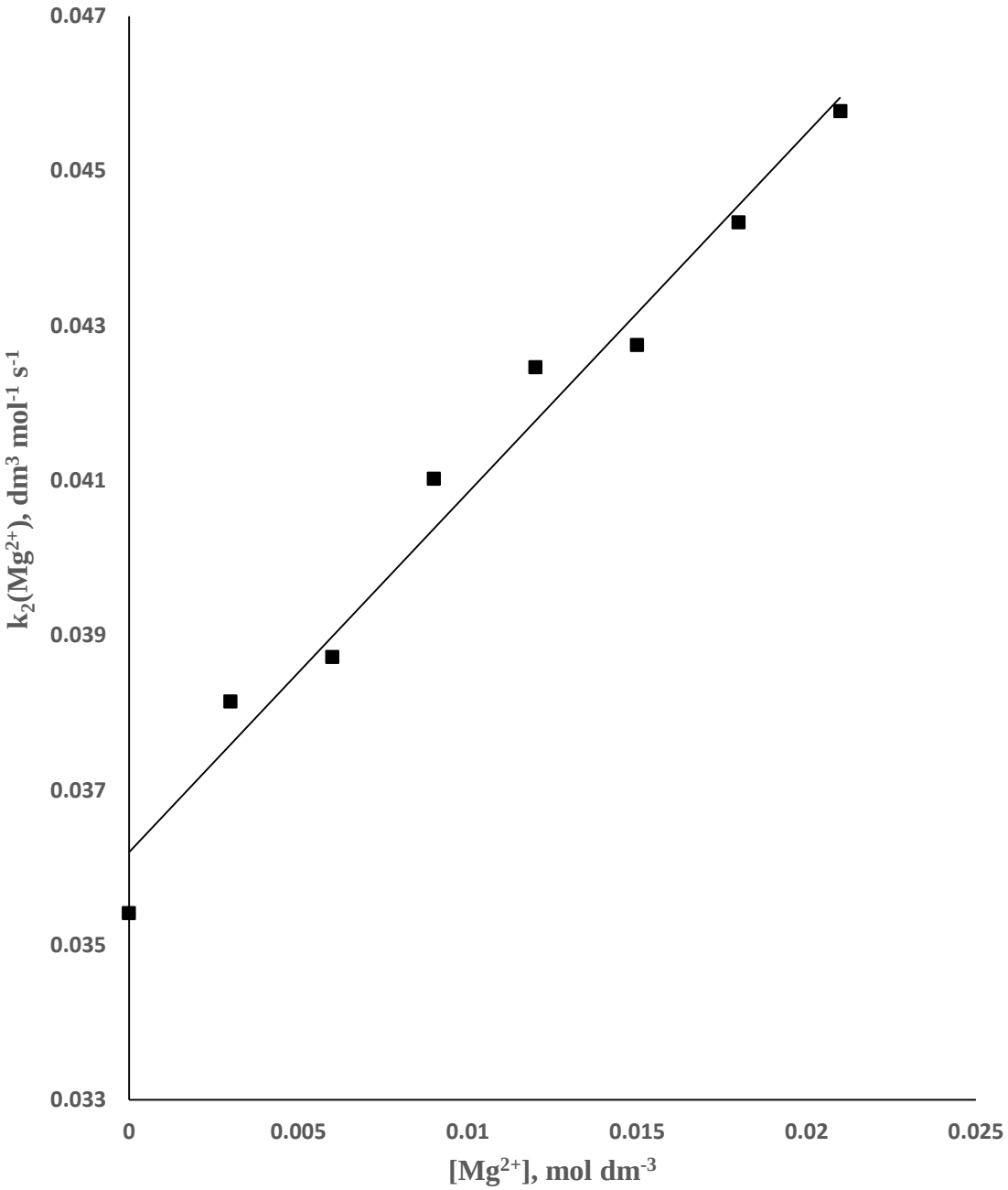


Figure 4.72: Plot of k_2 versus $[Mg^{2+}]$ for the redox reaction of $[Co(salophen)]^+$ and $S(R)_2$ at $[Co(salophen)^+] = 2.0 \times 10^{-4}$ mol dm^{-3}, $[S(R)_2] = 16.0 \times 10^{-2}$ mol dm^{-3}, $[H^+] = 5.0 \times 10^{-2}$ mol dm^{-3}, $\mu = 0.2$ C^2 mol dm^{-3}, D = 77.42, T = 305 K and λ_{max} = 470 nm

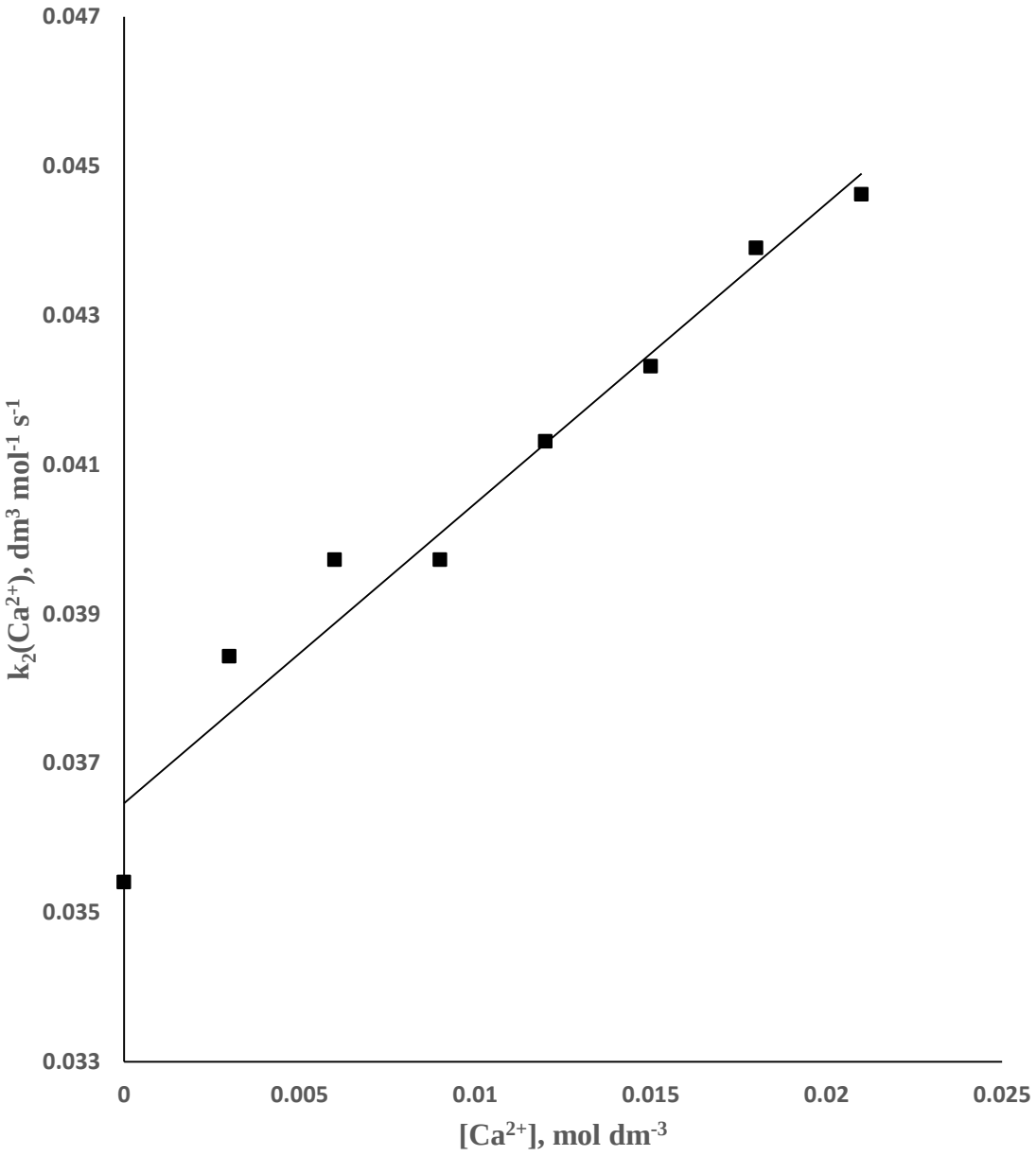


Figure 4.73: Plot of k_2 versus $[Ca^{2+}]$ for the redox reaction of $[Co(salophen)]^+$ and $S(R)_2$ at $[Co(salophen)^+] = 2.0 \times 10^{-4}$ mol dm^{-3}, $[S(R)_2] = 16.0 \times 10^{-2}$ mol dm^{-3}, $[H^+] = 5.0 \times 10^{-2}$ mol dm^{-3}, $\mu = 0.2$ C^2 mol dm^{-3}, D = 77.42, T = 305 K and λ_{max} = 470 nm

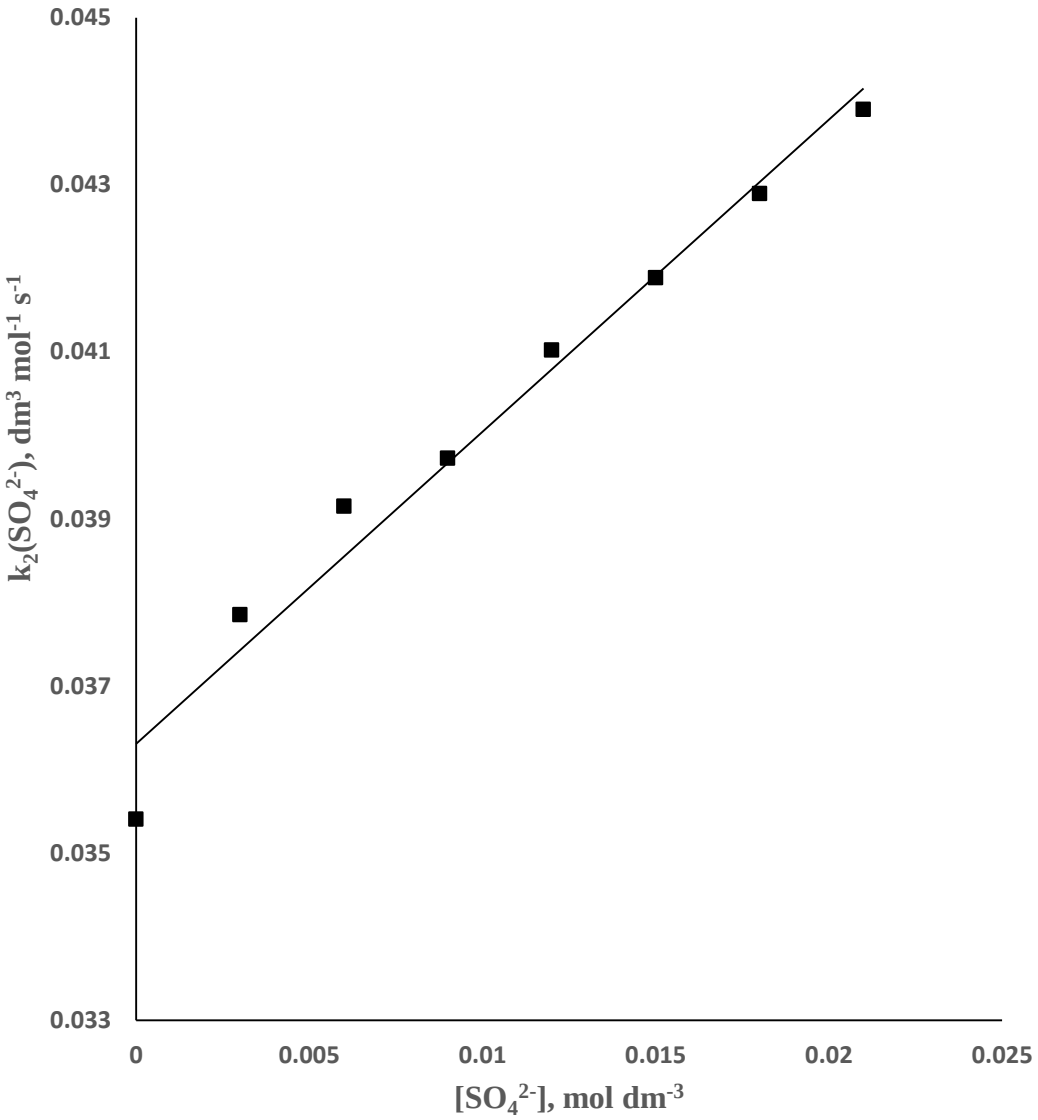


Figure 4.74: Plot of k_2 versus $[SO_4^{2-}]$ for the redox reaction of $[Co(salophen)]^+$ and $S(R)_2$ at $[Co(salophen)^+] = 2.0 \times 10^{-4}$ mol dm^{-3}, $[S(R)_2] = 16.0 \times 10^{-2}$ mol dm^{-3}, $[H^+] = 5.0 \times 10^{-2}$ mol dm^{-3}, $\mu = 0.2$ C^2 mol dm^{-3}, D = 77.42, T = 305 K and λ_{max} = 470 nm

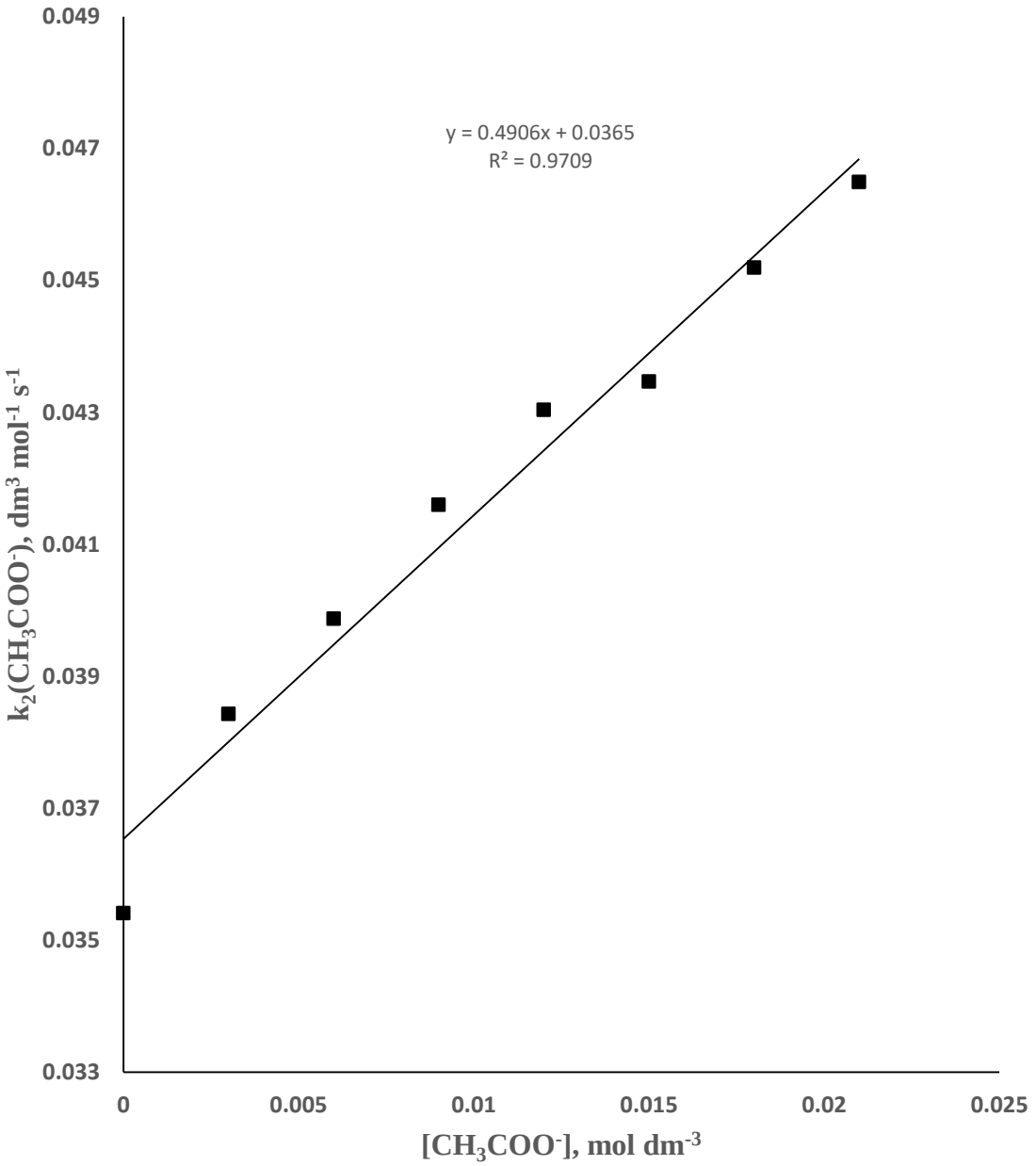


Figure 4.75: Plot of k_2 versus $[CH_3COO^-]$ for the redox reaction of $[Co(salophen)]^+$ and $S(R)_2$ at $[Co(salophen)^+] = 2.0 \times 10^{-4}$ mol dm^{-3}, $[S(R)_2] = 16.0 \times 10^{-2}$ mol dm^{-3}, $[H^+] = 5.0 \times 10^{-2}$ mol dm^{-3}, $\mu = 0.2$ C^2 mol dm^{-3}, D = 77.42, T = 305 K and λ_{max} = 470 nm

4.9 Dependence of Reactions Rate on Temperature

Temperature-dependent rate constants and thermodynamic parameters are presented in Tables 4.42 - 4.51. The plots of ln (k_2/T) versus 1/T are presented in Figures 4.76 - 4.85.

4.10 Free Radical Test

Addition of acrylamide solution to the partially oxidised reaction mixtures of oxidants and reductants then excess methanol showed gel formation for all the systems studied except in the case of Co(salophen)$^+$ / DPCI and Co(salophen)$^+$ / TSCZ where no gel formation was observed.

4.11 Test for the Formation of Intermediate Complex

4.11.1 Kinetic test (Michaelis-Menten plot)

The Michaelis-Menten plots of $1/k_1$ versus 1/[reductant] were linear for all the systems with zero intercept. These plots are presented in Figures 4.86 – 4.95.

4.11.2 Spectroscopic test

The electronic spectra of partially reacted mixture were run between 400 - 700 nm for the Co(salophen)$^+$ - reductants for all the systems and no shift in λ_{max} were observed. The results are depicted in Figures 4.96 - 4.105.

Table 4.42: Temperature dependent rate constants and activation parameters for the redox reaction of $[Co(salophen)]^{+}$ and LSH at $[Co(salophen)^{+}] = 2.0 \times 10^{-4}$ mol dm^{-3}, $[LSH] = 12.0 \times 10^{-3}$ mol dm^{-3}, $[H^{+}] = 1.0 \times 10^{-3}$ mol dm^{-3}, $\mu = 0.1$ C^2 mol dm^{-3}, D = 74.84 and λ_{max} = 470 nm

T, K	**10^3 k_1, s^{-1}**	**k_2, dm^3 mol^{-1} s^{-1}**
300	8.20	0.68
305	12.41	1.03
310	15.13	1.26
315	15.25	1.27
320	18.82	1.57
325	22.57	1.88

$\Delta \mathbf{H}^{\ddagger}$ = +27.77 kJ mol^{-1}, $\Delta \mathbf{S}^{\ddagger}$ = -157.87 J mol^{-1} K^{-1}, $\Delta \mathbf{G}^{\ddagger}$ = +74.14 kJ mol^{-1} at 300 K

$\mathbf{E_a}$ = +29.37 kJ mol^{-1}

Table 4.43: Temperature dependent rate constants and activation parameters for the redox reaction of $[Co(salophen)]^{+}$ and RSH at $[Co(salophen)^{+}] = 3.0 \times 10^{-4}$ mol dm^{-3}, $[RSH] = 15.0 \times 10^{-3}$ mol dm^{-3}, $[H^{+}] = 1.4 \times 10^{-3}$ mol dm^{-3}, $\mu = 0.1$ C^2 mol dm^{-3}, D = 74.19 and λ_{max} = 470 nm

T, K	**10^3 k_1, s^{-1}**	**k_2, dm^3 mol^{-1} s^{-1}**
300	5.34	0.36
305	10.43	0.69
310	13.70	0.91
315	20.13	1.34
320	24.69	1.65
325	29.13	1.94

$\Delta \mathbf{H}^{\ddagger}$ = +50.62 kJ mol^{-1}, $\Delta \mathbf{S}^{\ddagger}$ = -83.53 J mol^{-1} K^{-1}, $\Delta \mathbf{G}^{\ddagger}$ = +75.68 kJ mol^{-1} at 300 K

$\mathbf{E_a}$ = +53.11 kJ mol^{-1}

Table 4.44: Temperature dependent rate constants and activation parameters on the redox reaction of $[Co(salophen)]^{+}$ and TSH at $[Co(salophen)^{+}] = 3.0 \times 10^{-4}$ mol dm^{-3}, $[TSH] = 7.50 \times 10^{-3}$ mol dm^{-3}, $\mu = 0.1$ C^2 mol dm^{-3}, D = 74.04 and λ_{max} = 470 nm

T, K	**10^3 k_1, s^{-1}**	**k_2, dm^3 mol^{-1} s^{-1}**
300	10.71	1.43
305	32.45	4.33
310	37.01	4.95
315	71.97	9.59
320	84.77	11.30
325	91.34	12.18

$\Delta \mathbf{H}^{\ddagger}$ = -75.96 kJ mol^{-1}, $\Delta \mathbf{S}^{\ddagger}$ = +11.91 J mol^{-1} K^{-1}, $\Delta \mathbf{G}^{\ddagger}$ = -79.54 kJ mol^{-1} at 300 K

$\mathbf{E_a}$ = -73.47 kJ mol^{-1}

Table 4.45: Temperature dependent rate constants and activation parameters for the redox reaction of $[Co(salophen)]^+$ and TSCZ at $[Co(salophen)^+] = 2.0 \times 10^{-4}$ mol dm^{-3}, $[TSCZ] = 8.0 \times 10^{-2}$ mol dm^{-3}, $[H^+] = 1.0 \times 10^{-2}$ mol dm^{-3}, $\mu = 0.1$ C^2 mol dm^{-3}, D = 74.41 and $\lambda_{max} = 470$ nm

T, K	**10^3 k_1, s^{-1}**	**k_2, dm^3 mol^{-1} s^{-1}**
306	9.70	0.12
312	11.26	0.14
317	13.27	0.17
322	15.73	0.19
327	18.08	0.23
332	21.58	0.27
337	23.97	0.30

$\Delta \mathbf{H}^{\ddagger} = +23.92$ kJ mol^{-1}, $\Delta \mathbf{S}^{\ddagger} = -184.84$ J mol^{-1} K^{-1}, $\Delta \mathbf{G}^{\ddagger} = +80.48$ kJ mol^{-1} at 306 K

$\mathbf{E_a} = +26.47$ kJ mol^{-1}

Table 4.46: Temperature dependent rate constants and activation parameters for the reaction of $[Co(salophen)]^+$ and DPCI at $[Co(salophen)^+] = 1.0 \times 10^{-4}$ mol dm^{-3}, DPCI = 25.0×10^{-3} mol dm^{-3} $[H^+] = 0.1$ mol dm^{-3}, $\mu = 0.5$ C^2 mol dm^{-3}, D = 75.83 and $\lambda_{max} = 470$ nm

T, K	**10^3 k_1, s^{-1}**	**k_2, dm^3 mol^{-1} s^{-1}**
300	9.88	0.66
305	11.14	0.74
310	13.10	0.87
315	14.68	0.98
320	16.95	1.13
325	18.28	1.22

$\Delta H^{\ddagger} = +18.03$ kJ mol^{-1}, $\Delta S^{\ddagger} = -188.32$ J mol^{-1} K^{-1}, $\Delta G^{\ddagger} = +74.53$ kJ mol^{-1} at 300 K

$E_a = +20.53$ kJ mol^{-1}

Table 4.47: Temperature dependent rate constants and activation parameters for the redox reaction of $[Co(salophen)]^+$ and CH_3CHO at $[Co(salophen)^+] = 3.0 \times 10^{-4}$ mol dm^{-3}, $[CH_3CHO] = 13.5 \times 10^{-2}$ mol dm^{-3}, $[H^+] = 4.0 \times 10^{-2}$ mol dm^{-3}, $\mu = 0.2$ C^2 mol dm^{-3}, D = 75.67 and $\lambda_{max} = 470$ nm

T, K	**10^3 k_1, s^{-1}**	**10^2 k_2, dm^3 mol^{-1} s^{-1}**
302	5.69	4.21
308	10.96	8.12
313	18.84	13.95
318	32.85	24.33
323	43.53	32.24
328	76.14	56.40

$\Delta \mathbf{H}^{\ddagger} = +81.01$ kJ mol^{-1}, $\Delta \mathbf{S}^{\ddagger} = -3.33$ J mol^{-1} K^{-1}, $\Delta \mathbf{G}^{\ddagger} = +82.02$ kJ mol^{-1} at 302 K

$\mathbf{E_a} = +83.53$ kJ mol^{-1}

Table 4.48: Temperature dependent rate constants and activation parameters for the reaction of $[Co(salophen)]^+$ and HCHO at $[Co(salophen)^+] = 3.0 \times 10^{-4}$ mol dm^{-3}, [HCHO] $= 18.0 \times 10^{-3}$ mol dm^{-3}, $[H^+] = 0.1$ mol dm^{-3}, $\mu = 0.2$ C^2 mol dm^{-3}, D = 74.78 and $\lambda_{max} = 470$ nm

T, K	**10^3 k_1, s^{-1}**	**k_2, dm^3 mol^{-1} s^{-1}**
299	9.79	0.54
305	17.48	0.97
310	18.84	1.05
315	31.32	1.74
320	43.53	2.42
325	76.14	4.23

$\Delta \mathbf{H}^{\ddagger} = +57.95$ kJ mol^{-1}, $\Delta \mathbf{S}^{\ddagger} = -56.44$ J mol^{-1} K^{-1}, $\Delta \mathbf{G}^{\ddagger} = +74.83$ kJ mol^{-1} at 299 K

$\mathbf{E_a} = +55.46$ kJ mol^{-1}

Table 4.49: Temperature dependent rate constants and activation parameters for the reaction of $[Co(salophen)]^+$ and I^- at $[Co(salophen)^+] = 2.0 \times 10^{-4}$ mol dm^{-3}, $[I^-] = 16.0 \times 10^{-2}$ mol dm^{-3} $[H^+] = 0.40$ mol dm^{-3}, $\mu = 0.6$ C^2 mol dm^{-3}, D = 78.43 and λ_{max} = 470 nm

T, K	**10^3 k_1, s^{-1}**	**k_2, dm^3 mol^{-1} s^{-1}**
301	4.62	0.31
305	6.03	0.40
310	7.02	0.47
315	7.99	0.53
320	8.31	0.55
325	9.65	0.64

$\Delta \mathbf{H}^{\ddagger}$ = +21.16 kJ mol^{-1}, $\Delta \mathbf{S}^{\ddagger}$ = -184.02 J mol^{-1}, $\Delta \mathbf{G}^{\ddagger}$ = +76.55 kJ mol^{-1} at 301 K

$\mathbf{E_a}$ = +23.67 kJ mol^{-1}

Table 4.50: Temperature dependent rate constants and activation parameters for the redox reaction of $[Co(salophen)]^{+}$ and H_2A at $[Co(salophen)^{+}] = 3.0 \times 10^{-4}$ mol dm^{-3}, $[H_2A] = 12.0 \times 10^{-3}$ mol dm^{-3}, $[H^{+}] = 2.0 \times 10^{-3}$ mol dm^{-3}, $\mu = 0.1$ C^2 mol dm^{-3}, D = 74.11 and λ_{max} = 470 nm

T, K	**10^2 k_1, s^{-1}**	**k_2, dm^3 mol^{-1} s^{-1}**
306	2.89	2.40
311	2.95	2.46
317	5.41	4.51
322	5.67	4.72
327	8.84	7.37
333	12.03	10.03

$\Delta \mathbf{H}^{\ddagger}$ = +47.70 kJ mol^{-1}, $\Delta \mathbf{S}^{\ddagger}$ = -82.87 J mol^{-1} K^{-1}, $\Delta \mathbf{G}^{\ddagger}$ = +73.06 kJ mol^{-1} at 306 K

$\mathbf{E_a}$ = +50.24 kJ mol^{-1}

Table 4.51: Temperature dependent rate constants and activation parameters for the redox reaction of $[Co(salophen)]^+$ and $S(R)_2$ at $[Co(salophen)^+] = 2.0 \times 10^{-4}$ mol dm^{-3}, $[S(R)_2] = 16.0 \times 10^{-2}$ mol dm^{-3}, $[H^+] = 5.0 \times 10^{-2}$ mol dm^{-3}, $\mu = 0.2$ C^2 mol dm^{-3}, D = 77.42 and $\lambda_{max} = 470$ nm

T, K	**10^3 k_1, s^{-1}**	**10^2 k_2, dm^3 mol^{-1} s^{-1}**
305	5.67	3.54
312	7.55	4.72
317	9.56	5.97
322	12.02	7.51
327	14.26	8.91
332	17.50	10.94
337	19.53	12.21

$\Delta \mathbf{H}^{\ddagger} = +32.81$ kJ mol^{-1}, $\Delta \mathbf{S}^{\ddagger} = -165.60$ J mol^{-1} K^{-1}, $\Delta \mathbf{G}^{\ddagger} = +83.32$ kJ mol^{-1} at 305 K

$\mathbf{E_a} = +35.36$ kJ mol^{-1}

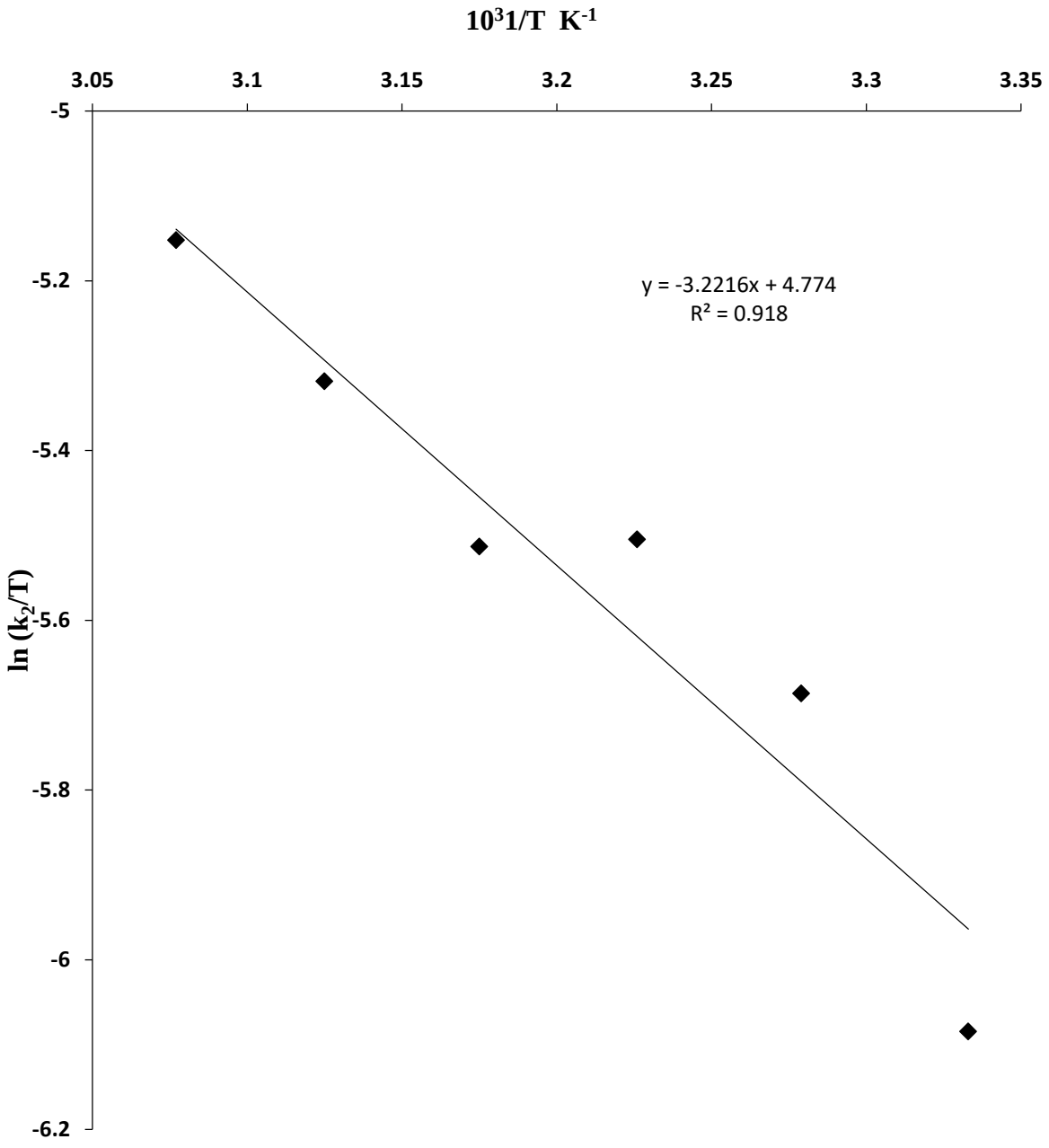


Figure 4.76: Plot of ln $\left(\frac{k_2}{T}\right)$ versus $\left(\frac{1}{T}\right)$ for the redox reaction of $[Co(salophen)]^+$ and LSH at $[Co(salophen)^+] = 2.0 \times 10^{-4}$ mol dm^{-3}, $[LSH] = 12.0 \times 10^{-3}$ mol dm^{-3}, $[H^+] = 1.0 \times 10^{-3}$ mol dm^{-3}, $\mu = 0.1$ C^2 mol dm^{-3}, D = 74.84, T = (300 – 325) K, and λ_{max} = 470 nm

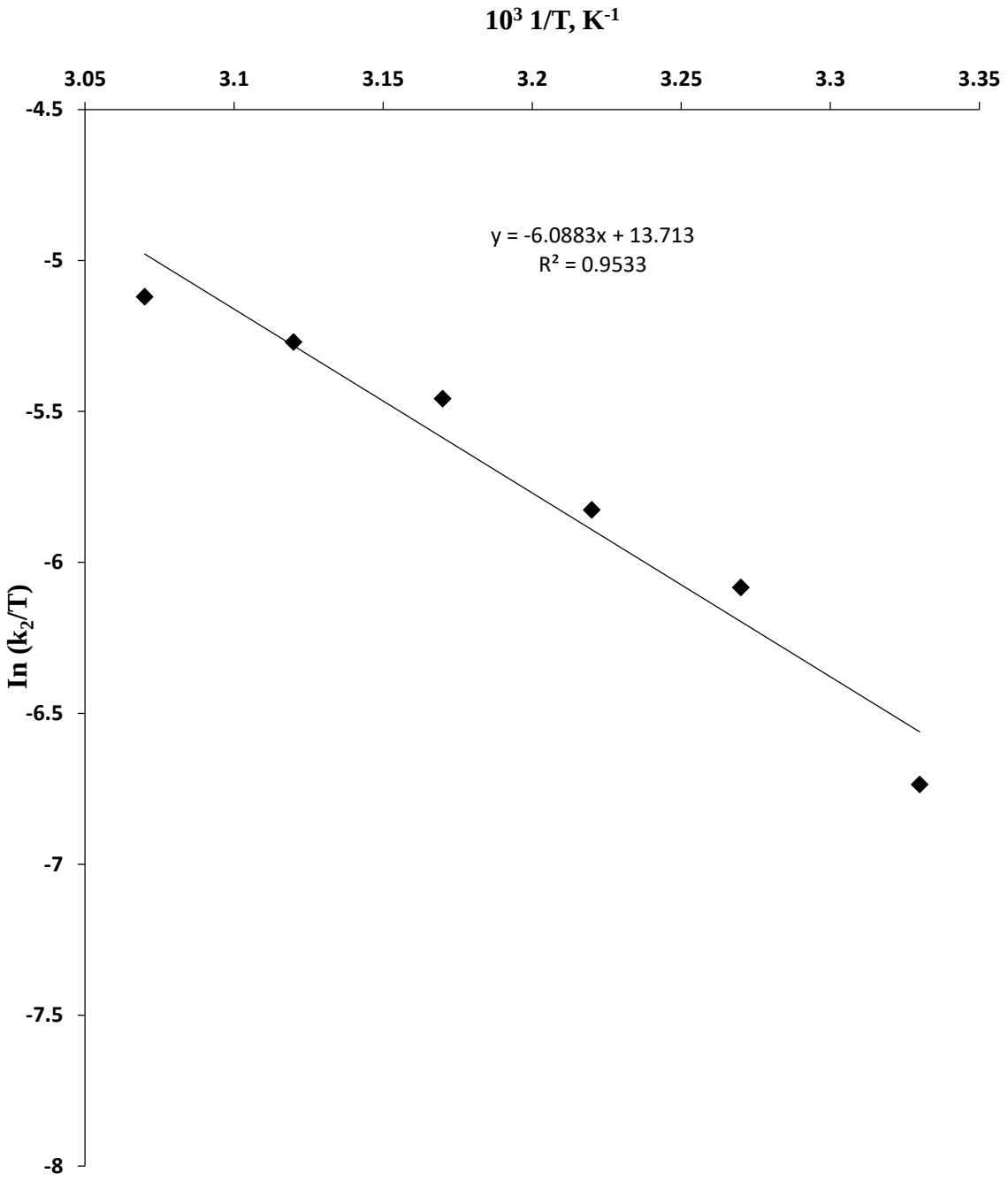


Figure 4.77: Plot of ln $\left(\frac{k_2}{T}\right)$ versus $(\frac{1}{T})$ for the redox reaction of $[Co(salophen)]^+$ and RSH at $[Co(salophen)^+] = 3.0 \times 10^{-4}$ mol dm^{-3}, [RSH] = 15.0×10^{-3} mol dm^{-3}, $[H^+] = 1.4 \times 10^{-3}$ mol dm^{-3}, $\mu = 0.1$ C^2 mol dm^{-3}, D = 74.19, T = (300 – 325) K, and λ_{max} = 470 nm

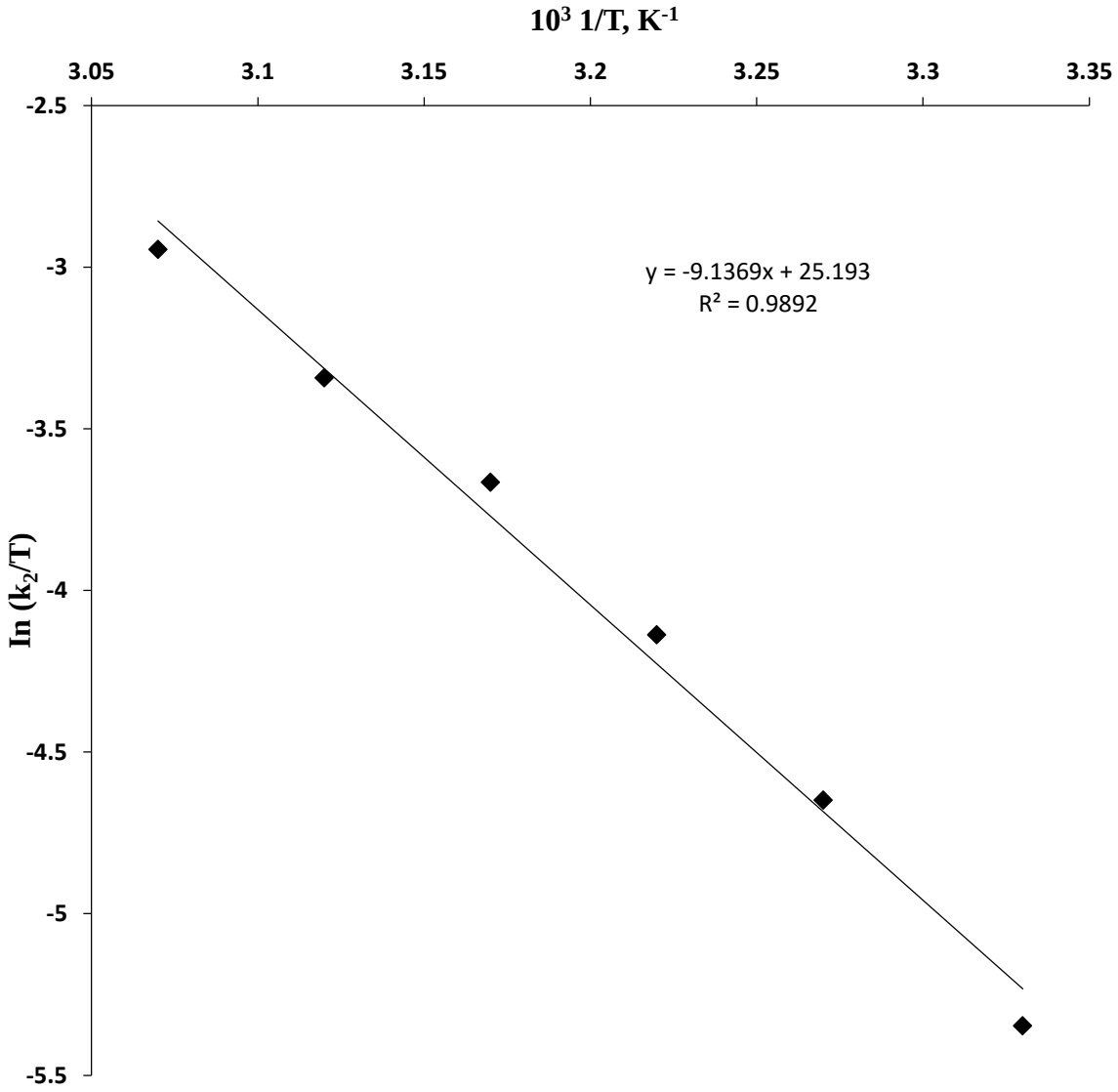


Figure 4.78: Plot of ln $\left(\frac{k_2}{T}\right)$ versus $(\frac{1}{T})$ for the redox reaction of $[Co(salophen)]^+$ and TSH at $[Co(salophen)^+] = 3.0 \times 10^4$ mol dm^{-3}, [TSH] = 7.50×10^{-3} mol dm^{-3}, $\mu = 0.1$ C^2 mol dm^{-3}, D = 74.04, T = (300 – 325) K, and λ_{max} = 470 nm

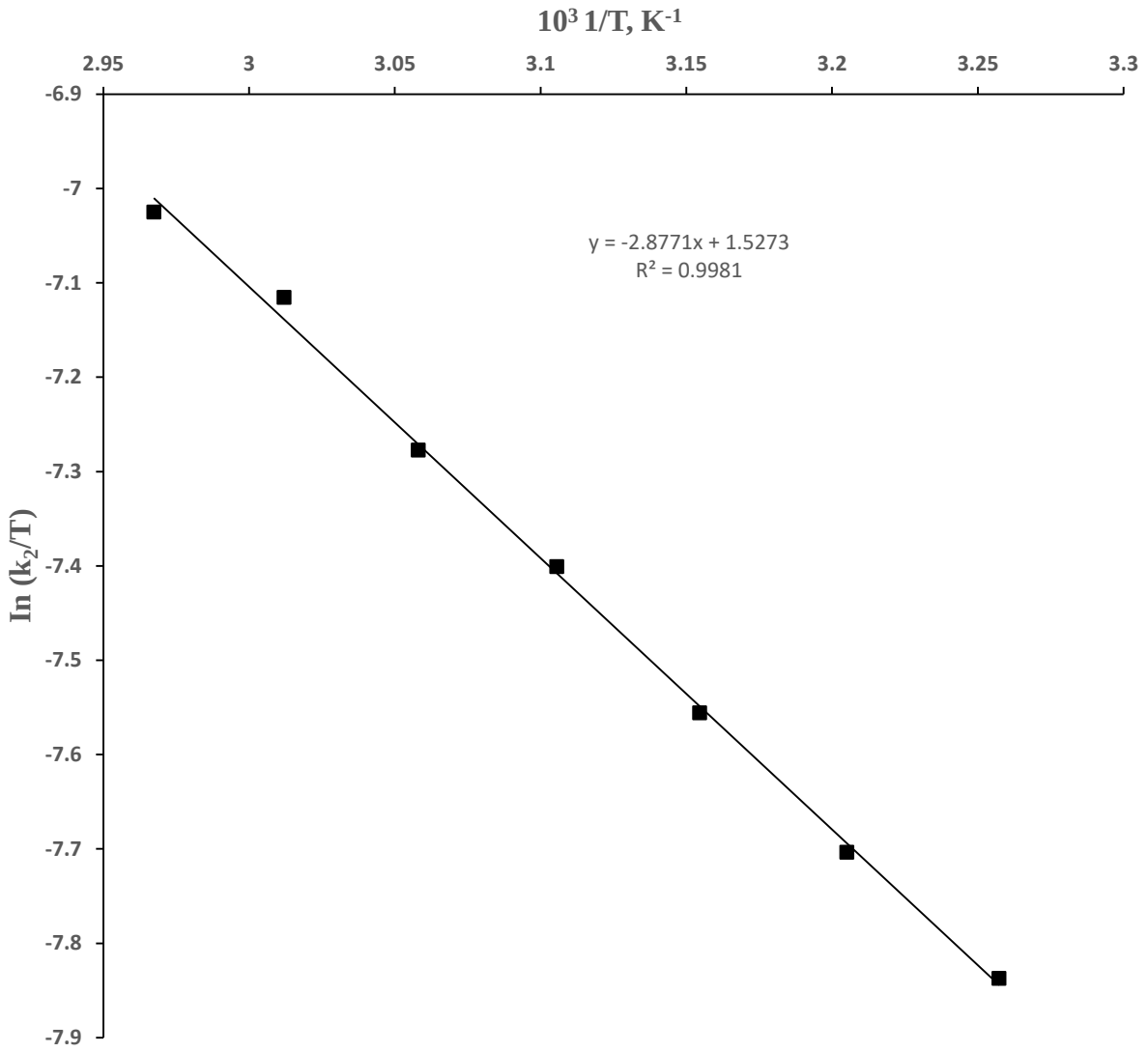


Figure 4.79: Plot of ln $\left(\frac{k_2}{T}\right)$ versus $(\frac{1}{T})$ for the redox reaction of $[Co(salophen)]^+$ and TSCZ at $[Co(salophen)^+] = 2.0 \times 10^{-4}$ mol dm^{-3}, [TSCZ] = 8.0×10^{-2} mol dm^{-3}, $[H^+] = 1.0 \times 10^{-2}$ mol dm^{-3}, $\mu = 0.1$ C^2 mol dm^{-3}, D = 74.41, T = (306 – 337) K and λ_{max} = 470 nm

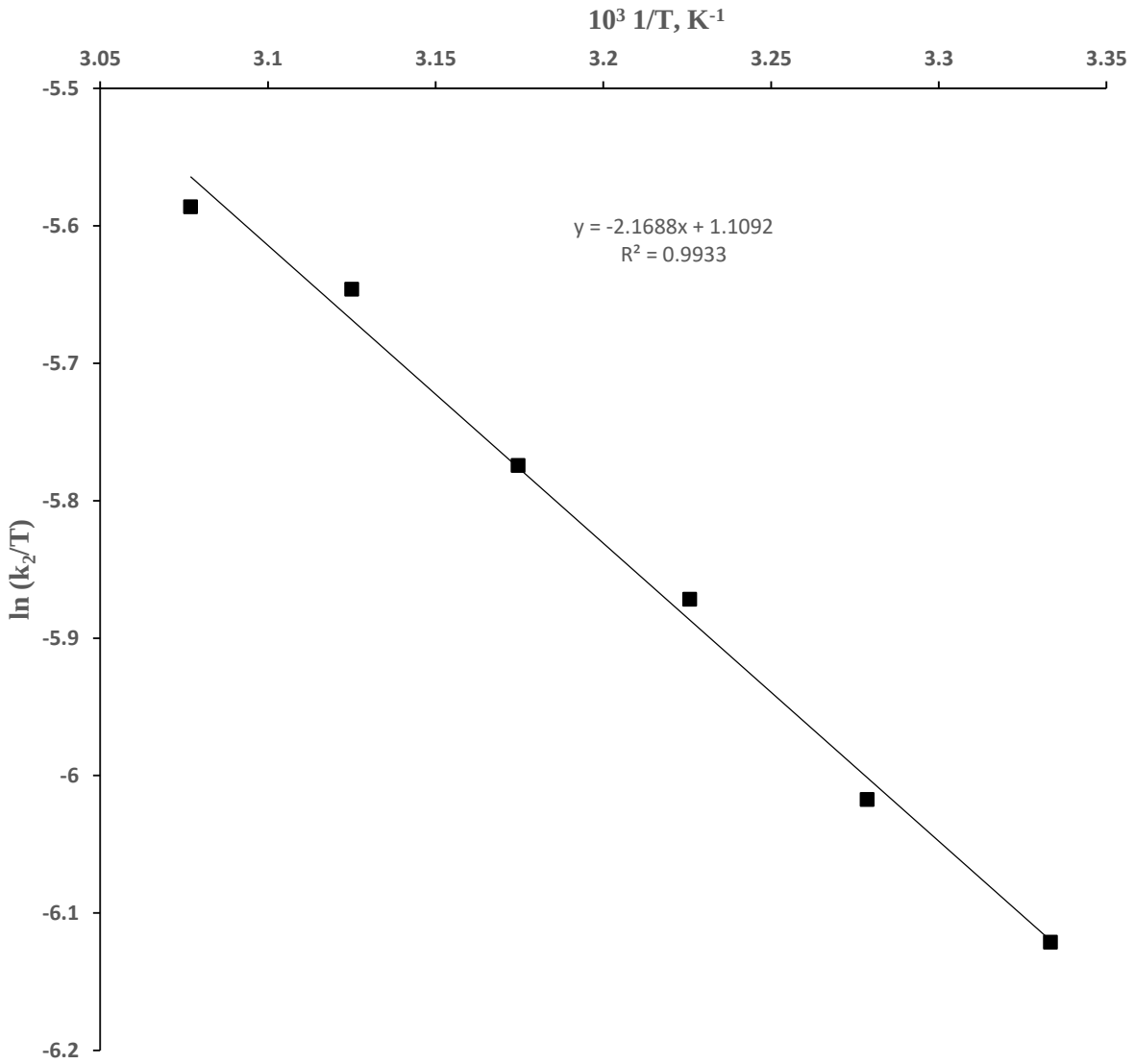


Figure 4.80: Plot of $\ln\left(\frac{k_2}{T}\right)$ versus $\left(\frac{1}{T}\right)$ for the reaction of $[Co(salophen)]^+$ and DPCI at $[Co(salophen)^+] = 1.0 \times 10^{-4}$ mol dm^{-3}, DPCI = 25.0×10^{-3} mol dm^{-3} $[H^+] = 0.1$ mol dm^{-3}, $\mu = 0.5$ C^2 mol dm^{-3}, D = 75.83, T = (300 – 325) K and λ_{max} = 470 nm

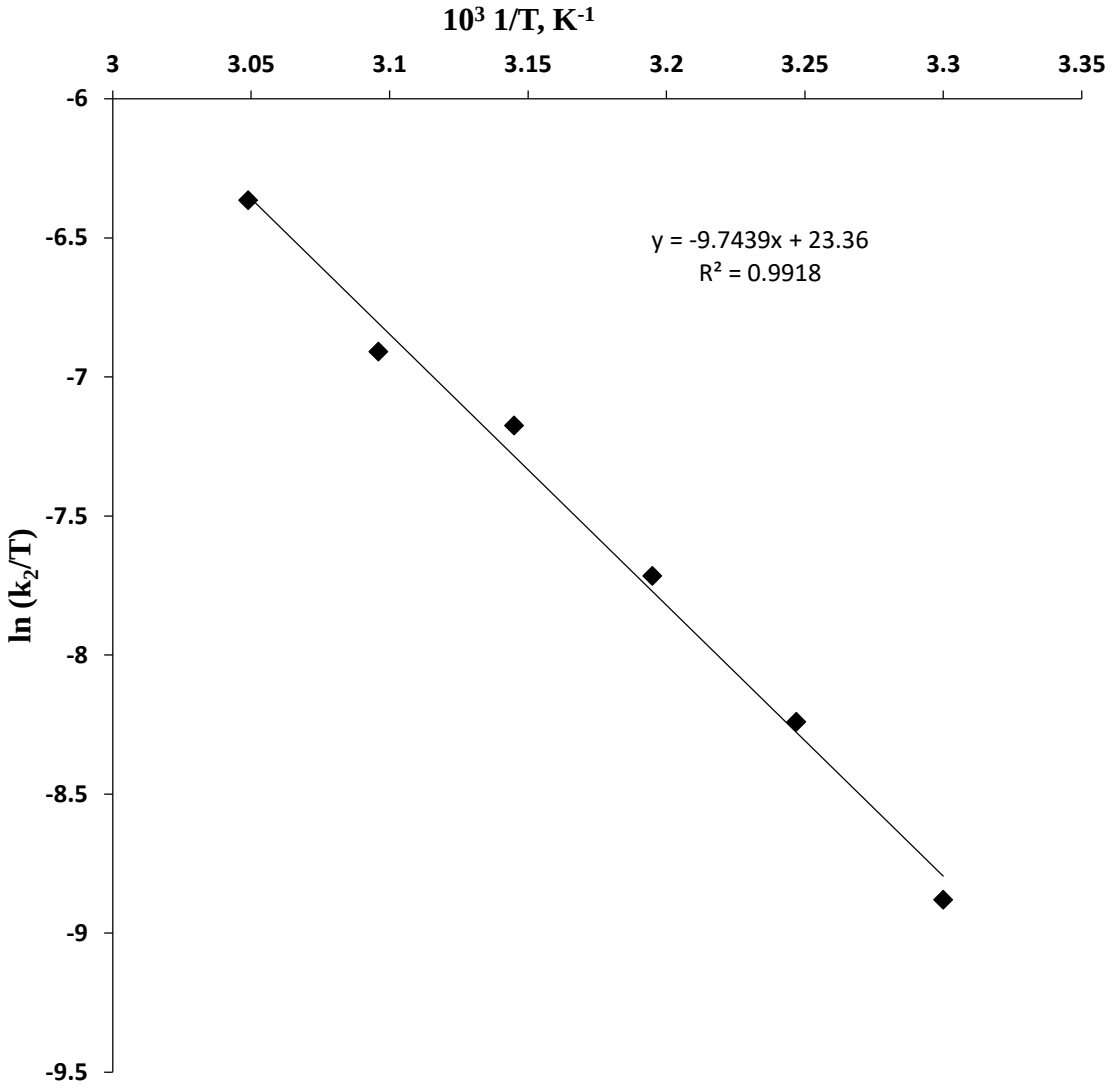


Figure 4.81: Plot of $\ln\left(\frac{k_2}{T}\right)$ versus $\left(\frac{1}{T}\right)$ for the redox reaction of $[Co(salophen)]^+$ and CH_3CHO at $[Co(salophen)^+] = 3.0 \times 10^{-4}$ mol dm^{-3}, $[CH_3CHO] = 13.5 \times 10^{-2}$ mol dm^{-3}, $[H^+] = 4.0 \times 10^{-2}$ mol dm^{-3}, $\mu = 0.2$ C^2 mol dm^{-3}, D = 75.67, T = (302 – 328) K and λ_{max} = 470 nm

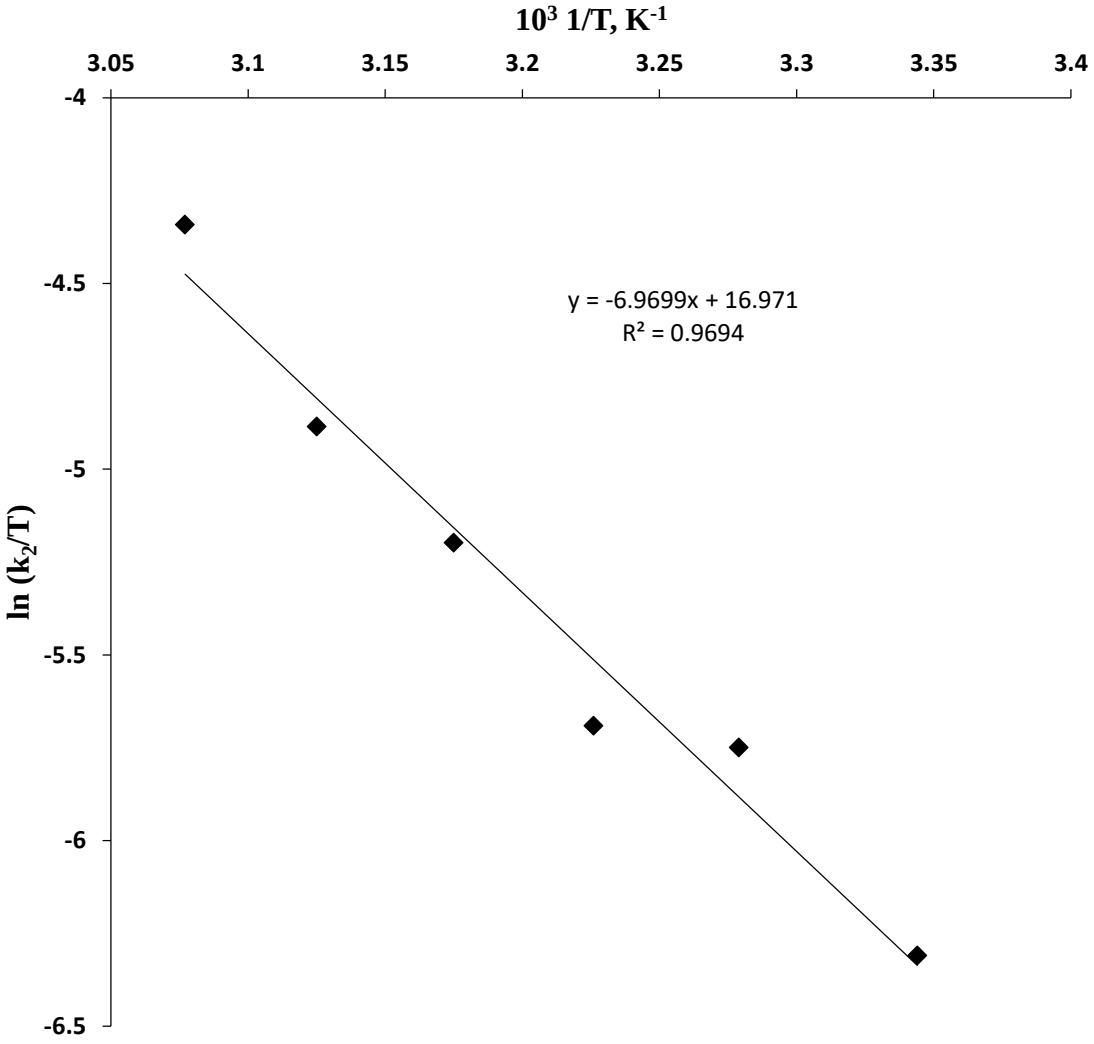


Figure 4.82: Plot of $\ln\left(\frac{k_2}{T}\right)$ versus $(\frac{1}{T})$ for the reaction of $[Co(salophen)]^+$ and HCHO at $[Co(salophen)^+] = 3.0 \times 10^{-4}$ mol dm^{-3}, $[HCHO] = 18.0 \times 10^{-3}$ mol dm^{-3}, $[H^+] = 0.1$ mol dm^{-3}, $\mu = 0.2$ C^2 mol dm^{-3}, D = 74.78, T = (299 – 325) K and λ_{max} = 470 nm

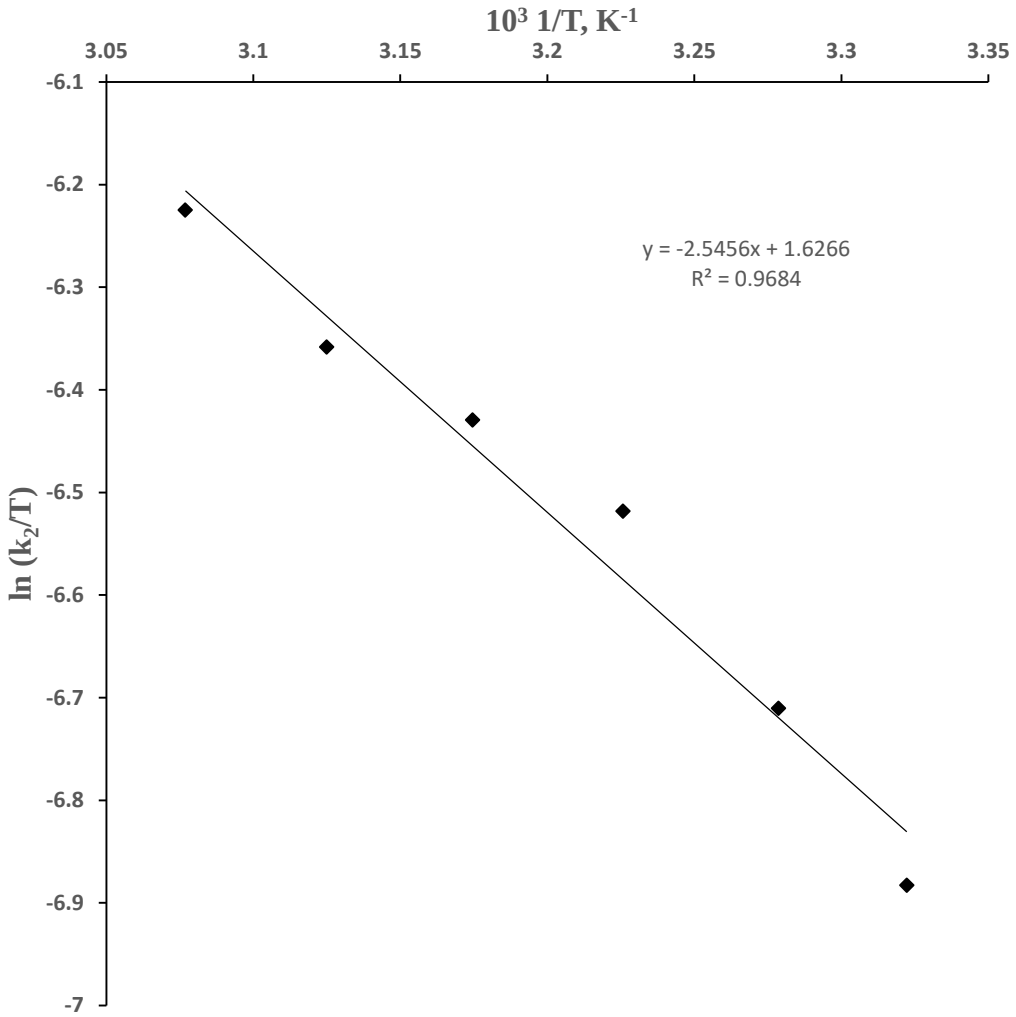


Figure 4.83: Plot of $\ln\left(\frac{k_2}{T}\right)$ versus $\left(\frac{1}{T}\right)$ for the reaction of $[Co(salophen)]^+$ and I^- at $[Co(salophen)^+] = 2.0 \times 10^{-4}$ mol dm^{-3}, $[I^-] = 16.0 \times 10^{-2}$ mol dm^{-3} $[H^+] = 0.40$ mol dm^{-3}, $\mu = 0.6$ C^2 mol dm^{-3}, D = 78.43, T = (301 – 325) K and λ_{max} = 470 nm

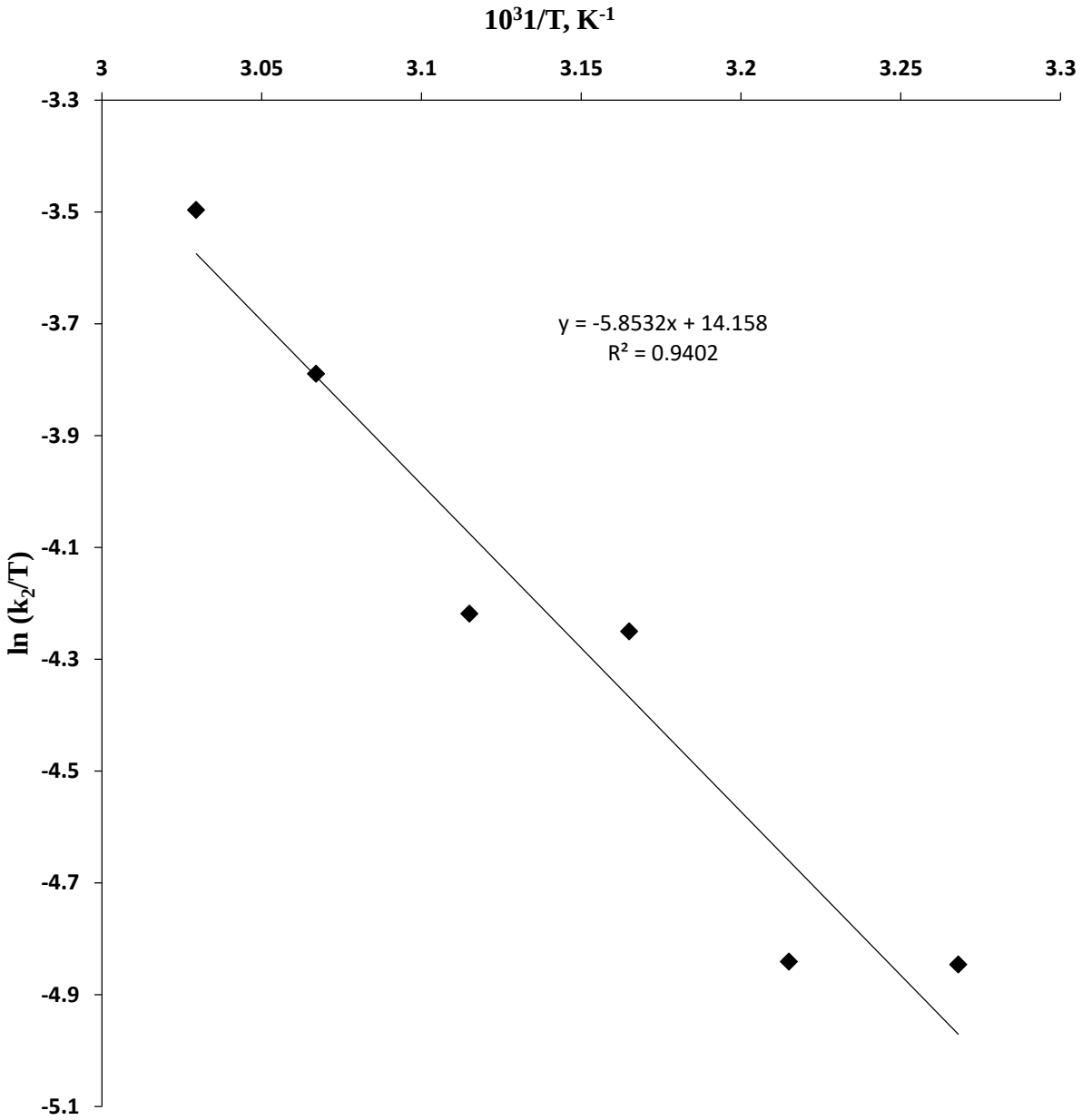


Figure 4.84: Plot of ln $\left(\frac{k_2}{T}\right)$ versus $\left(\frac{1}{T}\right)$ for the redox reaction of $[Co(salophen)]^+$ and H_2A at $[Co(salophen)^+] = 3.0 \times 10^{-4}$ mol dm^{-3}, $[H_2A] = 12.0 \times 10^{-3}$ mol dm^{-3}, $[H^+] = 2.0 \times 10^{-3}$ mol dm^{-3}, $\mu = 0.1$ C^2 mol dm^{-3}, D = 74.11, T = (306 – 333) K, and λ_{max} = 470 nm

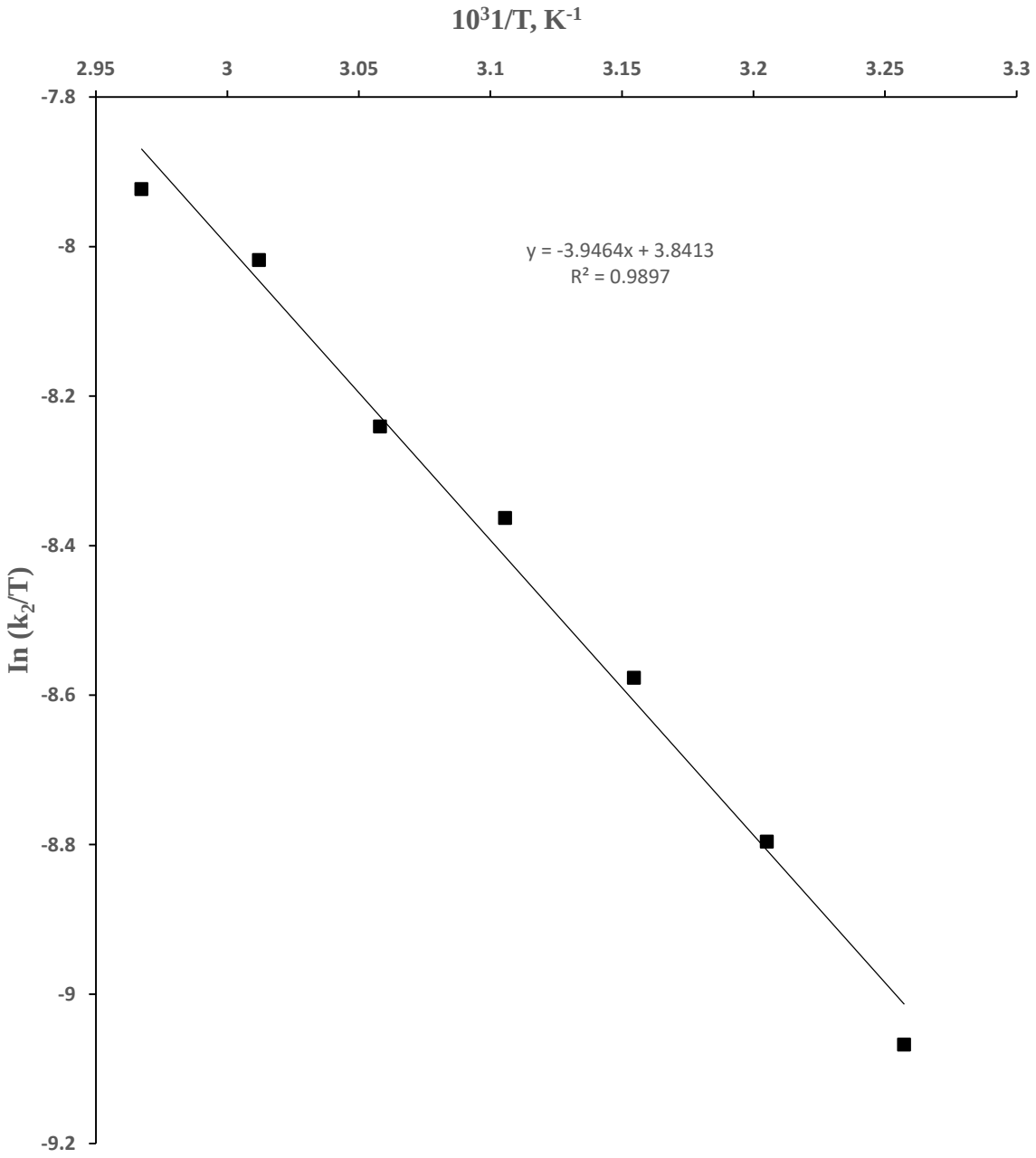


Figure 4.85: Plot of ln $\left(\frac{k_2}{T}\right)$ versus $\left(\frac{1}{T}\right)$ for the redox reaction of $[Co(salophen)]^+$ and $S(R)_2$ at $[Co(salophen)^+] = 2.0 \times 10^{-4}$ mol dm^{-3}, $[S(R)_2] = 16.0 \times 10^{-2}$ mol dm^{-3}, $[H^+] = 5.0 \times 10^{-2}$ mol dm^{-3}, $\mu = 0.2$ C^2 mol dm^{-3}, D = 77.42, T = (305 – 337) K and λ_{max} = 470 nm

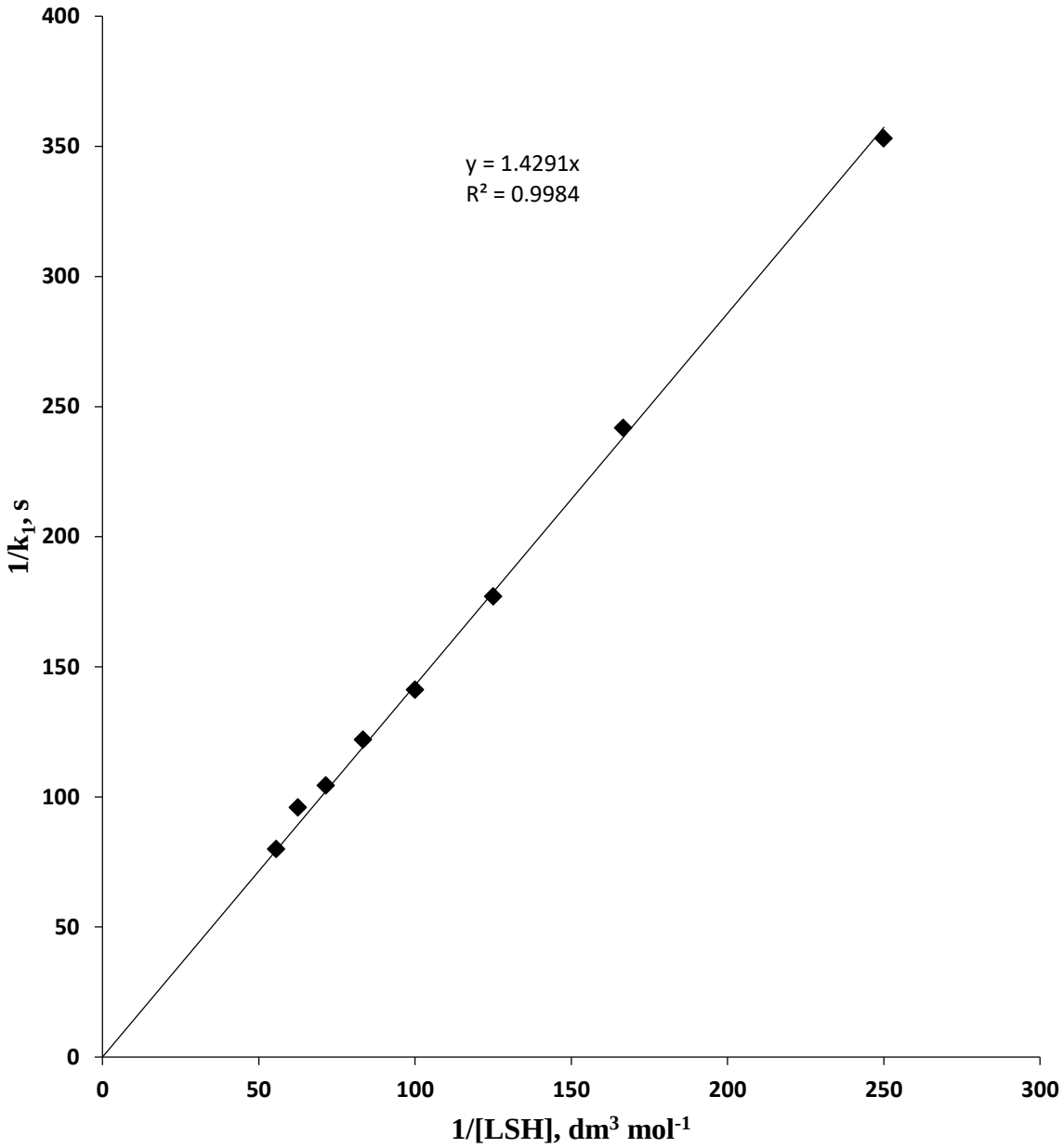


Figure 4.86: Michaelis-Menten plot for the redox reaction of $[Co(salophen)]^+$ and LSH at $[Co(salophen)^+] = 2.0 \times 10^{-4}$ mol dm^{-3}, [LSH] = 12.0×10^{-3} mol dm^{-3}, $[H^+] = 1.0 \times 10^{-3}$ mol dm^{-3}, $\mu = 0.1$ C^2 mol dm^{-3}, D = 74.84, T = 300 K, and λ_{max} = 470 nm

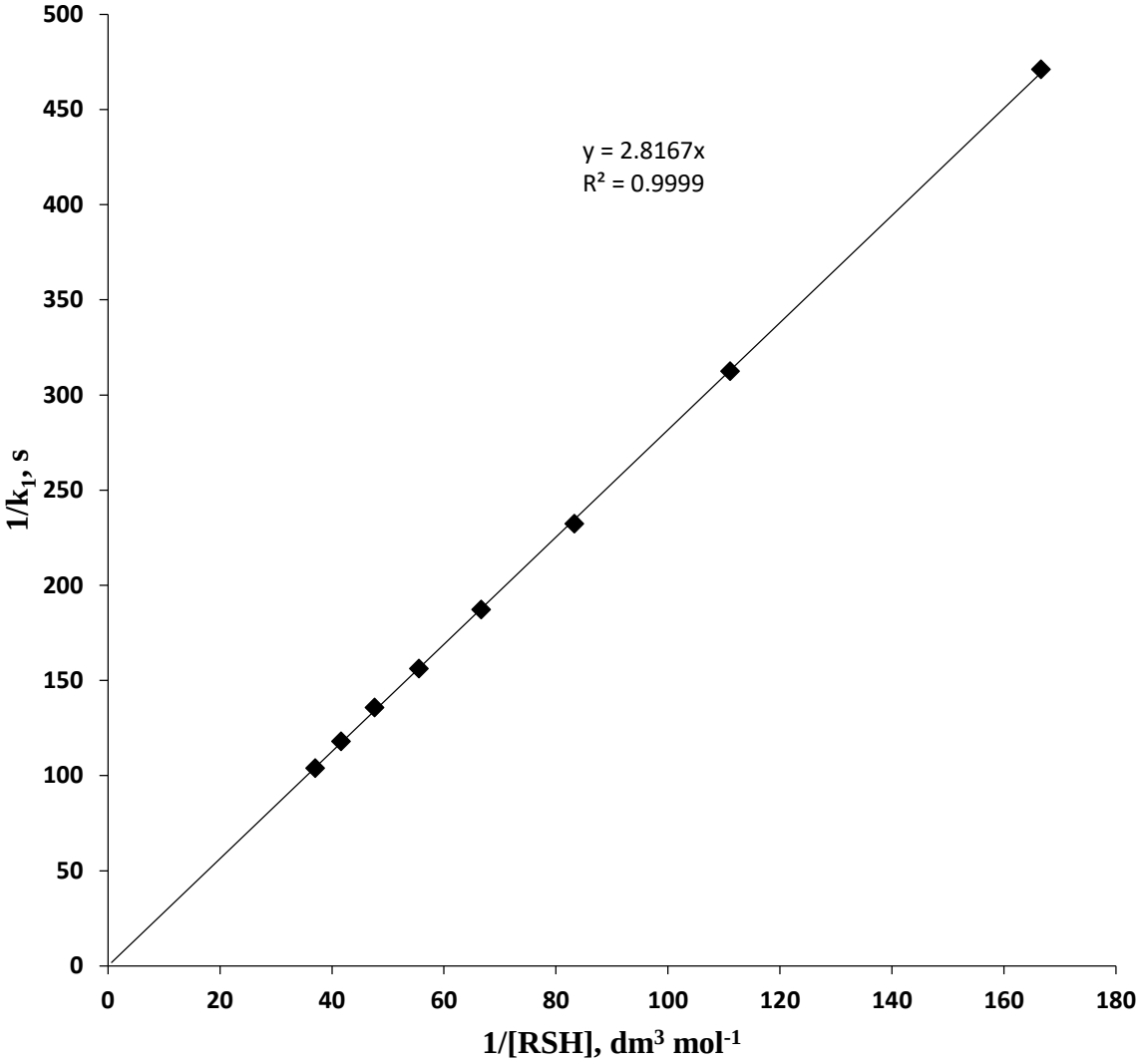


Figure 4.87: Michaelis-Menten plot for the redox reaction of $[Co(salophen)]^+$ and RSH at $[Co(salophen)^+] = 3.0 \times 10^{-4}$ mol dm^{-3}, [RSH] = 15.0×10^{-3} mol dm^{-3}, $[H^+] = 1.4 \times 10^{-3}$ mol dm^{-3}, $\mu = 0.1$ C^2 mol dm^{-3}, D = 74.19, T = 300 K, and λ_{max} = 470

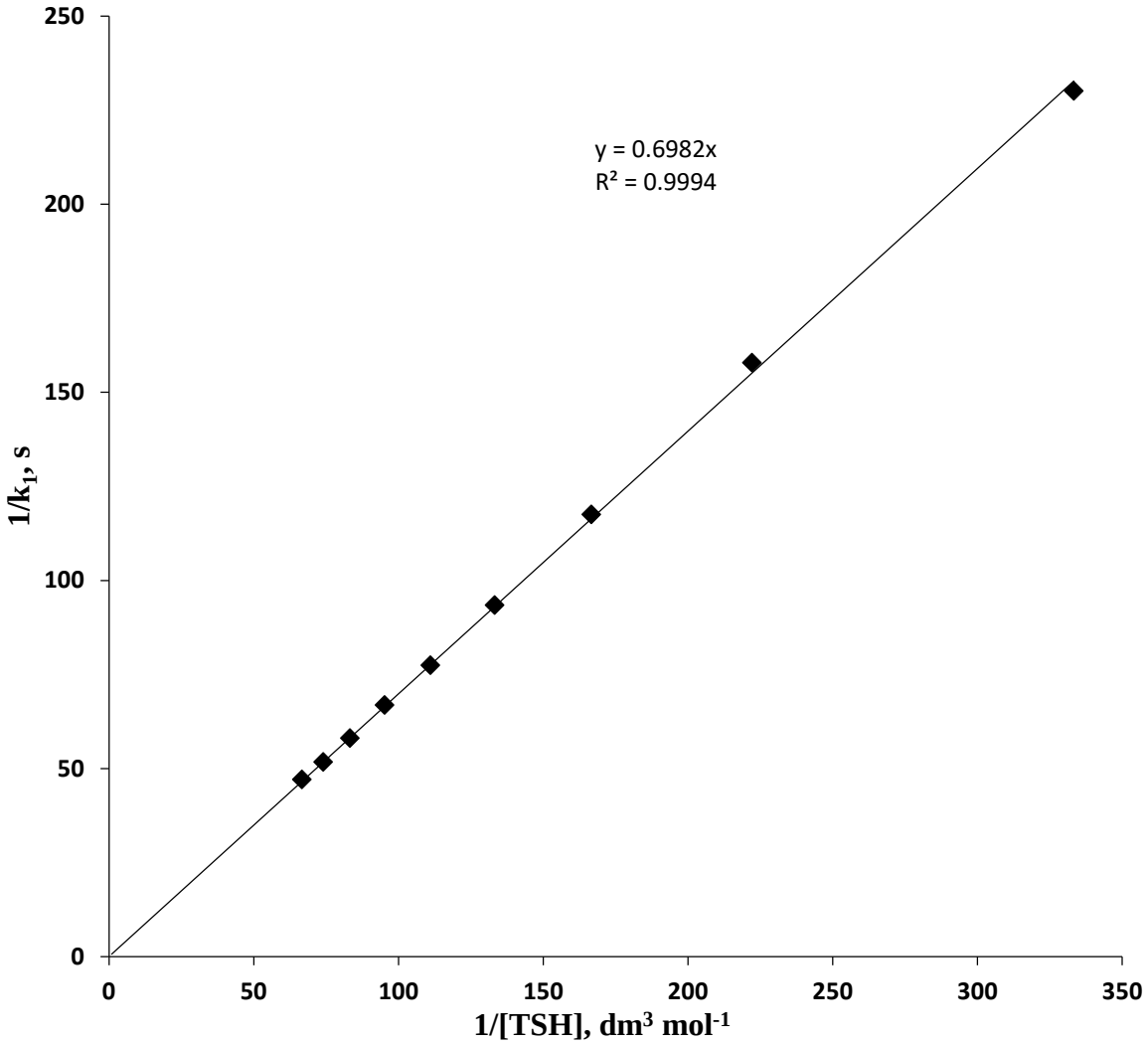


Figure 4.88: Michaelis-Menten plot for the redox reaction of $[Co(salophen)]^{+}$ and TSH at $[Co(salophen)^{+}] = 3.0 \times 10^{-4}$ mol dm^{-3}, [TSH] = 7.50×10^{-3} mol dm^{-3}, $\mu = 0.1$ C^2 mol dm^{-3}, D = 74.04, T = 300 K, and λ_{max} = 470 nm

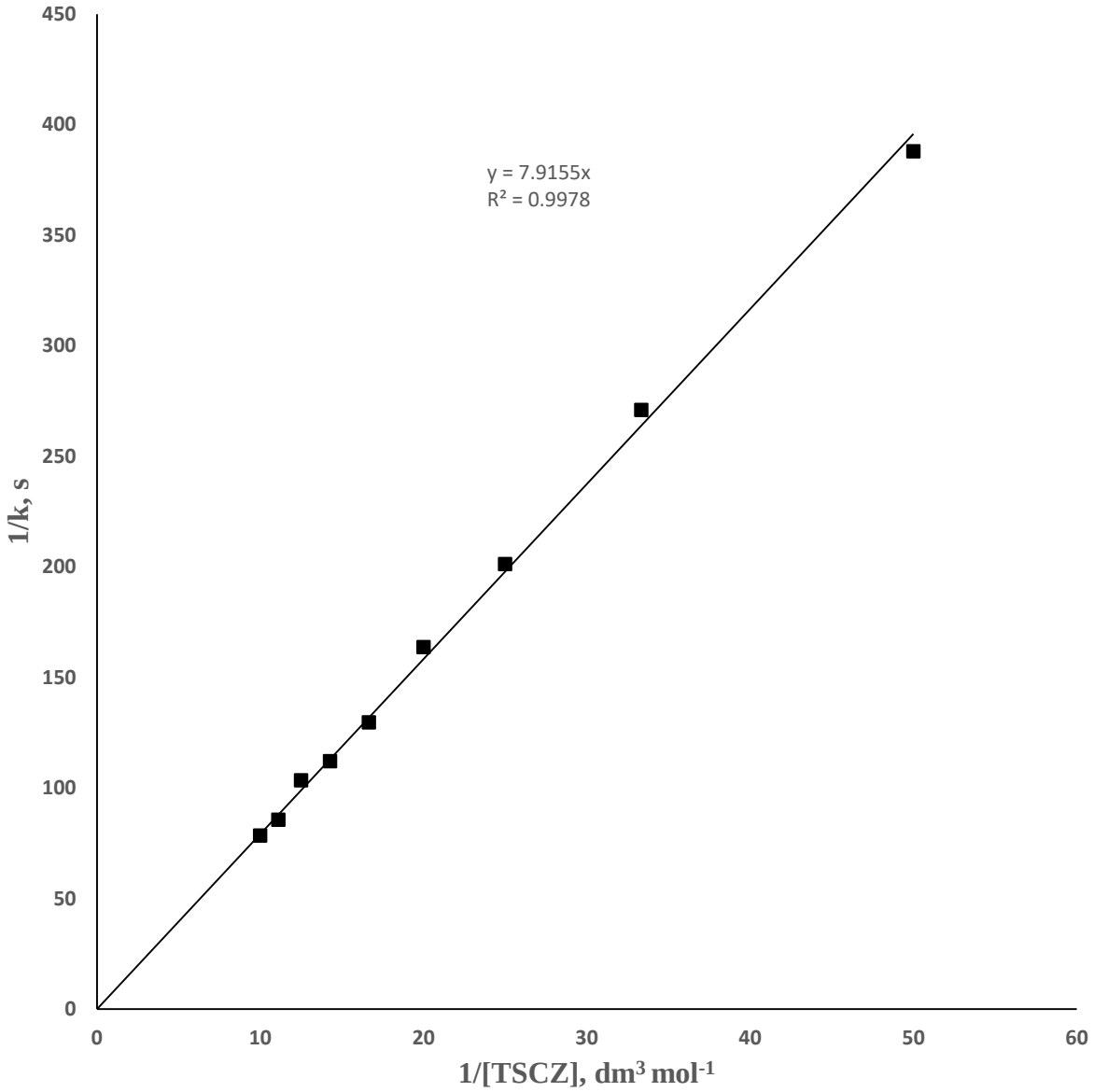


Figure 4.89: Michaelis-Menten plot for the redox reaction of $[Co(salophen)]^{+}$ and TSCZ at $[Co(salophen)^{+}] = 2.0 \times 10^{-4}$ mol dm^{-3}, [TSCZ] = 8.0×10^{-2} mol dm^{-3}, $[H^{+}] = 1.0 \times 10^{-2}$ mol dm^{-3}, $\mu = 0.1$ C^2 mol dm^{-3}, D = 74.41, T = 306 K and λ_{max} = 470 nm

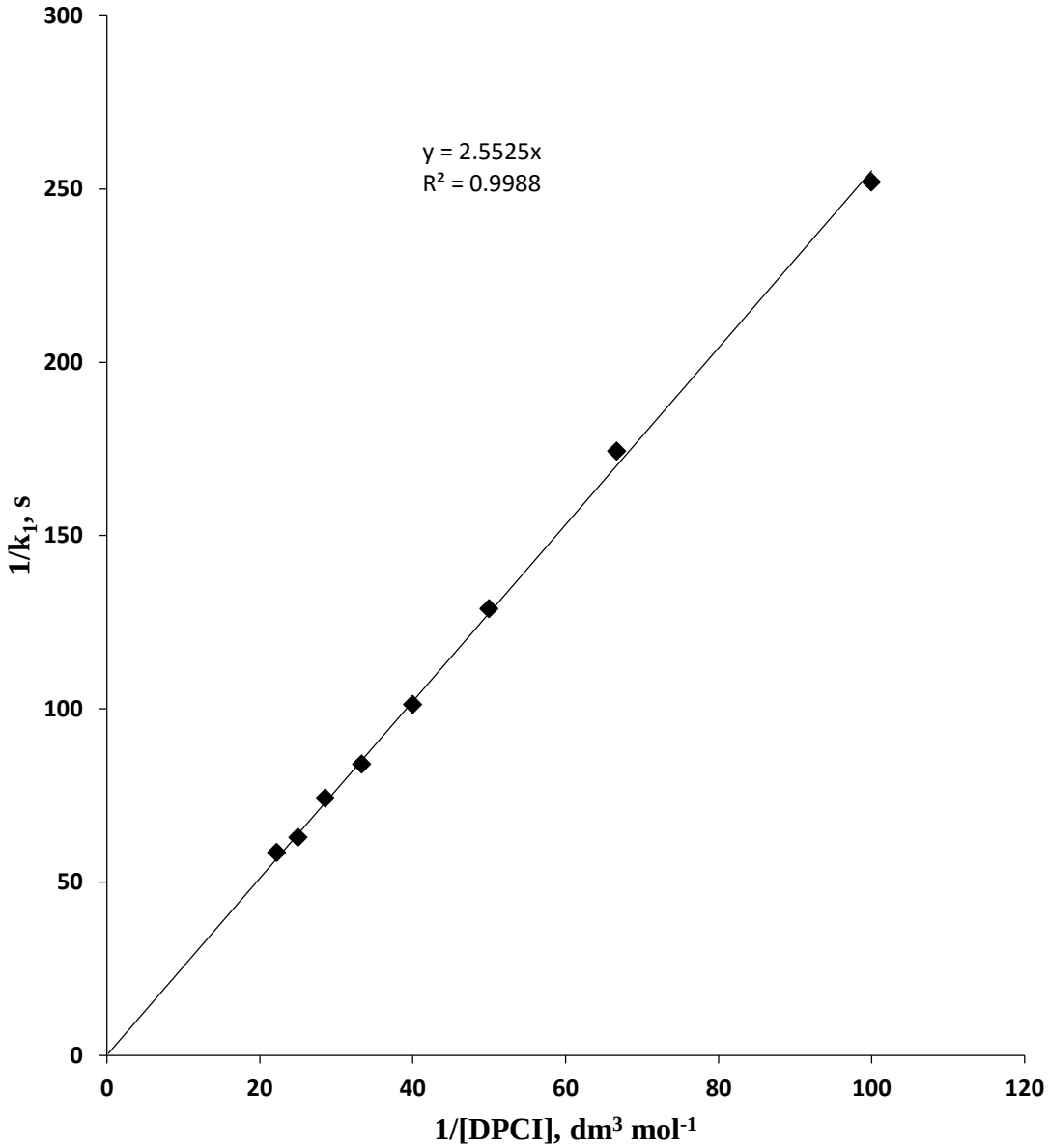


Figure 4.90: Michaelis-Menten plot for the redox reaction of $[Co(salophen)]^{+}$ and DPCI at $[Co(salophen)^{+}] = 1.0 \times 10^{-4}$ mol dm^{-3}, DPCI = 25.0×10^{-3} mol dm^{-3} $[H^{+}] = 0.1$ mol dm^{-3}, $\mu = 0.5$ C^2 mol dm^{-3}, D = 75.83, T = 300 K and λ_{max} = 470 nm

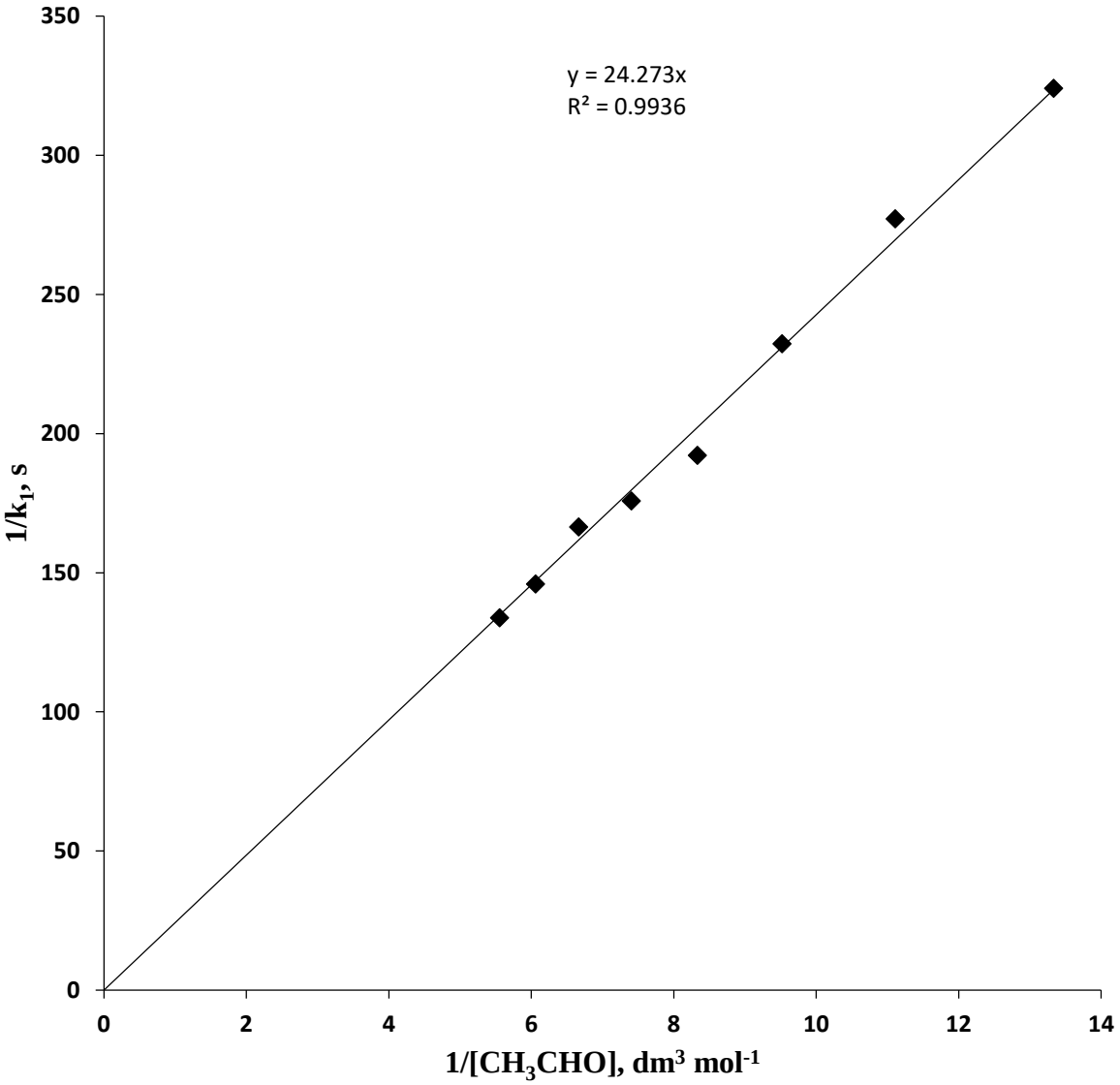


Figure 4.91: Michaelis-Menten plot for the redox reaction of $[Co(salophen)]^{+}$ and CH_3CHO at $[Co(salophen)^{+}] = 3.0 \times 10^{-4}$ mol dm^{-3}, $[CH_3CHO] = 13.5 \times 10^{-2}$ mol dm^{-3}, $[H^{+}] = 4.0 \times 10^{-2}$ mol dm^{-3}, $\mu = 0.2$ C^2 mol dm^{-3}, D = 75.67, T = 302 K and λ_{max} = 470 nm

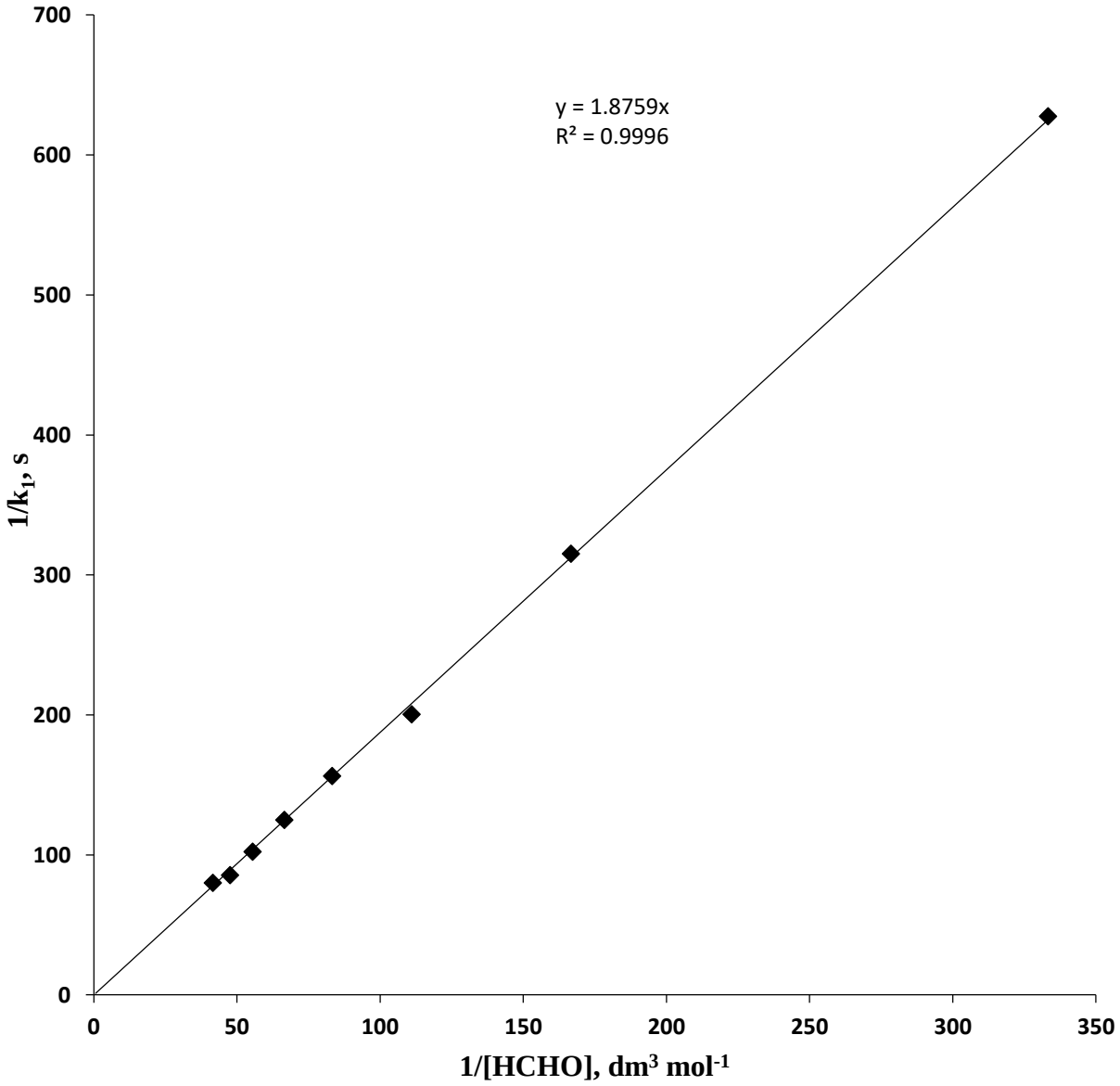


Figure 4.92: Michaelis-Menten plot for the redox reaction of $[Co(salophen)]^{+}$ and HCHO at $[Co(salophen)^{+}] = 3.0 \times 10^{-4}$ mol dm^{-3}, [HCHO] = 18.0×10^{-3} mol dm^{-3}, $[H^{+}]$ = 0.1 mol dm^{-3}, $\mu = 0.2$ C^2 mol dm^{-3}, D = 74.78, T = 299 K and λ_{max} = 470 nm

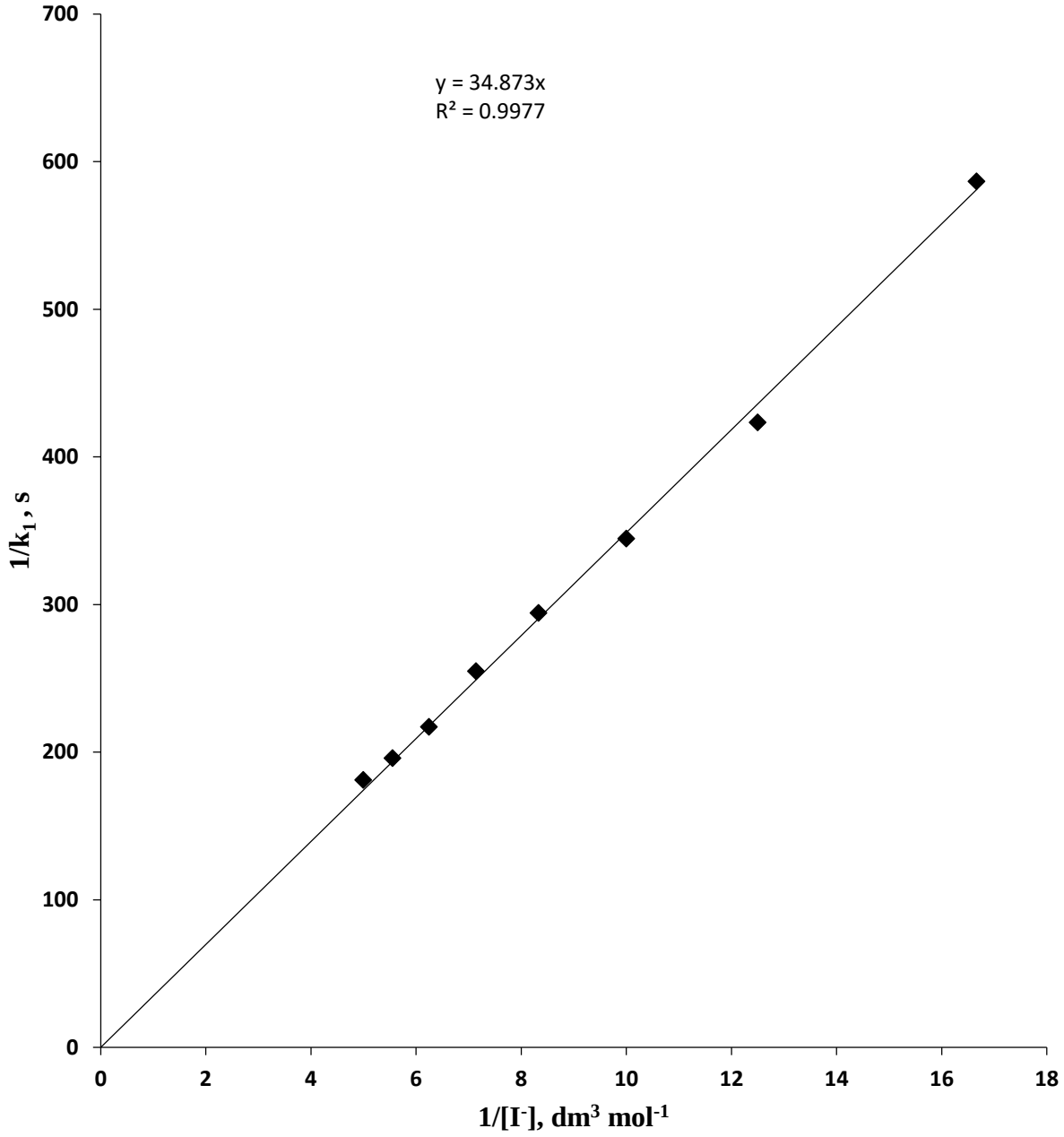


Figure 4.93: Michaelis-Menten plot for the redox reaction of $[Co(salophen)]^{+}$ and I^{-} at $[Co(salophen)^{+}] = 2.0 \times 10^{-4}$ mol dm^{-3}, $[I^{-}] = 16.0 \times 10^{-2}$ mol dm^{-3} $[H^{+}] = 0.40$ mol dm^{-3}, $\mu = 0.6$ C^2 mol dm^{-3}, D = 78.43, T = 301 K and λ_{max} = 470 nm

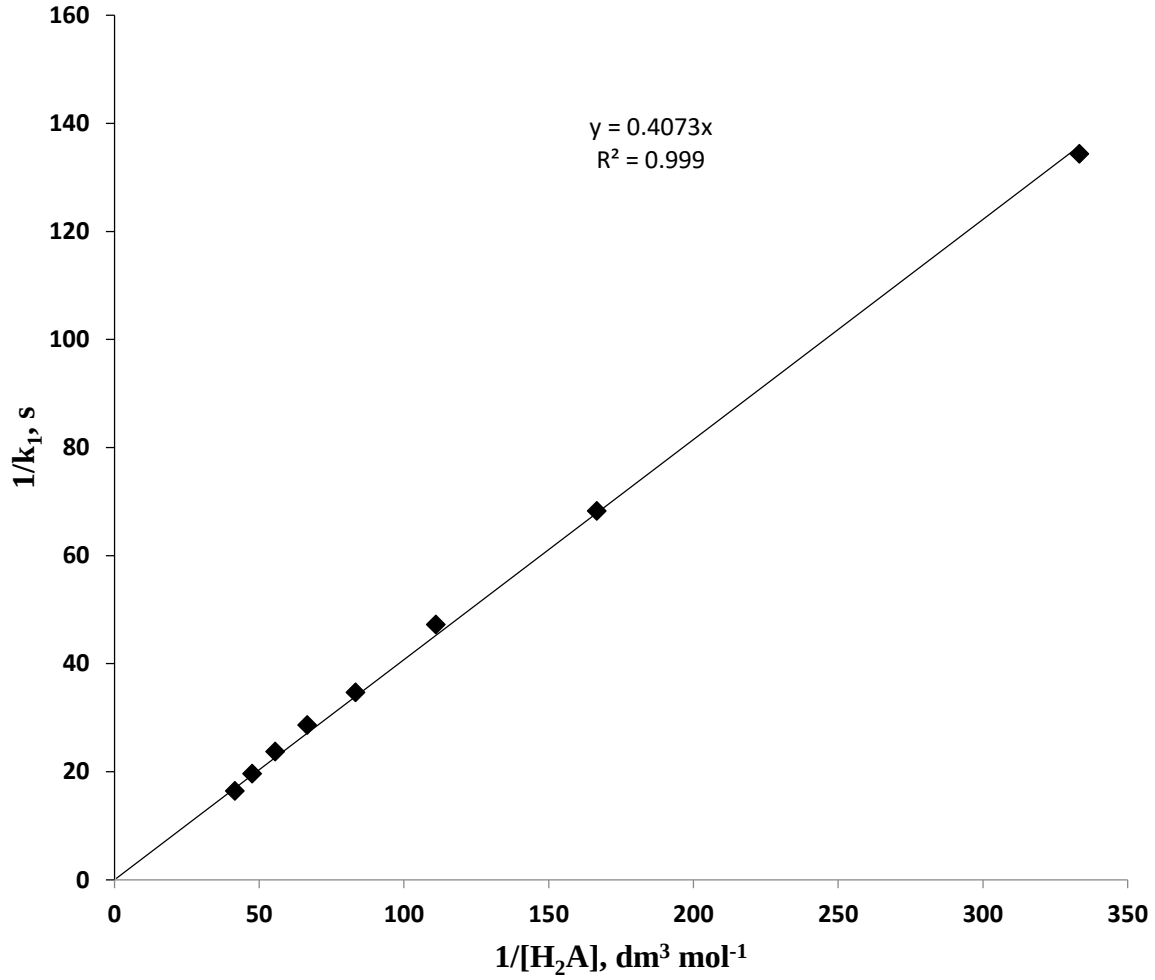


Figure 4.94: Michaelis-Menten plot for the redox reaction of $[Co(salophen)]^{+}$ and H_2A at $[Co(salophen)^{+}] = 3.0 \times 10^{-4}$ mol dm^{-3}, $[H_2A] = 12.0 \times 10^{-3}$ mol dm^{-3}, $[H^{+}] = 2.0 \times 10^{-3}$ mol dm^{-3}, $\mu = 0.1$ C^2 mol dm^{-3}, D = 74.11, T = 306 K, and λ_{max} = 470 nm

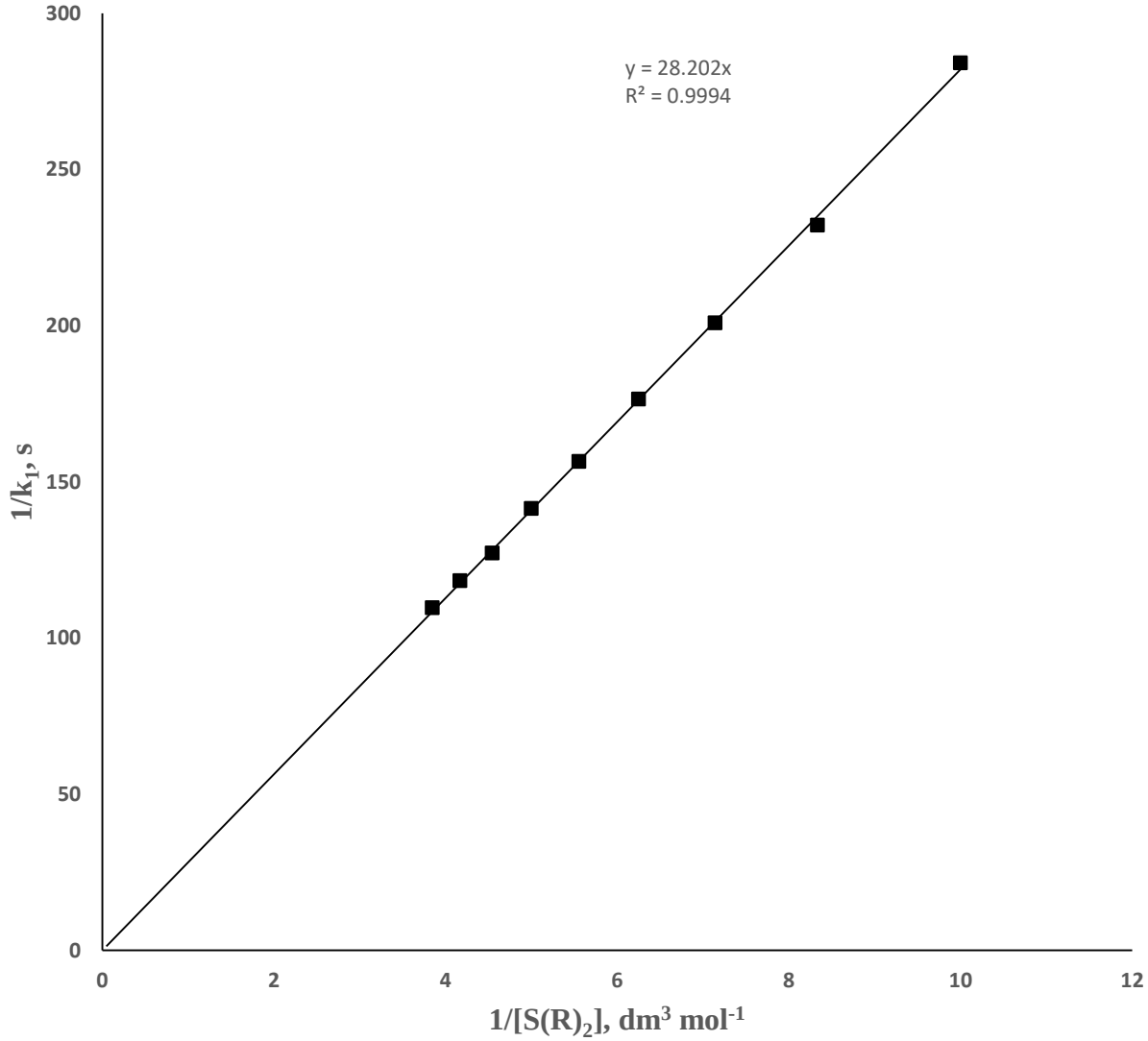


Figure 4.95: Michaelis-Menten plot for the redox reaction of $[Co(salophen)]^+$ and $S(R)_2$ at $[Co(salophen)^+] = 2.0 \times 10^{-4}$ mol dm^{-3}, $[S(R)_2] = 16.0 \times 10^{-2}$ mol dm^{-3}, $[H^+] = 5.0 \times 10^{-2}$ mol dm^{-3}, $\mu = 0.2$ C^2 mol dm^{-3}, D = 77.42, T = 305 K and λ_{max} = 470 nm

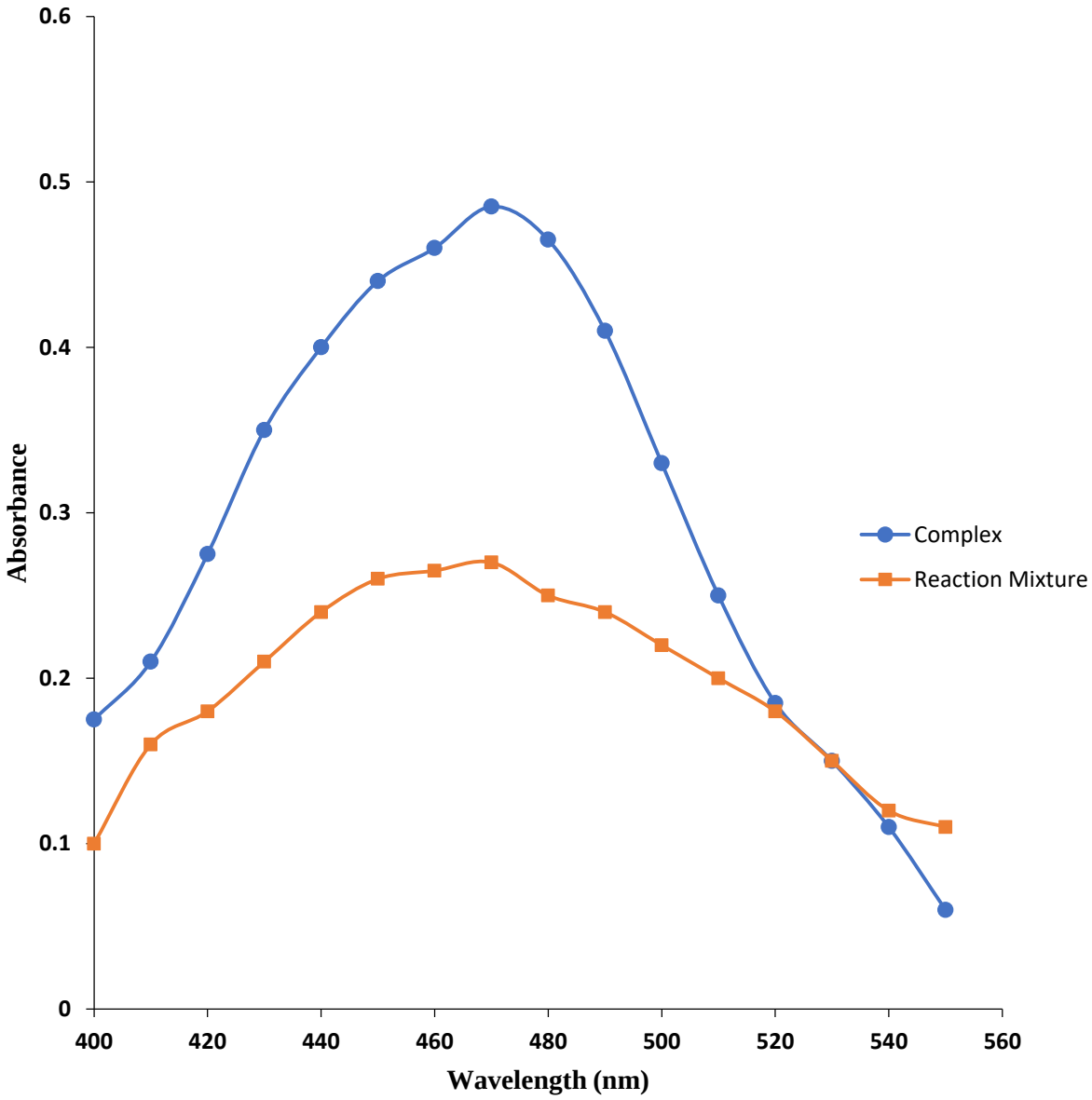


Figure 4.96: Plot for spectrophotometric test for the redox reaction of $[Co(salophen)]^{+}$ and LSH at $[Co(salophen)^{+}] = 2.0 \times 10^{-4}$ mol dm^{-3}, $[LSH] = 12.0 \times 10^{-3}$ mol dm^{-3}, $[H^{+}] = 1.0 \times 10^{-3}$ mol dm^{-3}, $\mu = 0.1$ C^2 mol dm^{-3}, D = 74.84, T = 300 K, and λ_{max} = 470 nm

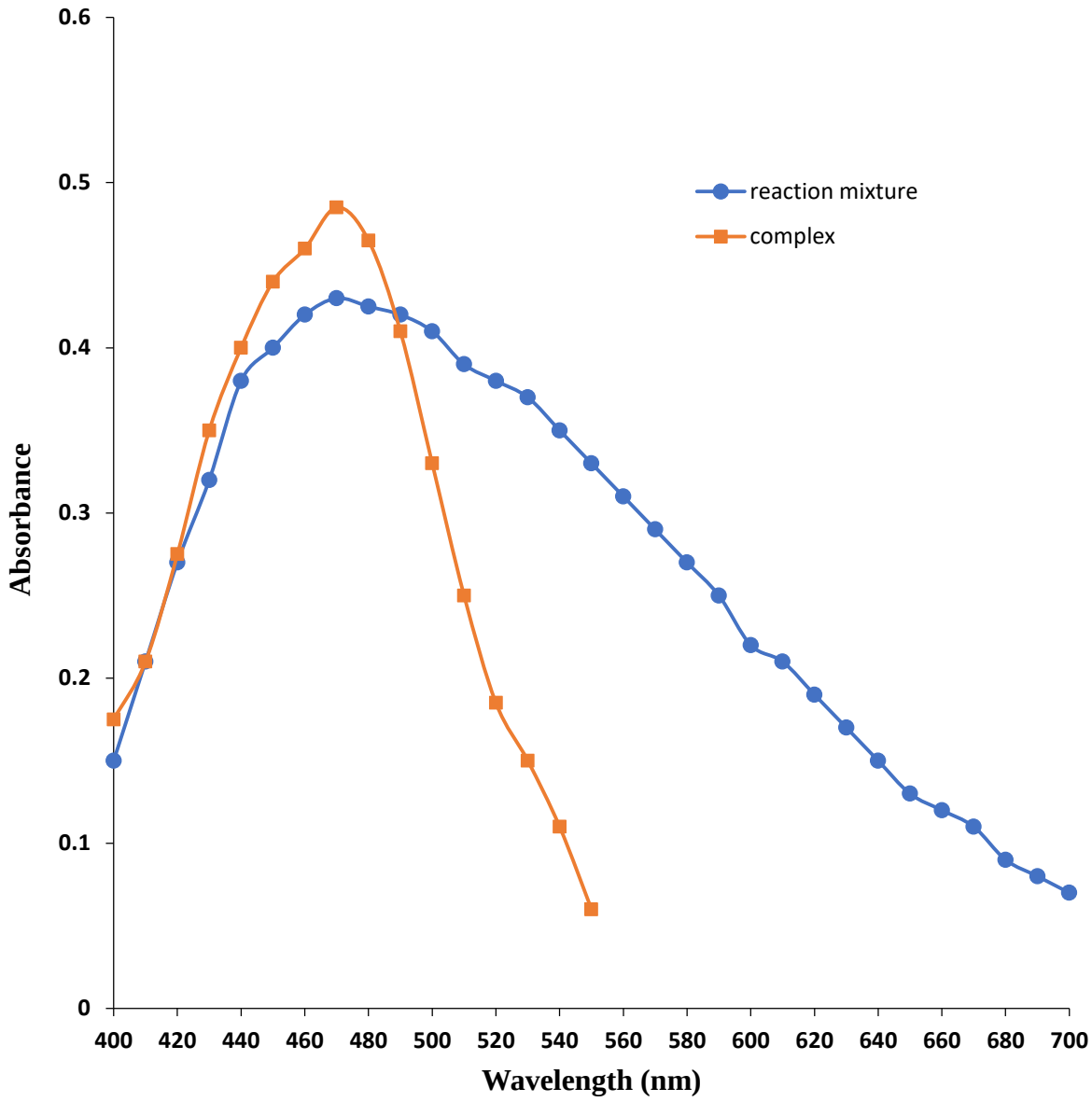


Figure 4.97: Plot for spectrophotometric test for the redox reaction of $[Co(salophen)]^{+}$ and RSH at $[Co(salophen)^{+}] = 3.0 \times 10^{-4}$ mol dm^{-3}, $[RSH] = 12.0 \times 10^{-3}$ mol dm^{-3}, $[H^{+}] = 1.4 \times 10^{-3}$ mol dm^{-3}, $\mu = 0.1$ C^2 mol dm^{-3}, D = 74.19, T = 300 K, and λ_{max} = 470 nm

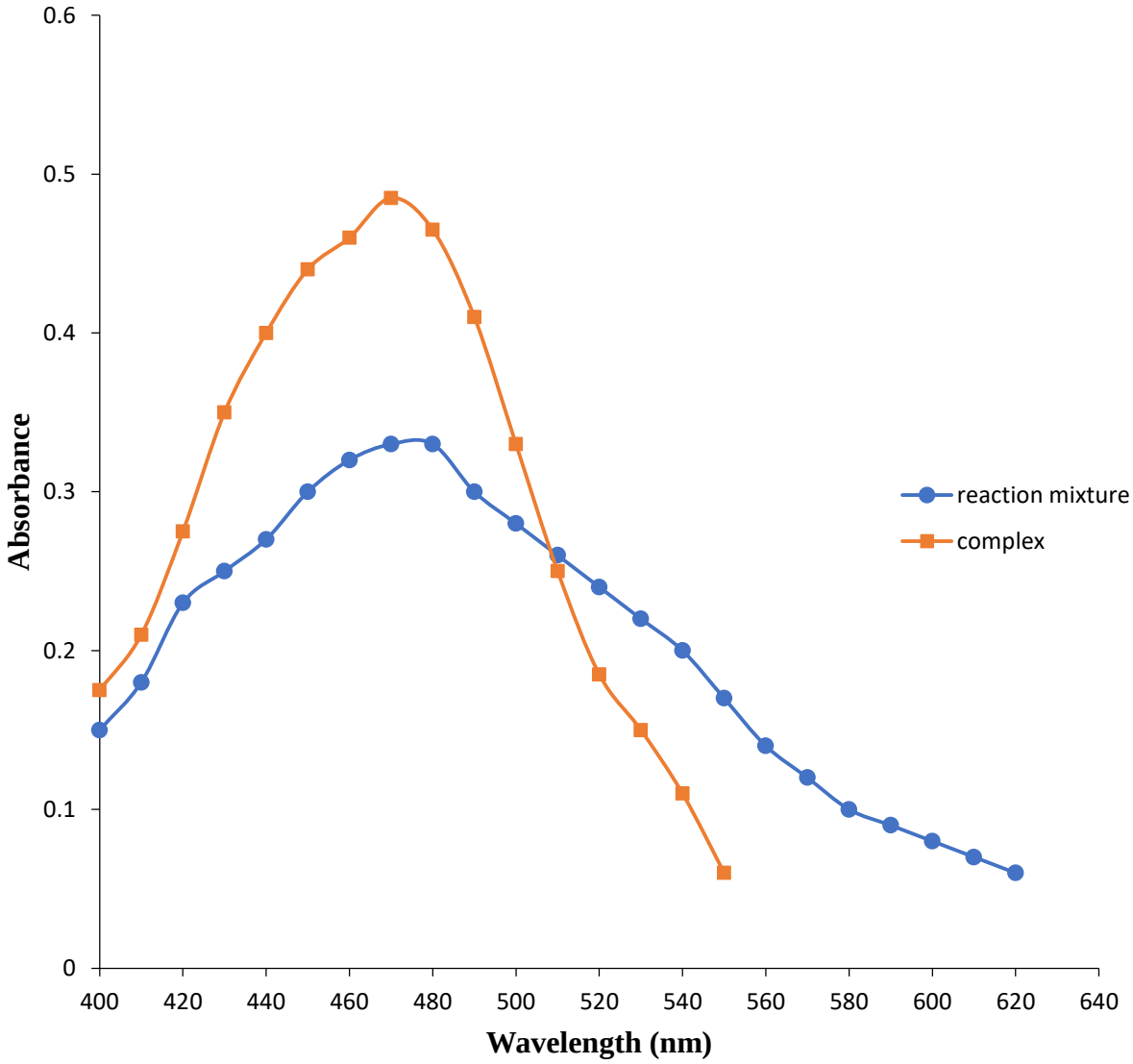


Figure 4.98: Plot for spectrophotometric test for the redox reaction of $[Co(salophen)]^{+}$ and TSH at $[Co(salophen)^{+}] = 3.0 \times 10^{-4}$ mol dm^{-3}, $[TSH] = 7.50 \times 10^{-3}$ mol dm^{-3}, $\mu = 0.1$ C^2 mol dm^{-3}, D = 74.04, T = 300 K, and λ_{max} = 470 nm

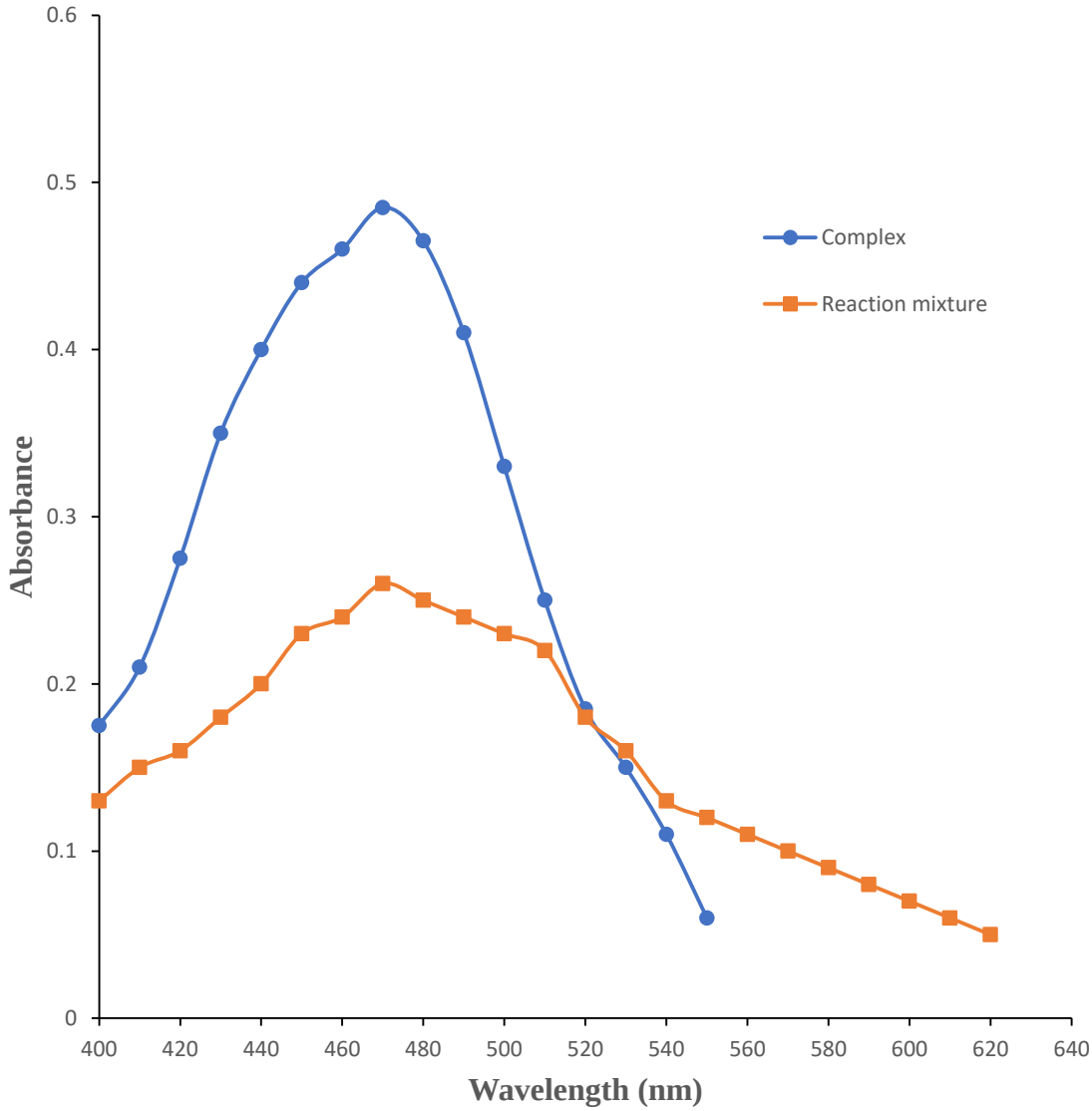


Figure 4.99: Plot for spectrophotometric test for the redox reaction of $[Co(salophen)]^{+}$ and TSCZ at $[Co(salophen)^{+}] = 2.0 \times 10^{-4}$ mol dm^{-3}, $[TSCZ] = 8.0 \times 10^{-2}$ mol dm^{-3}, $[H^{+}] = 1.0 \times 10^{-2}$ mol dm^{-3}, $\mu = 0.1$ C^2 mol dm^{-3}, D = 74.41, T = 306 K and λ_{max} = 470 nm

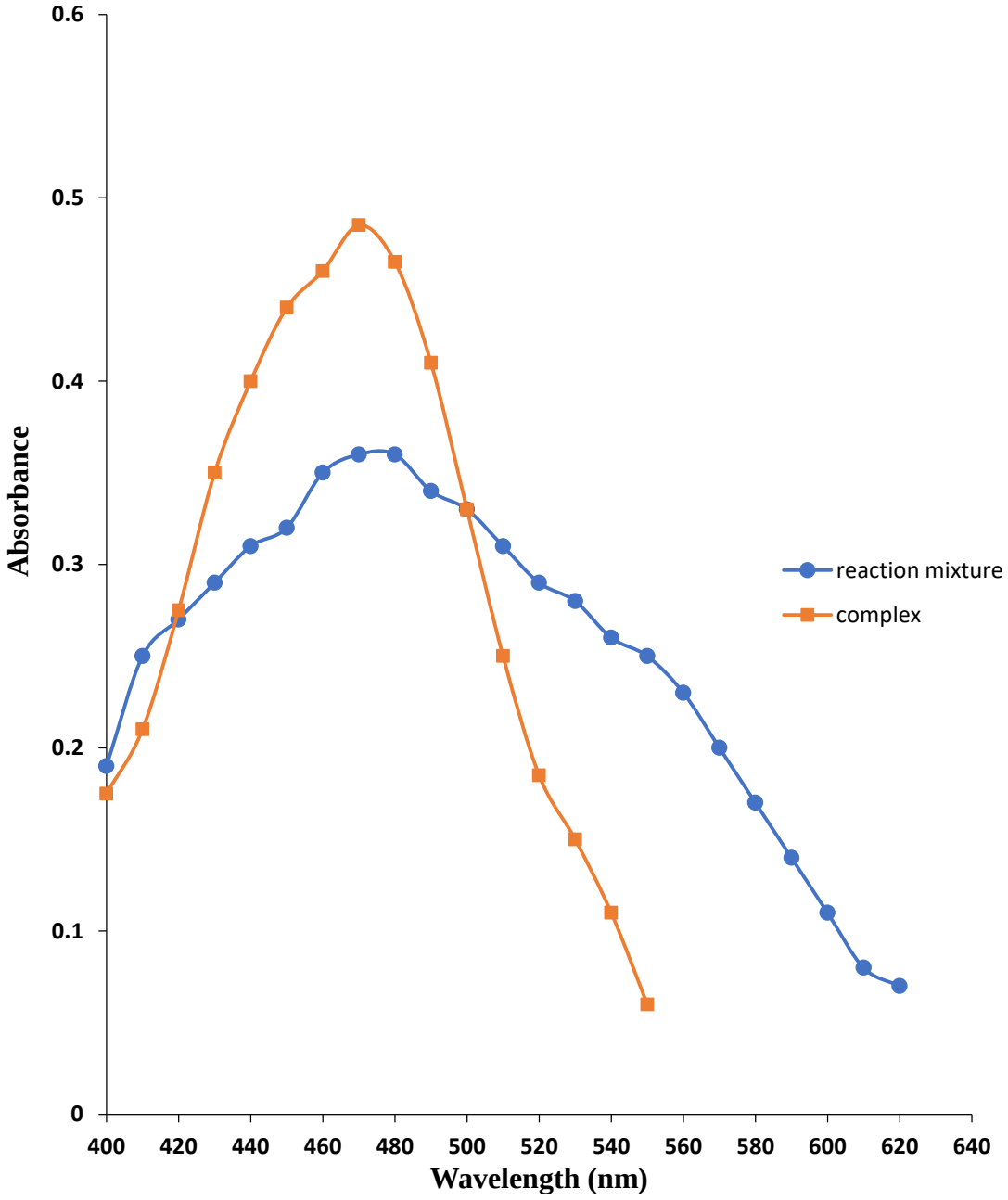


Figure 4.100: Plot for spectrophotometric test for the redox reaction of $[Co(salophen)]^{+}$ and DPCI at $[Co(salophen)^{+}] = 1.0 \times 10^{-4}$ mol dm^{-3}, DPCI = 25.0×10^{-3} mol dm^{-3} $[H^{+}] = 0.1$ mol dm^{-3}, $\mu = 0.5$ C^2 mol dm^{-3}, D = 75.83, T = 300 K and λ_{max} = 470 nm

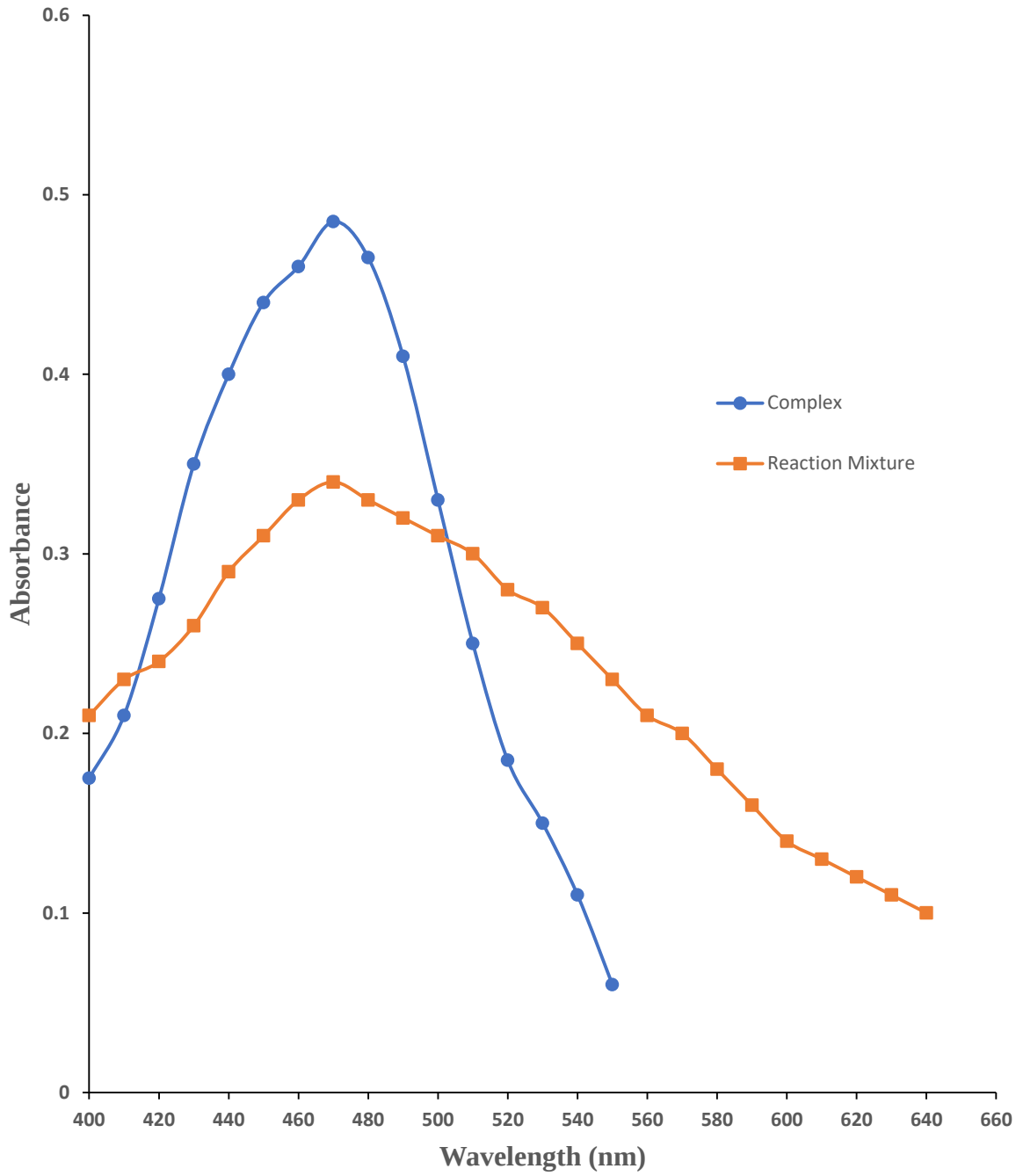


Figure 4.101: Plot for spectrophotometric test for the redox reaction of $[Co(salophen)]^{+}$ and CH_3CHO at $[Co(salophen)^{+}] = 3.0 \times 10^{-4}$ mol dm^{-3}, $[CH_3CHO] = 13.5 \times 10^{-2}$ mol dm^{-3}, $[H^{+}] = 4.0 \times 10^{-2}$ mol dm^{-3}, $\mu = 0.2$ C^2 mol dm^{-3}, D = 75.67, T = 302 K and λ_{max} = 470 nm

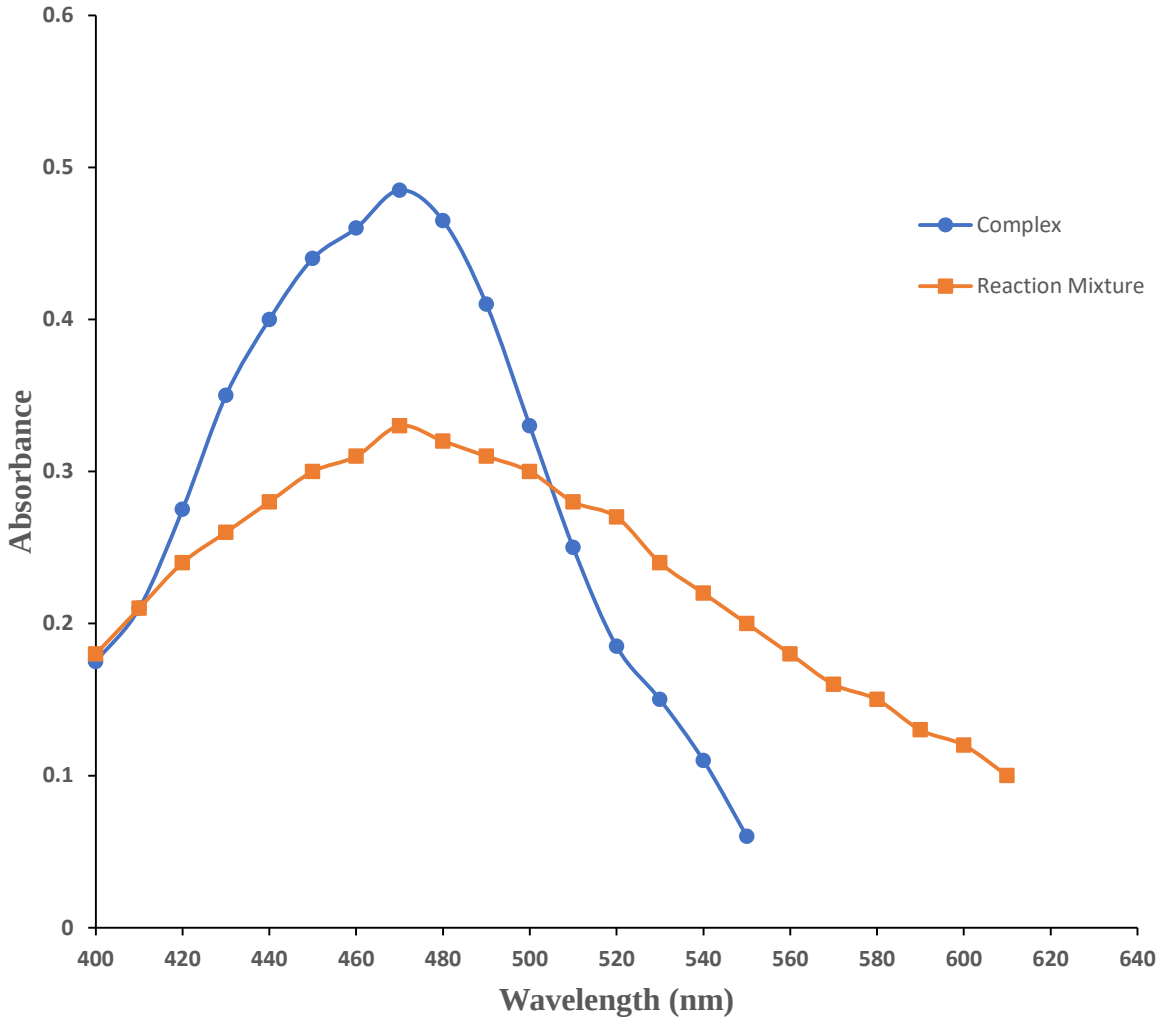


Figure 4.102: Plot for spectrophotometric test for the redox reaction of $[Co(salophen)]^{+}$ and HCHO at $[Co(salophen)^{+}] = 3.0 \times 10^{-4}$ mol dm^{-3}, $[HCHO] = 18.0 \times 10^{-3}$ mol dm^{-3}, $[H^{+}] = 0.1$ mol dm^{-3}, $\mu = 0.2$ C^2 mol dm^{-3}, D = 74.78, T = 299 K and λ_{max} = 470 nm

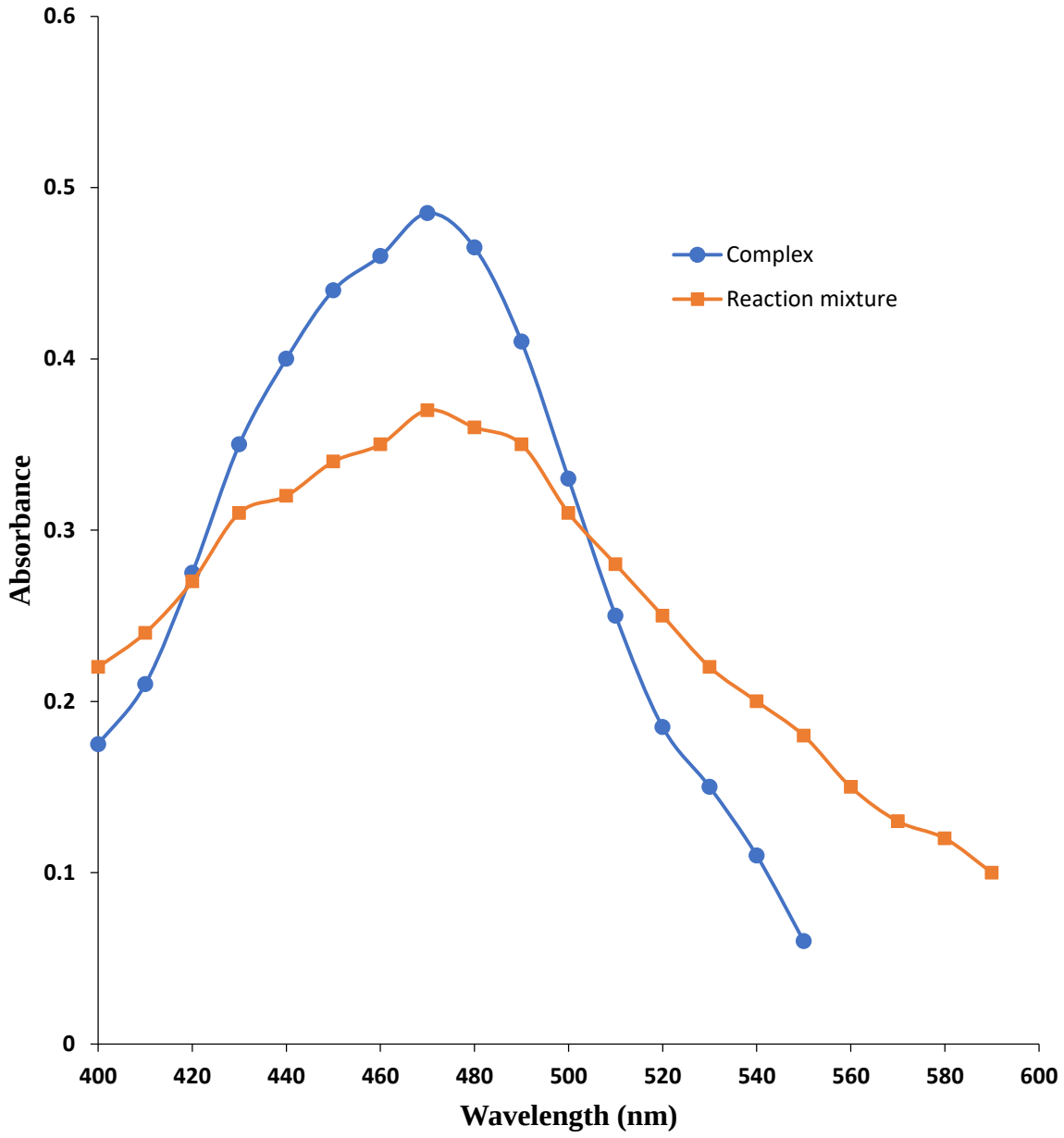


Figure 4.103: Plot for spectrophotometric test for the redox reaction of $[Co(salophen)]^{+}$ and I^{-} at $[Co(salophen)^{+}] = 2.0 \times 10^{-4}$ mol dm^{-3}, $[I^{-}] = 16.0 \times 10^{-2}$ mol dm^{-3} $[H^{+}] = 0.40$ mol dm^{-3}, $\mu = 0.6$ C^{2} mol dm^{-3}, D = 78.43, T = 301 K and λ_{max} = 470 nm

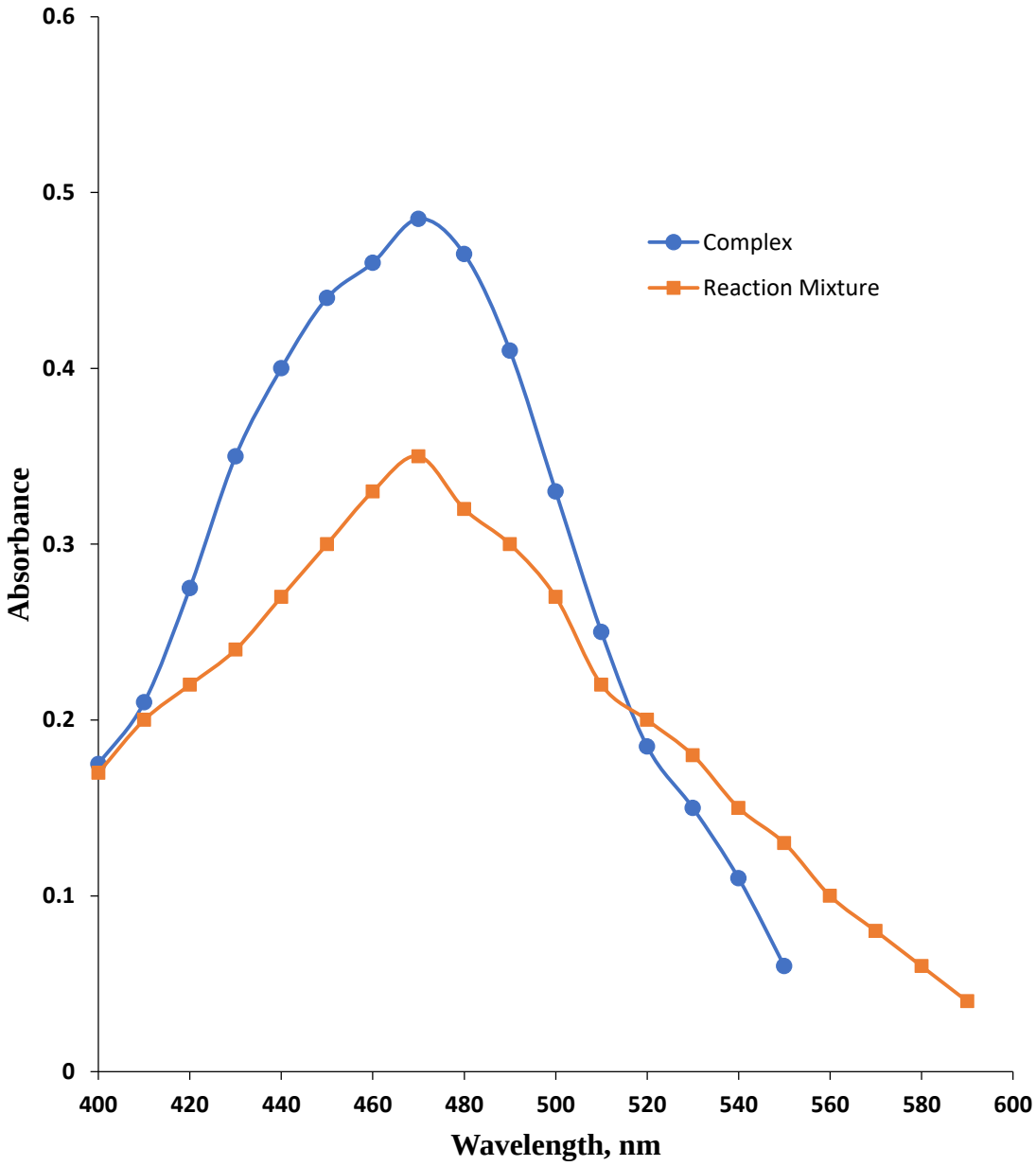


Figure 4.104: Plot for spectrophotometric test for the redox reaction of $[Co(salophen)]^{+}$ and H_2A at $[Co(salophen)^{+}] = 3.0 \times 10^{-4}$ mol dm^{-3}, $[H_2A] = 12.0 \times 10^{-3}$ mol dm^{-3}, $[H^{+}] = 2.0 \times 10^{-3}$ mol dm^{-3}, $\mu = 0.1$ C^2 mol dm^{-3}, D = 74.11, T = 306 K, and λ_{max} = 470 nm

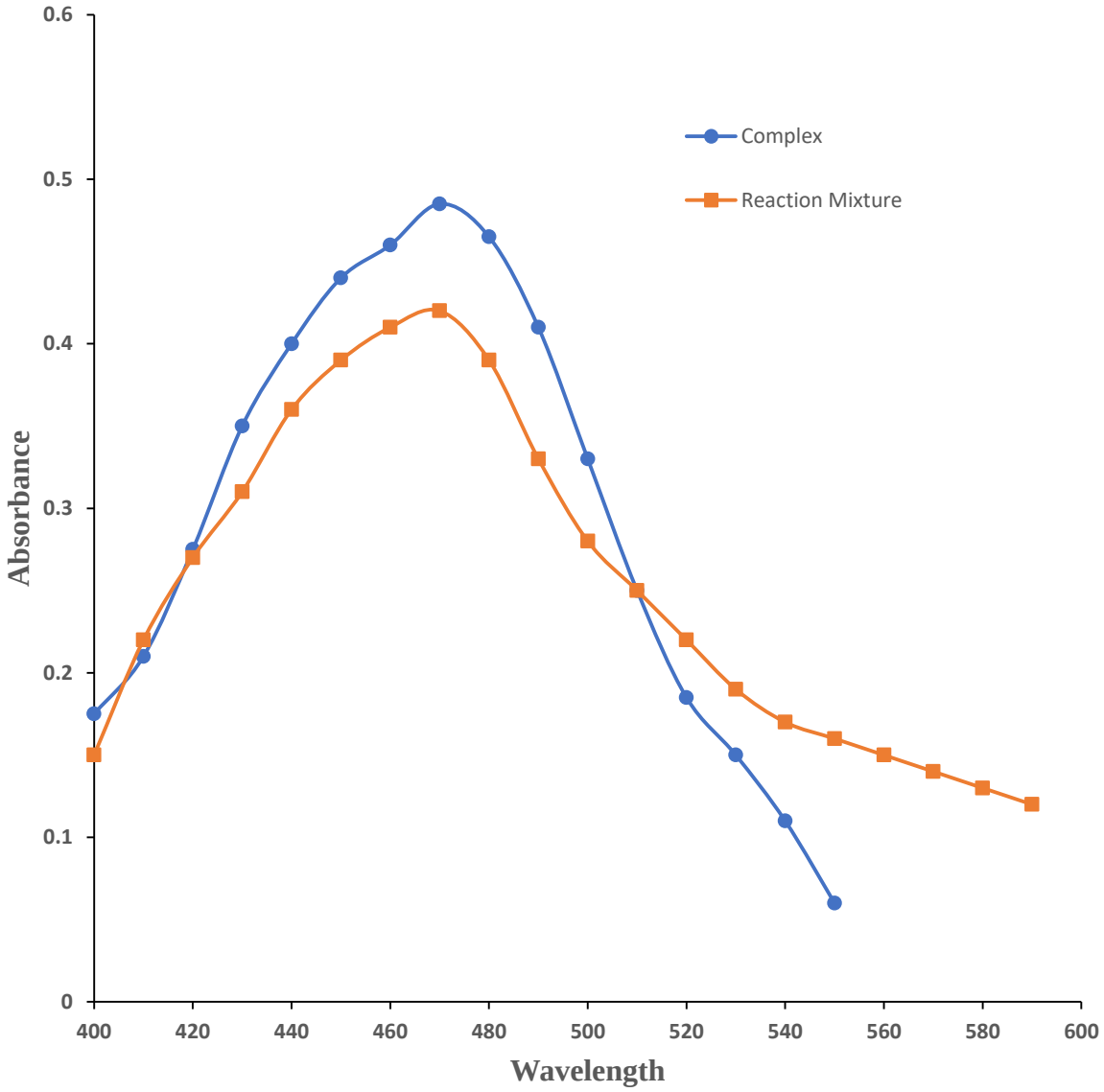


Figure 4.105: Plot for spectrophotometric test for the redox reaction of $[Co(salophen)]^{+}$ and $S(R)_2$ at $[Co(salophen)^{+}] = 2.0 \times 10^{-4}$ mol dm^{-3}, $[S(R)_2] = 16.0 \times 10^{-2}$ mol dm^{-3}, $[H^{+}] = 5.0 \times 10^{-2}$ mol dm^{-3}, $\mu = 0.2$ C^2 mol dm^{-3}, D = 77.42, T = 305 K and λ_{max} = 470 nm

CHAPTER FIVE

5.0 DISCUSSION

5.1 Reactions of $[Co(salophen)]^+$ with L-cysteine and Thioglycol

Stoichiometric results obtained in these studies showed a mole proportion (GSH: $Co(salophen)^+$) (where GSH represents LSH and RSH) of 1:1 based on the reactions of the complex with GSH (Figures 4.1 – 4.2), indicating oxidation of one mole of GSH by one mole of $[Co(salophen)]^+$. The stoichiometric equation 5.1 supports the reaction.

$$2[Co(salophen)]^+ + 2GSH \longrightarrow 2\,[Co(salophen)] + GSSG + 2H^+ \qquad (5.1)$$

Equation 5.1 is similar to equations 4.1 and 4.2.

A result of stoichiometry analogous to this research was reported previously in the reduction of heteropoly 11-tungstophosphovanadate(V) by L-cysteine (Komiyama *et al.,* 1999) and oxidation of 2-mercaptoethanol by heteropoly-11-tungsto-1-vanadophosphate (Shammugaprabha *et al.,* 2016). However, stoichiometry of 2:1 (complex: reductant) was established in the reduction of n-(2-hydroxyethyl)ethylenediaminetriacetatoiron(III) by thioglycol (Nkole *et al.,* 2018a), reaction of oxo-bridged ruthenium dimer with L-cysteine (Iyun *et al.,* 1996) and glutathione (Ayoko *et al.,* 1993). The 1:1 stoichiometry observed in the reactions of $Co(salophen)^+$ and the GSH (LSH and RSH) confirms that the thiols under study are one electron donor reductants.

The formation of disulphides as the only organic products in this investigation conforms to results of reactions involving thiols possessing the –SH functional group (Ayoko and Olatunji, 1983; Ayoko *et al.,* 1993; Shi *et al.,* 1996; Saha *et al.,* 2002; Idris, 2005; Sami *et al.,* 2009; Charkraborty *et al.,* 2012; Charkraborty *et al.,* 2013; Charkraborty and Banerjee, 2015; Shammugaprabha *et al.,* 2016; Nkole *et al.,* 2018a). The blue solution formed in the reaction

mixture after the addition of a few drops of potassium thiocyanate in excess acetone showed the presence of Co^{2+} (Osunlaja *et al.,* 2013).

The pseudo-first order plots of log $(A_t - A_\infty)$ against time were linear (Figures 4.11 and 4.12) suggesting a first order dependence in [Co(salophen)$^+$]. The order with respect to [GSH] determined from a plot of log k_1 against log [GSH] was unity, indicating that the reactions were first order in reductant concentrations (Figures 4.21 and 4.22). The kinetic studies of the oxidation of LSH and RSH by Co(salophen)$^+$, therefore, was second order overall. Equation 5.2 represents the rate law for the reaction.

$$\frac{-d[Co(salophen)^+]}{dt} = k_2[Co(salophen)^+][GSH] \qquad (5.2)$$

The values of k_2 for the systems at μ = 0.1 C^2 mol dm^{-3}; T = 300 K and λ_{max} = 470 nm are depicted in equations 4.11 and 4.12.

A first order dependence in thiols was previously reported in the reaction of trans-dichlorotetracyanoplatinate(IV) (Shi *et al.,* 1996), heteropoly 11-tungstophosphovanadate(V) (Sami *et al.,* 2009), 12-tungstocobaltate(III) and heteropoly-11-tungsto-1-vanadophosphate (Shammugaprabha *et al.,* 2015), while fractional order dependence in thiols was reported in the reaction of N-(2-hydroxyethyl)ethylenediaminetriacetatoiron(III) (Nkole *et al.,* 2018a) and Corey's reagent (Adari *et al.,* 2006).

Within the range of [H^+] of (1.0 - 18) × 10^{-3} mol dm^{-3} for LSH and (1.4 - 2.4) × 10^{-3} mol dm^{-3} for RSH, the reactions rate increased as [H^+] increases (Tables 4.1 and 4.2). Slopes of the plots of log k_1 against log [H^+] gave 0.89 and 0.84 for LSH and RSH systems respectively (Figures 4.31 and 4.32), indicating first order reaction in [H^+]. The plots of the acid dependent second order rate constant, $k_2(H^+)$ versus [H^+] for the LSH and RSH systems are given in Figures 4.35 and 4.36, and the relationship fits equations 4.21 and 4.22.

The nature of acid-dependence obtained, suggests that the reactions occur by two parallel reaction pathways involving a protonated ($HGSH^+$) which was acid dependent and unprotonated form (GSH) of the reductants which was acid-independent. These steps were formed in a rapid pre-equilibrium before electron transfer step (Idris *et al.*, 2015).

The general rate equation for the reactions is represented by equation 5.3 for LSH and RSH (GSH).

$$\frac{-d[Co(salophen)^+]}{dt} = (a + b\,[H^+])[Co(salophen)^+][GSH] \qquad (5.3)$$

The nature of acid dependence is shown in equation 5.4

$$GSH + H^+ \overset{K_{H^+}}{\rightleftharpoons} HGSH^+ \qquad (5.4)$$

Similar results of acid dependence was reported in the oxidation of thiols by 12-tungstocobaltate(III) (Ayoko and Olatunji, 1983) and $[Mn_4O_6]^{4+}$ (Chakraborty *et al.,* 2012).

From Tables 4.1 and 4.2, the reaction rate increased as the ionic strength of the medium of the reaction was increased. A straight-line graph was obtained from a graph of log k_2 against $\sqrt{\mu}$ with positive slope of approximately one (Figures 4.38 and 4.39), indicating a positive effect of salt based on Brønsted-Debye model (Onu *et al.,* 2009). This suggests that there is a like charged species reacting at the rate determining step. By varying the dielectric constant, D, of the reaction medium using DMSO-H_2O mixture, it was observed that the reaction rate decreased with a decrease in dielectric constant (Tables 4.12 and 4.13). This further confirmed the species at the rate determining step as observed from the effect of ionic strength of reaction medium on the rate (Iyun *et al.,* 1995; Mohammed *et al.,* 2014).

The reaction rate was found to be inhibited in the presence of added cations while anions catalysed it (Table 4.22 and 4.23). Inhibitive effect of added cations (Mg^{2+} and Ca^{2+}) could be

explained in terms of columbic forces of repulsion, as the activated complex in this reaction is made up of positively charged species, bringing in another positive charged species would lead to overall repulsion of the reacting species, thereby decreasing the rate of reaction. Also added anions (SO_4^{2-} and CH_3COO^-) led to electrostatic attraction which accelerated the reaction rate (Babatunde and Ajayi, 2013; Idris *et al.*, 2015).

The formation of a gel was observed on adding acrylamide, which is a radical scavenger, to partially reacted mixture in excess methanol suggesting the presence of free radicals in the reaction (Alioke *et al.*, 2012).

The results of temperature dependence on the rate constants and activation parameters for the reaction are depicted in Tables 4.42 and 4.43. The observed negative values of the entropy of activation ($\Delta S^{\ddagger}$ = -157.87 J mol^{-1} K^{-1} (LSH) and $\Delta S^{\ddagger}$ = -83.53 J mol^{-1} K^{-1} (RSH)), suggest that the activated complexes formed are more ordered which is a factor in favour of inner-sphere mechanism. But other earlier evidences do not support this position. Thus, the negative entropy of the activated complex may not be due to bridge formation at the activated complex by the reactant partner but due to solvent reorganisation around the activated complex. Also, the positive values of both $\Delta H^{\ddagger}$ and $\Delta G^{\ddagger}$ for LSH and RSH (+27.77 and +74.14 kJ mol^{-1}; +50.62 and +75.68 kJ mol^{-1} respectively) confirm the energy associated with bringing the reductant and oxidant together, and includes the work done to counter electrostatic repulsion (Housecroft and Sharpe, 2005; Fawzy *et al.*, 2017).

There was no shift in λ_{max} (470 nm) when the spectra of the reaction mixtures were compared with that of $[Co(salophen)]^+$ (Figures 4.96 and 4.97). Also, a Michaelis–Menten plot of $1/k_1$ versus 1/[GSH] had no intercept suggesting lack of evidence to support the presence of a stable and detectable intermediate in the reaction (Figures 4.85 and 4.86). This lack of evidence

for detectable intermediary complex indicates that the reactions are occurring through outer-sphere mechanistic pathway.

Based on the available evidences, an outer-sphere mechanism has been suggested for this reaction (equations 5.5 – 5.9). The choice of the mechanism was guided by:

i. The absence of intercept obtained from the plot of $1/k_1$ versus 1/[GSH] (Michaelis-Menten plot) suggesting an outer-sphere mechanism.
ii. The catalysis and inhibition of the reaction rate by added ions suggesting an outer-sphere mechanism.
iii. Lack of shift in λ_{max} (470 nm) when the spectra of the reaction mixtures were compared with that of $[Co(salophen)]^+$, indicative of no detectable intermediate complex.

$$GSH + H^+ \underset{}{\overset{K}{\rightleftharpoons}} HGSH^+ \tag{5.5}$$

$$[Co(salophen)]^+ + HGSH^+ \underset{k_{-3}}{\overset{k_3}{\rightleftharpoons}} [Co(salophen) - HGSH]^{2+} \tag{5.6}$$

$$[Co(salophen) - HGSH]^{2+} \xrightarrow[slow]{k_4} [Co(salophen)] + GS^{\bullet} + 2H^+ \tag{5.7}$$

$$[Co(salophen)]^+ + GSH \xrightarrow[slow]{k_5} [Co(salophen)] + GS^{\bullet} + 2H^+ \tag{5.8}$$

$$GS^{\bullet} + GS^{\bullet} \xrightarrow[fast]{k_6} GSSG \tag{5.9}$$

From the equations 5.7 and 5.8,

$$Rate = k_4[Co(salophen) - HGSH^{2+}] + k_5[Co(salophen)^+][GSH] \tag{5.10}$$

Applying steady state approximation on $[Co(salophen) - HGSH^{2+}]$;

$k_3[Co(salophen)^+] - k_{-3}[Co(salophen) - HGSH^{2+}] - k_4[Co(salophen) - HGSH^{2+}] = 0$ (5.11)

$$[Co(salophen) - HGSH^{2+}] = \frac{k_3[Co(salophen)^+][HGSH^+]}{k_{-3} + k_4} \quad (5.12)$$

From equation (5.5), $[HGSH^+] = K[GSH][H^+]$ (5.13)

Substituting equation 5.13 into equation 5.12 gives;

$$[Co(salophen) - HGSH^{2+}] = \frac{k_3K[Co(salophen)^+][GSH][H^+]}{k_{-3} + k_4} \quad (5.14)$$

Substituting equation 5.14 into equation 5.10 gives;

$$\text{Rate} = \frac{k_4k_3K[Co(salophen)^+][GSH][H^+]}{k_{-3} + k_4} + k_5[Co(salophen)^+][GSH] \quad (5.15)$$

$$\text{Rate} = \frac{k_4k_3K[H^+]}{k_{-3}k_4} + k_5([Co(salophen)^+][GSH]) \quad (5.16)$$

$$\text{Rate} = k([Co(salophen)^+][GSH]) \quad (5.17)$$

Equation 5.17 is similar to equations 4.11 and 4.12.

where $k = k_2 = \frac{k_4k_3K[H^+]}{k_{-3}k_4} + k_5$

5.2 Reaction of $[Co(salophen)]^+$ with Thioglycolic Acid

Spectrophotometric titration following the mole ratio method had sharp break at ratio 1:1. This implies that one mole of $[Co(salophen)]^+$ was reduced by one mole of TSH (equation 4.3). A stoichiometric ratio similar to this study has been reported in the oxidation of mercaptoacetic acid by 12-tungstocobaltate(III) (Ayoko and Olatunji, 1983), reduction of ethylenediaminetetraacetatoferrate(III) in bicarbonate buffer medium (Nkole *et al.*, 2018b),

reduction of heteropoly 11-tungstophosphovanadate(V) with TSH (Sami *et al.,* 2009) and reduction of octacyanomolybdate(V) with TSH (Saha *et al.,* 2002). This stoichiometric result differs from the one reported in the reduction of trans-dichlorotetracyanoplatinate(IV) with TSH in which 2:1 (thiol: complex) was observed (Shi *et al.,* 1996).

Formation of blue precipitate confirmed the reduction of Co(III) to Co(II) (Osunlaja *et al.,* 2013). Disulphide (TSST) was confirmed by the similarity in peaks when the mixture of reaction spectrum was compared with that of TSH and hydrogen peroxide (Appendix VI). The similarity in peaks as obtained in this investigation confirmed the presence of the disulphide (Idris, 2005).

Plot of log (A_t - A_∞) versus time was linear (Figure 4.13), suggesting a first order dependence in [Co(salophen)$^+$]. The slope of 1.00 (Figure 4.23) obtained from log k_1 versus log [TSH] plot also showed that the order with respect to [TSH] is one and second order overall. The rate law for the reaction has been presented in equation 4.13. A second order overall was previously reported in the TSH oxidation by ethylenediaminetetraacetatoferrate(III) complex (Nkole *et al.,* 2018b), while third order overall was reported in the oxidation of TSH by heteropoly 11-tungstophosphovanadate(V) (Sami *et al.,* 2009).

The increase in the ionic strength of the reaction medium (Table 4.3) led to the decrease in the rate of reaction. The slope (-1.27) of the graph obtained when log k_2 versus $\sqrt{\mu}$ was plotted (Figure 4.40), indicative of a negative contribution of Brønsted-Debye salt effect. The result shows the interaction of oppositely charged species with a magnitude of approximately unity at the rate determining step (Onu *et al.,* 2009; Idris *et al.,* 2015; Abdulsalam *et al.,* 2018).

The effect of hydrogen ion concentration on reaction rate showed a decrease in the reaction rate with increase in concentration of the acid, with the slope of 0.77 when the log k_1

was plotted against log $1/[H^+]$ (Figure 4.33). Also, plot of hydrogen ion second order rate constant ($k_2(H^+)$) against $[H^+]^{-1}$ had intercept which shows that both the deprotonated (thiolate, TS^-) and unprotonated thiol (TSH) were reactive species. Similar assumptions have been reported in the reaction of TSH with 11-tungstophosphovanadate(V) and ethylenediaminetetraacetatoferrate(III) complex (Sami *et al.,* 2009; Nkole *et al.,* 2018b). The acid dependence effect can therefore be represented by equation 5.18

$$TSH \underset{}{\overset{K_H^+}{\rightleftharpoons}} TS^- + H^+ \qquad (5.18)$$

The rate law for the reaction is represented in equation 4.26

Catalysis of the reaction by added ions (Mg^{2+}, Ca^{2+}, SO_4^{2-}) is consistent with the reaction occurring without bridging ligand participation at the activated complex. Also, the formation of white precipitate due to acrylamide polymerisation showed involvement of free radicals during the course of the reaction (Idris *et al.,* 2015; Onu, *et al.,* 2016).

The positive value of the entropy of activation ($\Delta S^{\ddagger}$ = +11.91 J mol^{-1} K^{-1}) suggests that the activated complex species are not formed due to bond formation and that the redox process is less ordered at the rate determining step (Osunkwo *et al.,* 2018).

Michaelis–Menten plot of $1/k_1$ versus 1/[TSH] (Figure 4.88) had no intercept suggesting the absence of a stable and detectable intermediate in the reaction. This lack of intermediate formation supports the reaction occurring outer-sphere mechanism. Also, the lack of shift in λ_{max} (470 nm) when the spectra of $[Co(salophen)]^+$ with that of $[Co(salophen)]^+$ /TSH were matched (Figure 4.98) further confirmed the disposition of the reaction to be occurring via outer-sphere path.

On the basis of the zero intercept from the Michaelis-Menten plot (Figure 4.88), lack of detectable intermediate complex, the positive value of the entropy of activation, and ion

catalysis, a plausible mechanistic pathway that supports the experimental results is proposed (equation 5.19 – 5.22):

$$TSH \underset{}{\overset{K}{\rightleftharpoons}} TS^- + H^+ \quad (5.19)$$

$$[Co(salophen)]^+ + TS^- \xrightarrow[slow]{k_3} [Co(salophen)] + TS^{\bullet} + H^+ \quad (5.20)$$

$$[Co(salophen)]^+ + TSH \xrightarrow[slow]{k_4} [Co(salophen)] + TS^{\bullet} + H^+ \quad (5.21)$$

$$TS^{\bullet} + TS^{\bullet} \xrightarrow[fast]{k_5} TSST \quad (5.22)$$

From equations 5.20 and 5.21,

$$Rate = k_3[Co(salophen)^+][TSH] + k_4[Co(salophen)^+][TS^-] \quad (5.23)$$

Considering equation 5.19: $[TS^-] = K[TSH]/[H^+]$ (5.24)

By substituting equation 5.24 into equation 5.23, equation 5.25 is obtained,

$$Rate = k_3[Co(salophen)^+][TSH] + Kk_4/[H^+][Co(salophen)^+][TSH] \quad (5.25)$$

$$Rate = \left(k_3 + \frac{Kk_4}{[H^+]} \right)[Co(salophen)^+][TSH] \quad (5.26)$$

Equation 5.26 is similar to equation 4.13 where $k_2 = \left(k_3 + \frac{Kk_4}{[H^+]} \right)$.

5.3 Reaction of $[Co(salophen)]^+$ with Thiosemicarbazide

The stoichiometry of the oxidation of thiosemicarbazide by $[Co(salophen)]^+$ complex was found to be 1:1 (Figure 4.4). A similar stoichiometry was reported in the oxidation of hydroxylamine, semicarbazide, and thiosemicarbazide by iron(III) in the presence of triazines (Ratman and Anapindi, 2012) but a stoichiometry of 1:2 ($[Mn^{IV}Mo_9O_{32}]^{6-}$: $2NH_2NHCSNH_2$) was established in the oxidation of thiosemicarbazide by Waugh-type 9-molybdomanganate(IV) in aqueous perchloric acid (More *et al.,* 2018).

When the plot of log (A_t-A_∞) against time was made (Figure 4.14), the graph was found to be linear in all the runs indicating first order behaviour with respect to the [oxidant] within the range investigated. The pseudo-first order rate constants, k_1 was found to increase (Table 4.4) as [thiosemicarbazide] increased from 2.0×10^{-2} to 10.0×10^{-2} mol dm^{-3} at constant [oxidant] of 2.0×10^{-4} mol dm^{-3}. The plot of log k_1 against log [TSCZ] was found to be linear with a slope of 1.00, indicating the order in the [reductant] to be one (Figure 4.24). The overall order of the reaction is therefore second order. Similar overall second order was reported by earlier researchers in the reaction of carbazides with iron(III) in the presence of triazines and with molybdenum(IV) complex (Ratman and Anapindi, 2012; More *et al.*, 2018).

The effect of $[H^+]$ on the reaction was studied by varying the hydrochloric acid concentration from $(1.0 - 8.0) \times 10^{-2}$ mol dm^{-3} at a constant ionic strength of 0.1 C^2 mol dm^{-3}. The rate of reaction was found to be unaffected by increase in $[H^+]$ (Table 4.4). This indicates that neither the oxidant nor the reductant was protonated or deprotonated prior to electron transfer step.

The effect of ionic strength and the polarity of the reaction medium were studied by keeping concentration of $[Co(salophen)]^+$, thiosemicarbazide and $[H^+]$ constant at 2.0×10^{-4} mol dm^{-3}, 8.0×10^{-2} mol dm^{-3} and 1.0×10^{-2} mol dm^{-3} respectively, and at 306 K. The rate of the reaction was unaffected while varying ionic strength and the dielectric constant of the reaction medium (Table 4.15). This suggests an interplay of ion-pair complex at the slow step.

Added ions were found to catalyse the rate of reaction and thus, implying outer-sphere mechanistic pathway can be invoked in this reaction. Addition of acrylamide to the partially reacted mixture followed by excess methanol did not lend credence to the formation of free radical in the reaction mixture.

The entropy of activation ($\Delta S^{\ddagger}$) and the enthalpy of activation ($\Delta H^{\ddagger}$) obtained from the intercept and slope of the plot of log k_2 against 1/T (Figure 4.79) are -184.84 J $mol^{-1}K^{-1}$ and +23.92 kJ mol^{-1} respectively (Table 4.45). The value of entropy of activation showed that there is an ordered activation complex at the slow step.

Spectroscopic evidence for the formation of intermediate of significant stability was ruled out due to lack of shift in the wavelength of maximum absorption (470 nm) of the complex (Figure 4.99). This assertion was further reinforced by lack of appreciable intercept obtained from the Michaelis-Menten's plot of $1/k_1$ versus 1/[TSCZ] (Figure 4.99).

The reaction is rationalised in favour of an outer-sphere mechanism (equation 5.27 – 5.31) based on the following findings:

i. The negligible negative intercept obtained from the plot of $1/k_1$ versus 1/[TSCZ].
ii. The catalysis and inhibition of the reaction rate by added ions.
iii. The absence of spectroscopically detectable intermediate complex of high formation constant.

$$[Co(salophen)]^+ + H_2NCSNHNH_2 \overset{K}{\rightleftharpoons} [Co(salophen)\ ,\ H_2NCSNHNH_2]^+ \quad (5.27)$$

$$[Co(salophen)\ ,\ H_2NCSNHNH_2]^+ \xrightarrow[slow]{k_3} [Co(salophen)] + H_2NCSNN_2 + H^+ \quad (5.28)$$

$$[Co(salophen)\ ,\ H_2NCSNHNH_2]^+ + H_2O \xrightarrow{k_4} [Co(salophen)] + H_2NCS(OH)NHNH_2 + H^+ \quad (5.29)$$

$$H_2NCS(O)NHNH_2 \xrightarrow{k_5} H_2NCSNNH_2 + H_2O \quad (5.30)$$

$$H_2NCSNNH_2 + H_2NCSNNH_2 \xrightarrow[fast]{k_6} (S(NH_2)C{=}NNH_2)_2 \quad (5.31)$$

From equation 5.28,

$$\text{Rate} = k_3[\text{Co(salophen)} \ , \ H_2NCSNHNH_2^+] \quad (5.32)$$

Also, from equation 5.27,

$$[\text{Co(salophen)} \ , \ H_2NCSNHNH_2^+] = K[\text{Co(salophen)}^+][H_2NCSNHNH_2] \quad (5.33)$$

Substituting equation 5.33 into 5.32 gives;

$$\text{Rate} = k_3K[\text{Co(salophen)}^+][H_2NCSNHNH_2] \quad (5.34)$$

Equation 5.34 is similar to equation 4.14 where $k_2 = k_3K = (1.26 \pm 0.03) \times 10^{-1}$ dm^3 mol^{-1} s^{-1}

5.4 Reaction of [Co(salophen)]$^+$ with 1,5-diphenylcarbazide

The study of the stoichiometry of the electron transfer reaction of [Co(salophen)]$^+$ complex and 1,5-diphenylcarbazide showed that for every one mole of [Co(salophen)]$^+$ reduced, one mole of diphenylcarbazide is oxidised (equation 4.5 and Figure 4.5). The stoichiometry of 1:1 obtained in this reactions is similar to the result obtained for the oxidation of diphenylcarbazide by tetrakis(2,2^1-bipyridine)-μ-oxodiiron(III) complex ([$Fe_2O_4^+$]) (Anweting, 2016).

The result of kinetic studies displays that the reaction is first order in [Co(salophen)]$^+$ due to the linearity of the plots of log ($A_\infty - A_t$) versus time (Figure 4.15). From the slope of the plots, k_1 was obtained. The logarithmic plot of k_1 versus [DPCI] was linear with a gradient approximately equal to unity (Figure 4.25), suggesting a first order with respect to [DPCI]. The second order rate constants, k_2, was found to be fairly constant (Table 4.5) within the range of the concentrations of diphenylcarbazide investigated. This further confirmed the reaction to be first order with respect to [DPCI], hence, second order overall.

The FTIR spectra of the reductant (diphenylcarbazide) and the product (diphenylcarbazone) gave bands at 764.1 cm^{-1} and 749.2 cm^{-1} which can be attributed the stretching mode of the phenyl group of the diphenylcarbazide and diphenylcarbazone (Appendices X and XI). Also, bands around 1654.9 cm^{-1} and 1666.1 cm^{-1} are assigned to the carbonyl ν(C=O) stretching mode of the reductant and the product. Furthermore, considering the spectra of the reductant and the product, it is obvious that the ν(C=O) stretching mode present in the reductant is still found in the product. The shift in the wavelength of maximum absorption (λ_{max}) from 280 nm which is the characteristic peak of the diphenylcarbazide to 305 nm (peak for diphenylcarbazone) confirmed the oxidation process.

Within the acid concentration range of 0.1 – 0.4 mol dm^{-3}, the rate of reaction was independent of change in $[H^+]$ (Tables 4.5). Similar acid independent result was previously reported in the reduction of $[Fe_2O^{4+}]$ by diphenylcarbazide (Anweting, 2016). Added ions catalysed the reaction rate (Tables 4.30 and 4.31). The effect of these ions suggests a possible electrostatic interaction between the reacting species and the ions. There was no gelatinous precipitate formation when acrylamide was added to the reaction mixture with excess methanol, suggesting that free radical was not important for the reaction.

The rate of reaction was observed to be independent of variation in ionic strength (Table 4.5). Non-dependence of reaction rate on ionic strength could likely be due to ion-pair effect at the rate determine step. Since ion-pair complex does not possess a formal charge, the rate of reaction will also not be affected by change in ionic strength (Iyun *et al.,* 1992; Abdulsalam *et al.,* 2016). The change in dielectric constant of the reaction medium has no effect on the reaction rate (Table 4.16). This suggests that the reaction occurred between charged ion (cation) and

neutral molecule. This assertion is consistent with a reaction involving ion-pairs with outer-sphere character (Iyun *et al.,* 1992; Onu *et al*., 2016; Nkole *et al.,* 2018a).

However, the entropy of activation ($\Delta S^{\ddagger}$) obtained from intercept of the plot of log k_2 against 1/T (Figure 4.80) is -188.32 J $mol^{-1}K^{-1}$ (Table 4.46). Indicative of a more ordered nature of the activated complex at the rate determining step.

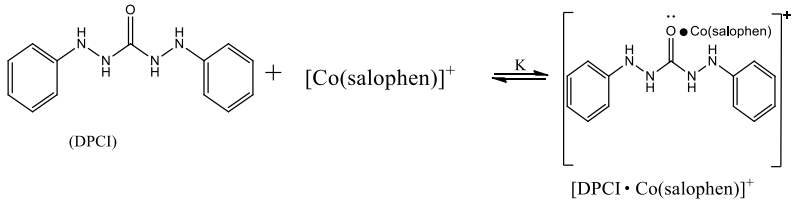
Spectroscopic test indicates absence of intermediate complex (Figure 4.100) of significant stability, and this result is further supported by the lack of intercept from the Michaelis-Menten's plot (Figure 4.90) (Osunlaja *et al.,* 2013; Abdulsalam *et al.,* 2015). Hence, the formation of stable intermediate was unimportant in the reaction as shown from both spectroscopic and kinetic evidence.

Taking into account the under-listed evidences, the reduction of $[Co(salophen)]^+$ by DPCI in aqueous HCl medium most probably occur by the outer-sphere mechanism (equation 5.35 – 5.40);

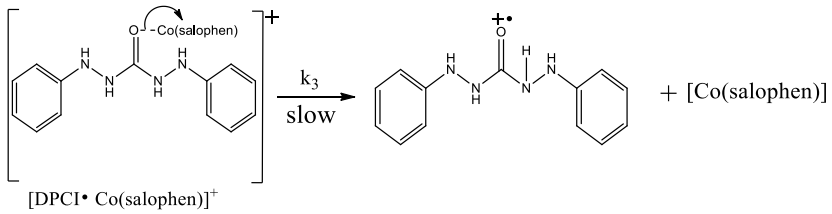
i. The negligible intercept of the Michaelis-Menten's plot.

ii. Catalysis of reaction rate by added ions.

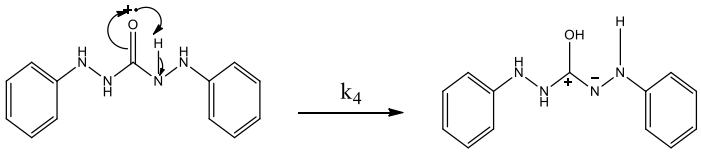
iii. The lack of intermediate complex of significant stability.



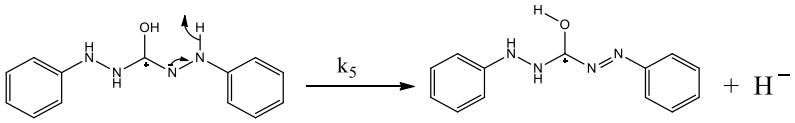
(5.35)



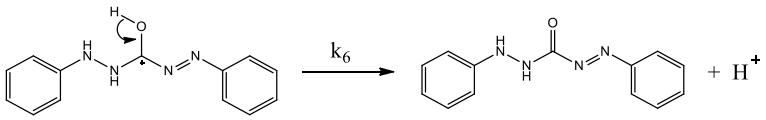
(5.36)



(5.37)

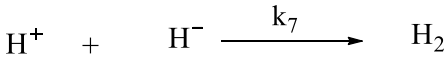


(5.38)



(5.39)

(DPCO)



(5.40)

$$\text{Rate} = k_3[\text{DPCI} \cdot \text{Co(salophen)}]^+ \quad (5.41)$$

From equation 5.35,

$$[\text{DPCI} \cdot \text{Co(salophen)}]^+ = K[\text{DPCI}][\text{Co(salophen)}]^+ \quad (5.42)$$

Substituting equation 5.42 into 5.41 gives,

$$\text{Rate} = k_3K[\text{DPCI}][\text{Co(salophen)}]^+ \quad (5.43)$$

Equation 5.43 is analogous to equation 4.15

5.5 Reaction of $[Co(salophen)]^+$ with Acetaldehyde and Formaldehyde

Stoichiometric studies of the oxidation of the aldehyde (RCHO) by $[Co(salophen)]^+$ indicated that for every mole of RCHO oxidised, two moles of $[Co(salophen)]^+$ were reduced. This stoichiometry is represented in equation 5.44.

$$2[Co(salophen)]^+ + RCHO + H_2O \longrightarrow 2[Co(salophen)] + RCOOH + 2H^+ \quad (5.44)$$

where R = H for HCHO and R = CH_3 for CH_3CHO.

The stoichiometry 2:5 (oxidant: reductant) has been reported for the oxidation of aldehyde by permanganate ion (Lohdip *et al.,* 1998). On the other hand, the result of 2:1 (oxidant: reductant) obtained in this study could be attributed to the participation of reactive free radical species in the reduction of the oxidant. A white precipitate that turns lime water milky due to the evolution of carbon dioxide with brisk effervescence confirmed the presence of carboxylic acid in the products (Vogel, 1996).

From kinetic studies, the reactions between $[Co(salophen)]^+$ and RCHO had first order dependence with respect to the oxidant concentrations, $[Co(salophen)^+]$. The evidence of this assertion is based on the linearity of the pseudo-first order plots of log $(A_t - A_\infty)$ versus time (Figures 4.16 and 4.17). Also, plots of log k_1 versus log [RCHO] were linear with the slopes of 1.02 and 1.01 for the CH_3CHO and HCHO systems respectively (Figures 4.26 and 4.27), suggesting first order dependence with respect to the [RCHO]. The majority of electron transfer reactions, particularly those involving organic substrates, have second order characteristics (Wilkins, 1991; Lohdip *et al.,* 1998). The overall rate law for the reaction, therefore, is written as equation 5.45;

$$-d[RCHO]/dt = k_2[Co(salophen)^+][RCHO] \quad (5.45)$$

The values of the second order rate constants k_2 at T = 302 K and 299 K for acetaldehyde and formaldehyde respectively are given in equations 4.16 and 4.17;

The rate of the reaction was found to be unaffected by hydrogen ion concentration within the range investigated (Tables 4.6 and 4.7). The observed independent of rate constant, k_2 on varying $[H^+]$ in the reactions of CH_3CHO/ $[Co(salophen)]^+$ and HCHO/ $[Co(salophen)]^+$,

suggests that neither the oxidant nor the reductant was protonated or deprotonated before or at the rate determining step of the reactions.

The rates of reaction of $[Co(salophen)]^+$ and RCHO were unaffected by variation of the ionic strength (Tables 4.6 and 4.7) and change in the dielectric constant of the reaction media (Tables 4.17 and 4.18). This pattern is obtained when reacting partners are uncharged, or one of the reactants is a neutral species or the reaction involved an ion – pair or adduct at the rate determining step (Mohammed, 2014). On addition of acrylamide to reaction mixture followed by excess methanol, polymerisation was induced. This is inferred from the formation of a gel, suggesting that free radicals participated in the reaction.

Added ions catalysed the reaction (Tables 4.32 - 4.35), but the negative values of activation entropies ($\Delta S^{\ddagger}$ = -3.33 and -56.44 J $K^{-1}mol^{-1}$) obtained for acetaldehyde and formaldehyde respectively suggest a more ordered activated complex. An ordered activated complex could suggest bridge formation by the reacting partners.

When the reaction mixture was scanned as reaction progressed, there was no shift in λ_{max} (470 nm), which is an indication that the reactions occurred without the formation of detectable intermediate complexes (Figures 4.101 and 4.102). This was further reinforced by lack of intercept obtained from the Michaelis-Menten's plot of $1/ k_1$ versus 1/[RCHO] (Figures 4.91 and 4.92).

On the basis of the above results, the possibility of the oxidation of RCHO by $[Co(salophen)]^+$ occurring via the outer-sphere pathway is very high. An outersphere mechanism (equations 5.46 – 5.49) involving hydration of aldehyde as reported by Lohdip *et al.* (1998) is proposed where the hydrated form of the reductants reacted with the oxidant at the rate determining step.

$$RCHO + H_2O \underset{}{\overset{K}{\rightleftharpoons}} RCH(OH)_2 \quad (5.46)$$

$$[Co(salophen)]^+ + RCH(OH)_2 \underset{k_{-3}}{\overset{k_3}{\rightleftharpoons}} [Co(salophen) - RCH(OH)_2]^+ \quad (5.47)$$

$$[Co(salophen) - RCH(OH)_2]^+ \xrightarrow[slow]{k_4} [Co(salophen)] + R\dot{C}(OH)_2 + H^+ \quad (5.48)$$

$$[Co(salophen)]^+ + R\dot{C}(OH)_2 \xrightarrow[fast]{k_4} [Co(salophen)] + RCOOH + H^+ \quad (5.49)$$

From equation 5.48;

$$Rate = k_4[Co(salophen) - RCH(OH)_2^+] \quad (5.50)$$

Applying steady state approximation,

$$k_3[Co(salophen)^+][RCH(OH)_2] - k_4[Co(salophen) - RCH(OH)_2^+] - k_3[Co(salophen) - RCH(OH)_2]^+ = 0$$

$$[Co(salophen) - RCH(OH)_2^+] = \frac{k_3[Co(salophen)^+][RCH(OH)_2]}{k_4 + k_3} \quad (5.51)$$

From equation 5.46,

$$[RCH(OH)_2] = K[RCHO] \quad (5.52)$$

Substituting equation (5.52) in equation (5.51) gives,

$$Rate = \frac{k_4k_3K[Co(salophen)^+][RCHO]}{k_4 + k_3} \quad (5.53)$$

where R = H for HCHO and R = CH_3 for CH_3CHO

Equation 5.53 is similar to equations 4.16 and 4.17

5.6 Reaction of [Co(salophen)]$^{+}$ with Iodide Ion

The spetrophotometric titrations showed oxidant - reductant ratio of 1:1 as represented by the stoichiometric equation 4.8. Stoichiometry 1:1 obtained in this reaction has been documented with reaction involving iodide ions (Nkole and Osunkwo, 2019).

The pseudo-first order plot is linear for the reaction (Figure 4.18). This implies that the order of the reaction is one with respect to [Co(salophen)$^{+}$] (Figure 4.28). The rate of the reaction increased with increase in [I^{-}] with a slope of 0.97, suggesting that the reaction is first order respect to [I^{-}] as shown in Table 4.8. A similar first order dependence of reaction rate was observed for iodide ion (Hubbard *et al.,* 2001; Nkole and Osunkwo, 2019). The rate law for the reaction is given as equation 4.18.

Within the range of [H^{+}] at constant ionic strength 0.6 C^2 mol dm^{-3}(NaCl) investigated, the rate of the reaction was unaffected by increase in [H^{+}] (Table 4.8). The change in ionic strengthof the reaction medium from 0.1 to 0.7 C^2 mol dm^{-3} had no effect on the observed rate constant, k_1 (Table 4.8). The variation of the dielectric constant of the reaction medium showed no effect on the reaction rate (Table 4.19). This is in conformity with the result obtained from the effect of ionic strength of the reaction medium. Also, the effect of added ions (Mg^{2+}, Ca^{2+}, SO_4^{2-} and CH_3COO^{-}) were insignificant on the rate of reaction (Tables 4.36 and 4.37), while free radicals participation in the course of the reaction was positive when the partially reacted solution of the reactants are mixed with a solution of acrylamide followed by excess methanol.

The rate of the reaction in this investigation was markedly catalysed when the temperature of the system was increased. The values of the activation parameters obtained from the study are: $\Delta S^{\ddagger}$ = -184.02 J K^{-1} mol^{-1} and $\Delta H^{\ddagger}$ = +21.16 kJ mol^{-1}. The negative value of $\Delta S^{\ddagger}$

implies the formation of activated complex where there is orderliness of solvated particles (James, 2002; Osunkwo *et al.*, 2018).

The plot of $1/k_1$ versus $1/[I^-]$ gave an insignificant intercept, which suggests absence of intermediate complex formation (Figure 4.93). When the reaction mixture was scanned as the reaction progressed, there was no appreciable shift in λ_{max} which is an indication that the reaction proceeded without the formation of an intermediate complex (Figure 4.103).

An outer-sphere mechanism is proposed (equations 5.54 – 5.57) for this reaction on the ground that among others, there were no detectable intermediate complex formation or if they were formed, they had small stability constant.

$$[Co(salophen)]^+ + I^- \underset{k_{-3}}{\overset{k_3}{\rightleftharpoons}} [Co(salophen)^+ - I^-] \quad (5.54)$$

$$[Co(salophen)^+ - I^-] \xrightarrow[\text{slow}]{k_4} [Co(salophen)] + I^{\bullet} \quad (5.55)$$

$$I^{\bullet} + I^- \xrightarrow{k_5} I_2^{\bullet -} \quad (5.56)$$

$$[Co(salophen)]^+ + I_2^{\bullet -} \xrightarrow[\text{fast}]{k_6} [Co(salophen)] + I_2 \quad (5.57)$$

Considering equation 5.55,

$$\text{Rate} = k_4[Co(salophen)^+ - I^-] \quad (5.58)$$

Applying steady state approximation

$$-\frac{d[Co(salophen)^+ - I^-]}{dt} = k_3[Co(salophen)^+][I^-] - k_{-3}[Co(salophen)^+ - I^-] - k_4[Co(salophen)^+ - I^-] = 0 \quad (5.59)$$

$$[Co(salophen)^+ - I^-] = \frac{k_3([Co(salophen)^+][I^-])}{k_{-3} + k_4} \quad (5.60)$$

Substituting equation 5.60 into 5.58 gives,

$$\text{Rate} = \frac{k_3k_4([Co(salophen)^+][I^-])}{k_{-3} + k_4} \quad (5.61)$$

Equation 5.61 conforms to the rate law at equation 4.18.

5.7 Reaction of $[Co(salophen)]^+$ with Ascorbic Acid

The mole ratio of the reaction is found to be 2:3 (Figure 4.9) and is represented in equation 4.9. A stoichiometry of 1:1 was reported in the reduction of [Fe(saloph)$_2$-μ-dicarpy] with ascorbic acid (Ukoha *et al.,* 2018), and oxidation of L-ascorbicacid by pentaamminecobalt(III) ion (Dixon *et al.,* 1995). Also, a stoichiometry of 2:1 was reported in the oxidation of ascorbic acid by hexacyanoferrate(III) (Jattinagoudar *et al.,* 2013) and reduction of ethylenediamine tetraacetatocobaltate(III) ion by L-ascorbic acid (Abiti *et al.,* 2018).

At the completion of the reaction, a blue solution was formed when potassium thiocyanate was added to the reaction mixture. This shows that the Co(III) in the complex has been reduced to Co(II) by the H_2A. Also, after mixing the reaction mixture with pyrrole in excess trichloroacetic acid, blue–green color was observed, confirming the oxidation of ascorbic acid to dehydroascorbic acid (Abiti *et al.,* 2018).

In the analysis of a plot of log ($A_t - A_\infty$) against time, a straight line was observed, implying the reaction to be first order with respect to [Co(salophen)$^+$] (Figure 4.19), while the order of the reaction with respect to [H_2A] was determined when log k_1 was plotted against log [H_2A]. The slope of the plot was calculated to be 0.99 (Figure 4.29). For the different values of [H_2A], the second order rate constants (k_2) were fairly the same (Table 4.9). With respect to the [reactants], the reaction showed second order overall (equation 4.19).

Similar second order overall have been previously reported in the reactions of H_2A by *N, N¹*- salicylideneiminatoiron(III) (Alioke *et al.*, 2012), hexacyanoferrate(III) (Jattinagoudar *et al.*, 2013), and *N, N¹*- ethylene*bis*(salicylideneiminato)Mn(III) (Salem and Gemeay, 1996).

The rate of the reaction was found to decrease with an increase in [H^+] (Table 4.9). Plot of k_2 against 1/[H^+] was liner and gave a positive intercept (Figure 4.37). This observation suggests that two parallel reaction pathways are involved in the reaction; an acid independent and inverse acid dependent pathway. The inverse acid pathway shows that there is a pre-equilibrium step before the rate determining step in which a proton is lost that is, both the protonated and the deprotonated form of the reductant (H_2A and HA^-) are reactive at the rate determining step (Gupta and Gupta, 1984). Acid dependence effect of this kind is represented in equation 4.24. The final rate law for the reaction is presented in equation 4.26. Similar acid independent pathway has been reported in the reaction of H_2A by [Fe(Saloph)$_2$-μ-dicarpy] complex (Ukoha *et al.*, 2018).

The result in Table 4.9 showed that increase in the ionic strength of the reaction medium decreased the rate of reaction. A plot of log k_2 versus $\sqrt{\mu}$ gave a slope of -1.06 (Figure 4.40), suggesting that the reaction proceeded via an interaction between oppositely charged species

([Co(salophen)]$^{+}$ and HA^{-}) at the rate determining step (Onu *et al.*, 2015; Abdulsalam *et al*., 2016).

Also, added ion (Ca^{2+}, Mg^{2+}, SO_4^{2-} and CH_3COO^{-}) in the reaction mixture was found to increase the rate of reaction (Tables 4.38 and 4.39). This ion catalysis is consistent with the reaction occurring in the presence of charged species at the rate determining step, evidence in support of the outer-sphere pathway of electron transfer (Abdulsalam *et al.,* 2015). A gelatinous precipitate was observed when radical scavenger (acrylamide) was added to a partially reacting mixture then excess CH_3OH, confirming the presence of free radicals in the reaction.

The result of temperature dependence on rate constant is shown in Table 4.50. The values of activation parameters ($\Delta H^{\ddagger}$ = +47.70 kJ mol^{-1}, $\Delta S^{\ddagger}$ = -82.87 J mol^{-1} K^{-1}) obtained from this investigation showed the strong interactions of the reactant species at the rate determine step and a reaction proceeding via an endothermic process (Dixon *et al.,* 1995).

When the spectrum of [Co(salophen)$^{+}$] was compared with that of the reaction mixture, no shift in the λ_{max} (470 nm) was observed (Figure 4.104). This suggests that the participation of an intermediate complex as the reaction progresses is unlikely, evidence in support of an outer-sphere mechanism (Abdulsalam, 2015; Idris *et al.,* 2015). The linear slope without an intercept observed in the Michaelis-Menten's plot further confirmed the absence of an intermediate complex with significant stability during the reaction (Figure 4.94).

Reaction scheme in equations 5.62 – 5.65 which is in favour of outer-sphere mechanism is hereby proposed based on the observed ion catalysis, zero intercept of Michaelis-Menten plot, and absence of stable and detectable intermediate complex.

$$H_2A \underset{}{\overset{K}{\rightleftharpoons}} H^{+} + HA^{-} \qquad (5.62)$$

$$[Co(salophen)]^{+} + HA^{-} \xrightarrow[slow]{k_3} [Co(salophen)] + HA^{\bullet} \quad (5.63)$$

$$[Co(salophen)]^{+} + H_2A \xrightarrow[slow]{k_4} [Co(salophen)] + HA^{\bullet} + H^{+} \quad (5.64)$$

$$H_2A + 2HA^{\bullet} + O_2 \xrightarrow[fast]{k_5} 3A + 2H_2O \quad (5.65)$$

Considering equations 5.63 and 5.64,

$$\text{Rate} = k_3[Co(salophen)^{+}][HA^{-}] + k_4[Co(salophen)^{+}][H_2A] \quad (5.66)$$

From equation (5.62),

$$[HA^{-}] = K\frac{[H_2A]}{[H^{+}]} \quad (5.67)$$

Substituting equation 5.67 into 5.66 gives,

$$\text{Rate} = \frac{Kk_3[Co(salophen)^{+}][H_2A]}{[H^{+}]} + k_4[Co(salophen)^{+}][H_2A] \quad (5.68)$$

$$\text{Also, Rate} = k^1([Co(salophen)^{+}][H_2A]) \quad (5.69)$$

where $k^1 = k_3 + Kk_4[H^{+}]^{-1}$

Equation 5.69 is similar to the experimental rate law equation 4.19.

5.8 Reaction of $[Co(salophen)]^{+}$ with Thiodiglycol

The result of stoichiometric study showed that a plot of absorbance versus mole ratio ($S(R)_2$: $[Co(salophen)]^{+}$) had a point of inflexion at ratio 1:2 (Figure 4.10). This implies that two moles of $[Co(salophen)]^{+}$ was reduced by one mole of $S(R)_2$ (equation 4.10). A similar

stoichiometry has been reported for the reaction of iron(III)-salen chloride with thiodiglycolic acid (Subramaniam *et al.,* 2014).

The product obtained in the reaction (Co^{2+}) was confirmed by the formation of a blue solution when two drops of KSCN in excess acetone was added to the reaction product (Osunlaja *et al.,* 2013). Also, the formation of an orange-coloured spot on the dried filter paper sprayed with dragendorff reagent confirmed the presence of sulphoxide (Suchomelova *et al.,* 1965).

The pseudo-first order plot of log ($A_t - A_\infty$) versus time was linear (Figure 4.20), indicating first order with respect to $[Co(salophen)]^+$. The plot of log k_{obs} versus log $S(R)_2$ (Figure 4.30) was also linear with slope approximately equal to unity (0.99), suggesting that the reaction was first order with respect to the reductant concentration, and a second order overall. A similar order has been reported with reactions of Co(III) and other reductants (Osunkwo *et al.,* 2018; Osunlaja *et al.,* 2013; Abiti *et al.,* 2018). The overall rate equation for the reduction of $[Co(salophen)]^+$ with $S(R)_2$ at constant temperature is therefore represented by equation 4.20.

The $[H^+]$ dependence on the reaction rate was investigated by varying $[H^+]$ from $(1.0 - 8.0) \times 10^{-2}$ mol dm^{-3} (Table 4.10). The result showed that varying the $[H^+]$ had no effect on the rate of reaction within the range investigated. A similar result was reported by earlier researchers on the reduction of Co(III) by other reductants (Mohammed *et al.,* 2014; Osunlaja *et al.,* 2013).

Increase in ionic strength of reaction medium in the range (0.1 – 0.7) C^2 mol dm^{-3} does not affect the reaction rate (Table 4.10). This is consistent with the interaction of cation - neutral or anion – neutral or neutral - neutral Brønsted-Debye salt-effect (Atkins and de Paula, 2018). The result is represented in Table 4.10. This salt effect is supported by the observed lack of dependence of the reaction rate on dielectric constant of the reaction mixture (Table 4.21). Test for polymerisation of acrylamide solution with the partially reaction mixture was positive in the

presence of excess methanol, an indication that participation of free radicals is important in this reaction (Onu *et al.,* 2015).

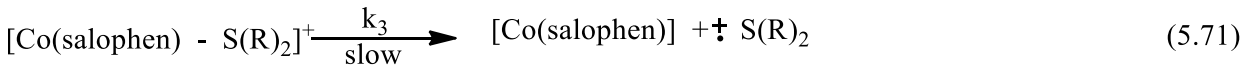
Added ions (Ca^{2+}, Mg^{2+}, SO_4^{2-} and CH_3COO^-) catalysed the rate of reaction. Ion catalysis has been implicated in the reactions that are thought to occur by the outer-sphere pathway. Although, the catalysis of cations in this case is not expected as the rate determining step is characterised with a positive charged ion-pair complex.

The observed negative value of the entropy of activation ($\Delta S^{\ddagger}$ = -165.60 J mol^{-1} K^{-1}), portrays the formation activated complex in the pre-equilibrium stage which is characterised with solvent reorganisation. Also, the positive values of both $\Delta H^{\ddagger}$ and $\Delta G^{\ddagger}$ (+32.81 and +83.65 kJ mol^{-1} respectively) confirm the energy associated with bringing the reductant and oxidant together, and includes the work done to counter electrostatic repulsion (Weissbekger, 1974; Housecroft and Sharpe, 2005; Fawzy *et al.*, 2017).

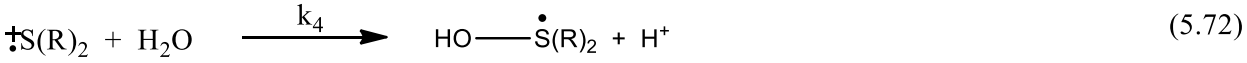
The Michaelis–Menten's plot of $1/k_1$ versus $1/[S(R)_2]$ was linear with no intercept (Figure 4.95), indicative of absence of intermediate complex, which further confirm the electron transfer to proceed via the outer-sphere mechanism. The spectroscopic investigation of intermediate complex showed no shift in λ_{max} in the spectrum of the partially reduced reaction mixture, also supporting the absence of stable intermediate complex formation during the course of the reaction (Figure 4.105).

On the basis of the above results, the possibility of the reduction of $[Co(salophen)]^+$ by $S(R)_2$ occurring via the outer-sphere pathway is very much likely. Hence, the following mechanistic steps (equations 5.70 – 5.74) are proposed:

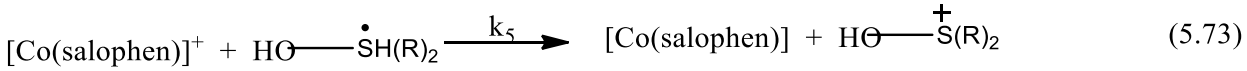
$$[Co(salophen)]^+ + S(R)_2 \underset{}{\overset{K}{\rightleftharpoons}} [Co(salophen) - S(R)_2]^+ \qquad (5.70)$$



(5.71)



(5.72)



(5.73)



(5.74)

$$\text{Rate} = k_3[\text{Co(salophen)} - \text{S(R)}_2^+] \quad (5.75)$$

From equation 5.70,

$$[\text{Co(salophen)} - \text{S(R)}_2^+] = K[\text{Co(salophen)}^+][\text{S(R)}_2] \quad (5.76)$$

Substituting equation 5.76 into 5.75 gives,

$$\text{Rate} = k_3K[\text{Co(salophen)}^+][\text{S(R)}_2] \quad (5.77)$$

Equation 5.77 conform with the experimental rate law in equation 4.20.

5.9 Comparative Study

5.9.1 Comparison of $[Co(salophen)]^+$ with thiols (LSH, RSH, TSH and $S(R)_2$) systems

The rate constant of the reduction of $[Co(salophen)]^+$ by LSH, RSH, TSH and $S(R)_2$ varied in the order $k_2 = (1.43 \pm 0.01)$ dm^3 mol^{-1} s^{-1} ($[Co(salophen)]^+$/ TSH) > $k_2 = (6.91 \pm 0.18) \times 10^{-1}$ dm^3 mol^{-1} s^{-1} ($[Co(salophen)]^+$/ LSH) > $k_2 = (3.55 \pm 0.02) \times 10^{-1}$ dm^3 mol^{-1} s^{-1} ($[Co(salophen)]^+$/ RSH), and > $k_2 = (3.54 \pm 0.03) \times 10^{-2}$ dm^3 mol^{-1} s^{-1} ($[Co(salophen)]^+$/ $S(R)_2$). The observed trend can be attributed to the pH of the reaction media as the redox potentials of TSH, LSH, RSH, $S(R)_2$ (E^0 = -0.74 V, -0.34 V, -0.22 V and +0.19 V at 25 ℃ respectively) vary with $[H^+]$ (Mojtaba, 2016). This trend can also be credited to the interplay of the functional

group of the reductants with carboxylic acid (TSH and LSH) followed by thiol with replaceable hydrogen ion (RSH) and lastly, the thiol with no replaceable hydrogen ion ($S(R)_2$).

5.9.2 Comparison of $[Co(salophen)]^+$ with carbazides systems

The reduction rate constant of $[Co(salophen)]^+$ by DPCI and TSCZ follows a decreasing order with the rate constants at $k_2 = (3.90 \pm 0.07)) \times 10^{-1}$ dm^2 mol^{-1} s^{-1} ($[Co(salophen)]^+$ / DPCI) $>$ $k_2 = (1.26 \pm 0.03) \times 10^{-1}$ dm^3 mol^{-1} s^{-1} ($[Co(salophen)]^+$ / TSCZ). The rationale behind DPCI having higher rate constant could be attributed to the high redox potential of it in aqueous solution ((E^0 = -0.6 V and +0.393 V for DPCI and TSCZ respectively). Their redox potentials are highly dependent on $[H^+]$ of the reaction mixture. Thus, the product of $[Co(salophen)]^+$ / DPCI is 1,5-diphenylcarbazone (DPCO) acid while $[Co(salophen)]^+$ / TSCZ is disulphide.

5.9.3 Comparison of $[Co(salophen)]^+$ with aldehydes systems

The electron transfer rate constant of $[Co(salophen)]^+$ with CH_3CHO and HCHO differed in the order $k_2 = (5.41 \pm 0.11) \times 10^{-1}$ dm^3 mol^{-1} s^{-1} ($[Co(salophen)]^+$/ HCHO) $>$ $k_2 = (4.14 \pm 0.11) \times 10^{-2}$ dm^3 mol^{-1} s^{-1} ($[Co(salophen)]^+$ / CH_3CHO), and it could be attributed to the presence of alkyl group of acetaldehydes and their redox potentials (E^0 = +0.71 V (HCHO) and -0.6 V(CH_3CHO)).

5.9.4 Comparison of $[Co(salophen)]^+$ with Thiols, Carbazides and Aldehydes systems

The general reduction rate constants of $[Co(salophen)]^+$ with thiols, carbazides and aldehydes follow a decline in the order $k_2 = 1.43 \pm 0.01$ dm^3 $mol^{-1}s^{-1}$ > $k_2 = (5.41 \pm 0.11) \times 10^{-1}$ dm^3 mol^{-1} s^{-1} > $3.90 \pm 0.07 \times 10^{-1}$ dm^3 $mol^{-1}s^{-1}$ respectively. This trend could be attributed to the nucleophilicity of the thiols, carbazides and aldehydes.

CHAPTER SIX

6.0 SUMMARY, CONCLUSION AND RECOMMENDATION

6.1 Summary

The redox kinetics of the oxidation of L-cysteine (LSH), thioglycol (RSH), thioglycolic acid (TSH), diphenylcarbazide (DPCI), thiosemicarbazide (TSCZ), acetaldehyde (CH_3CHO), formaldehyde (HCHO), iodide ion (I^-), ascorbic acid (H_2A) and thiodiglycol ($S(R)_2$) by *N, N′*-phenylenebis(salicyalideneiminato)cobalt(III) ion ($[Co(salophen)]^+$) were studied and mechanisms were proposed for these reactions. For the reactions with CH_3CHO, HCHO and $(S(R)_2$, the stoichiometries were determined to be 1:2 (reductant/ oxidant), for the reactions with LSH, RSH, TSH, DPCI, TSCZ, and I^-, a mole ratio of 1:1 was found while for reaction with H_2A 3:2 was determined. All the reactions showed a first order dependence with respect to both [oxidant] and [reductant]. The reactions with the TSH and H_2A showed an inverse acid dependence, while that with LSH and RSH showed direct acid dependence and the rest was not affected by acid. In the reaction with TSH, it was observed in preliminary tests that addition of acid seems to halt the reaction from taking place.

The deprotonation of H^+ ions from the TSH to TS^- and the H^+ ion from the acid contributed to the existence of excess H^+ ion which tends to halt the reaction. Based on the aforementioned reason, the reaction with TSH was allowed to proceed in the absence of acid. The rates of all of the reactions, apart from the one with LSH, RSH, TSH, and H_2A, were unaffected by change in μ and D. Added ions catalysis and inhibition was observed for all the reactions except for I^- ion reaction where catalysis nor inhibition was observed. Polymerisation was induced on addition of acrylamide in all the reactions except for the DPCI and TSCZ reactions, suggesting the participation of free radicals in the reactions. The entropy and enthalpy of activation parameters of the reactions were all negative and positive respectively, except for TSH, indicating orderliness of the activated complex at the transition state.

Spectroscopic investigations and Michaelis-Menten plots for all the reactions showed that there is no evidence for the formation of stable and detectable intermediate complex. Based on the aforementioned results, outer-sphere mechanistic pathways were proposed for all the systems.

6.2 Conclusion

i. The kinetic investigation of the redox reactions of $[Co(Salophen)]^{+}$ with l-cysteine, thioglycol, thioglycolic acid, thiodiglycol, thiosemicarbazide, diphenylcarbazide, acetaldehyde, formaldehyde, iodide ion, ascorbic acid and thiodiglycol in DMSO-H_2O medium was successfully carried out.

ii. The study has established the stoichiometries of the systems 1:1 for LSH, RSH, TSH, DPCI, TSCZ and I^-, 1:2 for CH_3CHO, HCHO and $S(R)_2$ and 3:2 for H_2A.

iii. First order with respect to the concentration of both the redox species was established for all the system, and second order overall in all the reactions.

iv. The participation of free radical species was essential for the reactions studied. Also, Ion-pair formation in the study was important for a reaction proceeding via an outer-sphere mechanistic pathway.

v. The participation of intermediate complexes was insignificant for all the reactions. Hence, an outer-sphere mechanistic route is implicated for the systems studied.

6.3 Recommendation

i. It is recommended that more work on the kinetics and mechanism on this complex (*N, N′*-phenylenebis(salicyalideneiminato)cobalt(III) ion) with more reductants should be carried out, so as to improve on its utilisation.

ii. Computational or theoretical studies should also be carried out in the investigations of the kinetics of the complex in order to compare the results generated with the empirical data obtained from the spectrophotometric method.

iii. Similar studies should be carried out in the presence of surfactant media for broader knowledge of the kinetics and mechanisms of the complex using micellar catalysis.

iv. Similar studies should be carried out on the oxo-bridged of the complex for broader knowledge on the kinetics and mechanisms of the complex and for comparison with the redox behavior of this present complex.

REFERENCES

Abdulsalam, S. (2015). Kinetics and Mechanisms of the Redox Reactions of Crystal Violet with Some Oxyanions in Aqueous Acidic Medium, Published M.Sc Thesis, Ahmadu Bello University, Zaria.

Abdulsalam, S. and Idris, S. O. (2015). Kinetic Approach to the Mechanism of Oxidation of Hexamethylpararosaniline Chloride by Bromate Ion in Acidic Medium. *Federal University Wukari Trends in Science and Technology Journal*. 1(2): 546 - 553.

Abdulsalam S. and Idris S. O. (2016). Kinetics and Mechanism of Redox Reaction of Crystal Violet and Metabisulphite Ion in Aqueous Acidic Medium. *Gashua Journal of Science and Humanities*. 2(2): 19 - 26.

Abdulsalam, S. and Idris, S. O. (2018). Kinetics Approach to the Mechanism of Redox Reaction of Hexamethylpararosaniline Chloride and Hypochlorite Ion in Aqueous Perchloric Acid Medium. *Nigerian Journal of Scientific Research*. 17(3): 365 - 371.

Abiti, B.Y., Onu, A. D., Idris, S. O., Ahmed, Y. and Ilyasu, S. S. (2018). Kinetics and Mechanism of the Catalysed Reduction of Ethylenediaminetetraacetatocobaltate(III) Ion by L-ascorbic Acid in Aqueous Acidic Medium. *Federal University Wukari Trends Science and Technology Journal*, 3(2B): 832 – 837.

Abu-Surrah, A. S., Abdel-Halim, H. M. and Feda'a, M. (2008). Synthesis of Cobalt(III), Iron(III), and Chromium(III) Complexes with Salicylaldiminato Ligands: Evaluation of the Complexes as Catalysts for Oxidation of L-cysteine. *Zeitschrift Für Naturforschung B*, 63(7): 848 – 852.

Adari, K. K., Nowduri, A. and Vani, P. (2006). Kinetics and Mechanism of Oxidation of L-cysteine by Corey's Reagent. *Transition Metal Chemistry*, 31(6): 745 – 748.

Adetoro, A., Iyun, J. F., and Idris, S. O. (2011). Kinetic Approach to the Mechanism of Redox Reaction of Pyrocatechol Violet and Nitrite Ion in Aqueous Hydrochloric Acid. *Research Journal of applied Sciences, Engineering and Technology. 3*(10), 1159 – 1163.

Aitken, C. E., Marshall, R. A. and Puglisi, J. D. (2008). An Oxygen Scavenging System for Improvement of Dye Stability in Single-molecule Fluorescence Experiments. *Biophysical Journal*, 94(5): 1826 – 1835.

Alioke, C. U., Ukoha, P. O., Ukwueze, N. N., Ujam, O. T. and Asegbeloyin, J. N. (2012). Kinetics and Mechanism of the Reduction of N, N'-salicylideneiminationiron(III) Complex Ion by L-ascorbicAcid in Aqueous Acidic Medium. *Chemistry and Material Research*, 2(7): 48 – 57.

Aly, M. M. (1998). Recent Developments in the Metallosupramolecular and Molecular Structures of the Cobalt, Iron and Vanadium Complexes of the Dianionic Tetradentate Schiff

Base Ligands of Salicylideneimine and Acetylacetoneimine. *Journal of Coordination Chemistry*, *43*(2–3): 89 – 113.

Amirnasr, M., Schenk, K. J., Gorji, A., and Vafazadeh, R. (2001). Synthesis and Spectroscopic Characterisation of $[Co^{III}(salophen)(amine)_2]ClO_4$ (Amine = Morpholine, Pyrrolidine, and Piperidine) Complexes. The Crystal Structures of $[Co^{III}(salophen)(morpholine)_2]ClO_4$ and $[Co^{III}(salophen)(pyrrolidine)_2]ClO_4$. *Polyhedron*, 20(7–8): 695 – 702.

Anweting, B. I. (2016). Kinetics and Mechanisms of Redox Reactions of Tetrakis(2,2'-bipyridine)- μ-oxodiiron(III) Complex and Some Reductants in Aqueous Hydrochloric Acid (Unpublished PhD dissertation). Ahmadu Bello University, Zaria, Nigeria.

Asemave, K., Yiase, S. G., Adejo, S. O. and Anhwange, B.A. (2012). Substitution Reaction of trans dichloro- bis-(ethylenediamine)cobalt(III) Chloride and Phenylalanine - A Kinetics and Mechanism Study. *International Journal of Modern Chemistry*, 1(2): 93 – 101.

Ashoor, S. E., Ashoor, F. M. and Salman, N. Y. (2013). Kinetics and Mechanism of Oxidation of (E)-1,5-Diphenylcarbazone Cobalt(II) by N-chloro-P-toluenesulphonamide. *Rasayan Journal of Chemistry*, 6(1): 1 – 6.

Asperger, S. (2003). *Chemical Kinetics and Inorganic Reaction Mechanism 2nd Edition*. Springer Science + Business Media LLC, New York. pp, 3.

Atkins, P. W. and de Paula, J. (2018). *Physical Chemistry (11th Edition)*. Oxford University Press, Oxford, P.798.

Ayoko, G. A. and Olatunji, M. A. (1983). Oxidation of L-cysteine, Mercaptoacetic Acid and β-Mercaptoethylamine by 12-tungstocobaltate(III). *Polyhedron*, 2(7): 577 – 582.

Ayoko, G. A., Iyun, J. F. and Ekubo, A. T. (1993). Oxidation of Glutathione by Diaquatetrakis-(2,2′-bipyridine)-μ-oxodiruthenium(III) Ion in Aqueous Acidic Solutions. *Transition Metal Chemistry*, 18(1): 6 – 8.

Babatunde, O. A. and Ajayi, J. O. (2013). Kinetic Approach to the Reduction of Toluidine Blue by Dithionate Ion in Aqueous Acidic Medium. *Global Journal of Science Frontier Research Chemistry*, 13(8): 20 – 30.

Banerji, K. K. (1972). The Kinetics of the Oxidation of Acetaldehyde by Acid Permanganate. *Zeitschrift Für Naturforschung B*, 27(7): 772 – 774.

Bianchini, C. and Zoellner, R. W. (1996). Activation of Dioxygen by Cobalt Group Metal Complexes. *Advances in Inorganic Chemistry* 44: 263 – 339.

Bitziou, E., Snowden, M. E., Joseph, M. B., Leigh, S. J., Covington, J. A., Macpherson, J. V. and Unwin, P. R. (2013). Dual Electrode Micro-channel Flow Cell for Redox Titrations: Kinetics and Analysis of Homogeneous Ascorbic Acid Oxidation. *Journal of Electroanalytical Chemistry*, 692: 72 – 79.

Bresson, C., Lamouroux, C., Sandre, C. and Tabarant, M. (2008). An Interdisciplinary Approach to Investigate the Impact of Cobalt in a Human Keratinocyte Cell Line. *Journal of Biochimie*, 88(1619–1629).

Böttcher, A., Takeuchi, T., Hardcastle, K. I., Meade, T. J., Gray, H. B., Cwikel, D., Kapon, M., and Dori, Z. (1997). Spectroscopy and electrochemistry of cobalt (III) Schiff base complexes. *Inorganic Chemistry*, *36*(12), 2498–2504.

Chakraborty, S. and Banerjee, R. (2015). Kinetics and Mechanism of Oxidation of 2-Mercaptoethanol by the Heteropolyoxovanadate $[MnV_{13}O_{38}]^{7-}$. *International Journal of Chemical Kinetics*, 47(1): 13 – 18.

Chakraborty, M., Mandal, P. C. and Mukhopadhyay, S. (2012). Mechanistic Studies on the Oxidation of Thiols by a $[Mn_4O_6]^{4+}$ Core in Aqueous Acidic Media. *Polyhedron*, 45(1): 213 – 220.

Chakraborty, M., Mandal, P. C. and Mukhopadhyay, S. (2013). Kinetic Studies on Oxidation of L-cysteine and 2-mercaptoethanol by a Trinuclear Mn(IV) Species in Aqueous Acidic Media. *Inorganica Chimica Acta*, 398: 77 – 82.

Chen, C., Ferreira, J. C. B., Gross, E. R. and Rosen, D. M. (2014). Targeting Aldehyde Dehydrogenase 2: New Therapeutic Opportunities. *Physiological Reviews*, 94 (1): 1–34. doi:10.1152/physrev.00017.2013.

Choi, Y. M., Xia, W. S., Park, J. and Lin, M. C. (2000). Kinetics and Mechanism for the Reaction of Phenyl Radical with Formaldehyde. *Journal Physical Chemistry. A*, 104: 7030 – 7035.

Cini, R., Moore, S. J. and Marzilli, L. G. (1998). Strong Trans Influence Methoxymethyl Ligand in B_{12} Cobaloxime and Imine/oxime Model Complexes: Structural, Spectroscopic, and Molecular Mechanics Investigations. *Inorganic Chemistry*, 37(26): 6890 – 6897.

Cohen, C. T. and Coates, G. W. (2006). Alternating copolymerization of propylene oxide and carbon dioxide with highly efficient and selective (salen) Co (III) catalysts: effect of ligand and cocatalyst variation. *Journal of Polymer Science Part A: Polymer Chemistry*, 44(17), 5182–5191.

Cristiani, F., Devillanova, F. A., Diaz, A., and Verani, G. (1981). Osmium Tetroxide Reduction with Thiourea in Perchloric Acid Solutions. *Inorganica Chimica Acta*, 50(C): 251 – 255.

Davies, M .B. (1992). Reactions of L-ascorbicAcid with Transition Complexes. *Polyhedron*, 11(3): 285 – 321.

Di Bella, S., Oliveri, I. P., Colombo, A., Dragonetti, C., Righetto, S. and Roberto, D. (2012) An Unprecedented Switching of the Second-order Non-linear Optical Response in Aggregate Bis (salicylaldiminato) Zinc (II) Schiff-base Complexes. *Dalton Transaction*, 41(23):7013–6.

Dixon, D. A., Sadler, N. P. and Dasgupta, T. P. (1995). Mechanism of the Oxidation of L-ascorbic Acid by the Pentaammineaquacobalt(III) Ion in Aqueous Solution. *Transition Metal Chemistry*, 20(3): 295 – 299.

Eichhorn, E. and Speiser, B. (1994). Electrochemistry of Oxygenation Catalysts: Part 4. Solvent Composition-dependent Isopotential Points in Cyclic Voltammograms of Co(salen). *Journal of Electroanalytical Chemistry*, 365(1–2): 207 – 212.

Eichhorn, E., Rieker, A., Speiser, B. and Stahl, H. (1997). Electrochemistry of Oxygenation Catalysts. 3.1 Thermodynamic Characterisation of Electron Transfer and Solvent Exchange Reactions of Co (salen)/[Co (salen)]$^{+}$ in DMF, Pyridine, and Their Mixtures. *Inorganic Chemistry*, 36(15): 3307 – 3317.

El-Hag, D. A. and Dahab, A. A. (2016). Identification and Characterisation of Disulphide Bonds in Therapeutic Proteins by using Raman Spectroscopy. *Advance Journal of Pharmaceutical Life Science Research*, 4(3): 50 – 59.

Fabian, I. and Gordon, G. (1997). The Kinetics and Mechanism of the Chlorine Dioxide – Iodide Ion Reaction. *Inorganic Chemistry*. 36: 2494 – 2497.

Fawzy, A., Gluesmi, N., Althagafi, I. I. and Asghar, B. H. (2017). A Study of Kinetics and Mechanism of Chromic Acid Oxidation of Isosorbide, a Chiral Biomass-derived Substrate in Aqueous Perchlorate Solution. *Transition Metal Chemistry*, 42: 229 – 236.

Ganjali, M. R., Shirvani-Arani, S., Norouzi, P., Rezapour, M. and Salavati-Niasari, M. (2004). Novel Nitrite Membrane Sensor Based on Cobalt(II) Salophen for Selective Monitoring of Nitrite Ions in Biological Samples. *Microchimica Acta*, *146*(1): 35 – 41.

Gault, N., Sandre, C., Poncy, J. L., Moulin, C. and Lefaix J. L. (2010). Cobalt Toxicity: Chemical and Radiological Combined Effects on Keratinocyte Cell Line. *Toxicology in Vitro*, 24(92–98).

Gaur, A., Shrivastava, B. D., Srivastava, K., Prasad, J. and Singh, S. K. (2012). XAFS Investigations of Copper(II) Complexes with Tetradentate Schiff Base Ligands. *X-ray Spectrom*, 41(6):384–92.

Ghosh, G. K., Misra, K., Baskim, M., Linert, W. and Moi, S. C. (2013). Kinetics and Mechanism of the Interaction of Di-μ-hydroxobis (1,10-phenanthroline)dipalladium(II) Perchlorate with Thioglycolic Acid and Glutathione in Aqueous Solution. *Journal of Solution Chemistry*, 42(3): 526 – 543.

Goswami, A. M. and De, K. (2005). A Kinetic and Mechanistic Study on Substitution of Aqua Ligands from Cis-diaqua- bis-(bipyridyl)ruthenium(II) Complex by Thiosemicarbazide in Aqueous Medium. *Transition Metal Chemistry*: 30: 677 – 683.

Gowda, T. B. and Rao, V. R. (1988). Kinetics and Mechanism of Oxidation of Thiosemicarbazide in the Pure State and in its Metal Complex by Chloramine T, Bromamine

T, and Dichloramine T in Acid Medium. *Journal of Chemical Society, Perkin Transactions 2*, 3: 355 – 361.

Gupta, K. S. and Gupta, Y. K.(1984).. Hydrogen-ion dependence of reaction rates and mechanism. *Journal of Chemistry Education* 61(11), 972.

Hamza, S. A., Iyun, J. F., and Idris, S. O. (2012). Kinetics and Mechanism of the Redox Reaction of Toluidine Blue and Nitrite Ions in Aqueous Acidic Medium. A*rchives of Applied Science Research*. 4(1): 10 – 18.

Hamzeh, M. A. (2001). Kinetics of Oxidation of L-ascorbicAcid by Cobalt(III) Complexes, *Journal of the Chemical Society of Pakistan*, 23(2): 69 - 73.

Henson, N. J., Hay, P. J. and Redondo, A. (1999). Density Functional Theory Studies of the Binding of Molecular Oxygen with Schiff's Base Complexes of Cobalt. *Inorganic Chemistry*, *38*(7):1618 – 1626.

Hirotsu, M., Kojima, M., Nakajima, K., Kashino, S. and Yoshikawa, Y. (1996). Stereochemistry and Electrochemistry of Cobalt(II) and Cobalt(III) Complexes Containing Optically Active Tetradentate Schiff Base Ligands. *Bulletin of the Chemical Society of Japan*, *69*(9): 2549 - 2557.

Hošt'álek, Z., Mundil, R., Císařová, I., Trhlíková, O., Grau, E., Peruch, F., Cramail, H. and Merna, J. (2015). Salphen-Co(III) Complexes Catalysed Copolymerisation of Epoxides with CO_2. *Polymer*, 63: 52 – 61.

Housecroft, C. E. and Sharpe, A. G. (2005). *Inorganic Chemistry*. Pearson Education Limited, Second Edition, pp. 766 – 799. ISBN: 0130-39913-2

Hubbard, C. D. and Eldik, R. V. (2001). Electrostriction and Counter Ion Effects in an Outer-sphere Electron Transfer Reaction. Kinetics of the Reduction of Hexachloroiridate(IV) by Iodide Ion. *Journal of Chemical Society, Dalton Transaction*. 2001: 1069 – 1075.

Idris, S.O. (2005). Some electron transfer reactions of Cr(VI) and of tetrakis(2,2$^{/}$- bipyridine)-µ-oxodiiron(III) complex. Unpublished *PhD. Thesis.* Chemistry Department, Ahmadu Bello University, Zaria.

Idris, S.O., Iyun, J.F. and Agbaji, E.B. (2008). Kinetics and Mechanism of Oxidation of Thiosulphate Ion by Tetrakis(2,2-Bipyridine)-µ-oxodiiron(III) Ion in Aqueous Acidic Medium. *ChemClass Journal*, 33: 103 – 108.

Idris, S. O., Tanimu, A., Iyun, J. F. and Mohammed, Y. (2015). Kinetics and Mechanism of the Reaction of Malachite Green and Dithionite Ion. *International Research Journal of Pure and Applied Chemistry*. 5(2): 177 – 184.

Iyun, J. F, Ayoko, G. A and Lawal, H. M. (1996). Kinetics of the Reduction of µ-oxobis-(aquobis(2,2'-bipyridine))ruthenium(III) by L–cysteine in Aqueous Solution. *Indian Journal of Chemistry*, 35(A): 210 – 213.

Iyun, J. F., Ayoko, G.A. and Lawal, H. M. (1992). Kinetics and Mechanism of the Oxidation of Iodide by Diaquote-trakis (2,2′-bipyridine)-μ-oxodiruthenium(III) Ion in Acid Medium. *Transition Metal Chemistry*, 17(1): 63 – 65.

Jagannadham, V. (2012). Electron Transfer Reactions: A Treatise. *American Journal of Chemistry*, 2(2): 57 – 82.

James, H. E. (2002), *Kinetics and Reaction Mechanisms Second Edition*. McGraw – Hill, pp. 156 - 160.

Jattinagoudar, L. N., Byadagi, K. S., Shirhatti, N. M., Nandibewoor, S. T. and Chimatadar, S. A. (2013). Oxidation of Ascorbic Acid by Hexacyanoferrate(III) in Aqueous Perchloric Acid Medium- A kinetic and Mechanistic Study. *Journal of Chemical and Pharmaceutical Research*: *5*(4): 290 – 300.

Jonnalagadda, S. B., Chinake, C. R., Olojo, R. and Simoyi, R. H. (2002). Kinetics and Mechanism of the Oxidation of 4-methyl-3-thiosemicarbazide by Acidic Bromate. *International Journal of Chemical Kinetics, 34*(4): 237 – 247.

Kianfar, A. H. and Khavasi, H. R. (2016). Synthesis and Crystal Structure of Cobalt(III) Complexes of Salen Type Schiff Bases and Tertiary Phosphanes as Ligands. *Inorganic Chemistry Research*, 1(2): 105 – 114.

Kim, H., Kim, W., Lough, A. J., Kim, B. M. and Chin, J. (2005). A Cobalt(III)−salen Complex with an Axial Substituent in the Diamine Backbone: Stereoselective Recognition of Amino Alcohols. *Journal of the American Chemical Society*. 127(48): 16776 – 16777.

Kleij, A. W., Kuil, M., Lutz, M., Tooke, D. M., Spek, A. L., Kamer, P. C. J., van Leeuwen, P. W. N. M. and Reek, J. N. H. (2006). Supramolecular zinc(II)salphen Motifs: Reversible Dimerization and Templated Dimeric Structures. *Inorganica Chimica Acta*, *359*(6): 1807 - 1814.

Kocak, A., Yilmaz, H., Faiz, O. and Andac, O. (2016). Experimental and Theoretical Studies on Cu(II) Complex of N,N′-disalicylidene-2,3-diaminopyridine Ligand Reveal Indirect Evidence for DNA Intercalation. *Polyhedron*, *104*: 106 – 115.

Kohlpaintner, C. Schulte, M., Falbe, J., Lappe, P. and Weber, J. (2008). Aliphatic Aldehydes. *Ullmann's Encyclopedia of Industrial Chemistry*, Wiley-VCH, Weinheim. doi:10.1002/14356007.a01_321.pub2.

Komiyama, M., Takeda, N. and Shigekawa, H. (1999). Hydrolysis of DNA and RNA by Lanthanide Ions: Mechanistic Studies Leading to New Applications. *Royal Society of Chemistry*. 16: 1443 – 1451.

Kothari, S., Sharma, V., Sharma, P. K. and Banerji, K. K. (1992). Kinetic Study of the Oxidation of Aliphatic Aldehydes by bis-(2,2′-bipyridyl)copper(II) Permanganate. *Proceedings of the Indian Academy of Sciences-Chemical Sciences*, *104*(5): 583 – 589.

Kurahashi, T. and Fujii, H. (2013). Unique Ligand-radical Character of an Activated Cobalt Salen Catalyst that is Generated by Aerobic Oxidation of a Cobalt(II) Salen Complex. *Inorganic Chemistry*, *52*(7): 3908 – 3919.

Llewellyn, B. D. (2014). Thiosemicarbazide-ferricyanide Reduction for the Histochemical Demonstration of Aldehydes in Tissue Sections. *Biotechnic and Histochemistry*, 89(3): 228 – 231.

Lohdip, Y. N., Davies, A. K. and Iyun, J. F. (1998). Kinetics and Mechanism of the Oxidation of Formaldehyde by Permanganate Ion in Aqueous Perchloric Acid. *Nigerian Journal of Textile Education*, 15(2): 57- 64.

López-Torres, E. and Dilworth, J. R. (2009). Reactivity of Thiosemicarbazides with Redox Active Metal Ions: Controlled Formation of Coordination Complexes Versus Heterocyclic Compounds. *Chemistry. A European Journal*: 15(12): 3012 – 3023.

Lu, X. and Wang, Y. (2004). Highly active, binary catalyst systems for the alternating copolymerization of CO_2 and epoxides under mild conditions. *Angewandte Chemie International Edition*, *43*(27), 3574–3577.

Luinstra, G. A., Haas, G. R., Molnar, F., Bernhart, V., Eberhardt, R. and Rieger, B. (2005). On the formation of aliphatic polycarbonates from epoxides with chromium (III) and aluminum (III) metal–salen complexes. *Chemistry–A European Journal*, *11*(21), 6298–6314.

Matsuura, T. (1977). Bio-mimetic oxygenation. *Tetrahedron*, *33*(22): 2869 – 2905.

McAuley, A. and Gomwalk, U. D. (1969). Metal-ion Oxidations in Solution. Part VI. Oxidation of Thiourea and its N-substituted Derivatives by Cobalt(III). *Journal of the Chemical Society A: Inorganic, Physical, Theoretical* (A): 977– 980.

Macartney, D.H. and McAuley, A. (1982). Kinetics and Mechanisms of the Oxidation of a Nickel(II) Oxime Complex by Cobalt(III) Aquo Ions in Acidic Aqueous Media. Formation of a Ni(IV) Complex. *Canadian Journal of Chemistry*, *60*(20): 2625 – 2628. https://doi.org/10.1139/v82-377

Mohammed, Y (2015). Kinetics and Mechanisms of the electron transfer reactions of diaquotetrakis (2, 2'- bipyridine)-μ-oxodiruthenium(III) ions and some reductants in aqueous medium. Ph.D thesis Submitted to Department of Chemistry, Ahmadu Bello University, Zaria, Nigeria.

Mohammed, Y., Idris, S. O. and Iyun, J. F. (2014). Redox Kinetics and Mechanism of the Oxidation of Thiourea by Diaquotetrakis(2,2'-bipyridine)-μ-oxodiruthenium(III) Ion in Aqueous Perchloric Acid. *International Research Journal of Pure and Applied Chemistry*, 4(6): 819 – 833.

Mohammad, A. N., Kaveh H., Ali A. (2019). Synthesis and characterization of Co(III) Salen Complex Immobilized on Cobalt Ferrite-silica Nanoparticle and their Application in the

Synthesis of Spirooxindoles. *Applied Organometallic Chemistry*, 35(5): e4743 doi.org/10.1002/aoc.4743

Mohanty, B., Behera, J., Acharya. S., Mohanty, P. and Patnaik, A. K. (2014). Kinetics and Mechanism of Oxidation of Glutathione by Cis-(diaqua)-bis-(ethylenediamine)cobalt(III) Ion. *International Journal of Advanced Chemistry*, 2(1): 39 – 43.

Mojtaba, M. (2016). Electrochemical Sensing of Thiodiglycol, The Main Hydrolysis Product of Sulfur Mustard, by using an Electrode Composed of an Ionic Liquid, Graphene Nanosheets and Silver Nanoparticles. *Microchimica Acta*, 183: 2396 – 2401.

More, S. S., Gurame, V. M. Gokavi, G. S. (2018). Kinetics and Mechanism of Oxidation of Thiosemicarbazide by Waugh-type 9-Molybdomanganate(IV) in Aqueous Perchloric Acid. *Journal of Applicable Chemistry*, *7*(3): 686 – 694.

Moustafa, I., Khateeb, M. and Alhamed, O. (2016). Kinetic Spectrophotometric Method for Determination of Vanadium in Syrian Oil Using 1,5-diphenylcarbazide Reagent. *International Letters of Chemistry, Physics and Astronomy*, 67: 42 – 49.

Munro, N. B., Talmage, S. S., Griffin, G. D., Waters, L. C., Watson, A. P., King, J. F. and Hauschild, V. (1999). The Sources, Fate, and Toxicity of Chemical Warfare Agent Degradation Products. *Environmental Health Perspectives*, 107(12): 933 – 974).

Nayak, S. P. and Gowda, B. T. (1992). Hydrazones by N-chlorobenzamide in Water. *Journal of Physical Organic Chemistry*, *5*: 755 – 763.

Nelson, D. R., Lehninger, A. L. and Cox, M. (2005). Lehninger Principles of Biochemistry. *W.H. Freeman, New York*, p. 148. ISBN: 0-7167-4339-6

Niederhoffer, E. C., Timmons, J. H. and Martell, A. E. (1984). Thermodynamics of Oxygen Binding in Natural and Synthetic Dioxygen Complexes. *Chemical Reviews*, 84(2): 137 – 203.

Nishinaga, Tsutsui, T., Moriyama, H., Wazaki, T., Mashino, T. and Fujii, Y. (1993). Structural Effect of Cobalt Schiff Base Complex Catalyst on its Catalytic Activity in Dioxygenolysis of 3-methylindole. *Journal of Molecular Catalysis*, 83(1–2): 117 – 123.

Nishinaga, Yamazaki, S. and Matsuura, T. (1988). Catalytic Dehydrogenation of Secondary Amines with Cobalt Schiff Base Complex-oxygen System. *Tetrahedron Letters*, 29(33), 4115 – 4118.

Nkole, I. U., Osunkwo, C. R., Onu, A. D. and Idris, S. O. (2018a). Kinetics and Mechanism of the Reduction of N-(2-hydroxyethyl)ethylenediaminetriacetatoiron(III) Complex by Thioglycol in Bicarbonate Buffer Medium. *International Journal of Advanced Chemistry*, *6*(1): 102 - 107.

Nkole, I. U., Onu, A. D., Osunkwo, C. R. and Idris S. O. (2018b). Kinetics Approach to the Mechanism of the Redox Reaction of Ehylenediaminetetraacetatoferrate(III) Complex

and Thioglycolic Acid in Bicarbonate Buffer Medium. *ATBU Journal of Science, Technology and Education*. 6(4): 6-19.

Nkole, I. U. and Osunkwo, C. R. (2019). Kinetic Approach to the Reduction of Ethylenediaminetetraacetatoferrate(III) Complex by Iodide Ion in Aqueous Acidic Medium. *Asian Journal of Physical and Chemical Sciences*, *7*(2): 1 – 8.

Nkole, I., Abdulsalam, S., Ibrahim, I. and Arthur D. E. (2021). Micellar Effect on Electron Transfer Reaction of 2-(hydroxyethyl)ethylenediaminetriacetatoiron(III) Complex with Thiocarbonate Ion: Kinetic Model. *Chemistry Africa*, doi: 10.1007/s42250-021-00241-z

Onu, A. D., Idris, S. O. and Iyun, F. J. (2016). Oxidation of Ethylenediaminetetraacetatocobaltate(II) Complex By Hydrogen Peroxide In Aqueous Acidic Medium: A Kinetic Study. *Journal of Chemical Society of Nigeria,* 41(2): 81 – 86.

Onu, A. D., Iyun, J. F. and Idris, S. O. (2009). The Kinetics of the Reduction of Tetraoxoiodate(VII) by N-(2-hydroxylethyl)ethylenediaminetriacetatocobaltate(II) Ion in Aqueous Perchloric Acid. *Transition Metal Chemistry, 34*(8): 849 – 853.

Onu, A. D., Iyun, J. F. and Idris, S. O. (2015). Kinetics and Stoichiometry of the Reduction of Hydrdogen Peroxide by Aminocarboxylatocobaltate(II) Complex in Aqueous Medium. *Open Journal of Inorganic Chemistry*, 5: 75 – 82.

Ortega, R., Bresson, C., Fraysse A., Sandre, C. and Devès, G. (2009). Cobalt Distribution in Keratinocyte Cells. *Toxicology Letter*, 188(26–32).

Osunkwo, C. R., Nkole, I. U., Onu, A. D. and Idris, S. O. (2018). Kinetics And Mechanism of the Reduction of Tris-(1,10-phenanthroline)cobalt(III) Complex by N-methylthiourea in Aqueous Acidic Medium. *Nigerian Research Journal of Chemical Sciences*, 5: 82 - 97.

Osunlaja, A. A., Idris, S. O. and Iyun, J. F. (2013). Kinetics and Mechanism of Thiourea Oxidation by Oxygenated $[Co_2(O_2)(NH_3)_{10}]^{5+}$ Complex. *Journal of Chemical and Pharmaceutical Research,.5*(2): 328 – 336.

Oyetunji, O. A., Gabalebe, M. and Sabure, N. (2006). Non-bridging Ligand Effects on the Kinetics of Reduction of Chloro- and Azido-pentaamminecobalt(III) by some Polypyridyl Complexes of Ruthenium(II). *Bulletin of the Chemical Society of Ethiopia, 20*(2): 227 - 234.

Özkan, Y., Özkan, E. and Şimşek, B. (2002). Plasma Total Homocysteine and Cysteine Levels as Cardiovascular Risk Factors in Coronary Heart Disease. *International Journal of Cardiology*, *82*(3): 269 – 277.

Pandeya, S. N., Srivastava, S. K., Priyanka, R. and Anita, S. (2012). Synthesis and Anticonvulsant Activity of Pyrimidine Hydrazones. *Journal of Scientific Research in Pharmacy*. 1(3): 92- 97.

Pillar, E. A., Guzman, M. I. and Rodriguez, J. M. (2013). Conversion of Iodide to Hypoiodous Acid and Iodine in Aqueous Microdroplets Exposed to Ozone. *Environmental Science and Technology*. 47(19): 10971 – 10979.

Pizzolato, E., Natali, M., Posocco, B., López, A. M., Bazzan, I., Di Valentin, M., Galloni, P., Conte, V., Bonchio, M. and Scandola, F. (2013). Light Driven Water Oxidation by a Single Site Cobalt Salophen Catalyst. *Chemical Communications*, *49*(85): 9941– 9943.

Polson, S. M., Cini, R., Pifferi, C. and Marzilli, L. G. (1997). Synthesis and X-ray Structures of Elusive Imine/oxime-type Organocobalt B_{12} Complexes. NMR Study Suggesting Steric Strain within the Axially Ligated Benzimidazole. *Inorganic Chemistry*, *36*(3): 314 – 322.

Rajmane, D. S. and Gokavi, G. S. (2014). Kinetics And Mechanism of Keggin Type 12 Tungstocobaltate(II) Catalysed Oxidation Hexacyanoferrate(II) Perborate. *Chemical Science Transactions*, 3(4): 1384 – 1389.

Ramírez, M. T., Morales-Pérez, A., Rojas-Hernández, A. and González, I. (1996). Electrochemical Study of 1,5-diphenylcarbazide and 1,5-diphenylcarbazone in 0.3 M $HClO_4$. *Journal of Electroanalytical Chemistry*, 410(2): 203 – 212.

Ratnam, S., Anipindi, N. R. (2012). Kinetic and Mechanistic Studies on the Oxidation of Hydroxylamine, Semicarbazide, and Thiosemicarbazide by Iron(III) in the Presence of Triazines. *Transition Metal Chemistry*, 37: 453 - 462

Read, J. F., Bewick, S. A., Graves, C. R., MacPherson, J. M., Salah, J. C., Theriault, A. and Wyand, A. E. H. (2000). The Kinetics and Mechanism of the Oxidation of S-methyl-L-cysteine, L-cystine and L-cysteine by Potassium Ferrate. *Inorganica Chimica Acta*, *303*(2): 244 - 255.

Rodrigo, A. M., José, C. G., Bruno R. F., Ericson, H. N. S. T., Franklin, F., Anderson M. S., Romildo, J. R., Gabriel L. C. S., Renato, G. F., Pedro, A. M. V. and Cristina, A. B. (2018). Electronic and Magnetic Properties of the [Ni(salophen)]: An Experimental and DFT Study. *Journal of Advanced Research*, 9: 27–33

Roesems, G., Hoet P. H., Dinsdale, D. and Demedts, M. (2000). In vitro Cytotoxicity of Various Forms of Cobalt for Rat Alveolar Macrophages and Type II Pneumocytes. *Toxicology and Applied Pharmacology*, 162(2–9).

Roy, K. (2005). Thiols and Organic Sulphides. *Ullmann's Encyclopedia of Industrial Chemistry*. Weinheim: Wiley-VCH. doi:10.1002/14356007.a26_767

Saha, B., Hung, M. and Stanbury, D. M. (2002). Reduction of Octacyanomolybdate(V) by Thioglycolic Acid in Aqueous Media. *Inorganic Chemistry*, 41(21): 5538 – 5543.

Salem, I. A. and Gemeay, A. H. (1996). Kinetics and Mechanism of the Oxidation of L-ascorbic Acid by the N, N′-ethylenebis-(salicylideneiminato)manganese(III) Complex in Aqueous Solution. *Transition Metal Chemistry*, 21(2): 130 – 134.

Sami, P., Venkateshwari, K., Mariselvi, N., Sarathi, A. and Rajasekaran, K. (2009). Studies on Electron Transfer Reactions: Reduction of Heteropoly 11-tungstophosphovanadate(V) by L-cysteine and Thioglycolic Acid in Aqueous Acid Medium. *Transition Metal Chemistry*, 35: 563 – 570

Santosh, K. Upadhyay (2006). *Chemical Kinetics and Reaction Dynamics.* Springer, New York with Anamaya Publishers, New Delhi, India, pp. 120 -234.

Senapati, S. (2014). Electron Transfer Reaction of Pyridoxine(Vitamin B6) with Keggin Type 12 Tungstocobaltate(III) in Aqueous Perchlorate Medium. *American Chemical Science Journal*, 4(2): 242 – 254.

Shanmugaprabha, T., Selvakumar, K., Rajasekaran, K. and Sami, P. (2016). A Kinetic Study of the Oxidations of 2-mercaptoethanol and 2-mercaptoethylamine by Heteropoly 11-tungsto- 1-vanadophosphate in Aqueous Acidic Medium. *Transition Metal Chemistry*, *41*(1): 77- 85.

Sherigara, B. S., Pinto, I. and Ishwar, B. K. (1994). Manganese(III) oxidations of Benzoylhydrazine, Aroxyacetylhydrazine, Semicarbazide, Thiosemicarbazide and Their Derivatives in Pyrophosphate Media. *Mikrochimica Acta*, 113(1–2): 61 – 69.

Shi, T., Berglund, J. and Elding, L. I. (1996). Kinetics and Mechanism for Reduction of Trans-dichlorotetracyanoplatinate(IV) by Thioglycolic Acid, L-cysteine, Dl-penicillamine, and Glutathione in Aqueous Solution. *Inorganic Chemistry*, 35(12): 3498 – 3503.

Solomon, M. B., Rawal, A., Hook, J. M., Cohen, S. M., Kubiak, C. P., Jolliffe, K. A. and D'Alessandro, D. M. (2018). Electroactive Co(III)-salen Metal Complexes and the Electrophoretic Deposition of Their Porous Organic Polymers onto Glassy Carbon. *RSC Advances*, 8(43): 24128 – 24142.

Speiser, B. and Stahl, H. (1995). Complexation of N, N′-bis-(salicylidene)-ethylenediiminato cobalt(III) by Anilines in Dimethylformamide. *Angewandte Chemie International Edition in English*, *34*(10): 1086 – 1089.

Staykov, A., Watanabe, M., Ishihara, T. and Yoshizawa, K. (2014). Photoswitching of Conductance through Salicylidene Methylamine. *Journal of Physical Chemistry*, 118 (47):27539–48.

Subramaniam, P., Vanitha, T., Kodispathi, T., Sundari, S. and Raj, C. (2014). Role of Iron(III)-salen Chloride as Oxidising Agent with Thiodiglycolic Acid: The Effect of Axial Ligands. *Journal of the Mexican Chemical Society*, 58(2): 211 – 217.

Suchomelova, L., Horak, V. and Zyka, J. (1965). New Method for the Detection of Sulphoxide. *Microchemical Journal*, 9: 196 – 200.

Tobe, M. L. and Burgess, J. (1999). *Inorganic Reaction Mechanisms*. Longman. Pp. 211 – 221 ISBN: 0582236770978058223677 6

Uebelacker, M. and Lachenmeier, D. (2011). Quantitative Determination of Acetaldehyde in Foods Using Automated Digestion with Simulated Gastric Fluid Followed by Headspace Gas Chromatography. *Journal of Automated Methods and Management in Chemistry,* doi:10.1155/2011/907317

Ugye, T., Uzairu, A., Idris, S. O. and Kwanashie, H. (2013). Spectrophotometric Measurement of the Stoichiometry of Formaldehyde and Plasma Albumin Reaction in Water Solution using the Method of Continous Variation (Job's Method) and the Mole Ratio Method. *Journal of Environmental Science, Toxicology and Food Technology*, 5(6): 42 – 45.

Ukoha, P. O. and Iyun, J. F. (1999). Kinetics and Mechanism of the Reduction of Tetraoxoiodate(VII) Ion by L-ascorbicAcid in Perchloric Acid Medium. *Nigerian Journal of Chemical Research*, 4(1): 9 – 14.

Ukoha, P. O., Anidobu, C. O., Iorungwa, P. D. and Oluigbo, I. C. (2018). Kinetics and Mechanism of Reduction of $(Fe(Saloph))_2$-μ-dicarpy Complex by L-ascorbicacid in Acid Medium. *Federal University Wukari, Trends in Science and Technology Journal*, 3(1): 158 – 162.

Veriansyah, B., Kim, J. D., and Lee, J. C. (2005). Supercritical Water Oxidation of Thiodiglycol. *Industrial and Engineering Chemistry Research*, 44(24): 9014 – 9019.

Vogel, A. I. (1996*). Vogels's Textbook of Quantitative Inorganic Analysis: Including Elementary Instrumental Analysis*. ELBS and Longman, London. Pp. 125 – 247.

Weissbekger, A. (1974). Investigation of Rates and Mechanism of Reactions in Techniques of Chemistry. John *Wiley and Sons Press*, p. 421.

Willems, G. J. and De Ranter, C. J. (1974). The Purity of Commercial Diphenylcarbazone. *Analytical Chimica Acta*, 68(1): 111 – 118.

Wezenberg, J. and Kleij, A. W. (2008). Material Applications for Salen Frame Works. *Journal of German Chemical Society*, 47(13): 2354 - 2364.

Wilkins, R. G. (2002). Kinetics and Mechanism of Reactions of Transition Metal Complexes. Second Edition, *Wiley-VCH Verlag GmbH and Co*., pp. 65 – 106. ISBNs: 3-527-28253-X (Hardback); 3-527-60082-5 (Electronic)

Yamada, S. (1999). Advancement in Stereochemical Aspects of Schiff Base Metal Complexes. *Coordination Chemistry Reviews*, 190: 537 – 555.

Yeh, J. I. (2009). Additives and Microcalorimetric Approaches for Optimisation of Crystallisation in Protein Crystallisation. *2nd Edition (Ed: T. Bergfors), International University Line, La Jolla, CA.* 9: 1729 – 1732. ISBN 978-0-9720774-4-6

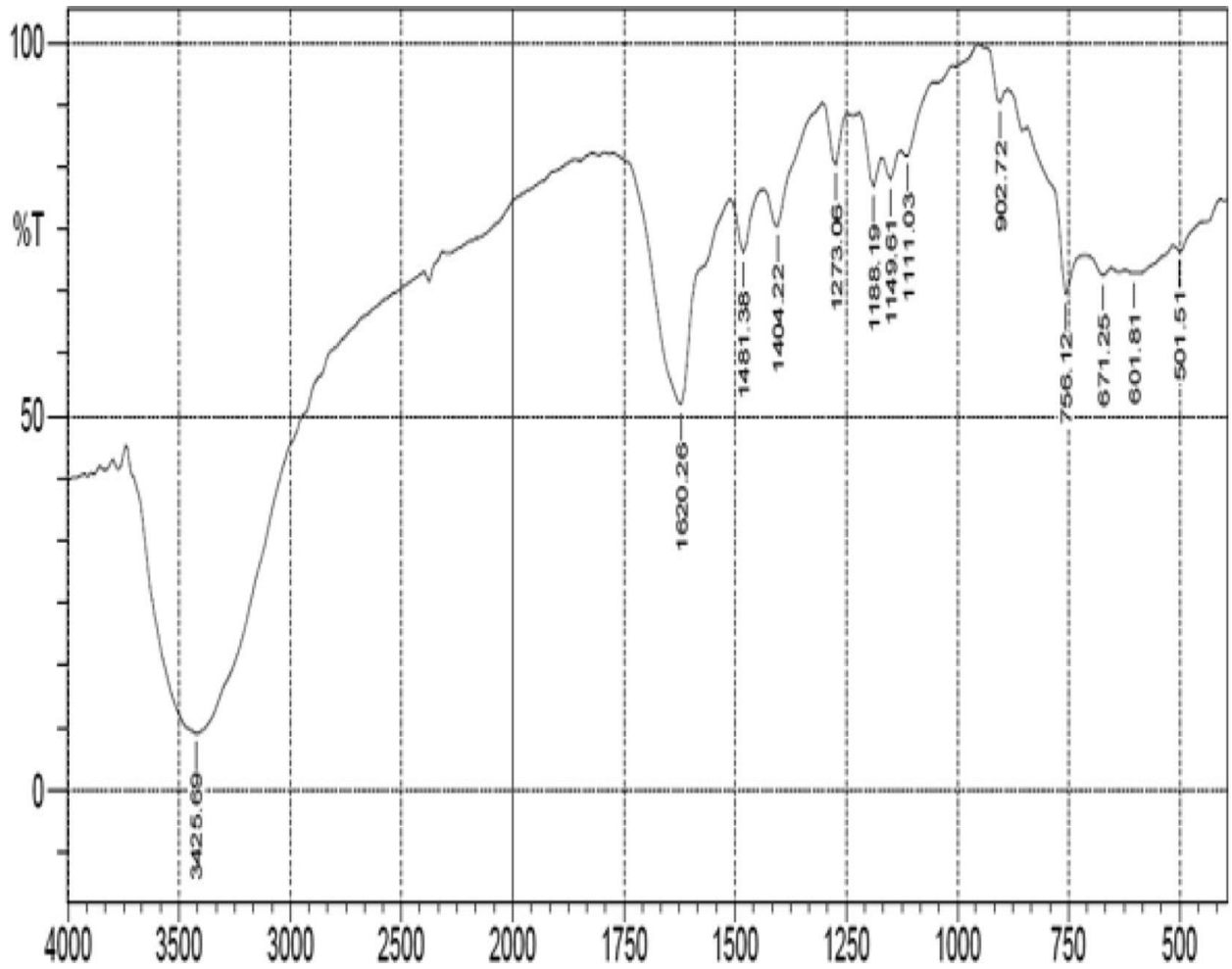
Yilmaz, H., Kocak, A., Dilimulati, M., Zorlu, Y. and Andac, M. (2017). A new Co(III) Complex of Schiff Base Derivative for Electrochemical Recognition ofNnitrite Anion. *Journal of Chemical Sciences*, 129(10): 1559 – 1569.

Yu-Ling, Z., Wen-Juan, R., Xiao-Jing, Z., Hong-Gen, W. and Zhi-Ang, Z. (2003). Synthesis and Characterization of Axial Coordination Cobalt(III) Complexes Containing Chiral Salen Ligands. *Polyhedron*, 22 (12): 1535-1545. doi.org/10.1016/S0277-5387(03)00261-4.

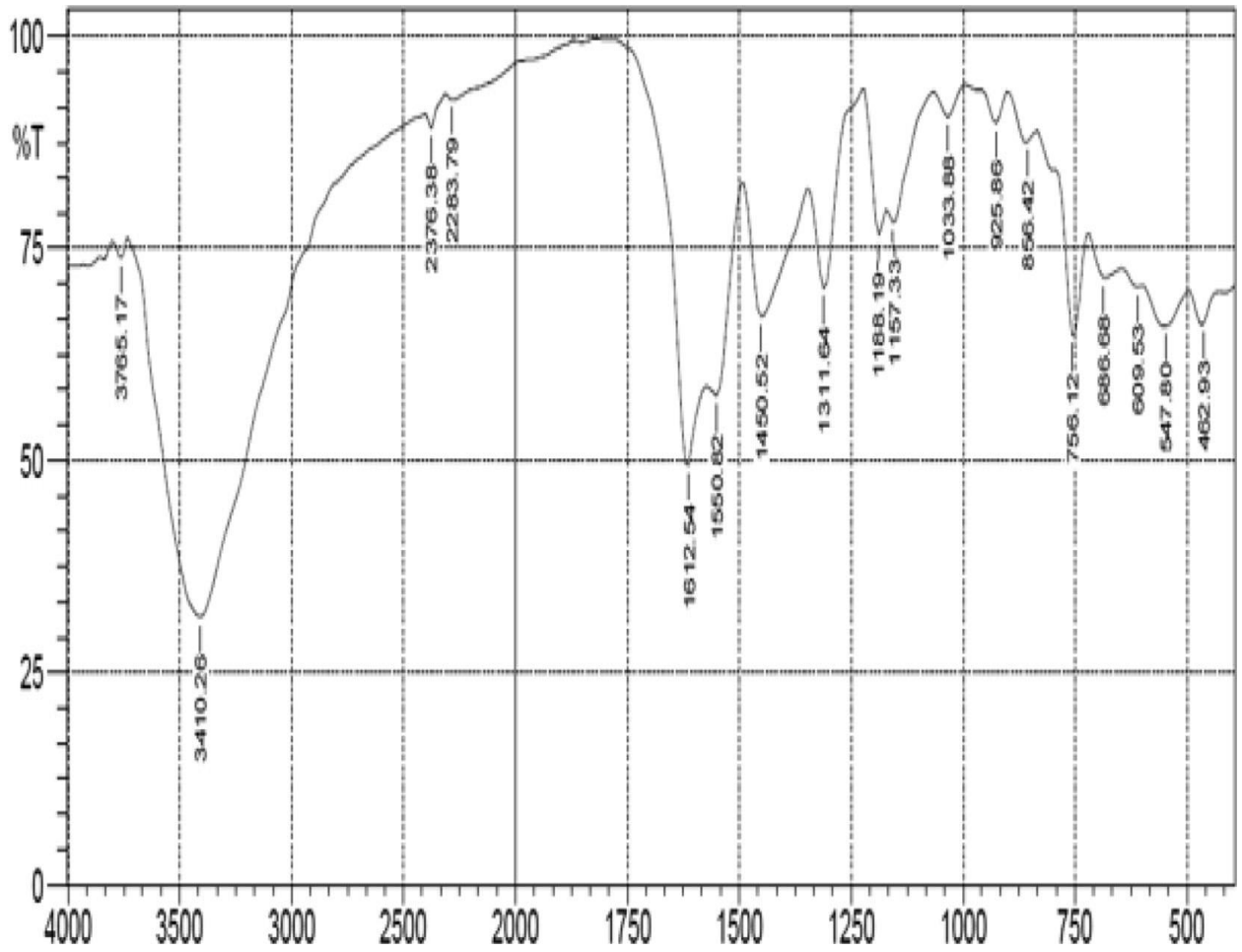
Zhang, C., Sutherland, M., Herasymchuk, K., Clarke, R. M., Thompson, J. R., Chiang, L., Walsby, C. J. and Storr, T. (2017). Octahedral Co(III) Salen Complexes: The Role of Peripheral Ligand Electronics on Axial Ligand Release Upon Reduction. *Canadian Journal of Chemistry*, 96 (2): 110 – 118.

LIST OF APPENDICES

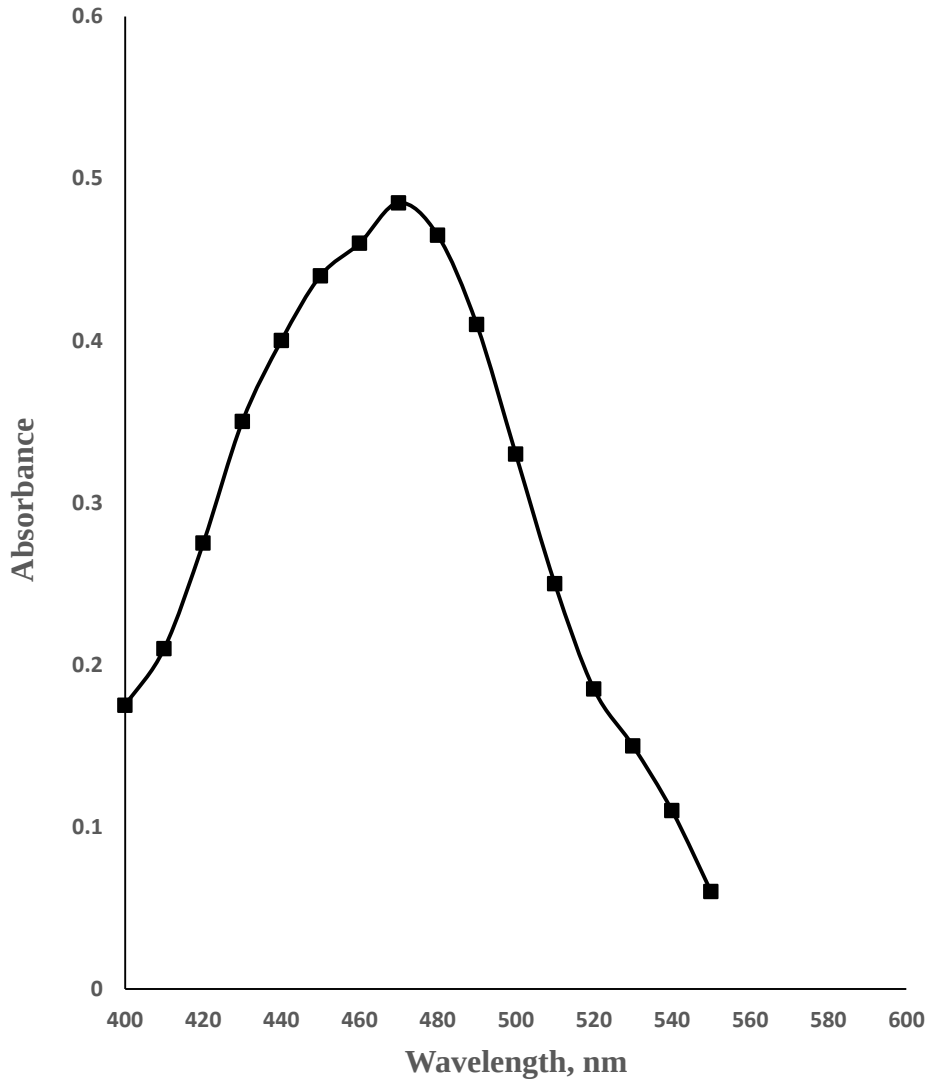
XII. FT-IR Spectrum of the Salophen Ligand



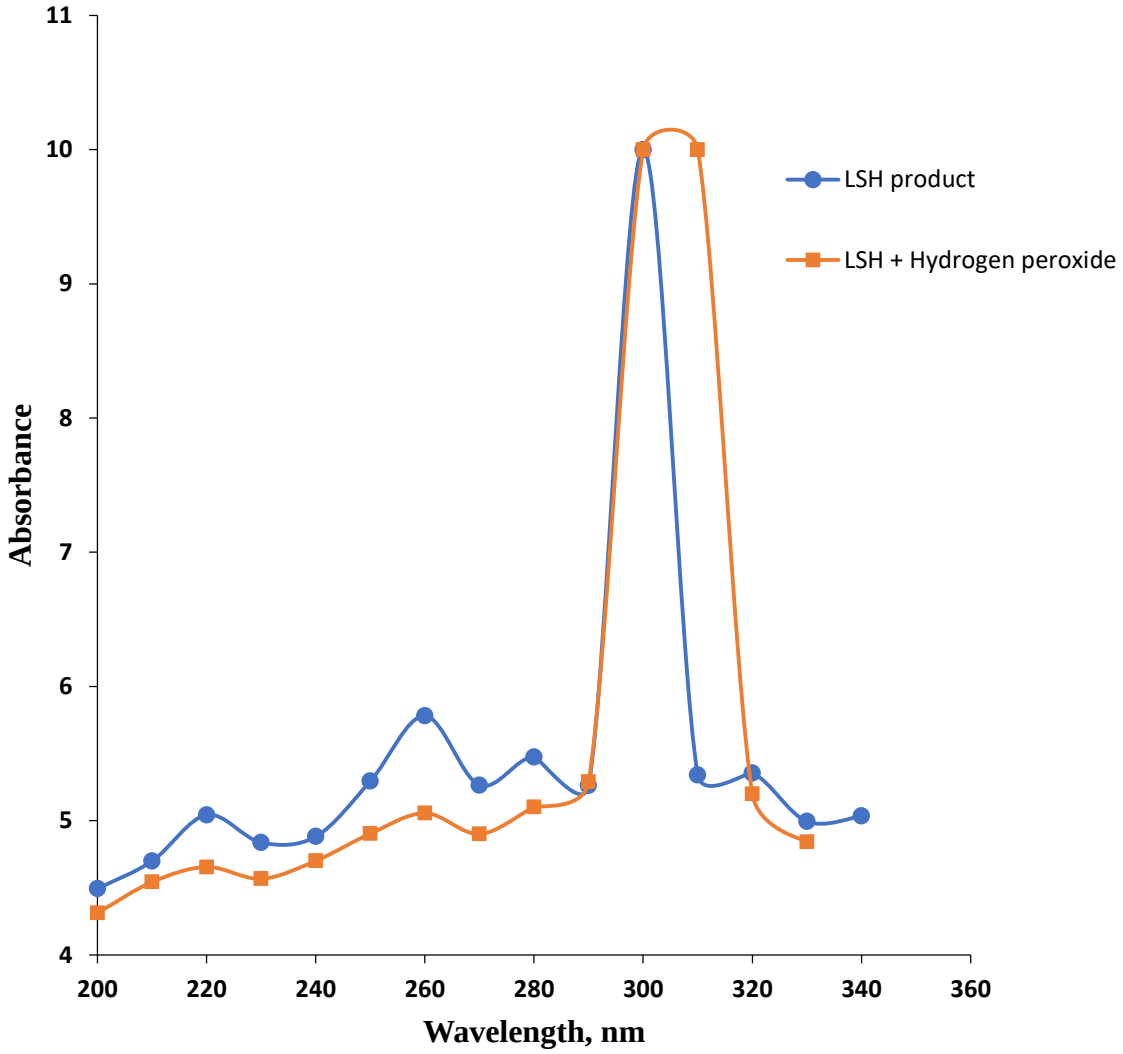
XIII. FT-IR Spectrum of the Co(III)Salophen Complex



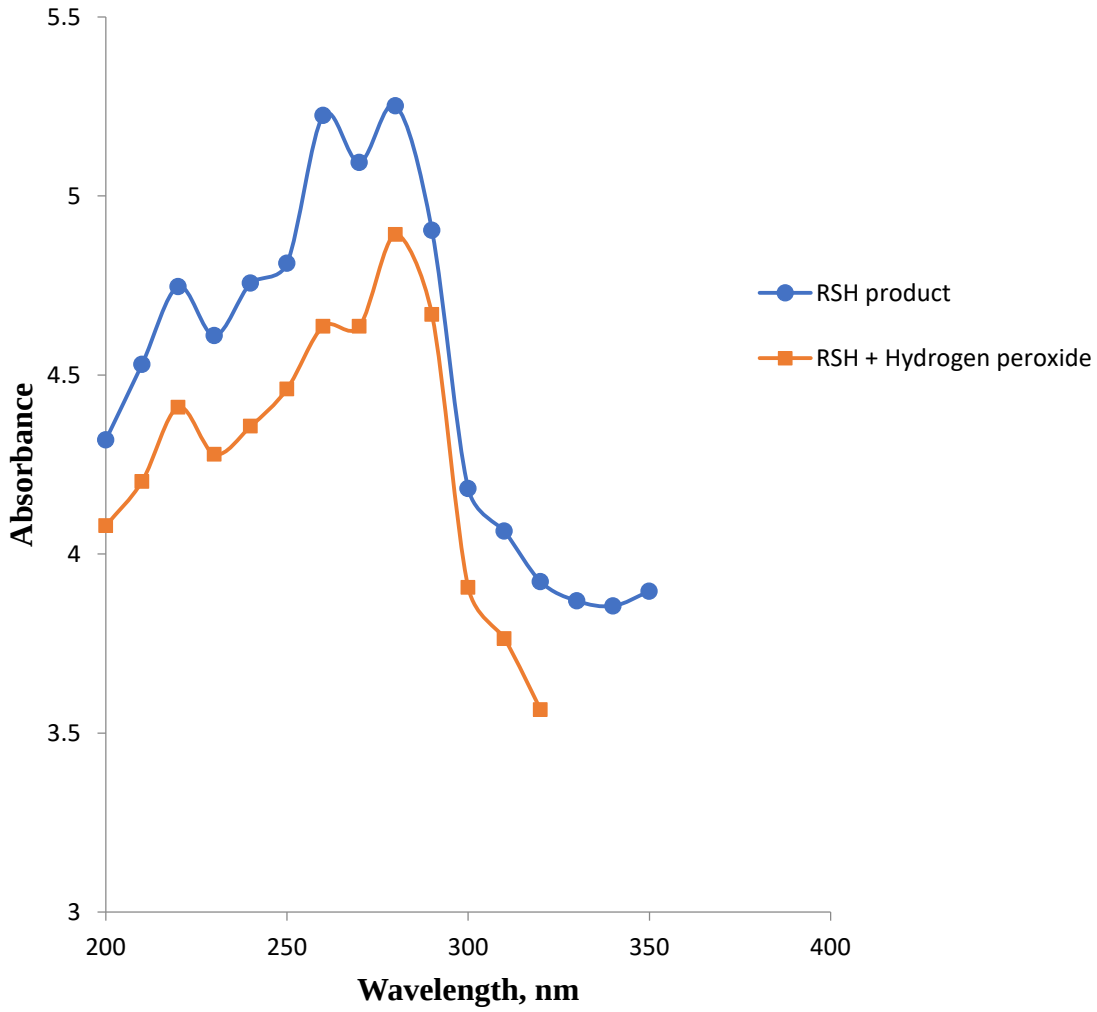
III. UV Visible Spectrum for DMSO/H_2O Solution of $[Co(salophen)]^+$ Complex at 4.0×10^{-4} mol dm^{-3}



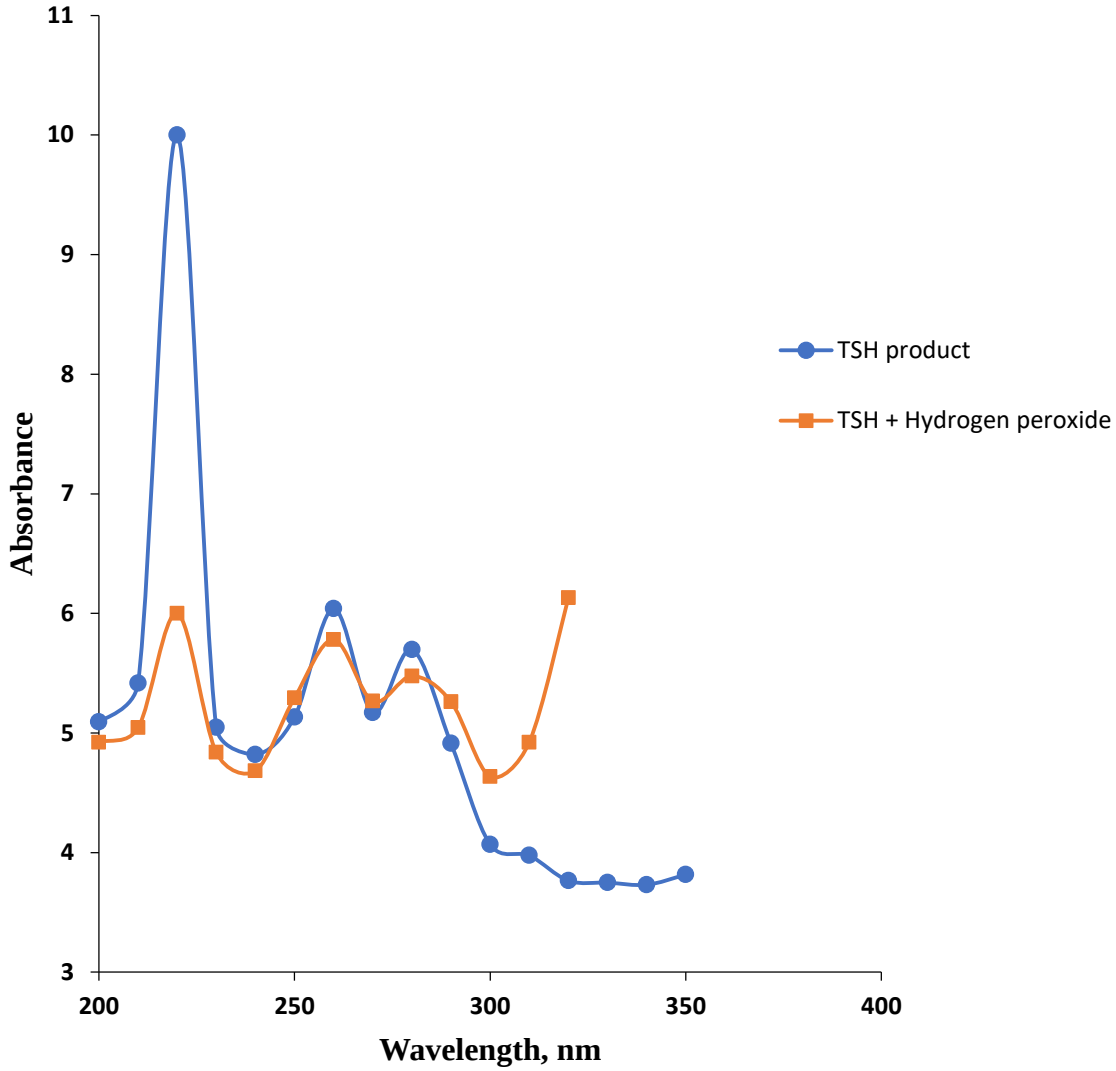
IV. UV- visible Spectrum of Product of LSH Oxidation by Co(salophen)$^{+}$ and Hydrogen Peroxide



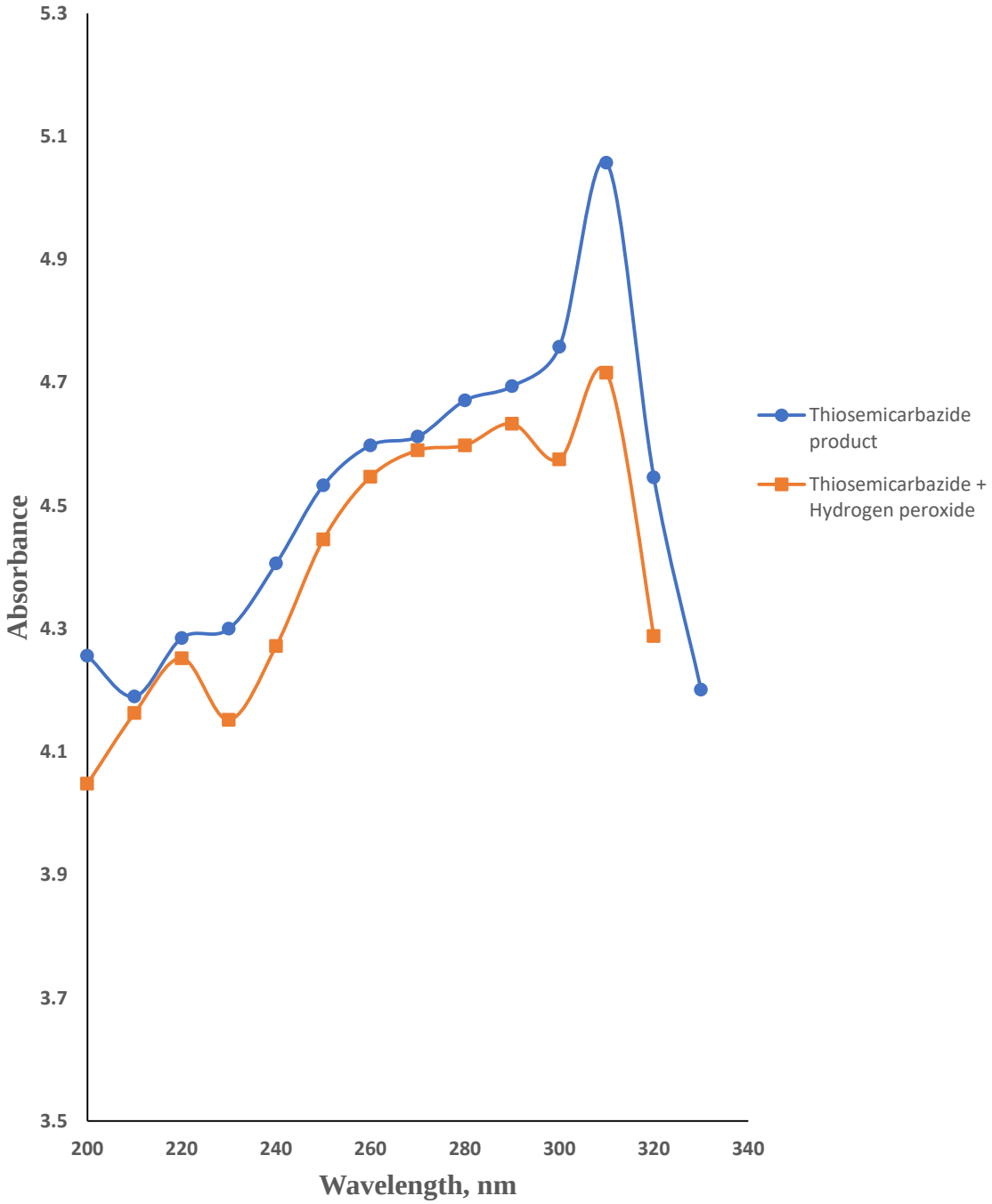
V. UV- visible Spectrum of Product of RSH Oxidation by Co(salophen)$^{+}$ and Hydrogen Peroxide



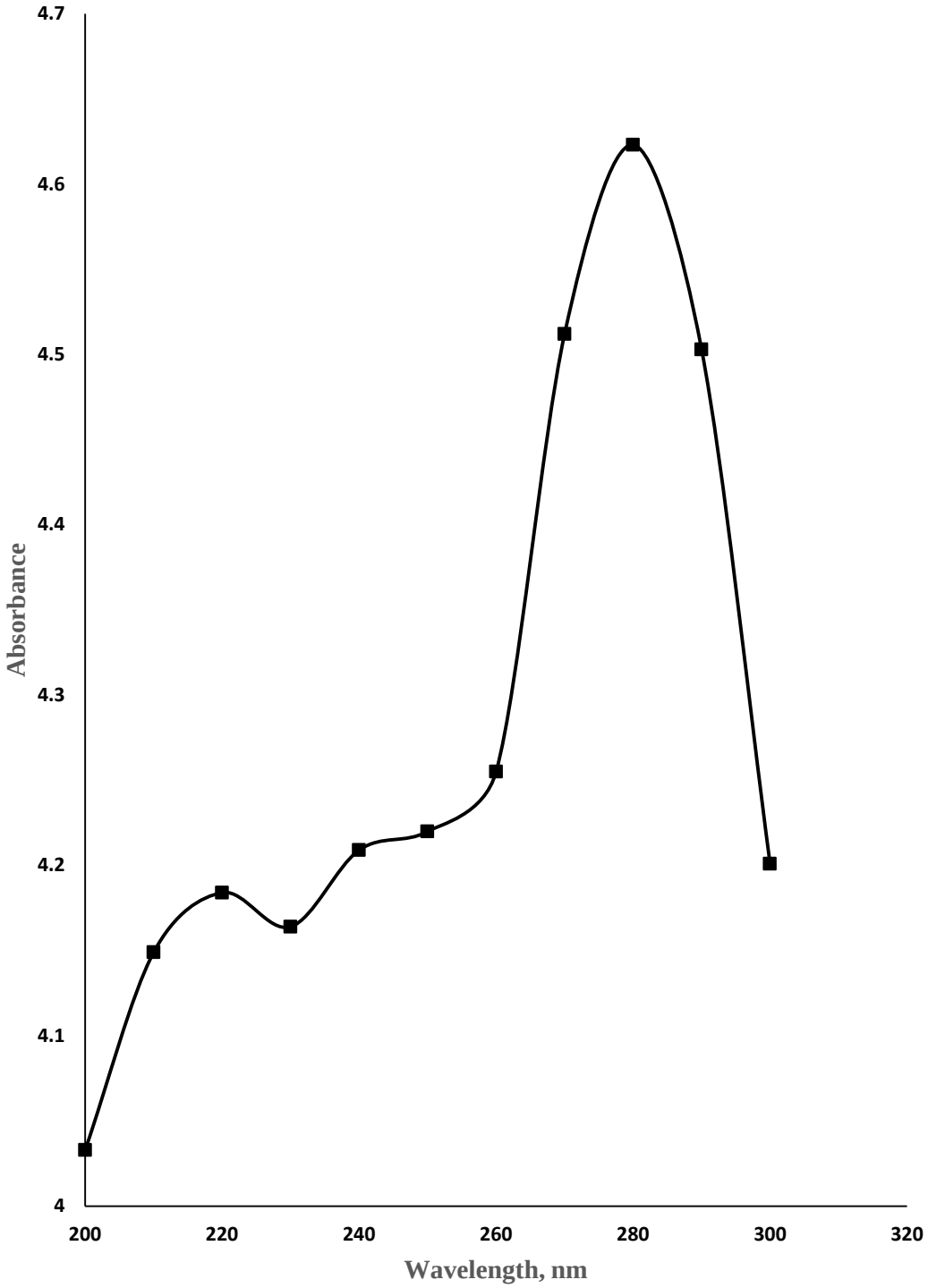
VI. UV- visible Spectrum of Product of TSH Oxidation by Co(salophen)$^{+}$ and Hydrogen Peroxide



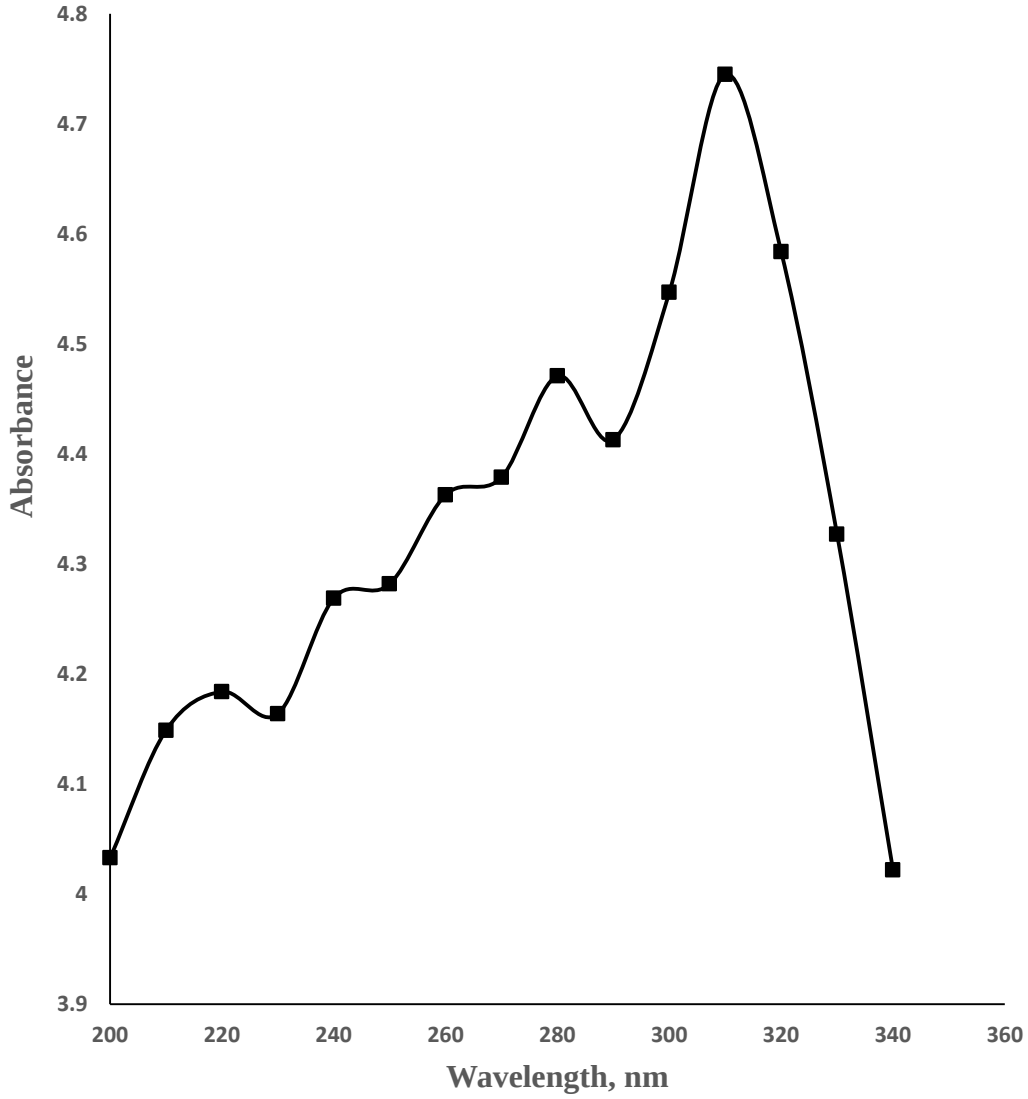
VII. UV- visible Spectrum of Product of TSCZ Oxidation by $[Co(salophen)]^{+}$ and Hydrogen Peroxide



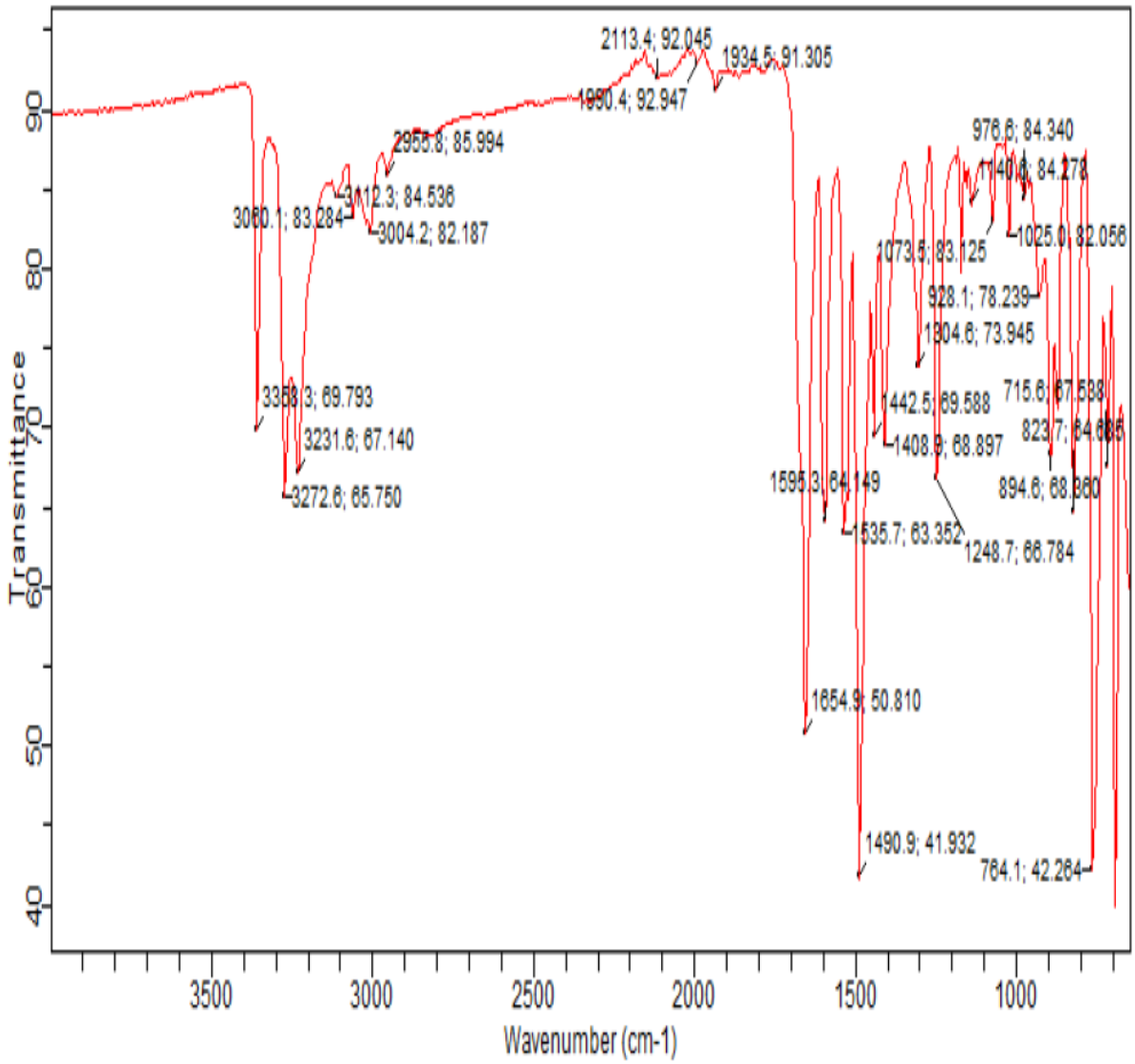
VIII. UV- visible Spectrum of Diphenylcarbazide (DPCI) in DMSO / Water Solvent


4.7
4.6
4.5
4.4
4.3
4.2
4.1
4
Absorbance
200
220
240
260
280
300
320
Wavelength, nm

IX. UV- visible Spectrum of Product of DPCI Oxidation by Co(salophen)$^{+}$ in DMSO / Water Solvent



X. FT-IR Spectrum of Diphenylcarbazide



XI. FT-IR Spectrum of the Product of Reaction of $[Co(salophen)]^{+}$/DPCI

